MULTIPLE MOTOR-UNIT MUSCLE MODELS FOR THE DESIGN OF FES SYSTEMS

Ahmed Omar HAMOUDA

School of Computing, Science and Engineering
College of Science and Technology
University of Salford, Salford, UK

Submitted in Partial Fulfilment of the Requirements of the

Degree of Doctor of Philosophy, September 2013

CONTENTS

LIST OF FIGURES

ACKNOWLEDGMENT

All praise and glory is due to Almighty Allah, the sole Lord of the universe, whose mercy and blessings have been bestowed constantly upon me. All achievements in this work surely only happened under His permissions. Peace and blessings be upon His final messenger Muhammad.

I wish to acknowledge and thank all those people who supported me during my research work and the writing of this thesis. First and foremost, I would like to express my sincere gratitude to my supervisor Prof David Howard for his continued guidance, sincere motivation and encouragement, thoughtful support, kindness and understanding throughout this work. His friendly approach and unbound patience have left a deep impression upon me. I am also grateful to my second supervisor Prof Laurence Kenney for his support and advice throughout this work.

It gives me great pleasure to appreciate and thank my fellow research colleagues for their help and support, their technical discussions and encouragement have been highly beneficial.

Finally, I gratefully acknowledge the love, understanding, patience and encouragement of my wife and children. I would also like to thank my parents and friends for their support during all these years. I am forever indebted to them.

NOTATION LIST

A: Muscle activation is the relationship between muscle force on one side, and on the other side: stimulation frequency, rise and fall times (effects of calcium dynamics), time delay, yield, sag, and effective length. Muscle activation A is mainly affected by stimulation frequency, A is unit-less ($0 \le A \le 1$). Only at certain conditions $A = 1$: tetanic stimulation frequency (the frequency that will produce maximum force, and prevents yield), isometric conditions (no effective length), enough time has elapsed since onset of stimulation (to pass the rise time, effect of sag, and natural time delay).

A_i: Level of activation of the i^{th} fibre-type, modelled in the same way as muscle activation A.

a, a', a_{v0}, a_{v1}, a_{v2}: Constants.

b, b', b_{v1}, .. , b_{v8} and b_v: Constants.

CE: The contractile element. *CE* is a device that represents the "active" properties of muscle (F-L and F-V relations). In the inactive state, *CE* does not hold any force and its length can be changed at will.

c_1, c_2, c_3, c_S, c_R, c_{v0}, c_{v1}, c_W: Constants.

c_{fi}: Slope of the frequency modulation line during voluntary contraction initiated by the CNS (representing the relationship between the natural stimulation input U and stimulation frequency of the i^{th} fibre-type after recruitment).

c_{Ri}: Hawkins recruitment constants for different fibre-types, determined experimentally. $c_{R1} = 1.1756$, $c_{R2} = c_{R3} = 0.6779$.

c_{TS}: The transient-state constant for stretch/shortening.

F_m: Total muscle force, including all active and passive forces (forces produced by the musculotendon complex).

$FL(l_{CE})$: The normalised *CE* isometric force as a function of its length (normalised with respect to the maximum isometric force), $FL(l_{CE}) = \dfrac{f_{iso}(l_{CE})}{f_{iso,\max}}$.

$FPCSA_i$: The fractional physiological cross-sectional area of the i^{th} fibre-type, dimensionless (unit-less), $FPCSA_i = \frac{\text{PCSA}_\text{i}}{\text{PCSA}} = \frac{\text{PCSA}_\text{i}}{\sum_{k=1}^{n} PCSA_k} \quad , i = 1,...,n$

$FV(v_{CE})$: The normalised CE force as a function of its velocity (normalised with respect to the maximum isometric force).

f_d: The steady-state force depression (after the end of the transient state).

f_e: The steady-state force enhancement (after the end of the transient state).

f_t: The passive force of the tendon.

f_{CE}: Instantaneous force produced by the contractile element *CE* (the muscle's active force excluding passive forces).

$f_{CE,i}$: Instantaneous "active" force produced by the i^{th} fibre-type.

$f_{iso}(l_{CE})$: The "active" isometric muscle force as a function of *CE* length l_{CE}.

$f_{iso,\max}$: Maximum CE isometric force at the plateau of the force-length relationship, $f_{iso,\max} = f_{iso}(l_{opt})$.

$f_{iso,\max,i}$: Maximum isometric force for the i^{th} fibre-type at the plateau of the force-length relationship, $f_{iso,\max,i} = f_{iso,i}(l_{opt})$.

f_{PE}: Combined passive forces of f_{PE1} and f_{PE2}, ($f_{PE} = f_{PE1} + f_{PE2}$).

f_{PE1}: Force produced by the parallel elastic element, representing the passive force which resists stretch in the muscle belly.

f_{PE2}: The passive resistance to compression of CE at short lengths of muscle belly.

f_{SE}: The passive force of the series elastic element (represents the combined tendon and aponeurosis).

f_{VE}: Force produced by the parallel viscosity element, representing, the viscous drag "passive" force created by non-recruited fibres resisting muscle movement, during both shortening and lengthening.

$freq$: FES stimulation frequency.

$freq_{0.5}$: The stimulation frequency required to produce 50% of maximal isometric force $f_{iso,\max}$ at the optimal muscle length l_{opt}, during voluntary contraction initiated by the CNS.

$freq_i$: The instantaneous stimulation frequency of the i^{th} fibre-type. If the stimulation frequency was not constant during stimulation (natural or FES); the stimulation frequency will be assumed adjustable, but not a real-time variable (i.e. ignoring dynamic changes in frequency).

$freq_i^{\max}$: The maximum stimulation frequency reached at maximum natural stimulation input ($U = 1$), during voluntary contraction initiated by the CNS.

$freq_i^{\min}$: The initial stimulation frequency of the i^{th} fibre-type (minimum stimulation frequency), during voluntary contraction initiated by the CNS.

i : Fibre-type identifier ($i = 1,2,3$), i can be 1 (single motor-unit models), 2 (slow and fast fibre types) or 3 (type-I, IIa, and IIb fibres).

ID : Index of force depression following shortening of recruited muscle ($0 < R \leq 1$) as a function of time (t).

ID_i : Index of force depression for the i^{th} fibre-type following shortening when recruited.

$ID_{\min}$: The minimum magnitude for the index of depression at the end of shortening.

$ID_{\min}$ =(minimum muscle force during shortening) / (isometric force corresponding to the instantaneous length at end of shortening).

ID_{SS} : The steady-state force depression index after 4 seconds.

ID_{∞} : The plateau level of the index of enhancement, this represents the index of depression after very large value of time ($t \to \infty$).

IE : Index of force enhancement following stretch of recruited muscle ($0 < R \leq 1$) as a function of time t.

IE_i : Index of force enhancement for the i^{th} fibre-type following stretch when recruited.

IE_{SS} : The steady-state force enhancement index after ($t = 4$ [sec]).

$IE_{\max}$: The maximum magnitude for the index of enhancement at the end of stretch.

$IE_{\max}$ =(maximum muscle force during stretch) / (isometric force corresponding to the instantaneous length at end of stretch).

IE_{∞} : The plateau level of the index of enhancement, this represents the index of enhancement after very large value of time ($t \to \infty$).

IF : Index of fatigue for the whole muscle.

IF_i : Index of fatigue for the i^{th} fibre-type (for a given fibre-type).

$IF_{i,j}$: Index of fatigue for the j^{th} motor-unit of fibre-type i.

$IF_{\min}$: The minimum fitness of the muscle at which fatigue rate = 0 of the fully recruited muscle (i.e. the minimum value for the index of fatigue).

j : Motor-unit identifier, $j = 1,2,...,m_i$.

k : Hill's parameter.

k_p : Stiffness of the linear un-damped purely elastic element in parallel.

k_s : Stiffness of the linear un-damped purely elastic element in series.

l_{CE} : Instantaneous length of the contractile element *CE*.

$\bar{l}_{CE}$: The instantaneous *CE* length l_{CE} normalized with respect to the optimal *CE* length l_{opt} , $\bar{l}_{CE} = \frac{l_{CE}}{l_{opt}}$.

l_{ER} : Instantaneous length of the elastic rack, this is the same as the instantaneous *CE* length ($l_{ER} = l_{CE}$).

$l_{ER,f}$: Final length of the elastic rack at end of stretch/shortening (which is the *CE* length at end of stretch).

$l_{ER,o}$: Initial length of the elastic rack just before beginning of stretch/shortening (this equals the length of *CE* just before beginning of stretch).

($l_{ER} - l_{ER,o}$): Instantaneous displacement of the elastic rack during stretch/shortening.

l_m : Instantaneous length of the muscle belly (without tendon).

$l_{\max}$: The maximal length of the muscle fibres at the maximal anatomical length (maximal in situ) of the muscle (i.e. the maximal length that the muscle experience at the anatomical limits of motion of the musculoskeletal system).

$l_{m,opt}$: Optimal length of muscle belly, measured with line of action of the tendon.

l_{mt} : Instantaneous length of the musculotendon complex, this includes the muscle fibres, aponeurosis, and tendon.

l_0 : Length of *CE* at the moment of initial recruitment.

l_{opt} : Optimal length of the contractile element *CE* at which the resulted isometric force in the force-length relationship is maximal.

l_{opt}^t : Tendon optimal length, measured at the maximum isometric force ($f_{CE} = f_{iso,\max}$).

l_{PE} : Instantaneous length of the parallel elastic element.

l_{rest}: The resting length of the *CE* (at the unique resting state), representing the slack length of the muscle belly.

l_S^m: The slack length of the muscle belly (at the unique resting state), the length beyond which the muscle belly begins to develop force.

l_{SE}: Instantaneous length of the series elastic element (represents the tendon).

l_S^{mt}: The slack length of the musculotendon complex (at the unique resting state), the length beyond which the musculotendon complex begins to develop force.

l_S^t: Tendon slack length (at the unique resting state), the tendon length beyond which the tendon begins to develop force.

l_t: Instantaneous length of the tendon.

M: Number of recruited motor-units.

m: Total number of all motor-units in the muscle model. These motor-units are hypothetical units (unreal), the value of (m) is chosen by the user to give the required force resolution and does not correspond to real number of motor-units, ($m \leq 1000$).

m_i: Number of motor-units in fibre-type i, $m_i = m \times FPCSA_i$.

n: Number of fibre-types in the muscle model, the fibre-type can be modelled as single-type (for a single motor-unit model), two types (slow and fast), or three types (fast-twitch type is modelled as two different types; type-IIa and type-IIb).

PA: Amplitude of the electrical stimulation pulses.

PCSA_m: The physiological cross sectional area of the whole muscle (sum of all fibre-type).

$PCSA_i$: The physiological cross-sectional area of the i^{th} fibre-type.

PE: The passive elastic element in Hill-type models, ($PE = PE1 + PE2$).

$PE1$: The parallel elastic element-1, representing the passive elastic force of muscle belly which resists stretch.

$PE2$: The parallel elastic element-2, representing the resistance to compression of the thick filaments at short lengths of muscle belly.

PW: Width of the electrical stimulation pulses.

pw_i^{sat}: The saturation pulse width for the i^{th} fibre-type.

pw_i^{thr}: The threshold pulse width for the i^{th} fibre-type (this can be partial or full depending on sub-model used).

pw_{sat}: The saturation pulse width, at which all motor-units are recruited.

pw_{thr} : The threshold pulse width, at which first motor-unit is recruited.

R : The normalized portion of recruited motor-units (recruitment level). R has the value between 0 (no recruitment) and 1 (all motor-units are recruited), $0 \le R \le 1$. R is used with both artificially stimulated muscle contraction using FES and voluntary contraction initiated by the CNS (Central Nervous System).

R_i : The normalized recruited proportion of the i^{th} fibre-type, calculated as the $PCSA$ of recruited proportion of the i^{th} fibre-type divided by the $PCSA_i$ of the same fibre-type, $0 \le R_i \le 1$. R_i is the analogue output of the recruitment sub-model.

$R_{i,j}$: The binary recruitment of the j^{th} motor-unit of the i^{th} fibre-type, this can only be either 0 or 1 (100% recruited or not recruited at all).

SE : The series elastic element, representing the tendon.

T_{end} : Endurance time of the muscle, time from onset of recruitment to the time when fatigue starts (when force reduction is detected).

$T_{end,i}$: Endurance time of the i^{th} fibre-type.

T_{fat} : Time constant for fatigue, it can have largely different values for different muscles and different fibre types.

T_{rec} : Time constant for recovery.

t : Time.

t_{end}^{fat} : Time at which FES stopped (of the same cycle).

t_o^{fat} : Time at which FES started for any cycle of the intermittent FES.

t_{end}^{rec} : Time at which recovery stopped (of the same cycle) and FES started (of the next cycle).

t_o^{rec} : Time at which recovery started (of the same cycle).

U : The natural stimulation input for a muscle under voluntary contraction initiated by the CNS. U will modulate both the number of recruited motor-units and the stimulation frequency (of recruited motor-units). U is dimensionless, The value of U, at any time, is normalised to the maximum natural stimulation input. $U = 1.0$ at MVC (maximum voluntary contraction) that will produce maximum force when all motor-units are recruited at maximum stimulation frequency.

U_{eff}: An intermediate natural stimulation input that models the rise and fall times (effects of calcium dynamics). U_{eff} models the transient-state when there is a change in the input activation U, the steady-state of the effective activation U_{eff} will be the new value of input activation U.

U_i^{sat}: The value of U at which the i^{th} fibre-type becomes fully recruited (all motor-units of this fibre-type are recruited), $U_n^{sat} = U_{sat}$.

U_i^{thr}: The threshold level at which the i^{th} fibre-type becomes recruited, the recruitment can be either analogue or binary, depending on the sub-model used.

U_{sat}: The value of U at which all motor-units have been recruited (equivalent to pw_{sat} in the case of FES).

U_{thr}: The threshold level, at which first motor-unit is recruited (equivalent to pw_{thr} in the case of FES).

VE: The viscous passive element, representing the resistance to muscle contraction in either direction (shortening or lengthening).

v_{CE}: Instantaneous CE velocity, assumed the same for all motor-units. $v_{CE} = dl_{CE}/dt$, $v_{CE} < 0$ for muscle shortening.

$\bar{v}_{CE}$: Instantaneous CE velocity normalised with respect to the absolute value of its maximum shortening velocity ($v_{CE,\max}$), $\bar{v}_{CE} = \dfrac{v_{CE}}{|v_{CE,\max}|}$.

$v_{CE,\max}$: Maximum shortening velocity of *CE*, beyond which $f_{CE} = 0$.

$v_{CE,\max}^{str}$: Maximum stretch velocity, beyond which f_{CE} does not increase and stays at its maximum.

v_m: Instantaneous velocity of the muscle belly along the same line of action of the tendon, assumed the same for all fibre-types in the muscle model, $v_m = dl_m/dt$.

$\bar{v}_m$: Instantaneous velocity of the muscle belly normalised with respect to the absolute value of its maximum shortening velocity $v_{m,\max}$, ($\bar{v}_m = \dfrac{v_m}{|v_{m,\max}|}$).

$v_{m,\max}$: Maximum shortening velocity of muscle belly, beyond which muscle force = 0.

v_{mt}: Instantaneous velocity of the musculotendon complex (including muscle fibres and tendon), $v_{mt} = dl_{mt} / dt$.

α: Pennation angle (angle between the fibre line of action and the tendon line of action).

$\Delta l_{ER} = (l_{ER,f} - l_{ER,o})$: Total displacement of the elastic rack from the length at initial recruitment after end of stretch/shortening.

Δl_{mt}: Displacement of the musculotendon complex from the unique resting state.

ABBREVIATIONS

ADP: Adenosine Diphosphate.

ATP: Adenosine Triphosphate.

ATPase: Adenosine Triphosphatase.

CE: Contractile Element.

CNS: Central Nervous System.

CPG: Central Pattern Generator.

dep.: Depression.

ES: Electrical Stimulation.

enh.: Enhancement.

FES: Functional Electrical Stimulation.

F-L: Force-Length.

F-V: Force-Velocity.

MMU: Multiple Motor-Unit.

MU: Motor-Unit.

MVC: Maximum Voluntary Contraction.

PA: Pulse amplitude (amplitude of the electrical stimulation pulses).

PE: Parallel Element.

PE1: The parallel elastic element-1, representing the passive elastic force of muscle belly which resists stretch.

PE2: The parallel elastic element-2, representing the resistance to compression of the thick filaments at short lengths of muscle belly.

PW: Pulse width (width of the electrical stimulation pulses).

SCI: Spinal Cord Injury.

SE: Serial Element.

SMU: Single Motor-Unit.

sec: second.

VE: Viscous Element.

VM: Virtual Muscle modelling package.

ABSTRACT

Many functional electrical stimulation (FES) controllers have been developed using a simulation approach, the performance of these controllers depends on the muscle model accuracy. Realistic models of neuro-musculoskeletal systems can provide a safe and convenient environment for the design and evaluation of FES controllers. A typical FES system consists of FES controller, an electrical stimulator, electrodes and sensors.

During FES, the stimulation level can change in a continuous fashion such that different motor-units are recruited at different muscle lengths and at different times. Furthermore, it is also not accurate to use the instantaneous length as input to the force-length relationship in dynamic (non-isometric) situations. Although instantaneous *CE* length is commonly used in FES control studies, empirical data from the literature were reviewed and it was concluded that the *CE* length at initial recruitment l_o is a key parameter influencing total muscle force.

The author presents a new multiple motor-unit Hill-type muscle model that accounts for different motor units being recruited at different *CE* lengths and different times. Hence the model can account for a continuously changing recruitment level whilst using the individual motor unit lengths at initial recruitment as input to the force-length relationship. Moreover, the model is capable of modelling fatigue and force enhancement & depression for the individual motor-units (i.e. the recruitment and time history effects). The model can also take account of the different force-length and force-velocity relationships for different fibre types by modelling these properties for the individual motor-units.

The new multiple motor-unit model is described in detail, implemented and tested in Matlab. Open-loop simulation protocols are made on single/multiple motor-unit models using different *CE* lengths for the force-length relationship; on single/multiple motor-unit fatigue sub-models; and on single/ multiple motor-unit force enhancement & depression sub-models.

A general model that can be used to represent all relevant models from the literature was developed. This model can also be used to build new models at different levels of complexity. Such a “General Model” could be used to study the effect of model complexity on FES controller design so that appropriate trade-offs between model complexity and accuracy could be determined. Results, limitations and possible future work are discussed.

Chapter 1: Introduction

1.1. Background

Electrical stimulation (ES) is the use of electrical pulses applied to the neuromuscular system to generate action potentials in nerves and hence innervated muscles [1, 2, 3]. ES uses short duration electrical pulses (typically several hundred microseconds) of low amplitude (typically several tens of milliamps) to generate action potentials in intact lower motor neurons and thereby cause contraction in associated muscle fibres [1, 3, 4, 5]. Providing that the stimulation intensity (proportional to charge, or pulse width/amplitude) is sufficiently high (to trigger an action potential) and the rate at which the pulses are delivered is sufficient to generate a fused (smooth) contraction, stimulation will result in potentially useful contractions in whole muscles [1, 2].

By controlling the intensity and timing of stimulation, muscle force output and hence resultant limb motion can be controlled [1, 6] and this application of ES is termed functional electrical stimulation (FES). Specifically, FES is the controlled use of ES to generate movements which mimic normal voluntary movements, and thus restore function in people with motor impairments following central nervous system injury (e.g. stroke, spinal cord injury) [1, 2, 3, 4, 5, 7, 8].

A wide range of FES systems exist for individuals with disabilities, including systems for hand grasping, drop-foot correction, standing, walking, stationary rowing, and stationary cycling [2, 9, 10, 11]. A generic FES system consists of FES controller, an electrical stimulator, stimulation electrodes, and different types of sensors [10, 11]. An overview of various grasping and walking FES systems can be found in [10].

For control engineers, the musculoskeletal system of a patient is considered as the plant to be controlled. The position, velocity and acceleration of a body segment are the plant states. The muscles that power the system are the actuators. The electrical pulses activating the muscles are the control signals. The FES controller is the device by which the desired controls are generated. The controller modulates the intensity of the stimulus delivered to the muscle by either changing the pulse amplitude or the pulse width [1, 3, 4]. Modulation of pulse amplitude or pulse width modulates the number of motor-units in the target muscle that are

recruited which in turn modulates muscle force. The time history of the plant states in response to the control signals is the joint-angle trajectory or torque profile [12].

Realistic models of neuro-musculoskeletal systems can provide a safe and convenient environment for the design and evaluation of controllers for FES prior to clinical trials. However, the performance of a controller is highly dependent on the accuracy with which a given model represents the response of a muscle (or muscles) to stimulation [13].

1.2. Why further modelling research is needed?

Most FES systems in use today are open-loop controlled (including finite state control approaches). This is surprising, given the complexities of the human musculoskeletal system, following neurological injury, and hence the potential advantages of closed-loop control over alternative approaches. Among the difficulties in widespread implementation of closed loop FES control approaches are the limitations with current models used to represent muscle response to stimulation.

As will be explained in Chapter 2, current models of muscle behaviour do not adequately represent the muscle's response to continuously varying recruitment levels $R(t)$ and muscle length (l_{CE}). In closed loop FES control, muscle recruitment levels and muscle length may vary continuously, and hence inaccuracies in the way models represent the muscle response to such inputs may lead to degraded controller performance. Specifically, in the thesis it is shown that current models do not properly represent the effects of the length of the contractile element *CE* at initial recruitment on muscle force response, fatigue and force enhancement & depression.

1.3. Objectives

The main question of this research is: Can multiple motor-unit models properly account for continuously varying recruitment levels at different muscle lengths and different times?

The primary goal is to develop a multiple motor-unit model that can account for continuously varying recruitment levels at different muscle lengths and different times. In order to achieve this, it is also necessary to develop a new comprehensive muscle model (General model) that

can be modified to represent all relevant instances from the literature and can be adapted to allow for multiple motor-units to be represented. Where suitable sub-models are not available, new models are created and tested against published experimental data.

Therefore the detailed aims required to achieve the primary goal are to:

i. Develop a new multiple motor-unit model using the *CE* length at initial recruitment (l_o) as the input to the force-length relationship.

ii. Compare performance of the multiple motor-unit model and the single motor-unit model using the basic Hill model. Appropriate input protocols are used to test the responses of the two models when recruitment level (R) and instantaneous length of *CE* (l_{CE}) vary with time.

iii. Analyse the results from previous step to identify which approach can better model the effects of length at initial recruitment, fatigue, and force enhancement & depression for partially recruited muscles with continuously varying stimulation levels at different muscle lengths and at different times.

1.4. Overview of the thesis

The organisation of the thesis reflects the sequence of steps taken in the development of the new multiple motor-unit model and the "General model".

Chapter 2: This chapter begins with a description of skeletal muscle and its physiological recruitment under voluntary contraction, followed by introduction to electrical stimulation and how force is produced in electrically stimulated muscles. FES is then introduced, followed by discussion on the complexity of FES control challenges using open-loop and closed-loop control strategies. Different schools of thought within muscle modelling are then introduced, followed by a discussion on how muscle models can assist in the development of FES systems. The next section of this chapter is a review of key features of muscle models; a summary of the behaviour of the various muscle properties which affect muscle response to FES is included. The last section discusses the need for multiple motor-unit models in FES application and how the accuracy of a muscle model can be improved using the multiple motor-unit modelling approach.

Chapter 3: This chapter addresses the problem of muscle modelling for continuously varying R and hence different values of l_o for different motor-units. Open-loop simulation protocols are made on the multiple motor-unit model and the single motor-unit model using both the instantaneous length and the length at initial recruitment for the force-length relationship, results are discussed at the end.

Chapter 4: This chapter addresses the problem of muscle modelling for continuously varying R and hence different time histories of recruitment for different motor-units. Open-loop simulation protocols are made on the multiple motor-unit model and the single motor-unit model using both the multiple motor-unit fatigue sub-model and single motor-unit fatigue sub-model, results are discussed at the end.

Chapter 5: This chapter addresses the same problem as in chapter three but using models of force enhancement & depression. Open-loop simulation protocols are made on the multiple motor-unit model and the single motor-unit model using both the multiple motor-unit force enhancement & depression sub-model and single motor-unit force enhancement & depression sub-model, results are discussed at the end.

Chapter 6: In this chapter, a general model that can be used to represent all relevant models from the literature is developed. The model, capable of representing the alternative sub-models (for each muscle property) and the inter-connection of these sub-models (model topology), could be used to represent any of the alternative muscle models presented in Chapter 2 or to build new models at different levels of complexity. Such a "General Model" could be used to study the effect of muscle model complexity on FES controller design. The topology of the "General Model" is presented showing the arrangement of sub-models and the interlinking model variables, i.e. the inputs and outputs of the various sub-models. The arrangement of the passive elements is also presented. Finally, the proposed general forms for the sub-models required in muscle modelling for FES controller design are presented.

Chapter 7: In this chapter the conclusions and recommendations for future work are presented.

Chapter 2: Literature Review

2.1. Introduction

This chapter begins with a description of skeletal muscle and its physiological recruitment under voluntary contraction, followed by introduction to electrical stimulation (ES) and how force is produced in electrically stimulated muscles. Functional electrical stimulation (FES) is then introduced, beginning with the applications of FES to control the neuromuscular system in people with upper motor neuron lesions, followed by discussion on the complexity and challenges of FES in open-loop and closed-loop control.

Different schools of thought within muscle modelling are then introduced, followed by an overview of basic Hill-type model that represents muscle as a contractile element, together with passive spring(s). The key muscle models used in FES studies are discussed and the limitations with these models highlighted. The following section reviews the key features of the sub-models used to represent individual aspects of a muscle's behaviour. The main aspects of behaviours modelled are recruitment of motor-units, muscle's active force-length relationship, muscle's active force-velocity relationship, muscle fatigue, force enhancement following active stretch and force depression following active shortening, and finally the passive behaviour of the musculotendon complex. A summary is provided of the various published models, showing their similarities and differences. Based on this review, the last section discusses the need for a new model for FES application, presented in subsequent chapters.

2.2. Skeletal muscle and its physiological recruitment

There are three types of human muscle tissue: skeletal, cardiac and smooth. This study is concerned with skeletal muscle only, whose principal functions are to produce movement, maintain body position, and generate heat [14].

2.2.1. Muscle fibres and force generation

Skeletal muscle is made of long cylindrical cells known as muscle fibres. The muscle fibre is composed of discrete bundles of myofibrils parallel to each other, see Figure 2.1. The repeated unit in the myofibril is called a sarcomere, which forms the basic contractile unit of a

skeletal muscle, see Figure 2.2. The sarcomere is composed of long fibrous proteins that slide past each other during contraction. The thick filament is called myosin and the thin filament is called actin. Adjacent sarcomeres are bordered with Z-lines.

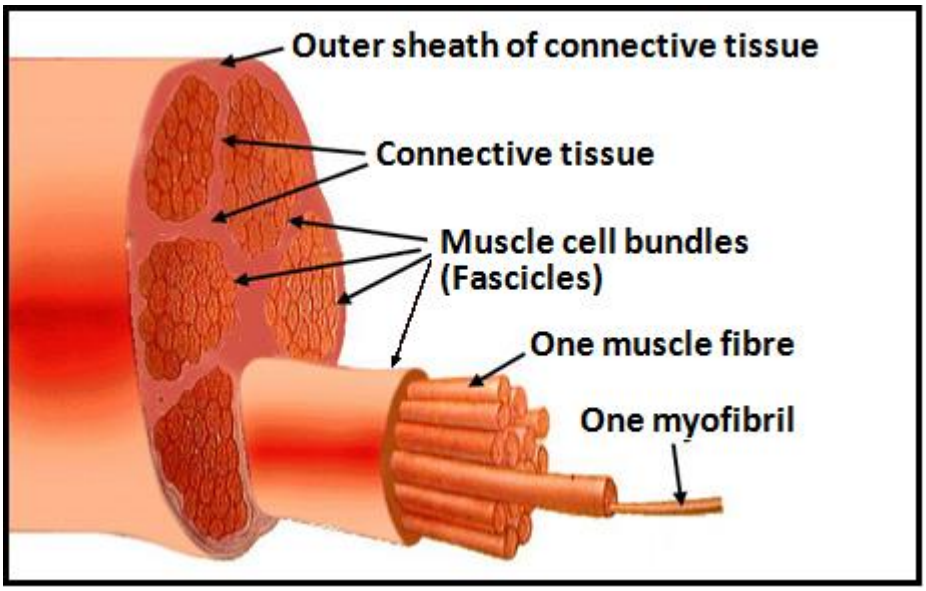

Figure 2.1: Skeletal muscle fibres. (From [15]).

There exist alternative theories of muscle force production; the most cited theory in the literature is the cross-bridge theory [16]. It is assumed in the cross-bridge theory that contraction occurs through the cross-bridge interaction cycle between the myosin cross-bridges and the actin filaments (Figure 2.2). During the cross-bridge cycle, the myosin cross-bridges will combine with specialised sites on the actin, and contraction and hence force development occurs through the rotation of the cross-bridge heads by pulling the actin across the myosin in the direction of sarcomere centre. The cyclic interaction of myosin cross-bridges with the actin filaments in the cross-bridge theory are illustrated in Figure 2.3, and summarised as follows: (a) Starting from the rest state; the actin is covered by tropomyosin-troponin complex at the attachment site. (b) Upon activation, calcium concentration increases and calcium Ca^{2+} binds to troponin. (c) The myosin cross-bridge combines with the actin. The ATP (adenosine triphosphate) splits into ADP (adenosine diphosphate) and P_i (inorganic phosphate) and produces the contraction force. (d) The myosin cross-bridge detaches from the actin and a new ATP attaches to the myosin cross-bridge making it ready for a new interaction with the actin.

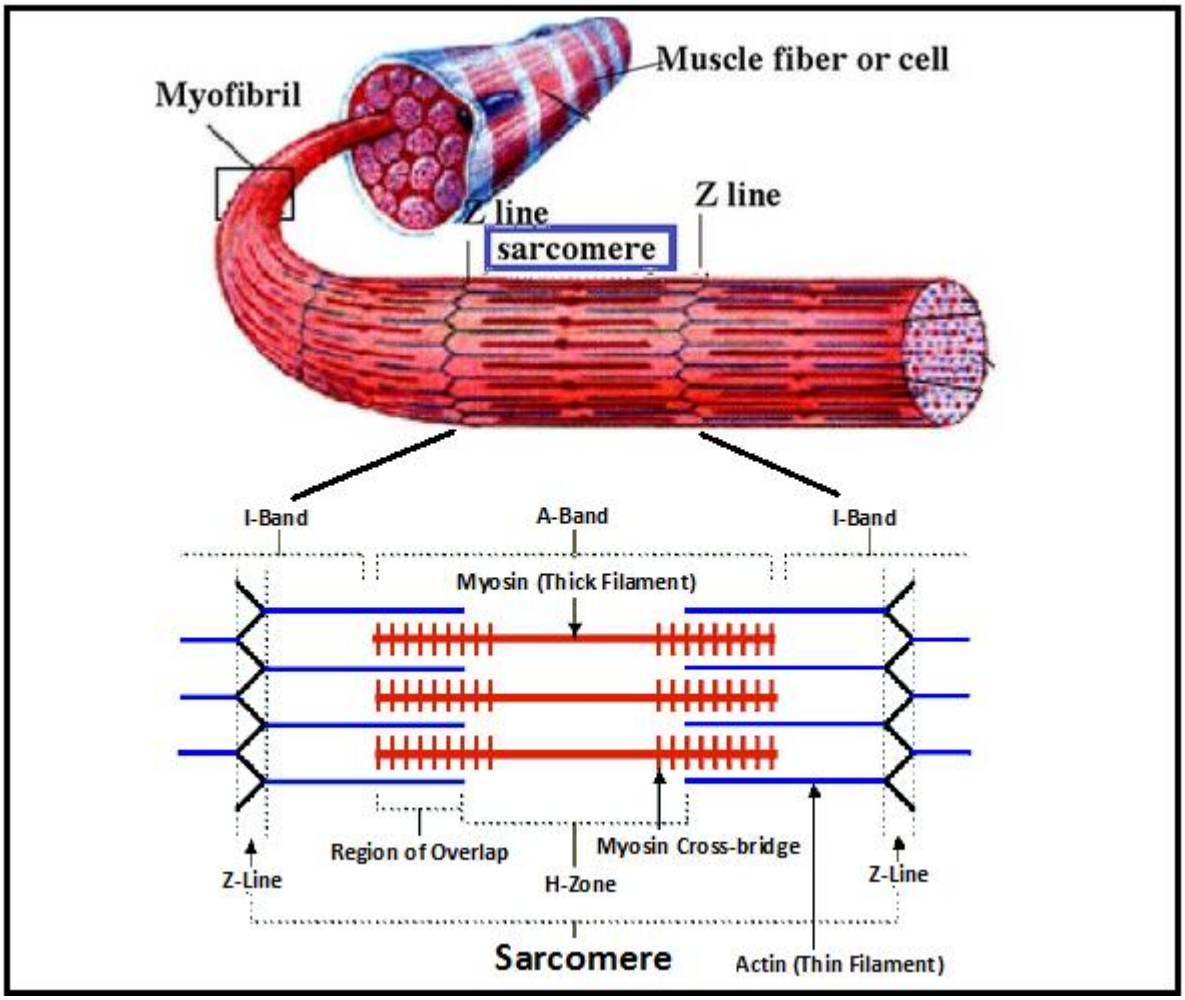

Figure 2.2: Schematic illustration of the sarcomere in a myofibril. (Adapted from [14]).

Although some animal muscles have a uniform appearance, most muscles including human muscles, have a mixed composition, where the fibres in the same muscle have different contractile properties. These differences are due to the innervation of the fibres and the different ways in which they are used [17]. It has been shown that muscle fibres may be classified into three main types [15].

Type-I fibres are characterised by high fatigue resistance because they primarily utilize fatty acid oxidation (using oxidative enzymes) and have high levels of mitochondria and myoglobin (and hence they are red in colour). The high level of blood flow provides high capacity for aerobic (oxidative) metabolism to generate ATP (Adenosine Triphosphate). These fibres also show a slow twitch response to a contractile impulse, develop relatively low levels of force, and have the slowest maximum velocity of contraction. Type-I fibres are also known as tonic, red, slow twitch, S (slow-contracting) and SO (slow-oxidative).

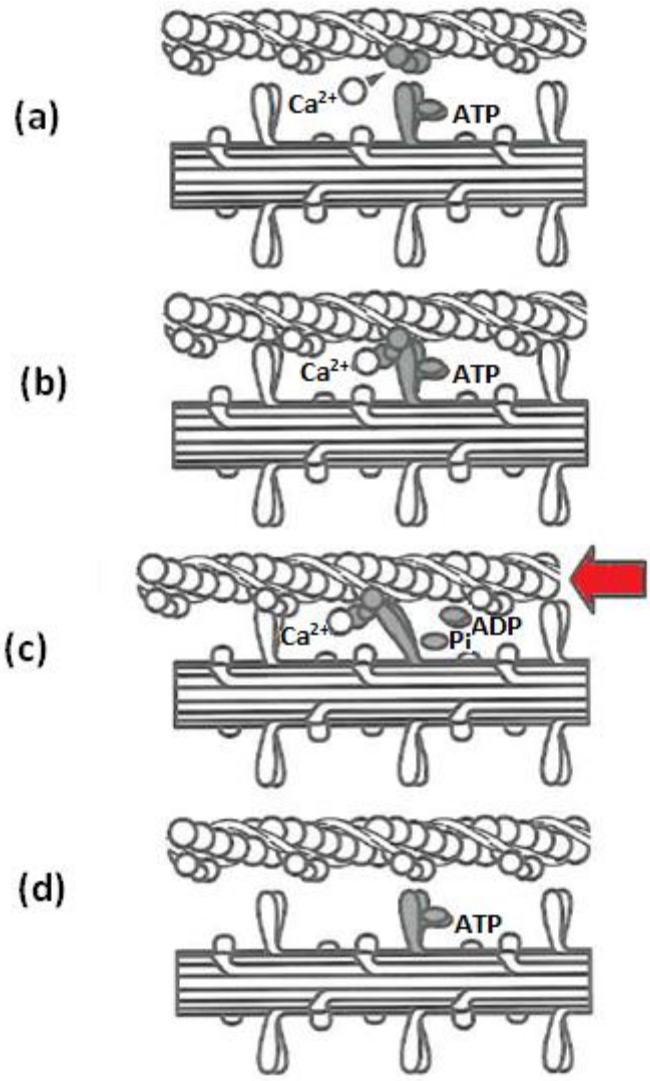

Figure 2.3: Schematic illustration of the cyclic interaction of myosin cross-bridges with the actin filaments in the cross-bridge theory. (From [18]).

Type-IIb fibres produce relatively high force because they primarily utilize glucose oxidation to pyruvate for ATP production (anaerobic metabolism), but they fatigue fast due to the high activity of ATPase (Adenosine Triphosphatase), the main function of the ATPase enzyme is to hydrolyse the ATP which provides energy for attachment to another active site on the actin molecule. Type-IIb fibres contain low level of mitochondria and myoglobin (and hence they are white in colour). The relatively high force of type-IIb fibres is due to the large anaerobic capacity. Type-IIb fibres also show a fast twitch response, and the fastest maximum velocity of contraction. These fibres are well equipped for brief intense activity but they are the least efficient because they use high amounts of energy. Type-IIb fibres are also known as FF (fast-contracting, fast-fatigue) or FG (fast-glycolytic).

Type-IIa fibres can utilize both anaerobic (as in type-IIb) and aerobic (as in type-I) metabolisms for ATP production, and hence they have intermediate properties. The fibres show a fast twitch response, develop moderate levels of force, and are fatigue resistant. These fibres are well equipped for prolonged activity, but in addition, they have the ability to produce high power output. Type-IIa fibres are also known as FR (fast-contracting, fatigue-resistant) and FOG (fast-oxidative-glycolytic). More details about muscle fibre-type classification can be found in [19].

The ratio between the three main types of muscle fibres in a muscle depends on the function of the muscle and this ratio determines the force-velocity relationship of the muscle [20]. As an example, the functional tasks in the cat triceps surae group are divided to some extent among the muscles. The soleus is mainly made up of type-I fibres [21] making it suitable for situation when low force and fatigue resistance are required, while the gastrocnemius consists of about 25% type-I fibres and 75% type-II fibres, making it dominant in situations when large and sudden force demands are needed [22, 23]. The composition of a muscle can change over time, depending on the type of contractions to which it is subjected [24]. For example, sprinters develop a higher proportion of type-II (both types IIa and IIb) fibres in their leg muscles than distance runners.

Skeletal muscle fibres are protected by connective tissue coverings. The connective tissues also provide pathways for the passage of nerves and blood vessels. As shown in Figure 2.4, there are multiple types of connective tissue, surrounding the muscle (fascia and epimysium), fascicle (perimysium) and muscle fibre (Endomysium).

A tendon connects muscle to bone and is capable of withstanding tension; the tendon is made of tough band of fibrous connective tissue. Bones move because of the combined work of tendons and muscles. Aponeuroses are layers of broad flat tendons, the primary function of an aponeurosis is to join the muscle with the part of the body the muscle act upon (this can be another muscle or bone).

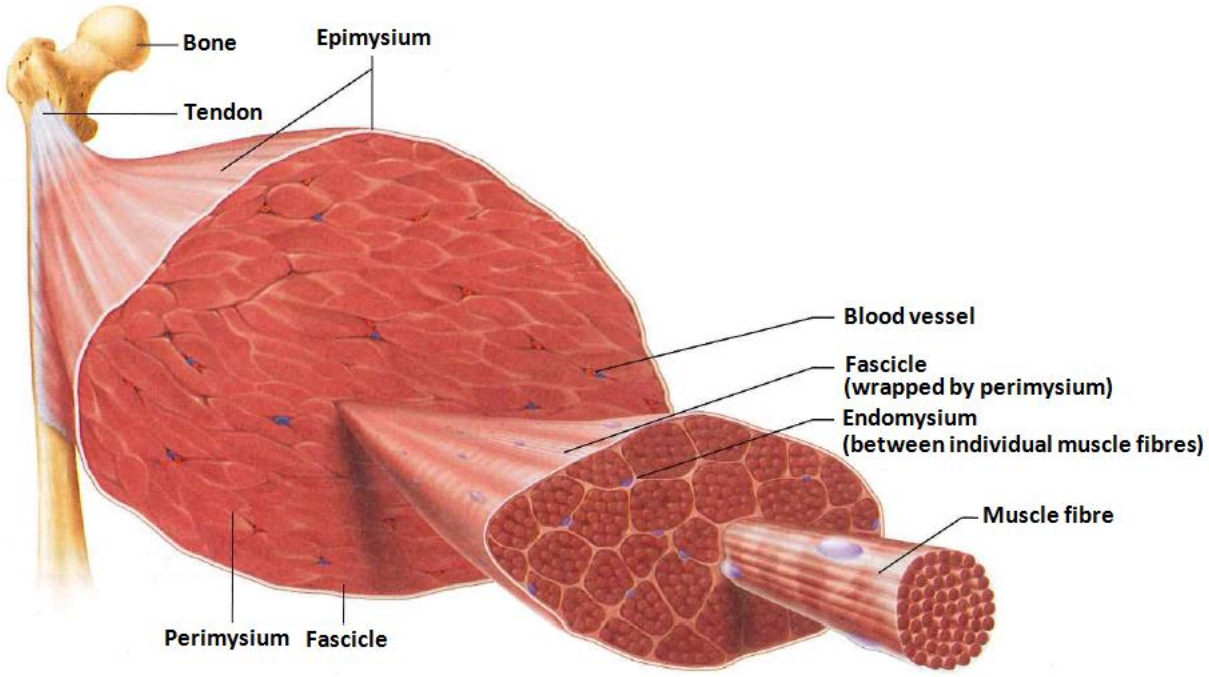

Figure 2.4: Structure of skeletal muscle. (From [14]).

2.2.2. The neuron and the action potential

The neuron is the core unit of the nervous system. A typical neuron consists of four main parts: the body of the cell (often called the soma), dendrites, axon, and synapse (Figure 2.5). Dendrites are thin structures and emerge from the soma; their function is to receive the command information and conduct them towards the soma. The soma is where the command information are integrated and then transferred through the axon. The axon is the only extension dedicated to transmitting the information outside the neuron; it travels for a distance as far as one metre in humans [25]. The information is conveyed outside the neuron through synapses to other neurons, muscle fibres or glands. The motoneurons carry command information from the central nervous system (CNS) to muscle fibres [26]. The axons are wrapped with myelin (the axon with the myelin wrapping is also called nerve fibre). Bundles of between 100 and 2000 nerve fibres form a nerve [25].

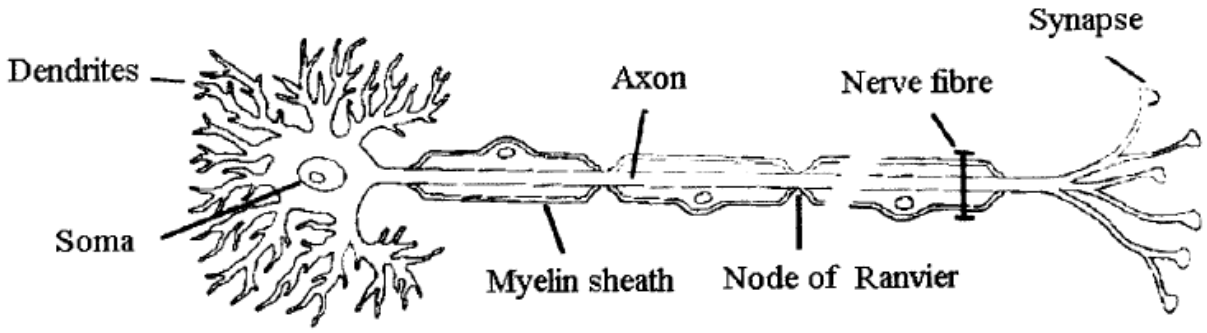

Figure 2.5: Schematic representation of the anatomy of a typical neuron. (From [27]).

The action potential

Neurons are electrically excitable cells, the concentration of ions in the inside and the outside of the cell are different. In the unexcited state (the neuron is not receiving any physiological or artificial stimulus), the membrane potential from inside to outside is negative and referred to as the "resting membrane potential". The resting membrane potential is typically in the range of (-70 to -90 mV). If the membrane potential changes by a large enough magnitude (around -55 mV), an electrochemical pulse called "action potential" is generated (Figure 2.6), and this voltage change propagates rapidly as a nerve impulse along the axon for great distances without losing its strength [25]. The action potential is an all-or-none signal, lasts for several milliseconds, and up to 120 [mV] across the membrane [28]. For a given neuron cell, the voltage and duration of an action potential are not affected by the intensity, or origin of the stimuli (artificial or natural), and a stimulus just above threshold and much stronger stimulus will elicit the same action potential.

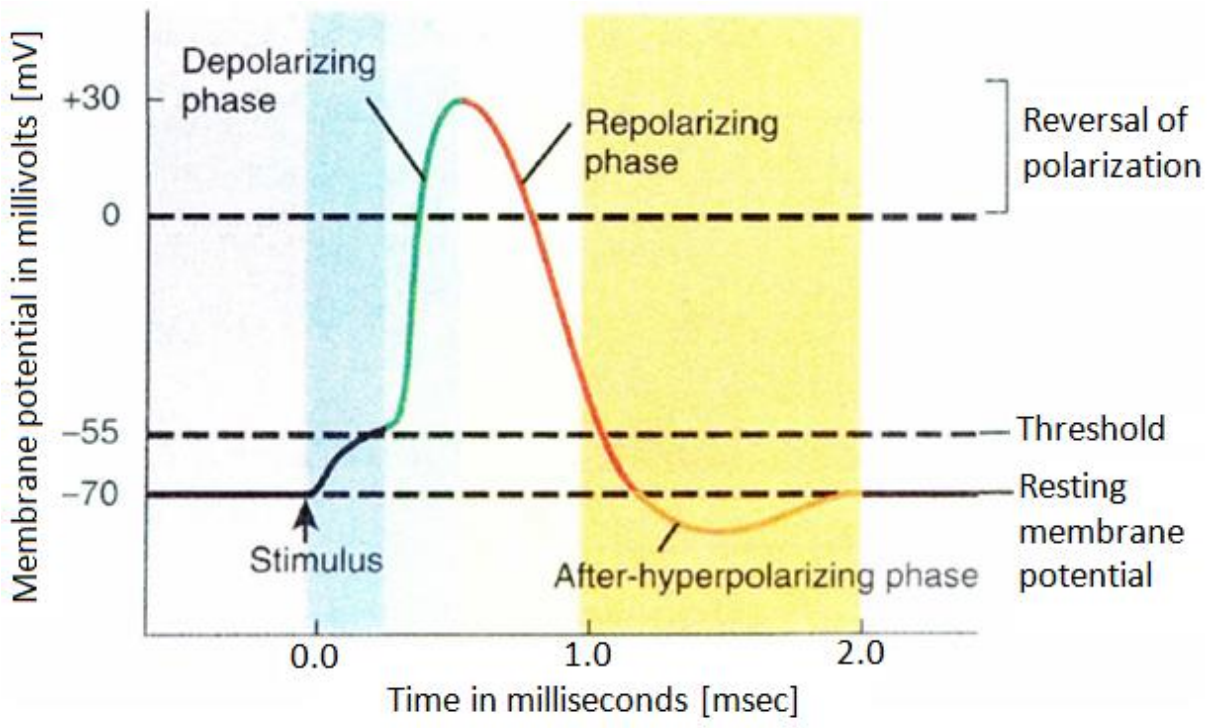

Figure 2.6: Schematic illustration of a single action potential. (From [29]).

Action potential generation can be summarised as follows:

- When an action potential is triggered by a stimulus above its threshold level, the voltage-dependent sodium channels are opened, allowing the sodium ions to flow into the neuron cell causing the depolarisation of the membrane potential and consequently closing the sodium channels.
- In the next phase the potassium channels open and allow potassium to leave the cell causing rapid repolarisation, the repolarisation continuous to a more negative than the resting membrane potential. This hyperpolarization prevents another action potential until the membrane potential is back to its resting level.
- The local depolarisation on one point on the axon causes movement of ions between neighbouring points and consequently depolarisation of neighbouring areas on the membrane leading to action potential propagation along the axon.
- If the action potential is triggered at one of the ends of an axon, it propagates in one direction only, either to muscle fibres or the CNS. If the action potential is initiated at another point in between the two ends of an axon (by external source, such as ES), it propagates away from that point in both directions (to both muscle fibres and the CNS) [28].

2.2.3. The motor-unit

The basic functional unit of force production is in fact the sarcomere, but usually the basic functional unit of movement is considered to be the motor-unit, which consists of a motoneuron and the muscle fibres that it innervates [15]. Muscle fibres of a particular motor-unit are of the same type and have the same metabolic properties so that, when they are recruited, they behave in the same manner. Each muscle fibre is innervated by a single axon; one motoneuron will supply through its axonal branches many fibres scattered throughout the muscle, the innervation is almost entirely random and adjacent muscle fibres are most likely to be supplied by branches from different motoneurons [17], see Figure 2.7.

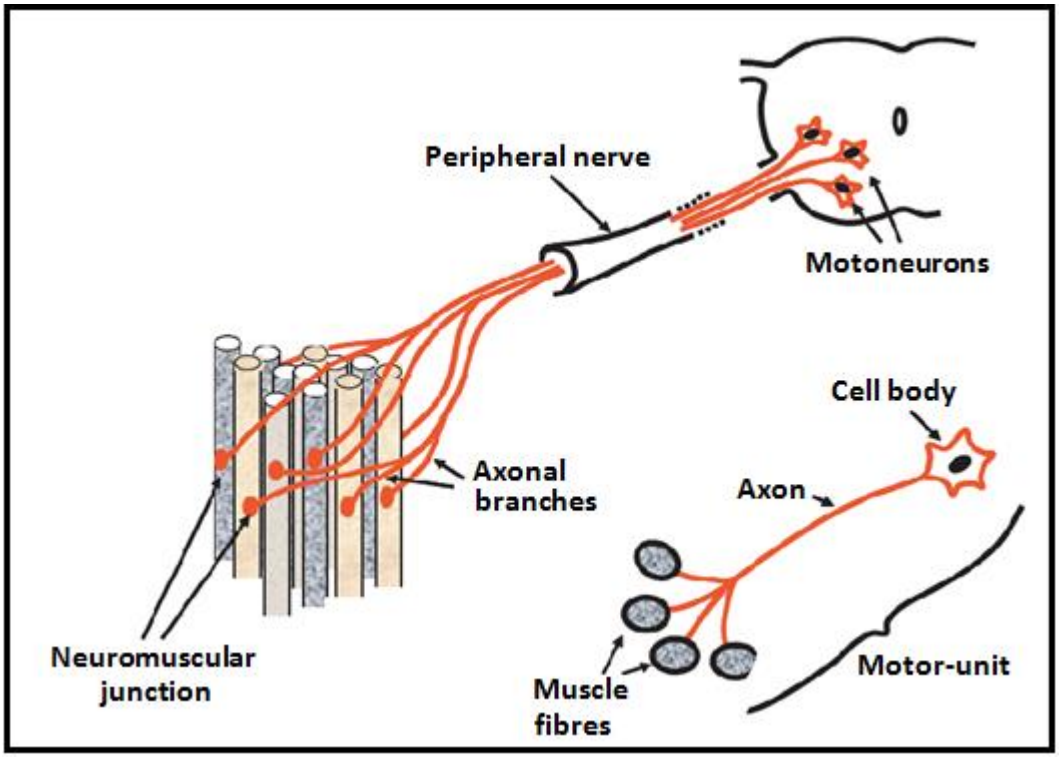

Figure 2.7: Concept of the motor-unit. A motor-unit consists of the motoneuron and all the scattered muscle fibres that it innervates. (From [17]).

The number of a skeletal muscle's motor-units depends on the size and function of the muscle, ranging from a few motor-units for small muscles up to several thousand for the largest human muscle [30]. Muscles that are involved in gross movements, such as leg muscles, have few motor-units (each of which includes a large number of muscle fibres). Muscles that are involved in fine movements (e.g. facial muscles) have many motor-units

(each of which includes a small number of muscle fibres), see Figure 2.8. Type-IIb have large axons that innervate many large fibres, they generate large forces but fatigue rapidly. Type-IIa have moderately sized axons that innervate many fibres, they generate moderate forces and do not fatigue a great deal. Type-I are composed of small axons that innervate a few small fibres, they generate low forces but maintain force for a long time.

Force generation in muscles is modulated by the central nervous system. After an action potential is triggered in a motor-unit; all the muscle fibres of this motor-unit will contract "synchronously", this motor-unit then is considered to be recruited. Muscle force modulation is achieved by recruiting varying numbers of motor-units [1].

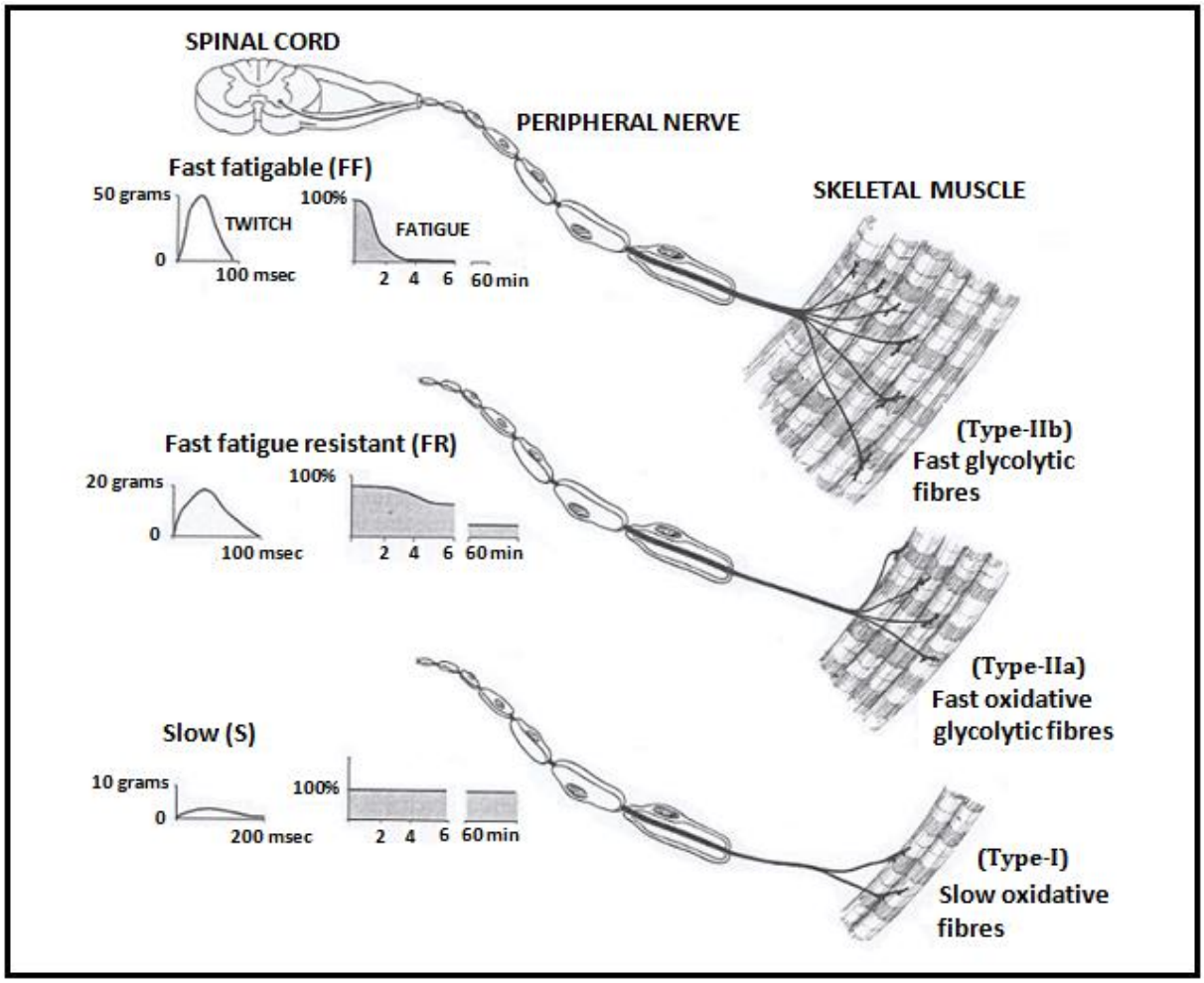

Figure 2.8: Schematic representation of the anatomic, physiologic, and histochemical properties of the three fibre types and how they are connected in motor-units. Type-IIb (top), type-IIa (middle), and type-I (bottom). (From [15]).

2.2.4. Natural recruitment of motor-units

A fast, transient contraction of a single motor-unit will result from a single impulse in a motoneuron. Therefore, a train of impulses has to be delivered by the motoneuron to its associated muscle fibres to maintain a smooth constant contraction (natural stimulation frequency depends on fibre-type and recruitment level of the whole muscle). The intensity of the resulting muscle force is determined by frequency of the impulses. During voluntary muscle contraction, the body achieves smooth contraction by using "asynchronous" recruitment of motor-units. Adjacent motor-units are activated at low frequency (of about 6-8 Hz) in a sequential manner, coordinated by the CNS [31], see Figure 2.9. The stimulation is timed by the intact CNS so that each motor-unit contracts before the previously stimulated motor-unit relaxes completely. The force of the whole muscle is the sum of the forces of the individual motor-units. This recruitment pattern of motor-units resists fatigue by allowing the various motor-units to share the task of maintaining smooth contraction.

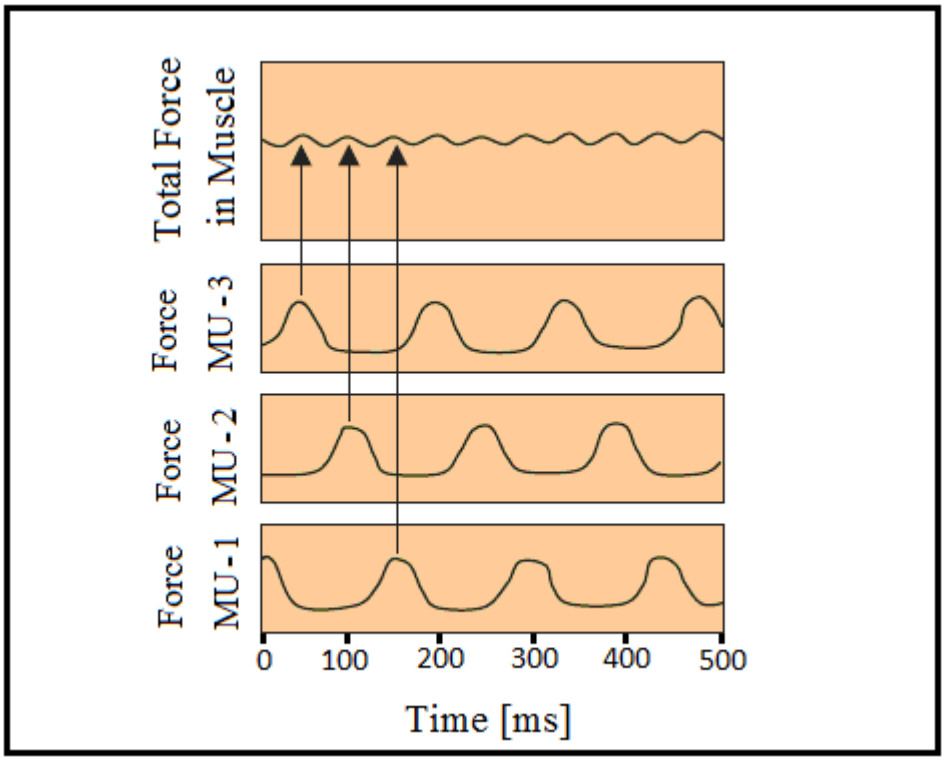

Figure 2.9: Summation of force in motor-units. Force production in skeletal muscle is accomplished by sequentially stimulating adjacent motor-units. (Adapted from [3]).

“Asynchronous" recruitment of motor-units happens only during sub-maximal contractions, where only some of the motor-units maintain the required force. During maximal contraction, when all motor-units of the muscle are recruited, asynchronous recruitment is impossible and hence fatigue cannot be prevented [32].

McPhedran et al [33] made a detailed study of motor-units in cat soleus muscle and Wuerker et al [34] made a similar study in cat medial gastrocnemius muscle. From these two studies; it was found that within the same muscle and also from one muscle to another, there are large differences in motor-units’ size. Small motor-units are usually made up of type-I fibres and large motor-units of type-II fibres (type-IIa and type-IIb) [35]. Motoneurons with thin axons belong to small motor-units (typically of type-I fibres) and are excited first (during voluntary contraction), motoneurons with thick axons belong to large motor-units (typically of type-II fibres) and are the least excitable (during voluntary contraction) [35]. Motor-units are therefore recruited according to the “size principle” where the smallest motor-units are recruited first and then progressively larger motor-units (as long as more force is required) until MVC is achieved [36].

For voluntary contracted muscles, fibres tend to be recruited at an initial frequency (firing rate) regardless of intensity of muscle contraction [37, 38, 39]. Once recruited, the frequency of recruited motor-units will be modulated approximately linearly with changes in the EMG signal. Gross EMG activity is representative of the natural stimulation input of a uni-functional muscle [40], so either the EMG signal or the CNS descending commands can be considered as reflecting the input to the muscle [41]. Changes in the natural stimulation input will simultaneously modulate both the number of recruited fibres and also the stimulation frequency [37, 39, 40, 42, 43, 44].

2.2.5. Summary

The biophysical mechanisms of skeletal muscle during voluntary contraction can be summarised as follows:

- The basic functional unit of movement is considered to be the motor-unit which consists of a motoneuron and the muscle fibres that it innervates [15]. Muscle fibres of a particular motor-unit are of the same type and have the same metabolic properties so that, when they are recruited, they behave in the same manner [15, 17, 30, 45].

- During voluntary “sub-maximal” contraction, the body achieves smooth contraction by using "asynchronous" recruitment of motor-units at low frequency (low firing rate) [1]. This recruitment pattern of motor-units resists fatigue by allowing the various motor-units to share the task of maintaining smooth contraction [1, 46].
- During voluntary maximal contraction, when all motor-units of the muscle are recruited, asynchronous recruitment at low frequency is impossible and the firing rate (natural stimulation frequency) will be high, and hence fatigue cannot be prevented [32].
- Motor-units were most easily classified into three main types: The first is type-I which contains few fatigue resistant (Type-I muscle) fibres and hence develops relatively small force. The second is type-IIb which contains relatively more Type-IIb muscle fibres and develops high force but also fatigue quickly. The third is type-IIa which has intermediate properties; it has a fast twitch, develops moderate force, and is fatigue resistant [15, 17, 45].

2.3. Electrical stimulation and challenges of functional electrical stimulation

Electrical stimulation (ES) involves artificially inducing a current to excitable tissue to induce a physiological response. In therapeutic applications, ES may enhance tissue health or voluntary function, but it is not used to provide the function directly. In functional applications, ES is applied to paralyzed muscles in precise sequence and magnitude to directly achieve functional tasks [2].

2.3.1. Electrical stimulation

ES pulses applied to an excitable motoneuron can elicit action potentials. The motoneuron receives ES pulses that are delivered using electrodes, these electrodes can be placed on the skin surface (transcutaneous electrodes), placed within a muscle (percutaneous electrodes), placed on the surface of the muscle (epimysial electrodes), or wrapped around the nerve that innervates a specific muscle (cuff electrodes) [4].The negative electrode (cathode) creates a localized electric field that depolarizes the cell membranes of nearby motoneurons. If the depolarization exceeded the threshold level, an action potential propagates along the axon in both directions away from the site of stimulation [3, 47]. The threshold charge required to elicit action potential in muscle fibres is much greater than the threshold charge required to

elicit action potentials in neurons [24]. Therefore, a fundamental principle is assumed that ES generally activates nerve rather than muscle fibres.

2.3.1.1. Recruitment order of electrically stimulated muscle

Unlike the "asynchronous" recruitment of motor-units that happens in the intact CNS, FES recruits motor-units in a "synchronous" manner. For this reason, a higher stimulation frequency (usually in the range of 20–40 Hz) is required to achieve smooth contractions when using FES [1]. The high frequency used in FES is the main cause of the increased rate of fatigue associated with FES as compared to voluntary contractions initiated by the CNS [24].

Furthermore, it is generally accepted that FES tends to recruit muscle motor-units in a "non-physiological" order [1, 46, 48]. The difference in recruitment order is believed to be due to the size of axons of the different motor units (and hence associated muscle fibre types). Type-IIb fibres are innervated by axons with the largest diameter, type-IIa fibres are innervated by axons with the second largest diameter, and type-I fibres are innervated by axons with the smallest diameter. The large diameter axons couple more of the electric field than the small diameter axons, so type-IIb fibres respond to FES at lower stimulation levels than type-IIa fibres which respond at lower stimulation levels than type-I [1, 3]. Since type-IIb fibres fatigue more quickly than other fibre types, the non-physiological order of motor-units' recruitment contributes to the increased rate of fatigue that occurs with FES, as compared to voluntary contractions initiated by the CNS.

Although the concept of non-physiological recruitment order of electrically stimulated muscle is generally accepted in the FES community, a debate exists with respect to the exact order of recruitment when surface electrodes are used:

- As reported in [3, 46, 48] recruitment order depends on two factors; the distance from the surface electrodes and the inverse-size order.
- Gregory and Bickel [49] and Singh et al [50] however suggested that motor-units recruitment order tends to be random and fibre-type has little effect, because threshold depends mostly on distance of the motor axon from the surface electrode (i.e. the axon size has little effect compared with the effect of the distance from the surface electrodes).

To achieve the physiological recruitment order in a heterogeneous muscle (consisting of different fibre types), several selective nerve-blocking techniques were developed [51, 52, 53]. Stimulation waveforms of special shape and nerve cuff electrodes are used in these techniques. The disadvantage of these techniques is that they require nerve cuff electrodes which must be surgically implanted.

2.3.1.2. Force production in electrically stimulated muscle

The proportion of motor-units recruited depends on stimulation intensity (pulse width *PW* and pulse amplitude *PA*). An increase in either pulse width or pulse amplitude generates a larger electric field of a sufficient value to initiate an action potential, and hence recruitment of more motor-units [54]. Pulse amplitude and pulse width both have an equivalent effect [3, 55], an increase in either (or both) will lead to an increase in the number of recruited motor-units and hence force, until all motor-units are recruited, see Figure 2.10. In this particular case (shown in this figure), at a pulse width of 200 [μsec], muscle force can be adjusted from threshold to near maximal by changing the pulse amplitude (which will change the current intensity) from 18 to 40 [mA]. In contrast, at current amplitude of 40 [mA], muscle force can be controlled by changing the pulse width from 40 to 200 [μsec] (frequency is fixed at 35 [Hz]).

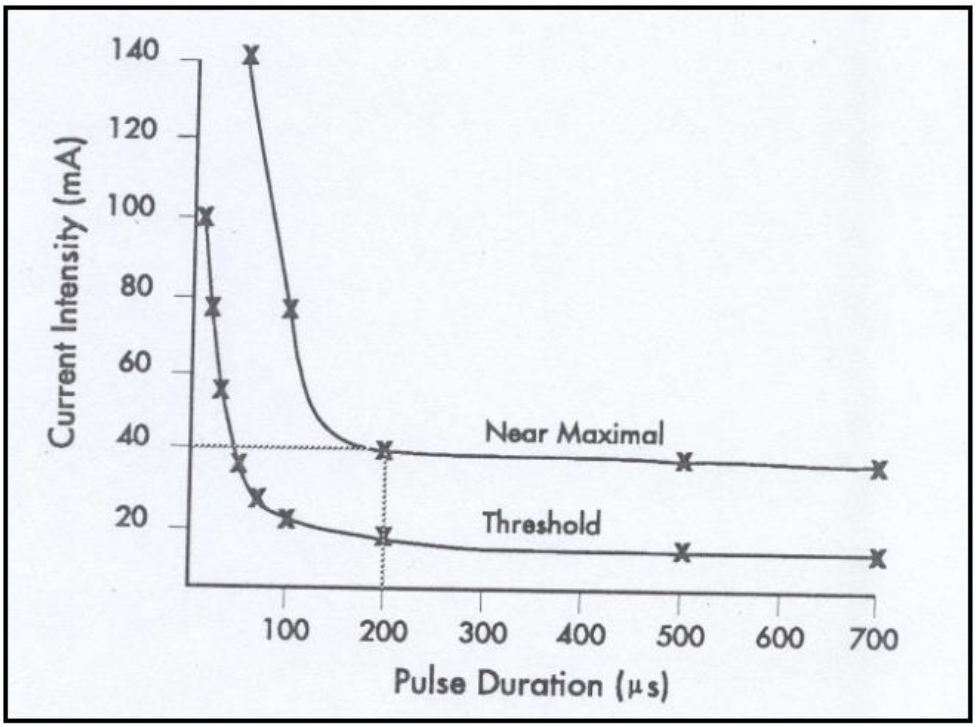

Figure 2.10: Variation of pulse amplitude and pulse width. (From [3]).

The force produced by ES can also be controlled by pulse repetition rate, or frequency. Low stimulation frequency causes the muscle to respond with a series of twitches. Therefore, the stimulation frequency has to be high enough to achieve smooth contractions. Higher stimulation frequencies will increase muscle force up to a maximum, but also increase the rate of muscle fatigue. Thus, a trade-off between produced muscle force and minimum rate of muscle fatigue is required (stimulation frequency is typically in the range of 20–40 Hz) [1].

Due to the problems of fatigue at the high end and non-tetanic contractions at the low end (frequency is not sufficiently high to produce smooth contraction), frequency is not suitable to modulate force. Therefore, ES systems usually use pulse amplitude or pulse width to modulate force. The stimulation frequency is set constant and as low as possible, while achieving a tetanic contraction, to reduce muscle fatigue [47]. A typical stimulation waveform used for transcutaneous (surface) FES is a biphasic square-wave pulse train with amplitude of (0–120) [mA], pulse width of (0–300) [μsec], and stimulation frequency in the range of 20–40 Hz [1].

2.3.2. Functional electrical stimulation

When electrically stimulated skeletal muscle contractions are coordinated in a way that provides function, this technique is referred to as functional electrical stimulation (FES). The purpose of FES intervention is to enable function by substituting or supporting the voluntary physical ability of a patient. The clinical application of FES is currently restricted to neurological disorders involving upper motor neuron lesion such as SCI, stroke, brain injuries, multiple sclerosis, and cerebral palsy [2].

FES application areas:

- **Upper-Limb Applications:** FES systems can assist the reach, grasp and release function for subjects with impaired upper limb function. The control signal for grasp is typically driven by the patient from preserved voluntary function (open-loop control). Examples of hand grasp FES systems are provided in [56, 57].
- **Lower-Limb Applications:** The initial application of FES in stroke patients focused on the stimulation of the peroneal nerve for foot drop correction. The development of lower-limb FES systems is much more advanced than upper-limb FES systems, but there are still several problems that restrict their clinical implementation [2]. The relatively simple multichannel FES systems, with 2-6 channels, are successful in

producing stepping and standing for patients with complete SCI [58]. However, walking with present lower-limb FES systems can only be used for short distances, and cannot be used as practical alternative to a wheelchair [2] because of the high metabolic energy required. A varied choice of lower-limb FES systems is available for patients of SCI, including standing [59, 60], stationary rowing [61], cycling [62, 63] and systems for supporting gait patterns during walking [64, 65, 66].

- **Other applications:** Other FES applications include bladder and respiratory FES systems.

2.3.3. State of the art and challenges

Controlling joint angles or torques by FES presents several significant control challenges. These challenges can be summarised in the following points:

1. Stimulated muscle force characteristics are nonlinear, dependent on muscle length and velocity (which vary with joint angle and angular velocity), and time-varying because of fatigue and changes in muscle composition over time due to regular use of FES.
2. The presence of spasticity and other hyperactive or inappropriate spinal reflexes in neurological patients add another layer of complexity to the response of electrically stimulated muscles. Spasticity and spinal reflexes are often unpredictable.
3. The neuromuscular system is highly coupled; each joint is actuated by at least two muscle groups (flexor and extensor muscles). Moreover, some muscles are biarticular (span two joints).
4. There is a significant time delay between stimulation and the onset of muscle contraction, this delay is about (10–50ms) depending on the muscle being stimulated, stimulation parameters and hardware [36].
5. There are also some technical difficulties involved with the improvement of the existing FES systems. Efforts to improve a simple existing FES system by adding more stimulation channels, multiple sensors, multiple electrodes, and other interfacing parts have resulted in more difficulties in handling and testing, in addition to the higher failure rate of such a complex FES system [67].

Open-loop and finite-state control systems are used in most FES systems available outside of research laboratories. Examples of commercially available open-loop controlled FES systems include:

- The H200 (BIONESS, Inc.) and the Free Hand system (Neurocontrol Corporation) where both can be used for the restoration of hand function.
- The Compex Motion stimulator (Compex SA) which can be used for a wide range of transcutaneous FES applications.
- The ParaStep system (Sigmedics, Inc.) which can be used in standing and ambulation for short distances.

Finite-state FES systems perform a predetermined stimulation sequence in an open-loop manner. Examples of commercially available finite-state controlled FES systems used to correct foot drop include:

- The WalkAide foot drop stimulator (NeuroMotion, Inc.).
- The Odstock dropped foot stimulator (Salisbury FES).
- The L300 (BIONESS, Inc.).

Finite-state control systems do not correct for model errors or disturbance and therefore they cannot be considered as closed-loop systems, even if they have feedback to monitor the condition of interest and hence the need for closed-loop control.

Closed-loop control systems

A few closed-loop FES cycling systems are commercially available, including the RT300 (Restorative Therapies, Inc.) and the Ergys2 (Therapeutic Alliances, Inc.). These devices use closed-loop control to keep the cycling cadence constant, as the muscle begins to fatigue, by increasing the stimulation intensity. However, the control challenges presented by other, more complex FES applications require more sophisticated real-time control of stimulation intensity (pulse width/amplitude) in addition to closed-loop compensation for external and internal disturbances.

2.3.4. Summary

The response of electrically stimulated muscle is nonlinear, time varying, coupled, and often accompanied by unpredictable disturbances. Only relatively, few patients have been assisted with FES products despite the fact that FES has been in existence for five decades [68]. This is due in part to many FES control challenges including the non-linear response of the paralysed muscle, muscle fatigue, muscle spasticity, spinal reflexes, muscle wasting, and FES system time delays.

2.4. Muscle models

In this section, different schools of thought within muscle modelling are introduced, followed by an overview of basic Hill-type model. An overview of key models used in FES is included, and the limitations with these models are highlighted. A discussion on how muscle models can assist in the development of FES systems is provided at the end.

2.4.1. Introduction to muscle modelling

Realistic models of neuro-musculoskeletal systems can provide a safe and convenient environment for the design and evaluation of controllers for FES prior to clinical trials. Accurate models would significantly enhance and accelerate the design and evaluation of closed-loop FES controllers [1, 67, 69, 70, 71]. The performance of an FES controller should also improve with improvements to muscle model accuracy [3, 6, 72, 73, 74, 75, 76, 77, 78, 79, 80].

Many models have been proposed in the literature to predict muscle force, these models vary in complexity level, ranging from simple models (e.g. the model proposed by Herzog [18]) to complex models which incorporate the effects of additional biophysical and mechanical variables (e.g. the complex set of models proposed by Brown [81, 82, 83, 84]).

Skeletal muscles are made up of two basic elements; electrically excitable contractile muscle fibres (active element), and passive connective tissue and tendon (passive viscoelastic element). The tendon attaches the muscle across joints, while the connective tissue coverings protect muscle fibres and also provide pathways for the passage of nerves and blood vessels. Force production of skeletal muscles is a result both of the active contraction of the muscle fibres and forces resulting from the velocity and length of the (passive) connective tissue and tendon, often modelled as spring/damper systems.

There are three schools of thought within muscle modelling. As described in the previous section, the first school directly model the biophysical and biochemical processes of cross bridge activity in muscle contraction. The origin of these models is usually referred to A. F. Huxley [16]. The processes within a single muscle fibre are modelled with the aim to describe muscle characteristics at a microscopic level. This requires identification of parameters at the level of muscle fibres, which are difficult to estimate, and their use in simulation would

involve solving a large number of partial differential equations. Partial differential equations are considerably more computationally intensive to solve than ordinary differential equations and hence are not well suited for use in FES feedback control systems.

The second school uses models from systems theory (black-box models) where force is related to stimulation pattern by a purely empirically-derived mathematical function. In such an approach, an appropriate mathematical function that best describes the relationship between measured input-output data is determined [78, 85, 86, 87, 88]. Other approaches in this school include the use of fuzzy models [89, 90, 91, 92, 93], and Adaptive Neuro-Fuzzy Inference System (ANFIS) models [94, 95, 96] to represent the passive and active muscle properties. This school of modelling makes no contribution to the understanding of the modelled system.

The third school follows phenomenological models first suggested by A. V. Hill [97]. The original so-called Hill model proposed that skeletal muscle can be represented as a "two-component system, consisting of an un-damped, purely elastic element in series with a contractile element" [97]. Whilst the microscopic mechanisms of muscle contraction are not modelled, these macroscopic models are able to represent many of the observed properties of muscle behaviour to a reasonable degree [98]. Further, the mechanical input-output behaviour of the model can be described using a small number of parameters in simple algebraic and ordinary differential equations. This makes the model computationally efficient in comparison with microscopic models and hence potentially suitable for FES control applications. As discussed below, there are several versions of Hill-type model in the literature. All assume that during the inactive state, the contractile element *CE* cannot sustain any force, and its length can be adjusted at will.

2.4.2. Alternative Hill-type models

Different structures of Hill model are reported in the literature. For example, the original Hill model consists of a *CE* in series with an *SE*. An extensive review of various modelling approaches can be found in [75, 99].

The most common form of the Hill model is the three-element model with parallel elements connected in parallel either with *CE* only [100, 101] or with *CE* and *SE* [18, 98, 102], shown in Figure 2.11. These two forms have been examined by many researchers [103, 104, 105,

106], and most of them (all except [104]) concluded that both forms are simplified representations of the complex biological muscle structure, but that form (a) was more accurate since *PE* represents the passive force of the muscle belly only (not the whole musculotendon complex) and hence should be parallel on *CE* only. The other study [104] concluded that both forms are similar.

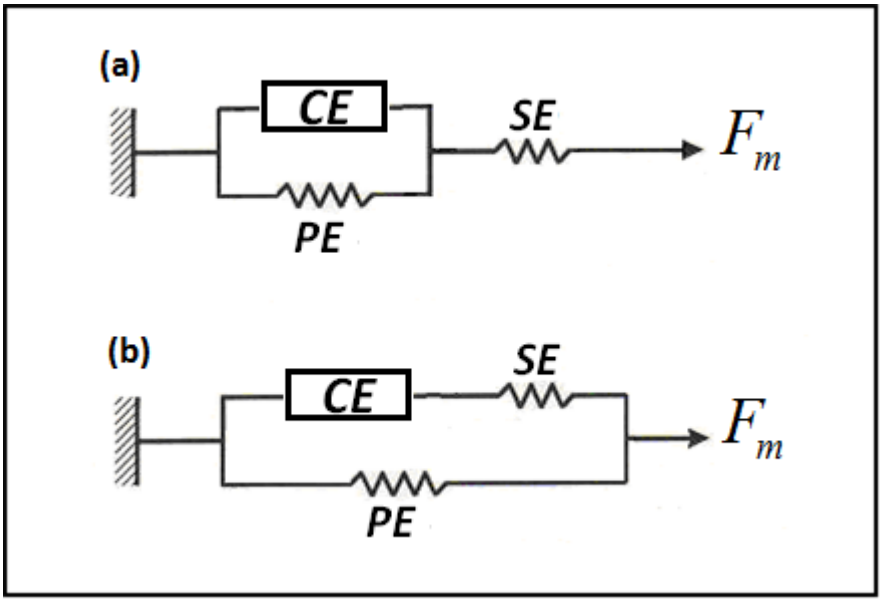

Figure 2.11: The two most common forms of Hill-type models used in the literature. The parallel element *PE* can be parallel on *CE* only or both *CE* and the series element *SE*.

However, the topology of form (b) is easier for parameter identification and more preferable for the following reasons:

- In the shortening range, if the muscle is recruited at the unique resting state (inactive, force-free), F_m is initially zero and thus the value of *PE* can be directly obtained for both forms. To obtain the value of *PE* in the other case when the muscle is not recruited ($F_m = 0$), if the muscle is stretched to a given displacement Δl_{mt}, F_m will be the same for both forms. But for form (a) *SE* and *PE* are in series, therefore as the muscle is stretched both *SE* and *PE* will be stretched, *PE* extension equals Δl_{CE} rather than Δl_{mt} and the measured force due to passive stretch results from extension of both spring elements. In form (b), *CE* and *PE* are in series and the force across *SE* is also zero, thus as the muscle is stretched, the measured force is only that due to *PE*.

- The parallel element *PE* in form (b) gives a good representation of the passive force of the musculotendon complex which results from connective tissue infrastructure including the musculotendon sheath, the muscle fibre membranes, and the overall fluid environment within which muscle tissue lives. There are also other passive elements that cross joints in parallel to the muscle; these passive elements can be lumped together mathematically. The experimental data that is available for the human system is usually for lumped passive joint properties, which makes form (b) more preferable.

For linear passive elements, the two forms (a) and (b) behave in a similar way and can replace each other using simple mathematical equation developed and proved by Fung [107]. For non-linear passive elements form (a) is more accurate as discussed earlier. For the reasons described above, the form (b) was chosen for the rest of thesis.

2.4.3. Overview of key models used in FES control

Various mathematical muscle models have been developed for FES control studies. These models vary in complexity and accuracy. Models of electrically stimulated muscles have been developed based on black-box approach [86, 108], Hill model [109, 110, 111, 112], Hill-based physiological model (Hill model combined with physiological processes underlying excitation and activation of human muscles) [72, 73, 74, 113], Huxley model [114, 115], or a combination of Hill-type and Huxley-type models [116, 117, 118].

Hill-based physiological models can be described as Hill-type models modified by incorporating some of the muscle's physiological properties into the basic Hill model, and thus improving the model behaviour, while preserving its simple structure. This type of model calculates the active muscle force as the product of three independent experimentally measured relationships, namely the force-length relationship, the force-velocity relationship and the recruitment (and/or activation) dynamics. These models assume that the muscle recruitment (and/or activation) and muscle contraction dynamics are uncoupled, see Figure 2.12 (b).

To the author's knowledge, the model by Riener (referred to from this point forward as the Riener-1 model) is the most complex of this type of models that have been used in FES

control studies. Other similar models [74, 113] are less complex and hence they account for fewer muscle properties. An overview of Riener-1 model is presented below.

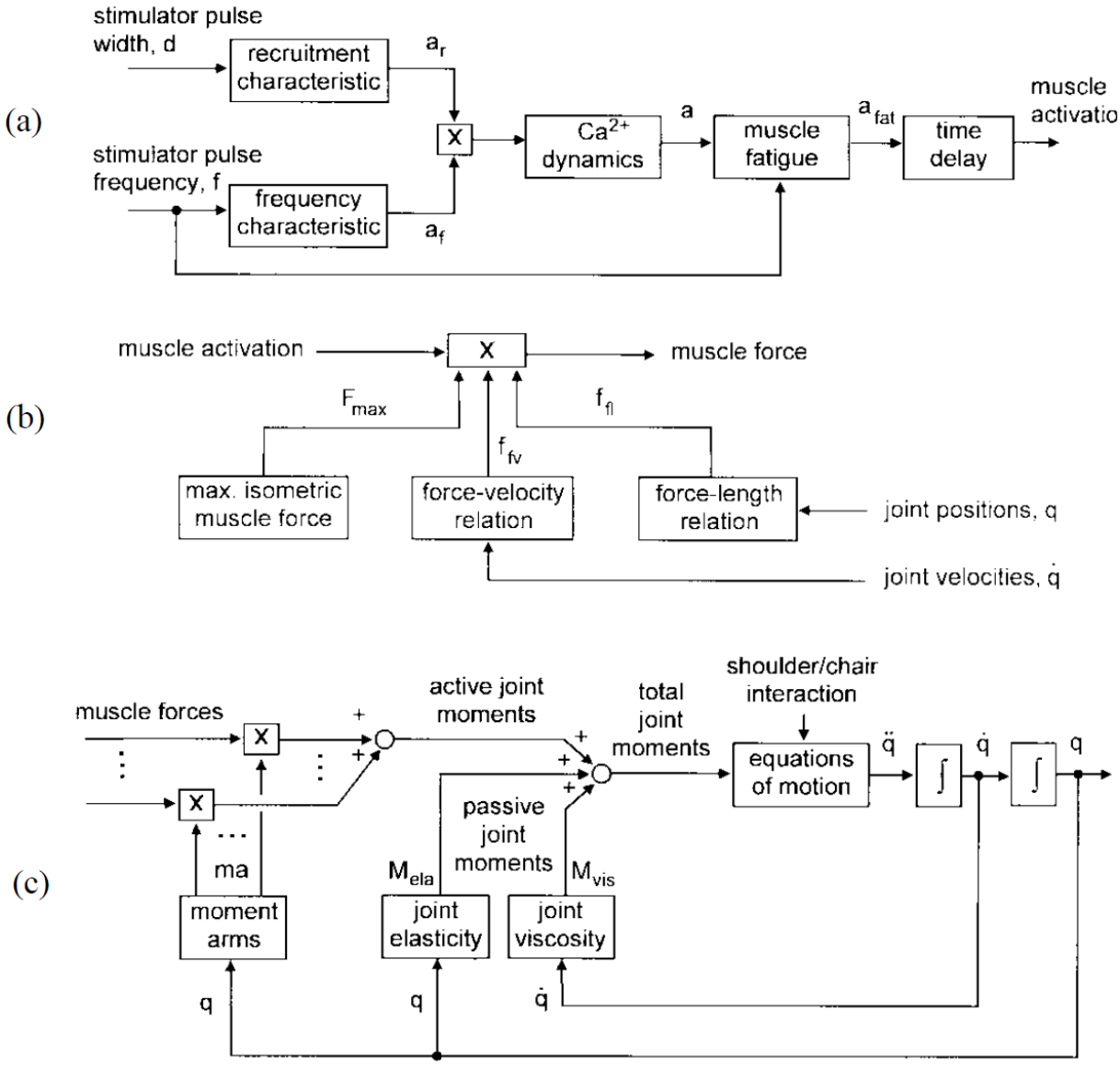

Figure 2.12: Riener-1 model: (a) activation dynamics, (b) contraction dynamics, and (c) body-segmental dynamics. (From [72]).

The Riener-1 model [72] describes the dynamics of the joint in response to electrically stimulated muscle contractions. As shown in Figure 2.12, the model comprises three parts; activation dynamics, contraction dynamics and body segmental dynamics. Activation dynamics are modelled as function of stimulation pulse width and frequency. Active muscle force is computed as the product of force- length relationship, force-velocity relationship and muscle activation (Hill-based). Passive muscle properties (viscous and elastic) are separated

from all muscles which span the joint and assigned to the joint (the tendon is assumed rigid, i.e. not modelled). Riener-1 model is based on experimentally obtained data which makes the identification process required to tune the model for a particular subject time consuming.

The Riener-1 model has been used by many researchers to develop control strategies for different FES systems [55, 72, 119, 120, 121, 122, 123, 124, 125, 126]. The main practical limitation of this model is the time-consuming identification process required to tune the model parameters for each particular subject.

Limitations with the Riener-1 and other models used in FES control

As will be explained in further detail in subsequent chapters, the Riener-1 model, in common with almost all other muscle models used in FES control, has two major limitations.

In closed loop FES control applications the number of activated motor-units in a given muscle will usually vary with time, as stimulation intensity increases, or decreases. As discussed in subsequent sections, the length of the *CE* associated with a given motor unit when initially recruited is believed to influence the total muscle force via the muscle's F-L relationship. As recruitment and muscle length may both vary continuously, the length of different *CE*'s at recruitment, will also vary. The Riener-1 model, in common with most previous work [1, 72, 74, 109, 113], represents the entire muscle's *CE* length as a single (instantaneous) *CE* length and hence a single length. Further, as discussed above, muscles contain different types of motor-units, which vary in their properties. This suggests that every single motor-unit should be modelled separately for the purposes of calculating the effect of the length at initial recruitment, fatigue, and other physiological properties specific to each fibre-type (i.e. recruitment order, F-L relationship, F-V relationship and fatigue). This argument is further developed at the end of this chapter.

Another physiological model was developed by Riener [73] (Riener-2 model) using the multiple motor-unit modelling approach. However, in this model the muscle length is assumed constant and the model can only be used under isometric conditions (not for dynamic conditions), which limits its use to FES isometric contractions only.

2.5. Review of key features of muscle models

Skeletal muscles have various complex properties; these properties are modelled separately in the literature with different modelling approaches and at different levels of complexity. This section reviews the models of the various muscle properties which affect muscle response to FES. These properties are: recruitment of motor-units, muscle's active force-length relationship, muscle's active force-velocity relationship, muscle fatigue, force enhancement following active stretch and force depression following active shortening, and finally the passive behaviour of the musculotendon complex.

Alternative sub-models were collected from muscle models available in the literature for electrically stimulated as well as naturally contracted muscles. When using models of natural voluntary contraction for FES control, two important points have been considered. Firstly, stimulation frequency is assumed constant during FES, and secondly, the non-physiological recruitment order during FES. Models of voluntary contracted muscles have to be modified accordingly before using them in FES control.

The muscle models produced by Brown and colleagues [41, 82, 84, 127, 128] were developed for naturally recruited muscles, and despite the high level of complexity some important properties are not included in the models (e.g. fatigue and force enhancement & depression). In the following section, the activation sub-model developed by Brown has been greatly simplified by assuming constant frequency and hence reducing a lot of un-necessary complexity in muscle models for FES control (for further detail, see Chapter 6).

2.5.1. Recruitment sub-models

The two terms, muscle activation and muscle recruitment are often poorly defined, or inaccurately used, in the literature, e.g. as in [18, 41, 82, 129, 130]. Sometimes both terms are used to describe the same characteristic, e.g. [18, 73], and sometimes they are different, e.g. [72, 81, 82, 83, 84, 113]. Sometimes a paper or a book refers to activation, when the term recruitment should be used (and vice versa).

In this study, the recruitment level R is defined as the normalized portion of recruited motor-units. R is the analogue recruitment of the muscle as a whole, R has the value between 0 (no recruitment) and 1 (all motor-units are recruited), $0 \le R \le 1$. The binary recruitment R_j represents the recruitment level of the motor-unit (of index j), which can only be either 0 or 1

(100% recruited or not recruited at all). Muscle activation A (also unit-less, $0 \le A \le 1$) is defined as the relationship between muscle force on one side, and on the other side: stimulation frequency, rise and fall times (effects of calcium dynamics), time delay, yield, sag, and effective length. Muscle activation will only be maximum ($A = 1$) in certain conditions, specifically stimulation at tetanic frequency (the frequency at which muscle force is maximum, and prevents yield), isometric conditions and when sufficient time has elapsed since onset of stimulation (to pass the rise time, effect of sag, and natural time delay). Effects of muscle activation on muscle force are discussed in Appendix 1.

The real mechanism of motor-units recruitment is complex and difficult to measure. Modelling approaches of this muscle property vary in complexity; hence different alternative sub-models are reported in the literature. However, most of them use piecewise linear function, the number of fibre types varies from one to three, and the number of motor-units varies from one to a thousand.

2.5.1.1. Summary of empirical data for recruitment behaviour

Comprehensive and accurate experimental data on recruitment are not available. For example, accurate values for muscle parameters such as the force produced by cross-sectional area of each fibre-type, size of each fibre-type, and number of fibres attached to each motor-units, etc., are not available in the literature. Accurate values for such parameters are required to get an accurate recruitment sub-model (i.e. the relationship between PW and recruitment of motor-units). Rather, experimental methods used to estimate the recruitment curve measure the relationship between PW and whole muscle isometric force. The isometric muscle force is used as indication of the normalised portion (or level) of recruited motor-units. Taking into account the large number of motor-units in a muscle, especially large muscles, this approximation is expected to have little effect on the accuracy of the recruitment sub-model.

Pulse amplitude and pulse width have an equivalent effect [3, 55], an increase in either (or both) will lead to an increase in the number of recruited motor-units and hence force, until all motor-units are recruited ($R = 1$). The general shape of the recruitment curve observed experimentally is similar to the curve shown in Figure 2.13. No response is observed ($R = 0$) until the threshold level is reached (about 15 [μ.sec]). On the other end of the curve, increasing PW beyond saturation level does not increase the force response ($R = 1$), maximum

force was obtained at about PW = 100 [μ.sec]. Muscle force can be adjusted from threshold to maximal ($R = 1$) by changing the pulse amplitude from 15 to 100 [μ.sec].

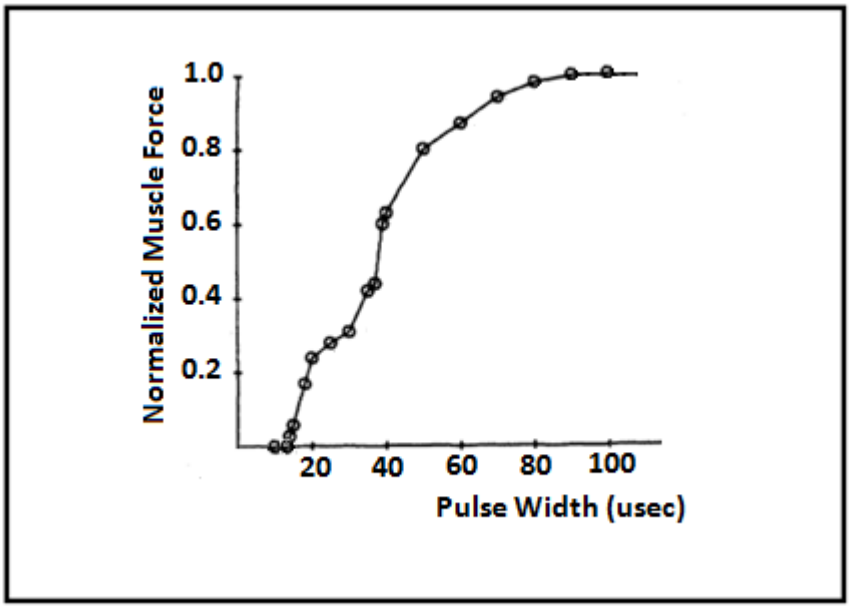

Figure 2.13: Effect of pulse width PW on recruitment of muscle fibres. The recruitment curve resulted by PW range of ($0-100\mu$.sec) at constant pulse amplitude ($PA = 2.7mA$) and constant stimulation frequency. (Adapted from [54].

Durfee et al [131] experimentally tested three different methods for estimating isometric recruitment curves of electrically stimulated muscles. The results of this study was that estimation of recruitment curves depends on the method used, and also that all tested methods are sensitive to short-term and long-term variations in muscle properties (e.g. recruitment history and fatigue).

Crago et al [54] reported the recruitment curves to be dependent on muscle length, but Levy et al [48] suggested the recruitment curve is independent of muscle length.

The recruitment curves for individual fibre types during FES are believed to be similar to the curves shown in Figure 2.14, assuming that motor axon adjacent to the surface electrodes are recruited first, and also that largest diameter and most fatigable motoneurons (type-IIb) are recruited first. This recruitment order was reported in [1, 46, 48, 72, 73] when using surface electrodes, i.e. type-IIb first, then type-IIa, and type-I last. Recruitment sequence is different with nerve-implanted electrodes.

The input to the recruitment sub-model is the artificial electrical stimulation level (PW / PA), and the output is the recruitment level R. Adjusting PW will change the number of recruited motor-units.

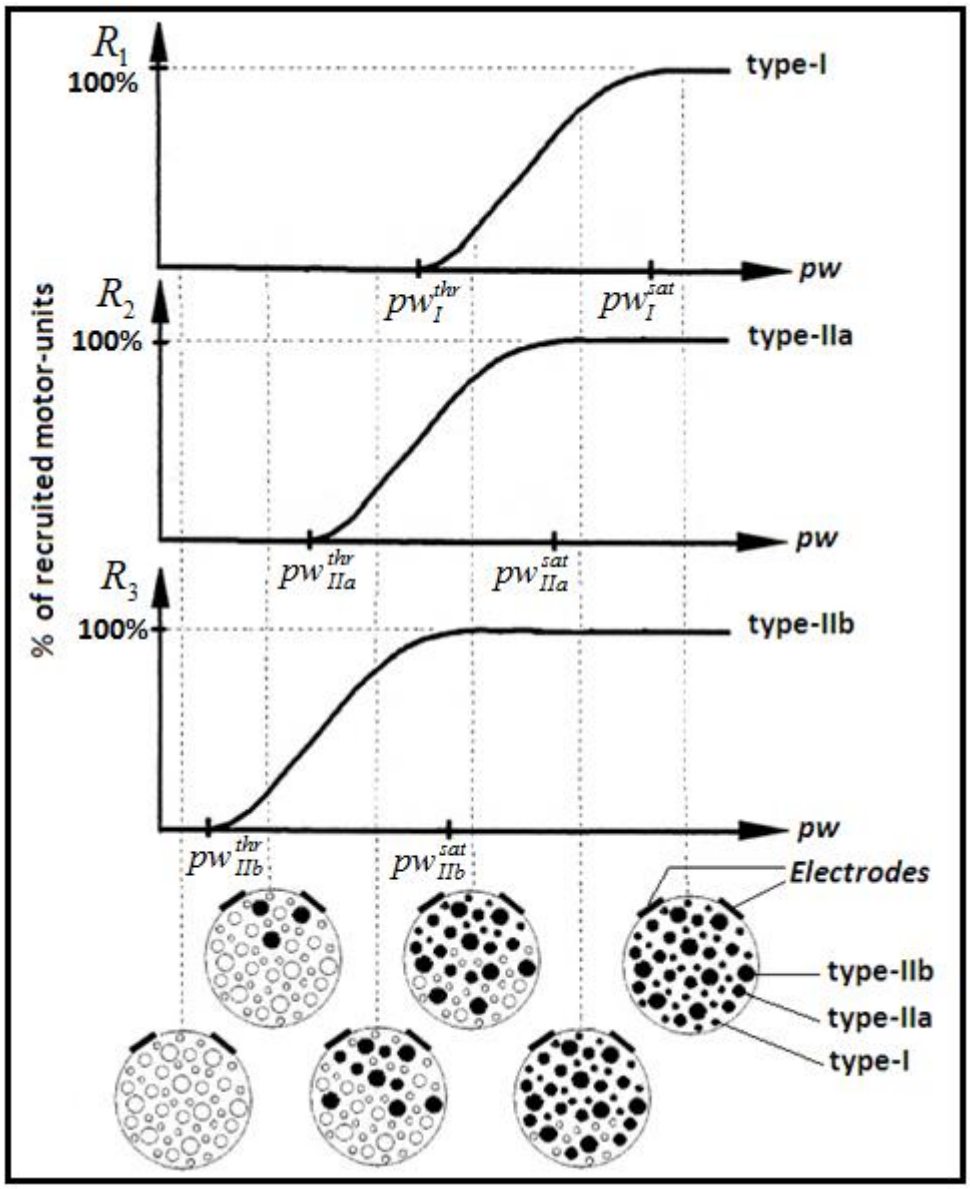

Figure 2.14: Typical non-linear and overlapping recruitment curves of different fibre types during FES. (Adapted from [119]).

2.5.1.2. Summary of key recruitment sub-models

Recruitment modelling approaches available in the literature can be classified into two main types; analogue recruitment (can be linear or non-linear), and analogue recruitment with

binary extension. Using this classification; different alternative recruitment sub-models are summarised below.

2.5.1.2.1. Analogue recruitment

Analogue recruitment can be linear or non-linear and with single or multi fibre-type.

i) Schauer recruitment sub-model

The recruitment curve of Schauer recruitment sub-model [113] is described by a piecewise linear function as follows:

$$R = \begin{cases} 0 & , \quad pw < pw_{thr} \\ \dfrac{pw - pw_{thr}}{pw_{sat} - pw_{thr}} & , \quad pw_{thr} \le pw \le pw_{sat} \\ 1 & , \quad pw > pw_{sat} \end{cases} \tag{2.1}$$

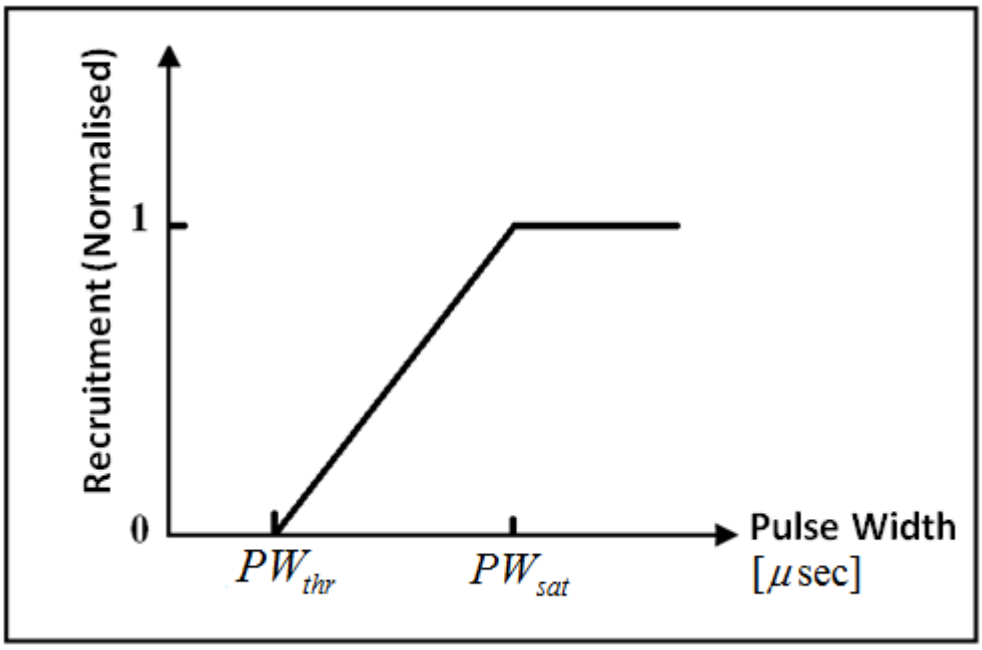

Figure 2.15: Linear recruitment curve. A piecewise linear function describes the recruitment curve of Schauer sub-model. (From [113]).

ii) Riener-1 recruitment sub-model

In Riener-1 recruitment sub-model [72], the muscle is treated as single motor-unit, and single fibre-type is assumed. The recruitment curve is similar to that shown earlier in Figure 2.14.

The normalized portion of recruited motor-units R, ($0 \le R \le 1$) is calculated as a function of pulse width *PW*.

$$R = c_1\{(pw - pw_{thr})\arctan[c_{thr}(pw - pw_{thr})] - (pw - pw_{sat})\arctan[c_{sat}(pw - pw_{sat})]\} + c_2 \quad (2.2)$$

c_1, c_2, c_{thr}, c_{sat}: are constants.

iii) Brown recruitment sub-model

This recruitment sub-model was proposed by Brown in his PhD thesis [41]. The muscle is divided into a number of slow-twitch and fast-twitch units; all units have the same *PCSA*. Total number of units is specified by the user (more units will increase model accuracy). Recruitment of motor-units is illustrated in Figure 2.16. Recruitment R_i and stimulation frequency $freq_i$ are modelled as functions of the natural stimulation input U. This sub-model follows the physiological recruitment order (slow units first).

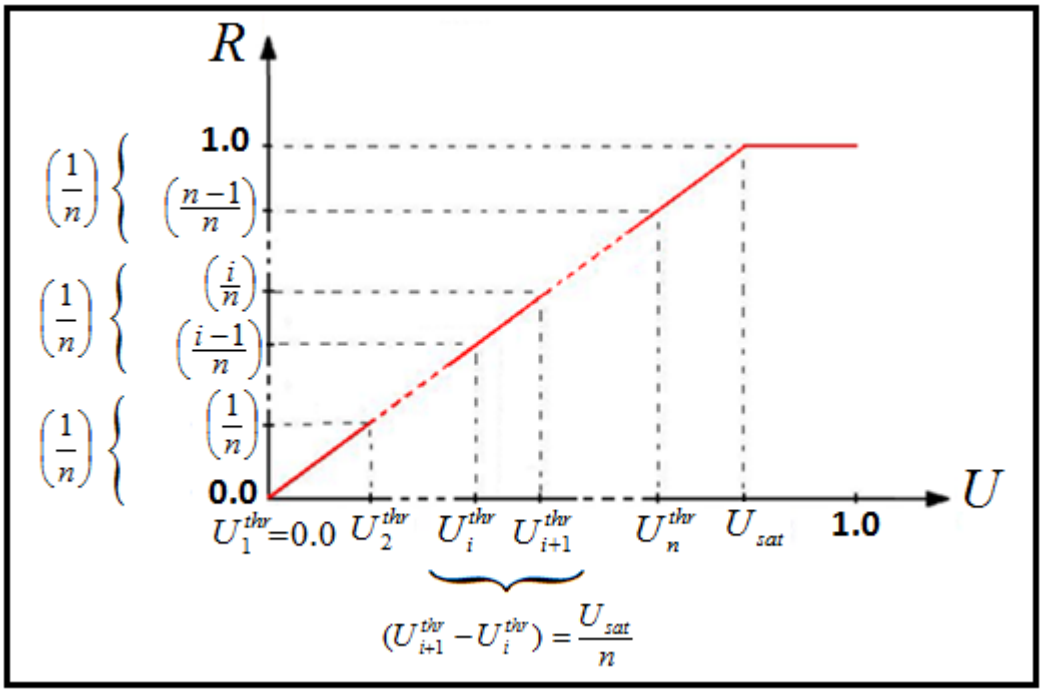

Figure 2.16: Brown recruitment sub-model. (Adapted from [41])

iv) The "natural continuous" recruitment sub-model of (VM 4.0)

This recruitment sub-model is used in the third alternative muscle model of (VM 4.0) [128], and was called "natural continuous" in [128]. This sub-model is similar to the original Brown

recruitment sub-model, but with single unit for each fibre-type (i.e. simplified version of Brown recruitment sub-model). Recruitment R_i and stimulation frequency $freq_i$ are modelled as functions of the natural stimulation input U. This sub-model follows the physiological recruitment order (slow units first).

v) The "intramuscular FES" recruitment sub-model of (VM 4.0)

This recruitment sub-model is used in the fourth alternative muscle model of (VM 4.0) [128]. This sub-model is similar to the "natural continuous" sub-model (in VM 4.0) with two differences; stimulation frequency is constant (because of its application to FES) and all motor-units have the same threshold and saturation levels. This model includes two types of motor-units (fast and slow response), both of which are recruited in a random sequence, based on the experimental results obtained by Singh et al [50].

vi) Hawkins recruitment sub-model

Hawkins model [101, 129, 130] was developed for voluntary contraction initiated by the CNS, the input is the natural stimulation input U. Hawkins assumed constant stimulation frequency (near to natural maximum frequency) for all model units and for any input. Three units are used, one unit for each fibre-type. The threshold level U_i^{th} and the normalized recruited proportion $(0 \le R_i \le 1)$ of the i^{th} unit are illustrated in Figure 2.17 using an example of possible relationship between recruitment R and natural stimulation input U in a heterogeneous muscle.

2.5.1.2.2. Analogue recruitment with binary extension

In this approach of modelling, recruitment of motor-units is incorporated as a binary extension to the analogue recruitment.

i) Riener-2 recruitment sub-model

In Riener-2 recruitment sub-model [73], the muscle is divided into 100 motor-units of slow-twitch (type-I) and fast-twitch (Types IIb and IIa). The inverse size-order recruitment with overlap is used in this model, as shown in Figure 2.14. The analogue recruitment sub-model (used to calculate the number of recruited motor-units of each type) is the same as that of Riener-1 model (equation 2.2) with different threshold and saturation levels for different fibre types ($i = 1,2$). Each motor-unit (of the one hundred) is either recruited or not (either 0 or 1).

As soon as R_i (of fibre type-i) exceeds the threshold value related to the motor-unit j, this motor-unit is recruited.

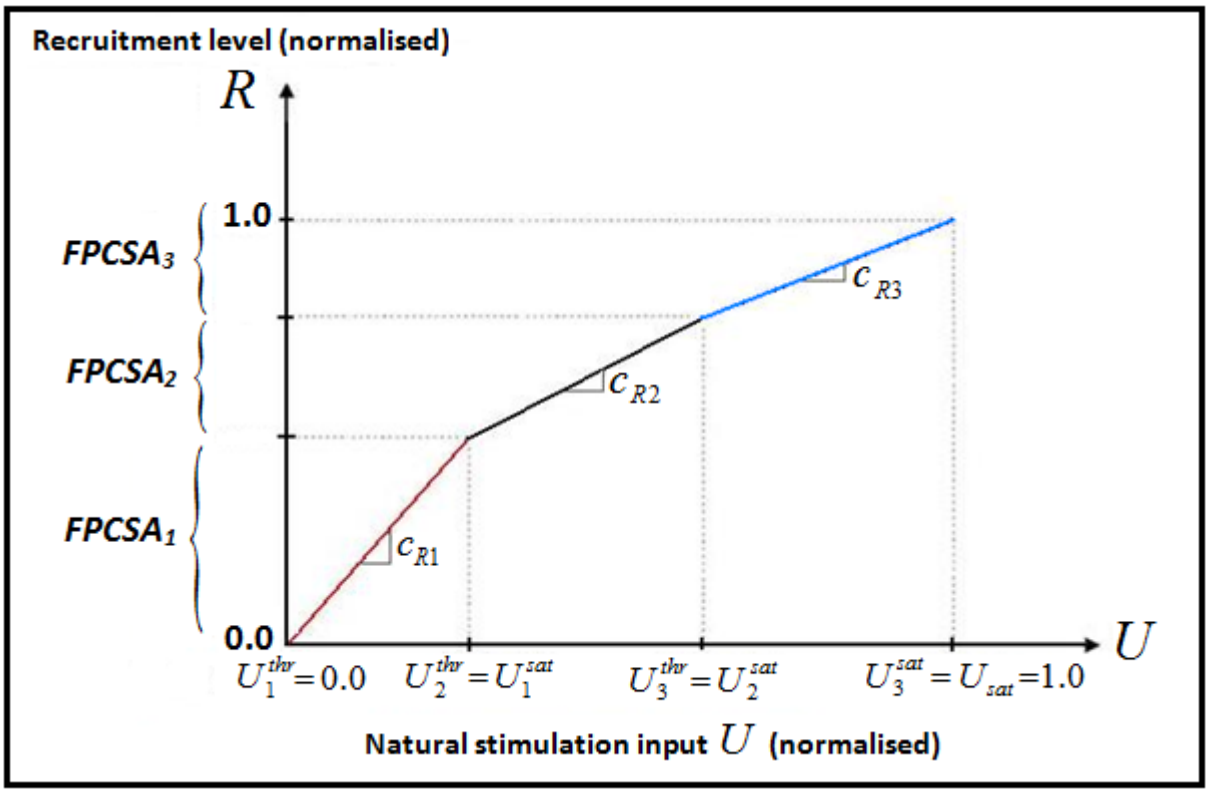

Figure 2.17: Hawkins recruitment sub-model. $(U_{i+1}^{thr} - U_i^{thr}) = \dfrac{FPCSA_i}{c_{Ri}}$, c_{Ri}: Hawkins recruitment constant for different fibre types is determined empirically. (Adapted from [101]).

$$R_{i,j} = \begin{cases} 0 & , R_i \le \left(\dfrac{j-1}{m_i}\right) \\ 1 & , R_i > \left(\dfrac{j-1}{m_i}\right) \end{cases} \qquad (2.3)$$

For fast motor-units:

$$R_{fast} = c_1\left\{(pw - pw_2^{thr})\arctan\left[c_{thr}(pw - pw_2^{thr})\right] - (pw - pw_2^{sat})\arctan\left[c_{sat}(pw - pw_2^{sat})\right]\right\} + c_2$$

$$m_2 = m \times \text{FPCSA}_2 = 100 \times \text{FPCSA}_2,\ 0 \le m_2 \le 100. \qquad (2.4)$$

Number of recruited fast motor-units = $R_2 \times m_2$

For slow motor-units:

$$R_{slow} = c_1\left\{(pw - pw_1^{thr})\arctan\left[c_{thr}(pw - pw_1^{thr})\right] - (pw - pw_1^{sat})\arctan\left[c_{sat}(pw - pw_1^{sat})\right]\right\} + c_2$$

$$m_1 = m \times \text{FPCSA}_1 = 100 \times \text{FPCSA}_1,\ 0 \le m_1 \le 100. \quad (2.5)$$

Number of recruited slow motor-units = $R_1 \times m_1$

ii) The "natural discrete recruitment algorithm" recruitment sub-model

This recruitment sub-model is used in (VM 3.0) [127] and also in the first and second alternative muscle models of (VM 4.0) [128]. It was called "natural discrete recruitment algorithm" in [128]. This sub-model is a modified version of the Brown recruitment sub-model with the addition of binary recruitment of motor-units (0 or 1), see Figure 2.18.The number of recruited units depends on the value of the natural stimulation input U ; all units will be recruited when natural stimulation input reaches U_{sat} (value of U_{sat} can be specified by the user). The user is allowed to modify the complexity of this sub-model including fibre types, and number of units. Although the addition of more units will increase model accuracy it will increase also the computational time [127]. Recruitment R_i and stimulation frequency $freq_i$ are modelled as functions of the natural stimulation input U . This sub-model follows the physiological recruitment order (slow units first).

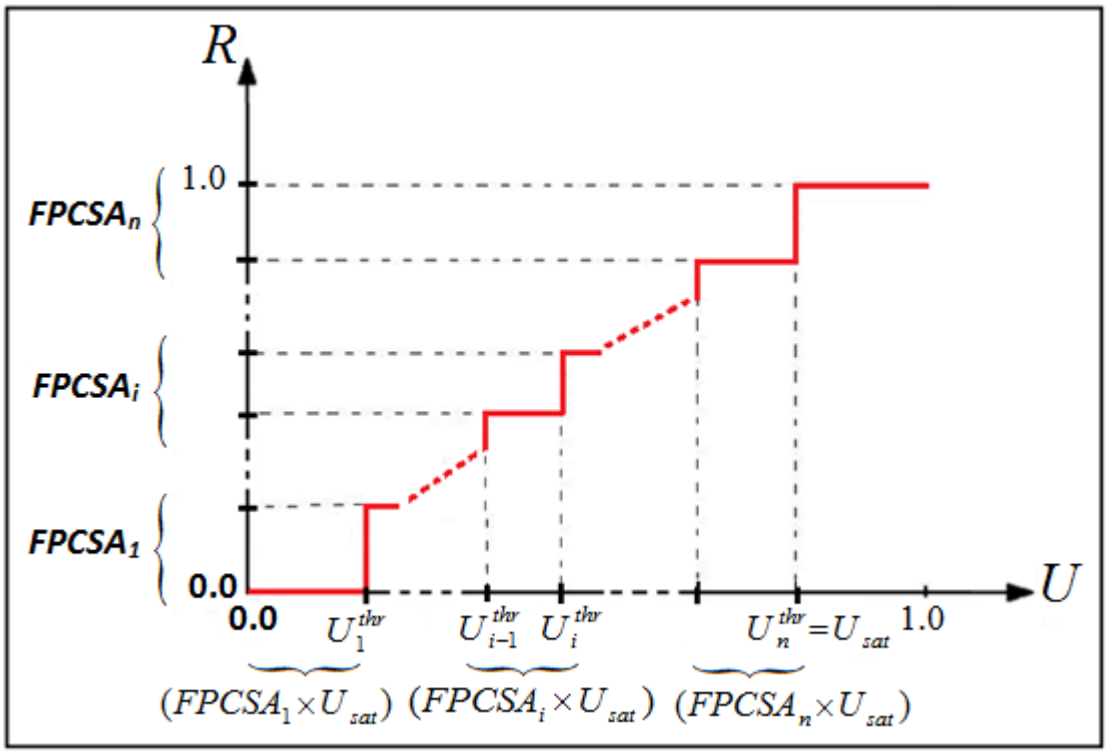

Figure 2.18: The recruitment sub-model used in the first version of Virtual Muscle (VM 3.*), also in the first and second alternative muscle models of (VM 4.0). (Adapted from [127, 128])

2.5.1.3. Implications of the application of recruitment sub-models on the single motor-unit model

A muscle consists of large number of motor-units and different fibre types which have different contractile properties. If a single motor-unit model is used, different contractile properties of the different fibre types cannot be incorporated into the muscle model. Moreover, in a realistic scenario R and l_{CE} are changing continuously during FES, the single motor-unit model cannot account for the effect of continuously varying R (i.e. length history-dependence and fatigue history-dependence of different motor-units). As described elsewhere in the thesis, a new comprehensive multiple motor-unit model has been developed to address these limitations. The multiple motor-unit model properly accounts for this realistic scenario and different contractile properties of the different fibre types since each motor-unit is modelled separately. As part of this research work, a new recruitment sub-model was developed during this research. This sub-model has one thousand motor-units and three different fibre types. Details are provided in Chapter 6.

2.5.2. F-L sub-models

The F-L relationship is estimated experimentally by using either separate fibres/motor-units or entire muscles. It is generally accepted that the active F-L curve of a single fibre consists of a steep ascending limb followed by a plateau and then a less steep descending limb [132].

2.5.2.1. Summary of empirical data for F-L relationship

Muscle models available in the literature, usually incorporate one generic curve of the force-length relationship for any muscle, fibre or motor-unit. However, the transformation of fibre F-L relationship to muscle F-L relationship is determined by muscle geometry [133]. Muscle architecture and fibre orientations can vary widely in different muscles. Muscle architecture has large effect on the shape of the F-L curve; Figure 2.19 shows the experimental F-L curves for nine different muscles of different architecture. These data were collected from nine different skeletal muscles, the muscles are: Tibialis Anterior (TA), Peroneus Brevis (PB), Peroneus Longus (PL), Extensor Digitorum Longus (EDL), Soleus (SOL), Tibialis Posterior (TP), Medial Gastrocnemius (MG), Lateral Gastrocnemius (LG) and Flexor Digitorum Longus (FDL).

Both the muscle force and optimal length are dependent on stimulation frequency $freq$, recruitment level R, and fibre-type. The force-length relationship is usually estimated experimentally at constant stimulation frequency and fully recruited muscles ($R = 1$), and then the empirical data is used to develop a simplified F-L sub-model. F-L relationships at different stimulation frequencies are shown in Figure 2.20. Force traces are shown to illustrate the effect of stimulation frequency on isometric force at different lengths (of muscle belly).

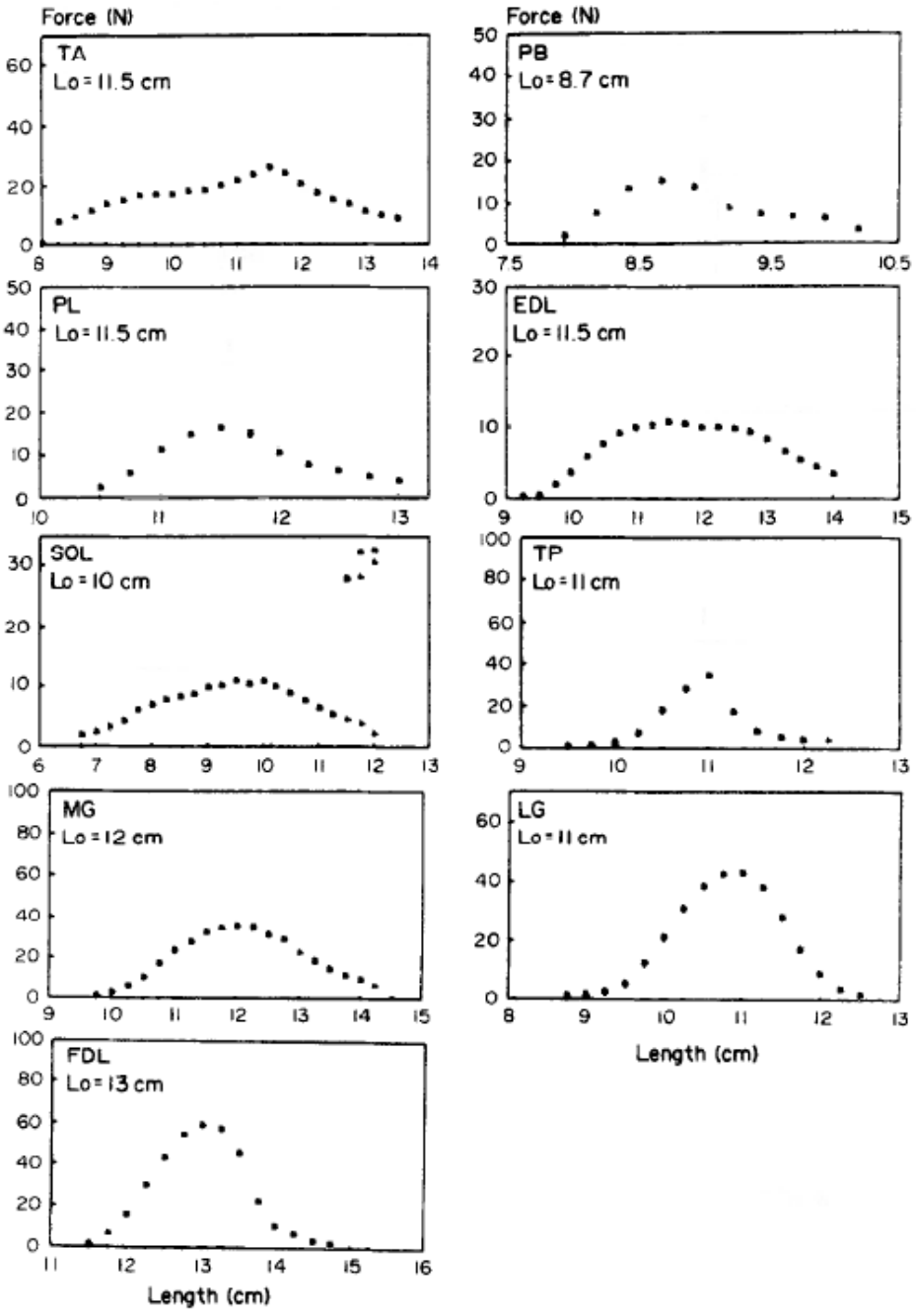

Figure 2.19: The F-L relationships for different skeletal muscles (in the hind-limb of the cat). (Adapted from [132]).

Constant stimulation frequency is assumed during FES. Therefore, the input to the force-length relationship (FL) is the length of either muscle fibres/motor-units or muscle belly (depending on the sub-model used), and the output is the normalised force of either the fibres/motor-units or the whole muscle.

Most models in the literature use the instantaneous *CE* length l_{CE} as input to the force-length relationship. However, this does not reflect the way in which the F-L relationship of a muscle (or muscle fibre) is believed to act as the input should be length at initial recruitment, not instantaneous length. Using the instantaneous length l_{CE} for dynamic contraction results in instability on the descending limb of the force-length relationship (see Appendix 2). Experimental data and comparison between the isometric forces corresponding to l_o and l_{CE} after protocols of stretch/shortening are presented in Appendix 2.

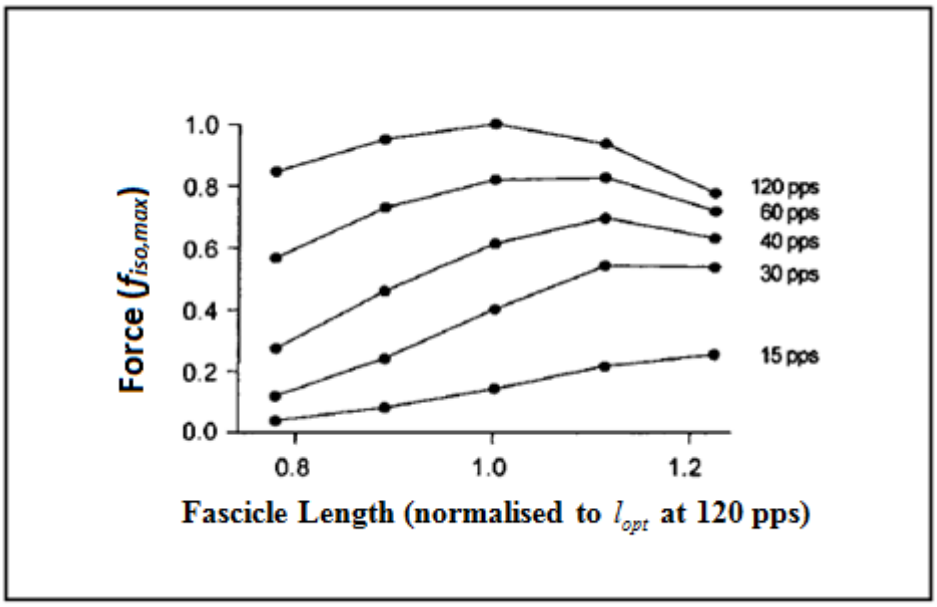

Figure 2.20: F-L relationships at different stimulation frequencies. The F-L curves measured at different stimulation frequencies are not congruent. (From [82])

2.5.2.2. Summary of key F-L sub-models

Summary of key F-L sub-models reported in the literature is provided in this section. Alternative mathematical equations are used in different muscle models to mathematically represent the empirical data of the force-length relationship at different complexity levels.

i) Otten F-L sub-model

Otten F-L sub-model [134] was incorporated into many muscle models reported in the literature, either modified, or as it is. Otten [134] suggested that the force-length relationship could be modelled by the following equation:

$$FL(l_m) = \exp\left(-\left[\frac{(\bar{l}_m)^{c_S} - 1}{c_W} \right]^{c_R} \right) \tag{2.6}$$

Constants: c_S, c_R, and c_W are used as curve shaping parameters; c_S controls curve skewness, c_R controls curve roundness, and c_W controls curve width.

Figures 2.21, 2.22 and 2.23 show the effect of c_S, c_R, and c_W (respectively) on the curve of Otten F-L sub-model. In each figure, one parameter varies and other parameters are kept constant at appropriate values in order to show clearly the effect of the varied parameter.

ii) Riener-1 F-L sub-model

In Riener-1 F-L sub-model [72], a simplified form of Otten F-L sub-model is used with ($c_S = 1$) and ($c_R = 2$), the value of c_W depends on the stimulated muscle (different muscles have different values).

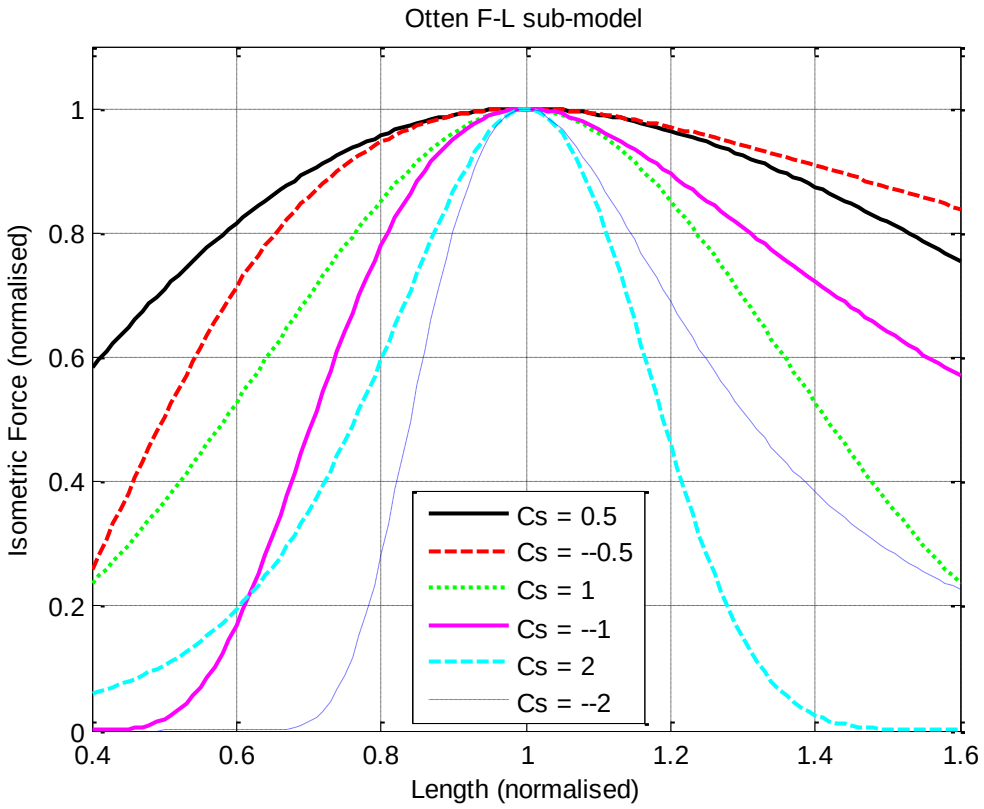

Figure 2.21: Effect of skewness parameter c_S on the curve of Otten F-L sub-model. c_S = (1, -1, 2, -2, 0.5, and -0.5), $c_R = 2$, $c_W = 0.5$. The curve is symmetrical only at: $c_S = 1$.

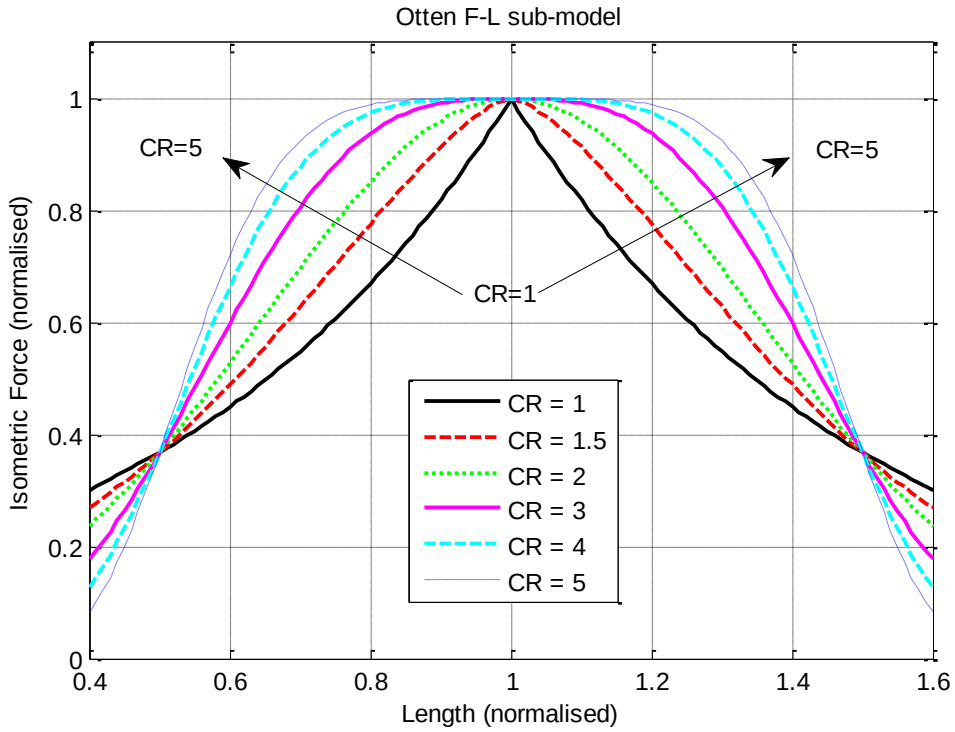

Figure 2.22: Effect of roundness parameter c_R on the curve of Otten F-L sub-model. c_R = (1, 1.5, 2, 3, 4, and 5), $c_S = 1$, $c_W = 0.5$.

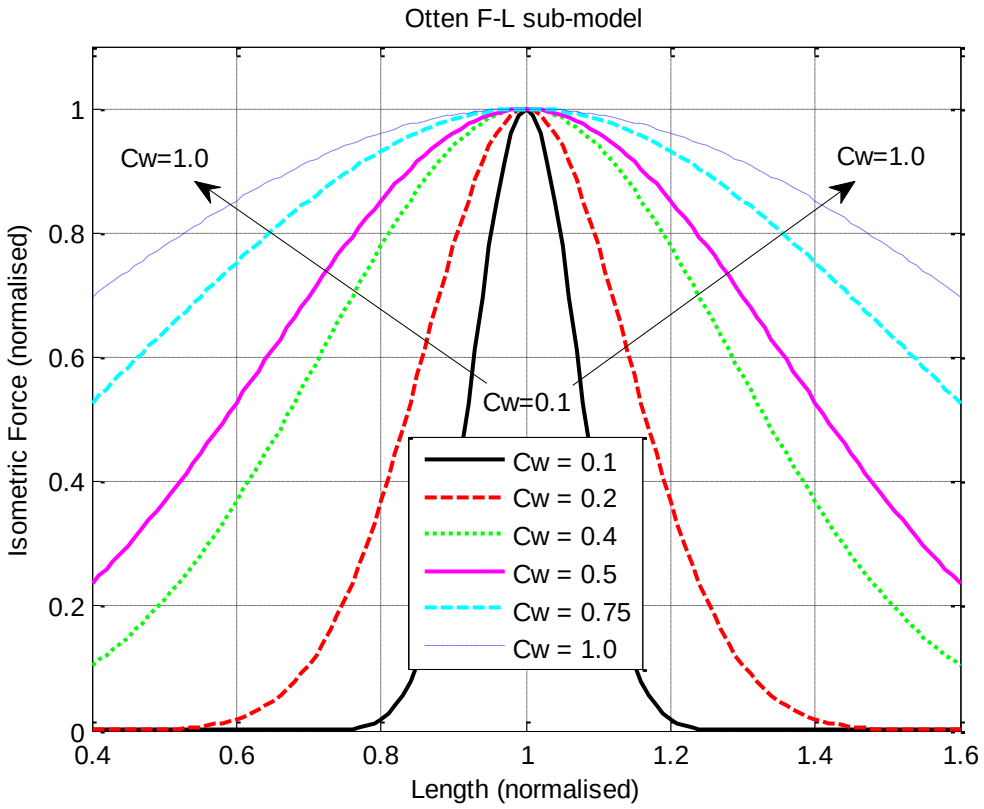

Figure 2.23: Effect of width parameter c_W on the curve of Otten F-L sub-model.

c_W = (0.1, 0.2, 0.4, 0.5, 0.75, and 1), $c_S = 1, c_R = 2$.

iii) Brown F-L sub-model

In Brown F-L sub-model [41, 82, 84, 127, 128], the same form as that of Otten F-L sub-model is used. However, if c_R was not selected as an integer, then the output of Otten equation might be a complex number with imaginary part. Therefore, Brown used the following equation:

$$FL(l_m) = \exp\left(-abs\left|\frac{(\bar{l}_m)^{c_S} - 1}{c_W}\right|^{c_R}\right) \qquad (2.7)$$

Slow-twitch and fast-twitch fibres have different force-length relationships, hence different values for equation parameters are used to model each fibre-type (l_{opt} is the same for both).

Note that, Brown F-L sub-model is for the active isometric force only, i.e. excluding f_{PE2} which resists muscle fibres compression at short *CE* lengths (less than $0.7\,l_{opt}$), f_{PE2} is

modelled separately in Brown muscle model, Brown f_{PE2} sub-model is summarised in section 2.5.6.2.

iv) Hawkins F-L sub-model

In Hawkins F-L sub-model [101, 129, 130], the length of fibres is used as the input to the F-L sub-model ($l_m = l_f \times \cos\alpha$). The normalised F-L relationship is given by:

$$FL(l_f) = \begin{cases} [-6.25(\bar{l}_f - 1)^2 + 1] & for: 0.6 \le \bar{l}_f < 1.1 \\ [-1.5625(\bar{l}_f) + 2.656] & for: 1.1 \le \bar{l}_f < 1.7 \\ 0.0 & for: 0.6 > \bar{l}_f \ge 1.7 \end{cases} \quad (2.8)$$

Fibres of different types have the same F-L relationship, all fibre in the muscle assumed to have the same length.

v) Herzog F-L sub-model

In Herzog F-L sub-model [18], the normalised isometric muscle force is approximated by the positive values of a parabola; this is given in the following equation:

$$FL(l_{CE}) = \begin{cases} c_1(\bar{l}_{CE} - 1)^2 + 1 & for \quad positve \quad values \\ 0.0 & for \quad negative \quad values \end{cases} \quad (2.9)$$

($l_{CE} = l_m$), c_1: constant.

vi) Garies et al F-L sub-model

Garies et al F-L sub-model [132] is an improved version of the original Otten F-L sub-model [134]. This sub-model was developed to model the complex F-L curves of some muscles which have complex architecture, for example when the F-L curve has more than one optimal length (e.g. the F-L curve of T.A.) or when the F-L sub-model cannot predict forces at extremes of length (F-L curve of MG), see Figure 2.19 shown earlier in this section.

Garies F-L sub-model is a "multi compartment" sub-model. The muscle is assumed to have more than one compartment and then each compartment is modelled separately. Each compartment has its own optimal length and scaled to its influence on the overall model. This sub-model is given by:

$$FL(l_m) = \sum_{i=1}^{N} c_i \times \exp\left(- abs \left| \frac{\left(\frac{\bar{l}_m}{\bar{l}_{opt,i}} \right)^{c_{S,i}} - 1}{c_{W,i}} \right|^{c_{R,i}} \right) \quad (2.10)$$

N : Number of compartments in the F-L sub-model.

c_i : Scaling factor representing the effective influence of the i^{th} compartment on the overall model.

$\bar{l}_{m,i}$: Instantaneous length of the i^{th} compartment normalised with respect to its own optimal length.

2.5.2.3. Implications of the application of F-L sub-models on the single motor-unit model

Different fibre types have different F-L relationships. If a single motor-unit model is used, only one F-L sub-model can be used. The multiple motor-unit model described in subsequent chapters is able to properly account for more than one F-L sub-model for different fibre types.

2.5.3. F-V sub-models

Hill-type muscle models use F-V sub-model similar to the original Hill equation given in [97], where muscle force decreases with increasing shortening velocity and increases with increasing stretch velocity. Hill [97] proposed a force velocity relationship for shortening muscle at optimal length using a part of rectangular hyperbola. A typical F-V curve of skeletal muscle is shown in Figure 2.24. The original Hill's force-velocity equation is given by:

$$(f_{CE} + a) \times (v_{CE} + b) = (f_{iso,\max} + a) \times b \quad (2.11)$$

a and b are constants with units of force and velocity respectively.

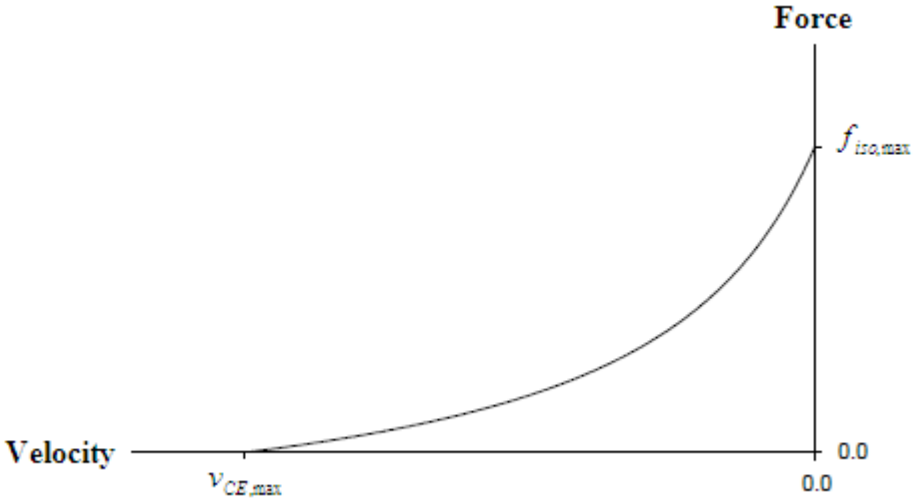

Figure 2.24: Relationship between muscle force and shortening velocity. Muscle force decreases as muscle shortening velocity increases.

2.5.3.1. Summary of empirical data for F-V relationship

The force-velocity relationship is mainly affected by velocity of muscle fibres, but it is also affected by fibre-type, muscle architecture (optimal length and pennation angle), recruitment level, recruitment order (physiological or non-physiological), "instantaneous" fibre length and stimulation frequency.

Recruitment order and recruitment level affect the F-V relationship in muscles composed of different fibre types (heterogeneous muscles). During non-physiological sequence, slow motor-units will be recruited first and hence at partial recruitment all or part of recruited motor-units is of the slow-type which have a lower maximum shortening velocity. During non-physiological sequence, fast motor-units will be recruited first and hence at partial recruitment all or part of recruited motor-units is of the fast-type which have larger maximum shortening velocity.

Figure 2.25 shows the force-velocity relationship for the medial gastrocnemius (MG) muscle of the cat at four different recruitment levels and two different recruitment sequences; physiological sequence (motor-units are recruited from slow to fast) and non-physiological sequence (motor-units are recruited from fast to slow). The MG muscle is composed of 25% slow-twitch fibres and 75% fast-twitch fibres [135].

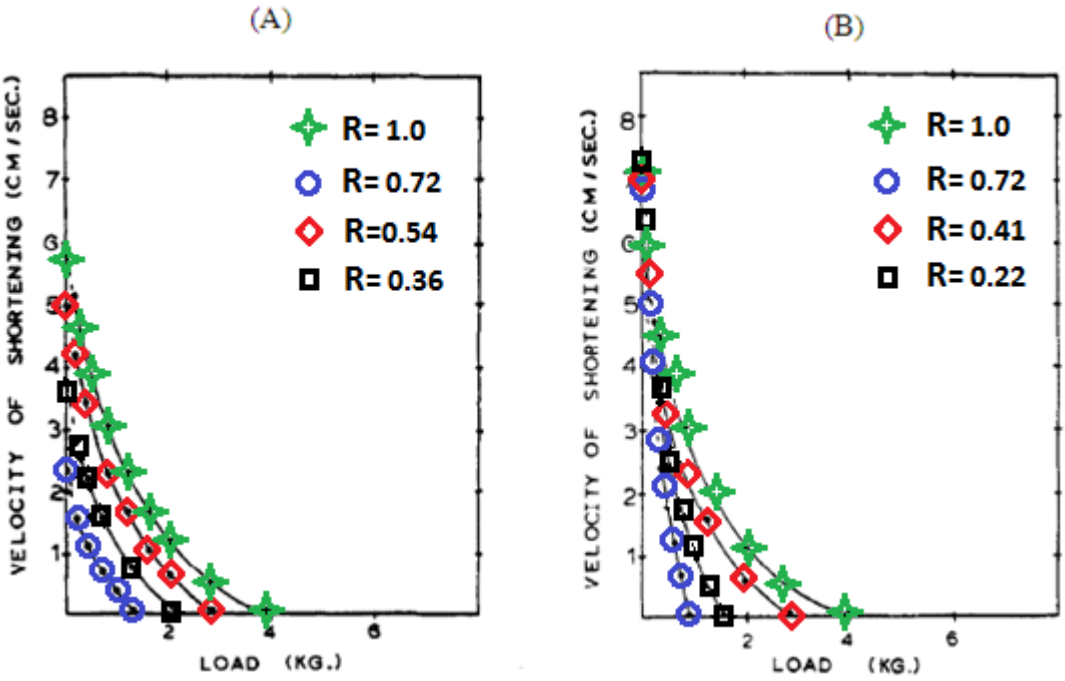

Figure 2.25: Force-velocity relationship for medial gastrocnemius (MG) at four levels of recruitment: (A) Physiological sequence (R = 1.0, 0.72, 0.54, 0.36). (B) Non-physiological sequence (R = 1.0, 0.72, 0.41, 0.22). (From [135]).

2.5.3.2. Summary of key F-V sub-models

Different "simplified" mathematical equations are used to represent the force-velocity relationship. These equations are of different complexity, but in all of them, muscle force decreases during shortening and increases during stretch.

i) Riener-1 F-V sub-model

In Riener-1 F-V sub-model [72], the F-V relationship is represented as a function of the velocity of the muscle belly (v_m):

$$FV(v_m) = 0.54 \arctan(5.69\bar{v}_m + 0.51) + 0.745 \qquad (2.12)$$

ii) Brown F-V sub-model

In Brown model [41, 82, 84, 127, 128], the force-velocity relationship is a function of v_m and l_m, and is modelled by the following equation:

$$FV(v_m, l_m) = \begin{cases} (1+\bar{v}_m)/(1-(c_{v0}+c_{v1}\bar{l}_m)\bar{v}_m) & , \quad \bar{v}_m \le 0 \\ (b_{v4}-(a_{v0}+a_{v1}\bar{l}_m+a_{v2}\bar{l}_m{}^2)\bar{v}_m)/(b_{v5}+\bar{v}_m) & , \quad \bar{v}_m > 0 \end{cases} \qquad (2.13)$$

c_{v0}, c_{v1}, a_{v0}, a_{v1}, a_{v2}, and b_{v4} are constants estimated from experimental data.

Different constants are used for different fibre types, including $v_{m,\max}$.

iii) Hawkins F-V sub-model

The original Hawkins muscle model [101, 129, 130] was re-formulated in order to be in the general form typically used by most Hill-type muscle models and also used in the standard topology (the third formula was formulated). The normalised force-velocity relationship is given by:

$$FV(v_f) = \begin{cases} 0.0 & for: \bar{v}_f \le -1 \\ [1+\bar{v}_f]/[1-(1/k)\bar{v}_f] & for: -1 < \bar{v}_f \le 0 \\ 1.3+(-0.3)\times\left(1-(\dfrac{1}{\bar{v}^{str}_{f,\max}})\bar{v}_f\right) & for: 0 < \bar{v}_f \le \bar{v}^{str}_{f,\max} \\ 1.3 & for: \bar{v}_f > \bar{v}^{str}_{f,\max} \end{cases} \qquad (2.14)$$

Different constants are used for different fibre types, including $v_{f,\max}$ and $v^{str}_{f,\max}$.

iv) AnyBody F-V sub-model

The second alternative in AnyBody Software [136] is a simple linear F-V relationship:

$$FV(v_m) = (1+\bar{v}_m) \qquad (2.15)$$

v) LifeMOD F-V sub-model

In the muscle model used in LifeMOD [137, 138], the normalised force-velocity relation is modelled by:

$$FV(v_m) = \begin{cases} 0 & , \quad \bar{v}_m \le -1 \\ (1+\bar{v}_m)/(1-c_{v0}\bar{v}_m) & , -1 < \bar{v}_m \le 0 \\ (1-a_{v0}\bar{v}_m)/(1+b_{v6}\bar{v}_m), & \bar{v}_m > 0 \end{cases} \qquad (2.16)$$

Constants: $c_{v0} = 4$, $a_{v0} = -2$, $b_{v6} = 1.5$.

vi) Herzog F-V sub-model

The original Herzog muscle model [18] was re-formulated in order to be in the general form typically used by most Hill-type muscle models and also used in the standard topology. The new form of Herzog F-V sub-model is represented by the following formulas:

$$FV(v_{CE}, FL(l_0)) = \begin{cases} 0 & for \quad \bar{v}_{CE} \le -1 \\ \dfrac{1+\bar{v}_{CE}}{1-\left(\dfrac{1}{b}\right)\bar{v}_{CE}} & for \quad -1 < \bar{v}_{CE} \le 0 \\ 1.5 + (-0.5) \times \dfrac{1-\left(\dfrac{1}{\bar{v}^{str}_{CE,\max}}\right)\bar{v}_{CE}}{1+\left(\dfrac{1}{b'}\right)\bar{v}_{CE}} & for \quad 0 < \bar{v}_{CE} \le \bar{v}^{str}_{CE,\max} \\ 1.5 & for \quad \bar{v}_{CE} > \bar{v}^{str}_{CE,\max} \end{cases} \tag{2.17}$$

a, b, a', b': Constants, their values depend on the individual muscle. These constants need to be adjusted for the stimulated muscle to fit its experimental data.

In Herzog F-V sub-model, the maximum shortening and stretch velocities depend on $f_{iso}(l_0)$.

$v_{CE,\max} = -FL(l_o)\dfrac{b}{a}$, $v^{str}_{CE,\max} = FL(l_o)\dfrac{b'}{a'}$ (both normalised to $f_{iso,\max}$).

Using velocity values normalised to the maximum CE velocity $v_{CE,\max}$:

$(\bar{v}_{CE,\max} = -1)$, $\bar{v}^{str}_{CE,\max} = \left(\dfrac{FL(l_o)\dfrac{b'}{a'}}{FL(l_o)\dfrac{b}{a}}\right) = \left(\dfrac{b' \times a}{a' \times b}\right)$ (both normalised to $v_{CE,\max}$).

2.5.3.3. Implications of the application of F-V sub-models on the single motor-unit model

Different fibre types have different F-V relationships. v_{CE}, l_{CE}, and R are continuously changing during FES. Hence, high accuracy muscle model should consider these variables as

inputs to the F-V sub-model. If a single motor-unit model is used, only one F-V sub-model can be used. The multiple motor-unit model properly accounts for more than one F-V sub-model for different fibre types and can also account for the recruitment order of different fibre types.

2.5.4. Fatigue sub-models

Muscle fatigue is defined as the "the failure to maintain the required or expected force". The fatigue rate depends on the muscle employed, the intensity of the activity, and whether the contractions are continuous or intermittent [45]. Muscle fatigue is also affected by other factors such as: age, gender, fitness, etc.

2.5.4.1. Summary of empirical data for muscle fatigue

In healthy subjects and for tasks and activities requiring low force, fatigue will not be accumulated, and the muscle is able to perform the task without fatigue [30]. When a force is generated and maintained, motor-units in the involved muscle are recruited gradually. Some motor units are recruited first. Later on, when they become fatigued, they are de-recruited and other motor units will be recruited to compensate for the force loss due to fatigue, and meanwhile, the fatigued units start to recover [30]. Based on this scenario, the motor units of the muscle involved in a task can be divided into three groups: those which are currently recruited, those already fatigued and are making recovery, and those in the rest state and have not been recruited yet. For tasks requiring large force (in healthy subjects), such as performing a sustained maximal voluntary contraction (MVC), the recovery mechanism cannot compensate for the force loss (due to fatigue) quickly enough. Therefore, after some time, all motor units in the muscle will eventually become completely fatigued and can no longer be recruited [139, 140, 141]. As discussed earlier, different fibre types have different fatigue resistance, depending on the fibre type composition.

Stimulation frequency has a great effect on muscle fatigue, higher frequency will produce higher force but also results in a faster fatigue rate, and vice versa. Fibre-type also has a great effect on fatigue. This is a fixed property of muscle fibres and will be considered as a constant (although as explained below fibre-type composition within muscles can be changed by regular exercise or paralysis).

Muscles that do not receive regular exercise undergo disuse atrophy and convert to a higher proportion of type-II fibres than regularly active muscles [24]. Many disabled people have extensive disuse atrophy in their paralysed muscles depending on how long the muscles have been paralysed [4]. Consequently, when applying FES, the affected muscles can fatigue quickly where they have become mostly type-II fibres. The force response of electrically stimulated muscle decays nonlinearly as the muscle begins to fatigue [3]. Eventually, the muscle is not able to produce any force. Figure 2.26 shows four possible fatigue patterns that are typically seen in SCI disabled subjects during FES sessions. These plots show the force exerted by the quadriceps muscle group versus time when subjected to FES. These empirical data were collected from a patient (all data collected from the same patient) who had SCI resulting in paraplegia [142].

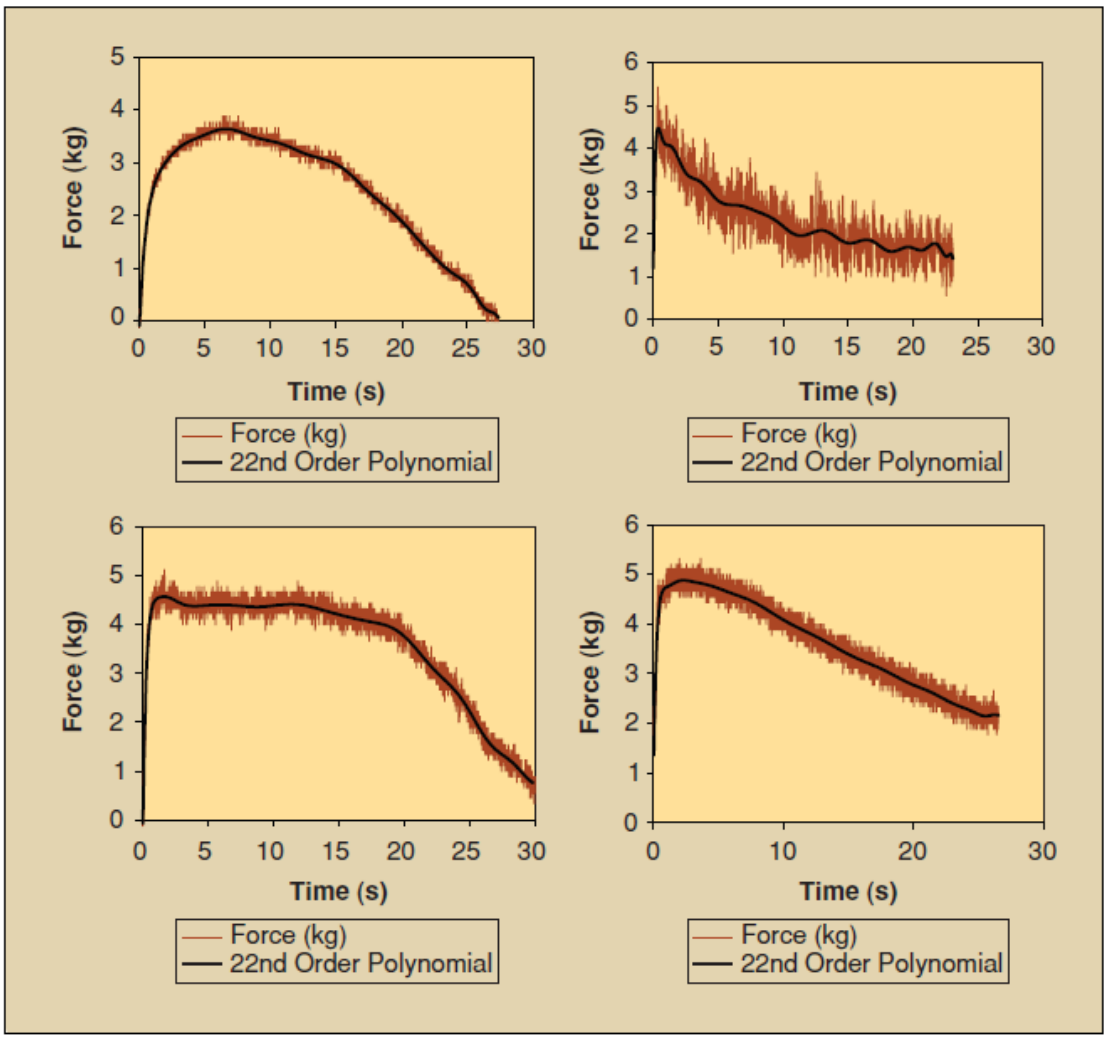

Figure 2.26: Four different force decay profiles representing some of the wide range of force profiles that can be seen as the muscle fatigues during FES. (From [1]).

2.5.4.2. Summary of key fatigue sub-models

Different mathematical equations have been reported in the literature at different complexity levels to represent the fatigue effect on muscle force. In all of them, muscle force decreases when FES is on. When FES is off, some of them have considered recovery and some have not. The fatigue sub-models considered in this chapter are only those which use "black-box" modelling approach to model fatigue, modelling of physiological details is not covered here.

Muscle fatigue can be measured and modelled as index of fatigue IF which is defined as "force of the fatigued muscle normalised to force of the same un-fatigued muscle under same conditions", IF is an instantaneous quantity that varies with time. Inputs to the fatigue sub-model are stimulation frequency $freq$ and recruitment level (when recruited fatigue occurs, when not recruited recovery occurs), the output of fatigue sub-model is IF .

Depending on the fatigue sub-model; IF can be the same or different for different fibre types (if a single motor-unit model is used, then there is only one IF . If multi fibre-type model is used then there can be separate IF_i for each fibre-type).

i) Giat fatigue sub-model

It is assumed in Giat fatigue sub-model [143, 144, 145, 146] that the fatigue related metabolic parameter *pH* reflects the force production capability of a muscle. The index of fatigue is calculated in two steps; *pH* level is calculated first then the index of fatigue IF is calculated. One curve for *pH* decay with respect to time during FES (Figure 2.27) and another curve for *pH* recovery with respect to time (Figure 2.28) are obtained empirically for the muscle of interest ($R=1$ during FES, and $R=0$ during recovery), these two curves are then used to calculate fatigue and recovery of muscle force for continuous or intermittent FES.

The decay of *pH* with respect to time during FES is presented mathematically as:

$$pH_{fat}(t) = c_1 - c_2 \tanh[c_3(t - c_4)] \qquad (2.18)$$

The increase of *pH* with respect to time during recovery is represented mathematically as:

$$pH_{rec}(t) = d_1 + d_2 \tanh[d_3(t - d_4)] \qquad (2.19)$$

Constants values (c_1, c_2, c_3, c_4, d_1, d_2, d_3, d_4) are determined experimentally for each muscle, and different muscles in the same subject can produce different fatigue and recovery curves, depending on fibre-type [143, 144].

Muscle force (of fatigued muscle) normalised to maximum isometric force (of un-fatigued muscle) is calculated by the following equation:

$$IF(pH) = d_5 \times (1 - \exp[d_6(pH(t) - d_7)]) \qquad (2.20)$$

This equation is used for both cases, during FES and during recovery.

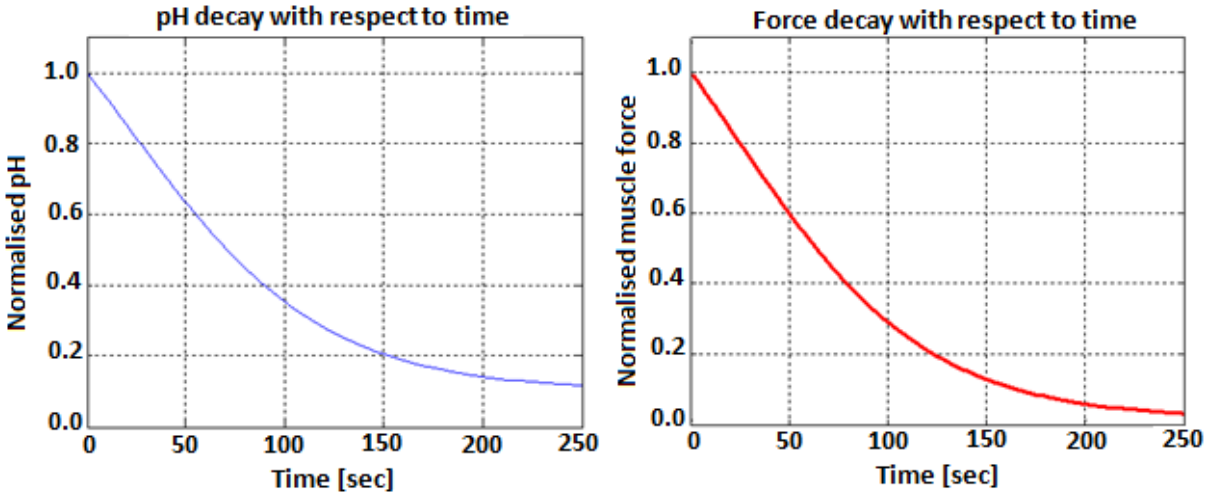

Figure 2.27: Giat Fatigue Sub-Model. Left: Decay curve of the normalised *pH* level with respect to time. This curve represents equation (2.18) with ($c_1 = 0.8527$, $c_2 = 0.75$, $c_3 = 0.1$, $c_4 = 2$). Right: Muscle force decay sub-model using the *pH* curve (left). This curve represents equation (2.20) with: ($d_5 = 113.6$, $d_6 = -0.0097$, $d_7 = 0.0885$).

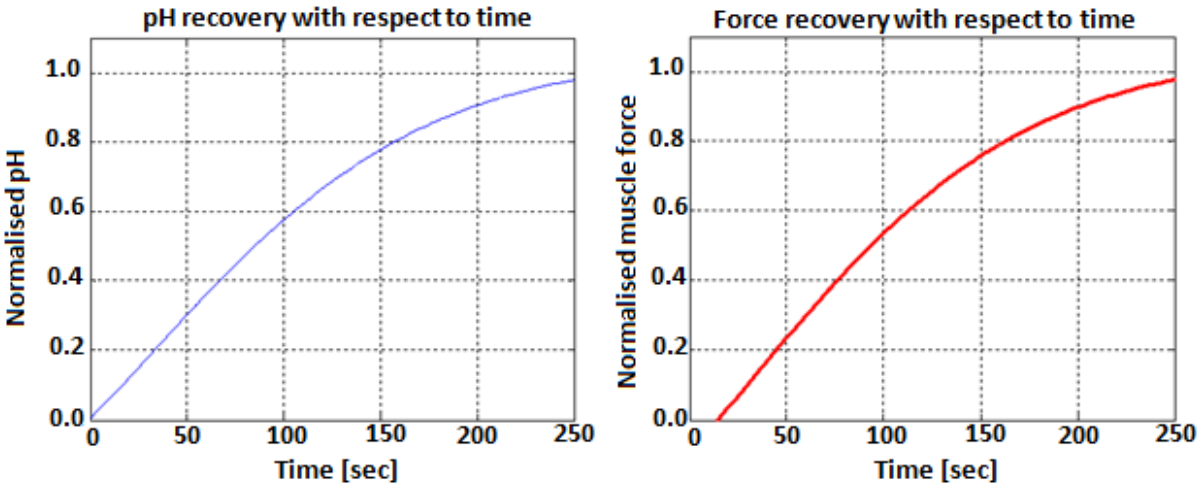

Figure 2.28: Giat Fatigue Sub-Model. Left: Recovery curve of the normalised *pH* level with respect to time. This curve represents equation (2.19) with ($d_1 = 0.179021$, $d_2 = 0.88$, $d_3 = 0.069$, $d_4 = 3$). Right: Muscle force recovery sub-model using the *pH* recovery curve (left). This curve represents equation (2.20) with: ($d_5 = 113.6$, $d_6 = -0.0097$, $d_7 = 0.0885$).

Modelling intermittent FES:

The time t_o^{rec} at which the recovery starts (of any cycle) is calculated by reversing equation (2.19):

$$t_o^{rec} = \frac{1}{d_3} \times \operatorname{arctanh}\left[\frac{pH_{fat} \times t_{end}^{fat} - d_1}{d_2}\right] + d_4 \qquad (2.21)$$

t_{end}^{fat} : Time at which FES stopped (of the same cycle).

The time t_o^{fat} at which FES starts again is calculated by reversing equations (2.18):

$$t_o^{fat} = \frac{1}{c_3} \arctan h\left[\frac{pH_{rec} \times t_{end}^{rec} - c_1}{c_2}\right] + c_4 \qquad (2.22)$$

t_{end}^{rec} : Time at which last recovery stopped and FES started.

ii) Riener-1 fatigue sub-model

Riener-1 fatigue sub-model [72] is a simplified version of Giat model, where the index of fatigue is calculated only in one equation. This model was developed first in [55] as a general simple model, then effect of recruitment and frequency was added in [72]. Fatigue and recovery rates at any time are given by the following first-order equation:

$$\frac{d}{dt}(IF) = \frac{(IF_{\min} - IF(t)) \times [R \times A_{freq} \times \lambda]}{T_{fat}} + \frac{(1 - IF(t)) \times (1 - [R \times A_{freq} \times \lambda])}{T_{rec}} \tag{2.23}$$

$$A_{freq}(freq) = \left(\frac{(freq)^2}{100 + (freq)^2} \right) \quad for: freq < 100Hz$$

$$\lambda(freq) = 0.4 + \left[0.6 \times \left(\frac{freq}{100} \right)^2 \right] \quad for: freq < 100Hz$$

R: Recruitment of the whole muscle.

A_{freq}: Muscle activation due to stimulation frequency only without the effect of other parameters which affect activation (i.e. without yield, sag, effective length and effective frequency).

λ: This term is used to model the effect of stimulation frequency on fatigue rate.

$IF_{\min}$: The minimum fitness of the muscle at which fatigue rate = 0 of the fully recruited muscle (i.e. the minimum value for the index of fatigue).

For all muscles: $T_{rec} = 30$ [sec].

($IF_{\min}$, T_{fat}) are estimated experimentally, they can have largely different values for different muscles.

Riener-1 fatigue sub-model can be used for the whole muscle, for the fibre-type, or for a single motor-unit (assuming $R_{i,j} = 1$ when recruited and $R_{i,j} = 0$ when not recruited) providing that appropriate values for model parameters are used.

iii) Hawkins fatigue sub-model

In Hawkins fatigue sub-model [101, 129, 130], stimulation frequency is assumed constant (near to maximum natural frequency). Recovery is not modelled; which means that index of

fatigue IF will stay the same during the recovery period of intermittent FES (i.e. when FES is switched off until next cycle of FES), endurance time and fatigue rate for different fibre types are shown in Figure 2.29.

For times longer than T_{end}, the rate of fatigue for the three fibre types is assumed linear.

$$IF = \begin{cases} 1.0 & , \quad t < T_{end} \\ 1 - \left[\left(\frac{d}{dt}(IF) \right) \times (t - T_{end}) \right] & , \quad t \geq T_{end} \end{cases} \qquad (2.24)$$

For type-I and type-IIa fibres under continuous FES (assumed near maximum natural stimulation frequency): $T_{end} = 6$ [sec], $\frac{d}{dt}(IF) = 0.00097$ [s^{-1}]

For type-IIb fibres under continuous FES (assumed near maximum natural stimulation frequency): $T_{end} = 23$ [sec], $\frac{d}{dt}(IF) = 0.0333$ [s^{-1}]

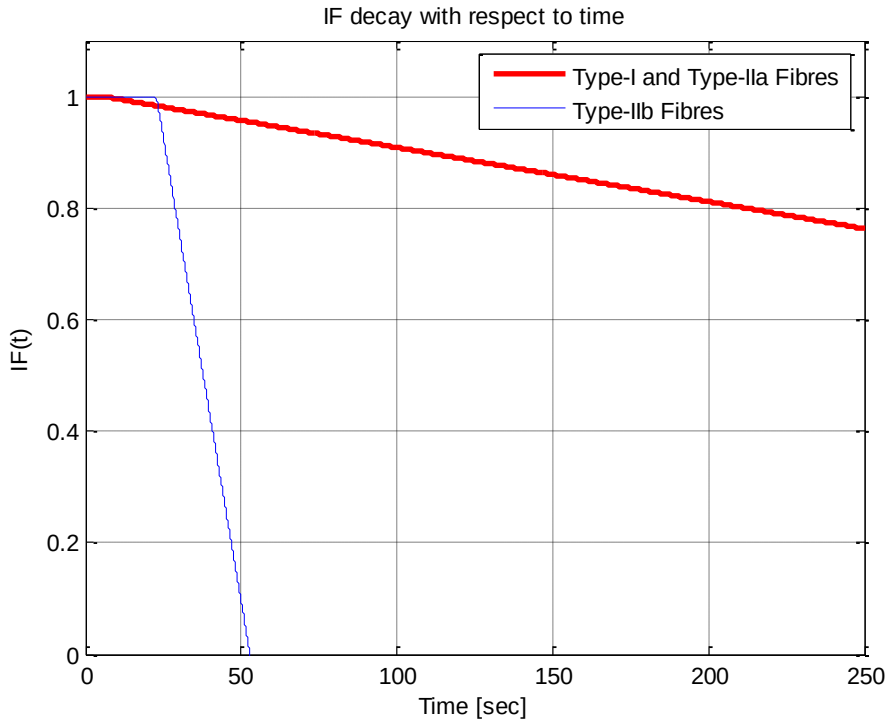

Figure 2.29: Endurance time and fatigue rate for different fibre types in Hawkins model.

iv) Freund and Takala fatigue sub-model

Freund and Takala fatigue sub-model [147] is a relatively simple fatigue sub-model which was developed for natural voluntary contraction assuming that recruitment R will increase during contraction (by the CNS) to compensate for the effect of fatigue on those recruited motor-units. However this can be used for FES with individual motor-units assuming ($R_{i,j}=1$) for recruited motor-units and ($R_{i,j}=0$) for non-recruited motor-units.

Fatigue rate is modelled as:

$$\frac{d}{dt}(IF) = -[\beta \times R] + [\alpha \times (1 - IF(t))] \qquad (2.25)$$

The first term represents fatigue, and the second term represents recovery. Constants need to be estimated from experimental data, they are provided in [147] as: $\alpha = 0.2$ $[\text{min}^{-1}]$, $\beta = 1.13$ $[\text{min}^{-1}]$. However, these values resulted in very fast fatigue; hence both were divided by 10 to get realistic curves. Figure 2.30 shows fatigue and recovery curves for fully recruited muscle (or single recruited motor-unit).

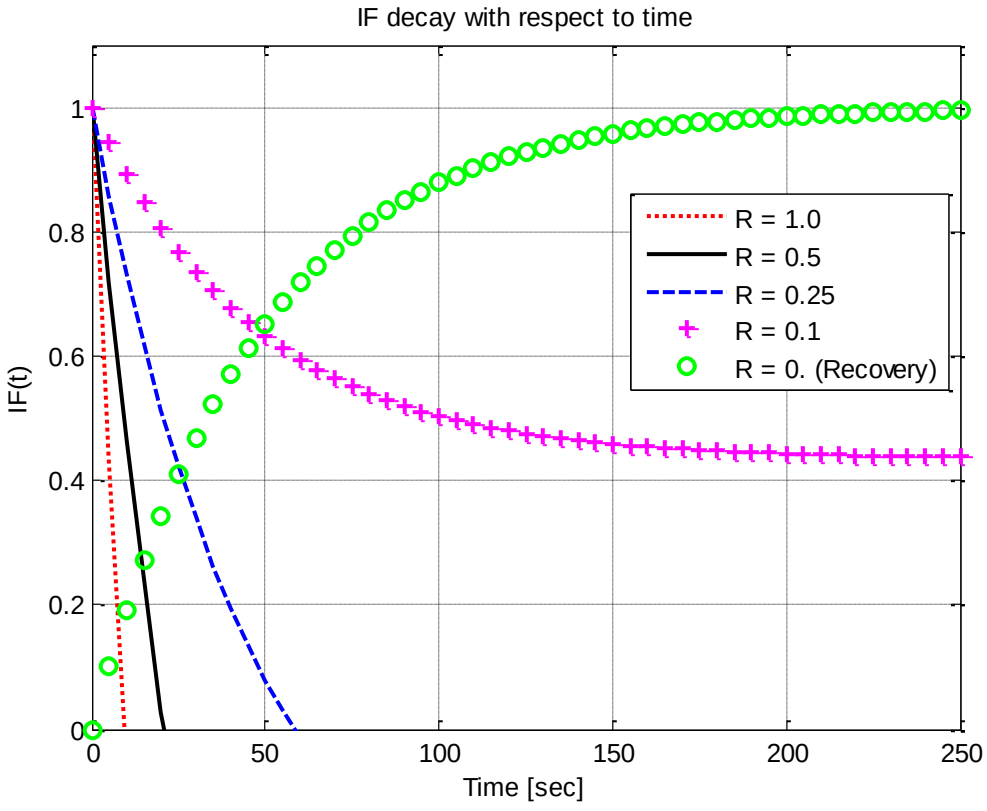

Figure 2.30: *IF* curve of Freund and Takala Fatigue Sub-model ($\alpha = 0.02$, $\beta = 0.113$)..

v) Ma fatigue sub-model

Model assumptions are similar to Freund and Takala fatigue sub-model. The fatigue part was developed first in [148], then the recovery part was incorporated into the model in [149]. During recruitment of the muscle, the fatigue rate is given by:

$$\frac{d}{dt}(IF) = -[k \times IF(t) \times R] + [r \times (1 - IF(t))] \qquad (2.26)$$

The first term represents fatigue, and the second term represents recovery, see Figure (2.31). $r = 2.4$, k is determined experimentally (not provided in related references [148, 149]).

During recovery ($R = 0$), the recovery curve is given by:

$$IF(t) = 1 + (IF(t_{end}^{fat}) - 1) \times \exp(-r \times t) \qquad (2.26A)$$

$IF(t_{end}^{fat})$: is the index of fatigue at the time when fatigue stopped and recovery started. At beginning of recovery: ($t = 0$).

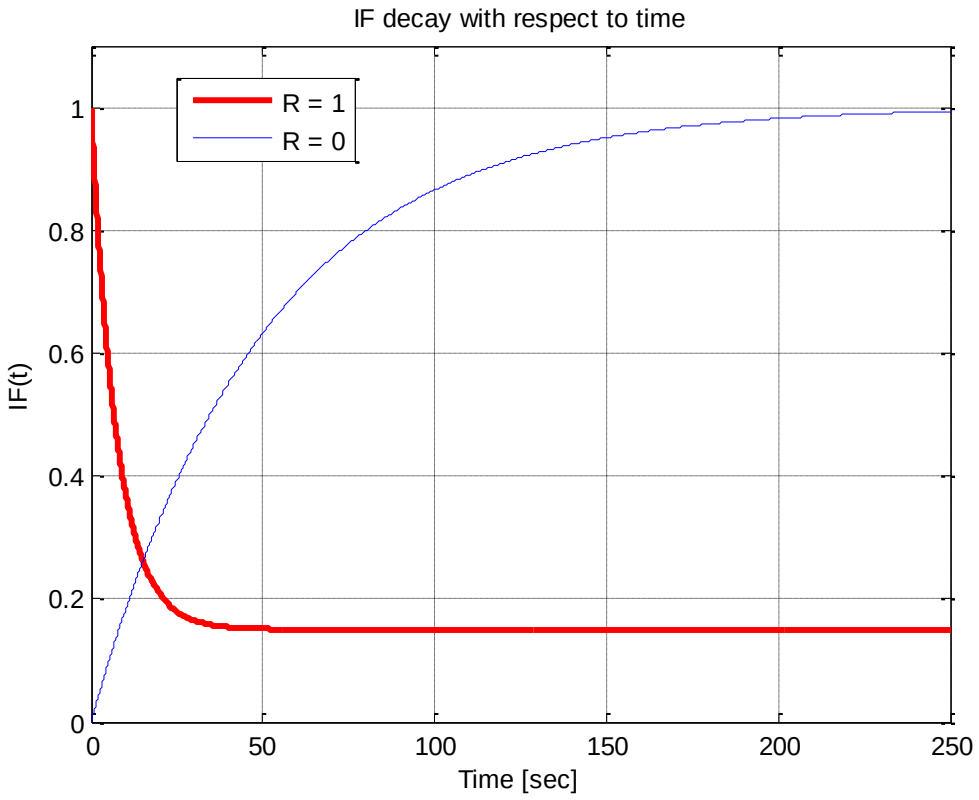

Figure 2.31: *IF* curve of Ma Fatigue Sub-model with ($r = 0.2$, $k = 1.13$). The red curve represents fatigue during full recruitment ($R = 1$), the blue curve represents recovery for non-recruited muscle ($R = 0$).

2.5.4.3. Implications of the application of fatigue sub-models on the single motor-unit model

The real muscle consists of large number of motor-units and different fibre types which have different rates of fatigue. If a single motor-unit model is used, the different fatigue sub-models of different fibre types cannot be incorporated into the model. Moreover, in a realistic scenario R is changing continuously during FES. The single motor-unit model cannot account for the effect of continuously varying R (i.e. fatigue of different motor-units) since each motor-unit fatigues and recovers, independent of other motor-units. The multiple motor-unit model properly accounts for more than one fatigue sub-model for different fibre types and also models each motor-unit separately.

2.5.5. Force enhancement & depression sub-models

The force enhancement & depression **(** f_e & f_d **)** is mainly affected by magnitude of stretch and shortening. It is also affected by velocity, recruitment level, and stimulation frequency during stretch/shortening [13]. The increase or decrease of muscle force **(** f_e *or* f_d **)** is determined relative to the purely isometric reference force corresponding to the *CE* length at the end of stretch or shortening (Figure 2.32).

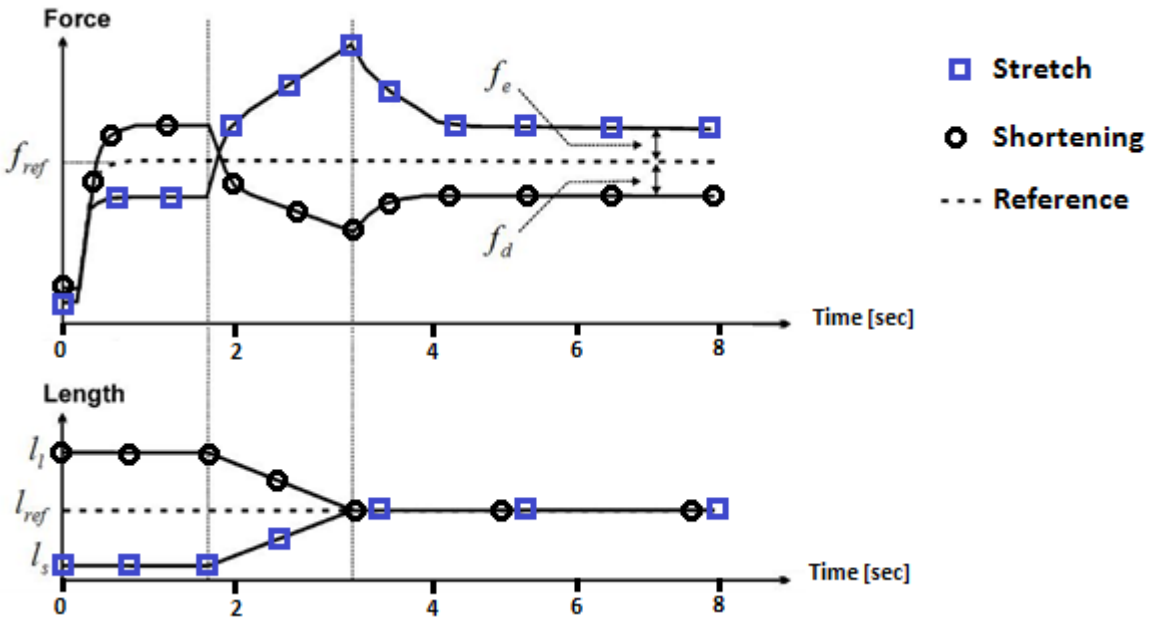

Figure 2.32: Force enhancement f_e following stretch, and force depression f_d following shortening of a recruited muscle. (From [13]).

2.5.5.1. Summary of empirical data for force enhancement & depression

Force enhancement and depression experimental data available in the literature show some complexity and some uncertainty. An example of empirical data is shown in Figure 2.33, which show the effect of stretch/shortening velocity v_{CE} and initial length l_o on force enhancement f_e following stretch and force depression f_d following shortening at different initial lengths l_o. The force enhancements and force depressions were less at shorter muscle lengths and higher speeds.

Force enhancement f_e is increased with increasing magnitudes of stretch, see left graph of Figure 2.34. The velocity of stretch was reported by some scientists to have no effect on force enhancement [150, 151] and to have a small effect on force enhancement by other scientists [152, 153]. The experimental data shown in Figure 2.33 show that the velocity of stretch has a small effect on force enhancement; this effect is greater at shorter lengths.

Force enhancement following stretch has been associated with the descending limb of the force–length relationship exclusively. However, there has been some controversy as to whether force enhancement could be obtained on the ascending limb of the force–length relationship. Some researchers' experimental results support the assumption that force enhancement also occurs on the ascending limb of the force–length relationship [13], but less than that on the descending limb; experimental data shown in Figure 2.33 support this assumption.

Force depression increases with increased magnitudes of shortening (Figure 2.34), for increased forces during shortening (when the minimum magnitude of force during shortening is higher, then force depression is higher), and for decreased speeds of shortening. These properties are well accepted although there remains slight controversy over the effects of speed of shortening on force depression [13, 152]. It has not been easy to identify whether force depression is independently related to the speed of shortening, or if the speed of shortening is indirectly associated with the magnitude of force during shortening (because during shortening the force magnitude decreases with increasing speed of shortening). For simplicity, the second option will be assumed; another reason is because the difference between the two assumptions seems to be small. Hence, only the first and the second properties will be considered (i.e. force depression is increased only for increased magnitudes of shortening and for increased forces during shortening).

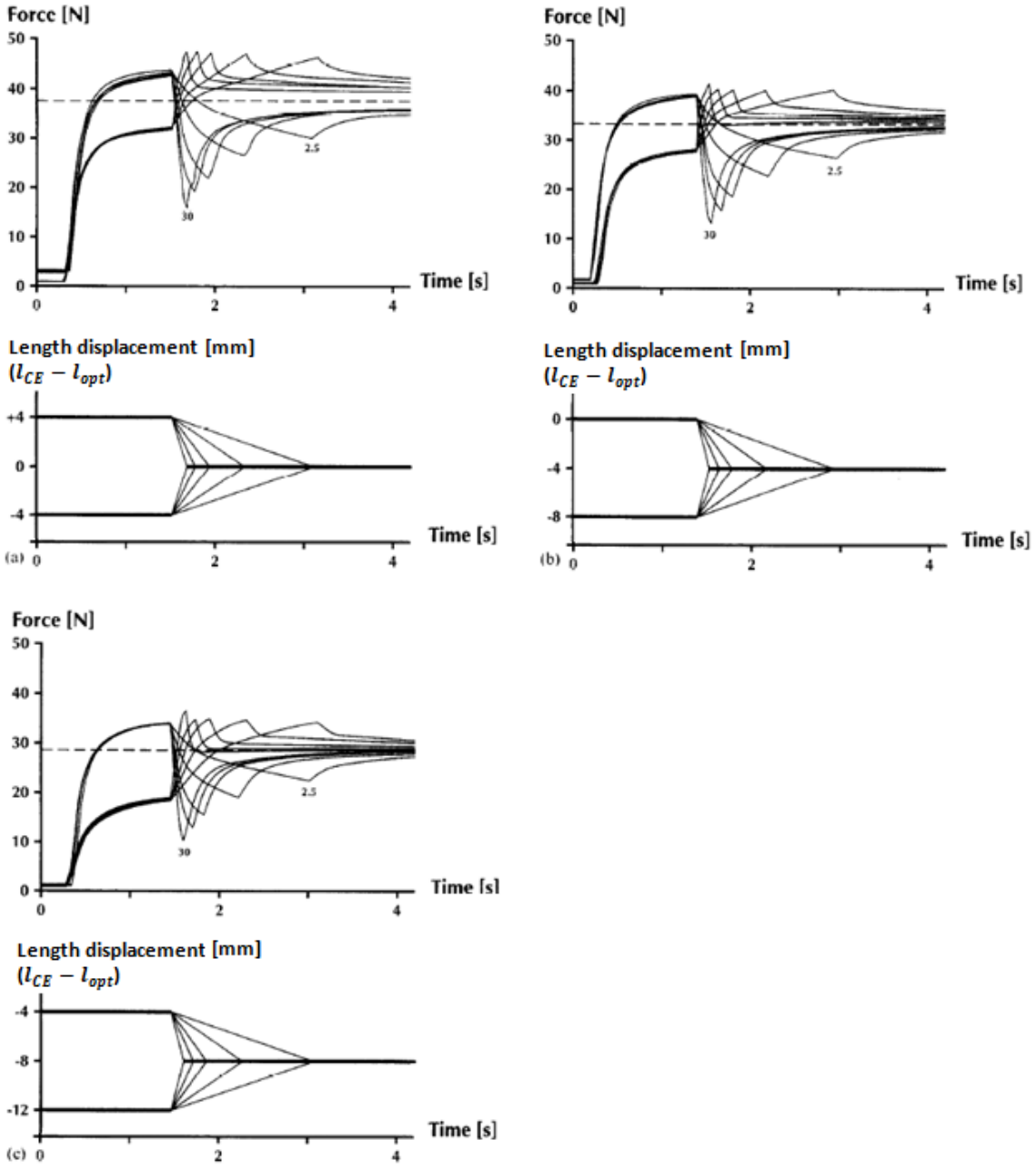

Figure 2.33: Three shortening and three stretch contractions, at speeds ranging from 2.5 to 30 [mm/s]. The steady-state isometric force of the muscle at the final length is indicated by horizontal line. The final length was 0, - 4, and - 8 mm in (a), (b), and (c) respectively. Length represents displacement from optimal length ($l_{CE} - l_{opt}$). (From [152]).

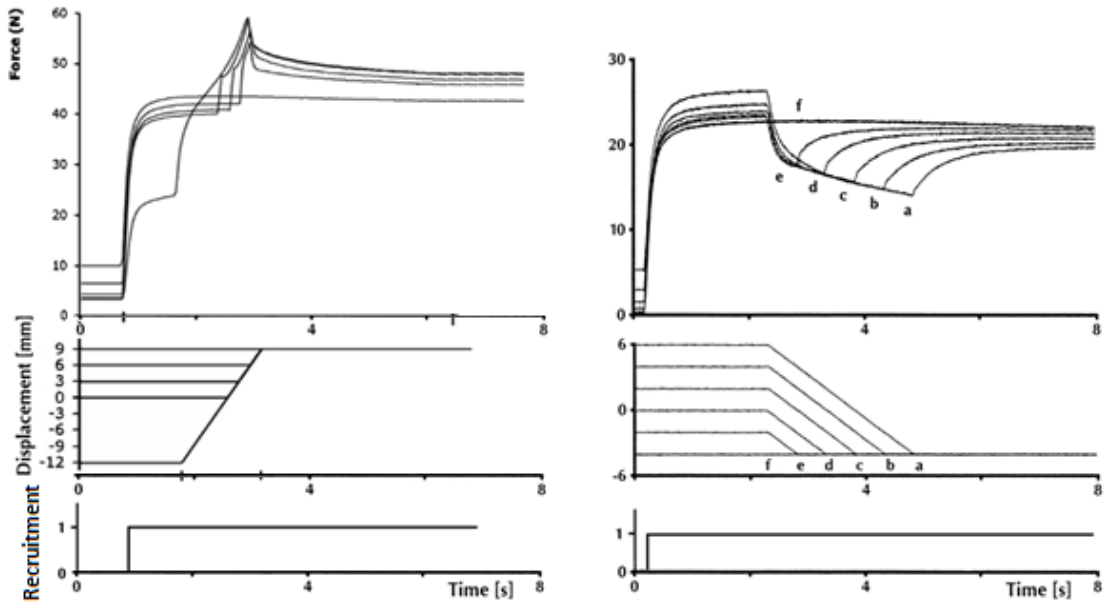

Figure 2.34: Effect of magnitude of stretch on force enhancement (left) and shortening on force depression (right). (Left graphs from [154], right graphs from [155]).

2.5.5.2. Summary of key force enhancement & depression sub-models

The *CE* length at initial recruitment l_o is thought to be a key parameter influencing total muscle force F_m. More details and comparison between *CE* instantaneous length l_{CE} and *CE* length at initial recruitment l_o are provided in Appendix 2.

Indices of enhancement & depression (*IE & ID*) are used to model the transient-state and the steady-state of the force enhancement/depression following stretch/shortening. *IE* is calculated as the instantaneous active muscle force after end of stretch divided by the isometric *CE* force corresponding to the length at end of stretch. *ID* is calculated as the instantaneous active muscle force after end of shortening divided by the isometric *CE* force corresponding to the length at end of shortening. (*IE & ID*) represent the new isometric *CE* force after end of stretch/shortening (f_{CE} corresponding to the length at end of stretch/shortening + transient-state and steady-state effects of stretch/shortening on recruited muscle force) normalised to the isometric *CE* force f_{CE} corresponding to the length at end of stretch/shortening. *IE & ID* is assumed the same for all fibre types in all sub-models. Only few force enhancement & depression sub-models are available in the literature.

i) Hawkins force enhancement sub-model

Force enhancement following stretch is modelled by the index of enhancement IE. Force depression following shortening is not modelled in Hawkins muscle model [101]. The index of enhancement IE_i (for fibre type-*i*) is the same for all fibre types. The index of enhancement is given by:

$$IE(t) = \begin{cases} IE_\infty + \left[(IE_{\max} - IE_\infty) \times \exp(c_{TS} \times t)\right] & for \quad t \le 4 \\ IE_{SS} & for \quad t > 4 \end{cases} \tag{2.27}$$

$$IE_{SS} = IE(t=4) = IE_\infty + \left[(IE_{\max} - IE_\infty) \times \exp(c_{TS} \times 4)\right] \tag{2.27A}$$

$$IE_\infty = \begin{cases} 0.505(IE_{\max}) + 0.403 & for: IE_{\max} \ge 1.2 \\ 1.0 & for: IE_{\max} < 1.2 \end{cases} \tag{2.27B}$$

$$c_{TS} = -0.301/(IE_{\max} - IE_\infty) \tag{2.27C}$$

Two examples are illustrated in Figure (2.35), both stretches were initiated on the descending limb of F-L curve, the lower curve corresponds to low stretch velocity, maximum eccentric force was not achieved the higher curve corresponds to higher stretch velocity where maximum eccentric force was achieved and hence the force enhancement is larger (Hawkins assumes that *IE* and eccentric force increase with increasing stretch velocity).

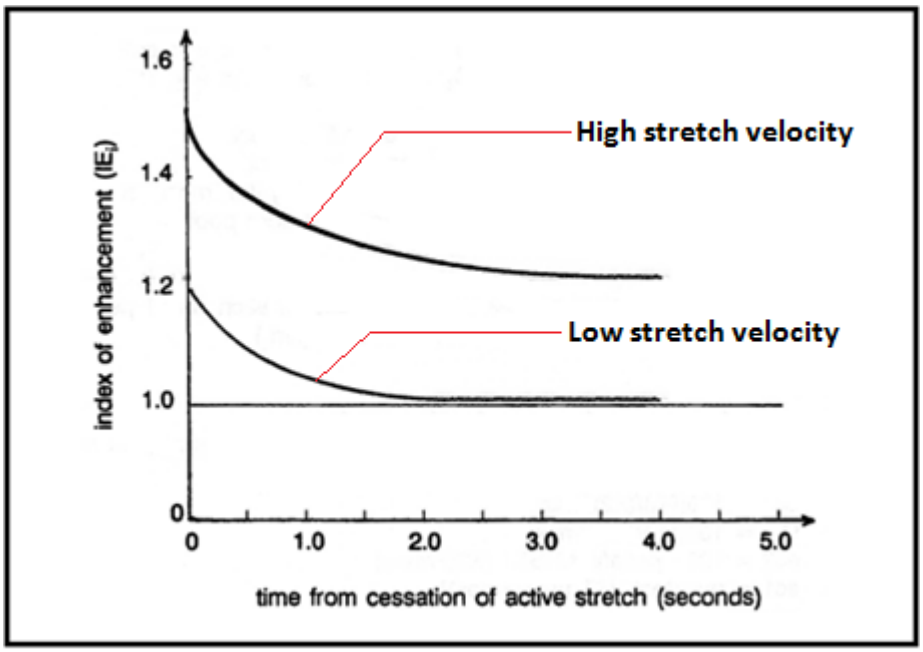

Figure 2.35: Two examples of Hawkins force enhancement sub-model for two muscles at MVC ($R = 1$) after cessation of stretch as function of time. (From [101]).

ii) Forcinito force enhancement & depression sub-model

In Forcinito model [156, 157], the initial length is used to calculate the isometric force [$f_{CE} = f_{iso}(l_o)$], where in the majority of Hill-type models the instantaneous length is used [$f_{CE} = f_{iso}(l_{CE})$]. For fully recruited muscle ($R = 1$), the steady-state force enhancement & depression is modelled by an extra parallel elastic rack (parallel to CE), where a relay will engage the elastic rack at the moment when the muscle is initially recruited. This relay will continue to be active as long as the muscle is still recruited ($R > 0$). The stiffness of the rack is given by: $(E.A/l_{ER,0})$, where A is the cross-sectional area of the elastic rack, and E is the modulus of elasticity. The stiffness of the rack decreases linearly with increasing initial length $l_{ER,0}$. The instantaneous active muscle force f_m including force enhancement & depression is given by:

$$F_m = f_{iso}(l_o) + \left(\frac{E.A}{l_{ER,o}} \times (l_{ER} - l_{ER,o}) \right) + \left(1 + \frac{E.A}{k \times l_{ER,o}} - \frac{E.A}{l_{ER,o}} \right) \times (l_{ER} - l_{ER,o}) \times \exp(-(k/c) \times t) \quad (2.28)$$

2.5.5.3. Implications of the application of *IE & ID* sub-models on the single motor-unit model

The real muscle consists of large number of motor-units. In a realistic scenario; R and l_{CE} are changing continuously during FES. The single motor-unit model cannot account for the effect of continuously varying R at different *CE* lengths (i.e. length history-dependence). The multiple motor-unit model properly accounts for this realistic scenario since each motor-unit is modelled separately, with its own initial length.

2.5.6. Passive elements sub-models

Skeletal muscles have complex passive viscoelastic structure; they are made of soft tissues with different material properties. A skeletal muscle consists of tendon, aponeurosis, connective tissues, and muscle fibres; each part of them has viscoelastic passive forces. The length and velocity of the whole muscle will affect the length and velocity of all muscle parts.

2.5.6.1. Summary of empirical data for passive behaviour

Passive elastic force of the whole muscle is a function of the length of the musculotendon complex l_{mt}. Passive elastic force of muscle belly resists stretch beyond its slack length; it also resists the compression of *CE* at short lengths. Passive elastic force of the tendon resists stretch beyond its slack length (the aponeurosis has similar properties to tendon). Passive elastic force can increase total muscle force when stretched beyond its slack length, and can decrease total muscle force when contracted to very short lengths. Passive viscous force is a function of the velocity of the musculotendon complex v_{mt}. The passive viscous force (of all muscle parts) resists movement during both shortening and lengthening.

The passive F-L curves determined experimentally for muscle belly can have different shapes for different muscles and can start at different lengths relative to the optimal length. Different muscles have different passive forces because of the effects of cross sectional area, length and muscle structure. However, the difference in the passive F-L relationship can be greatly reduced when normalised. In some cases, passive F-L curves for different specimens of the same muscle (from different animals) can vary a lot and do not tend to normalize well with respect to each other [158], an example is shown in Figure 2.36. Strap-like muscles are parallel-fibered muscles (i.e. pennation angle = 0) which have minimal aponeurosis (muscles used are five strap-like muscles of the cat hind limb: caudofemoralis, semitendinosus, sartorius anterior, tenuissimus, and biceps femoris anterior). The experimental data in this figure were collected using this type of muscles because the muscle belly length of this type of muscles provides an accurate indication of the active *CE* length [158] used in the model.

Different types of fibres were reported in the literature to have similar passive forces per unit area. Tendons of different muscles were also reported to have similar passive forces per unit area. Experimental passive elastic F-L curve of tendon is similar to that of muscle belly but with higher resisting force, see Figure 2.37.

Figure 2.38 shows the effect of the viscous drag "passive" force created by non-recruited fibres in the whole muscle. The soleus muscle is composed of 100% slow-twitch fibres, hence $v_{m,\max}$ is less at lower recruitment levels because of the viscous drag "passive" force. The viscous passive force created by non-recruited fibres (in a partially recruited muscle) reduces muscle force during shortening and stretch. It also reduces the maximum shortening velocity $v_{m,\max}$ during shortening. Recruited fibres also have viscous passive force, but it is already

included in the F-V relationship (as a hidden parameter). A viscous element is added in some muscle models for stability purposes during simulation (e.g. Brown muscle model).

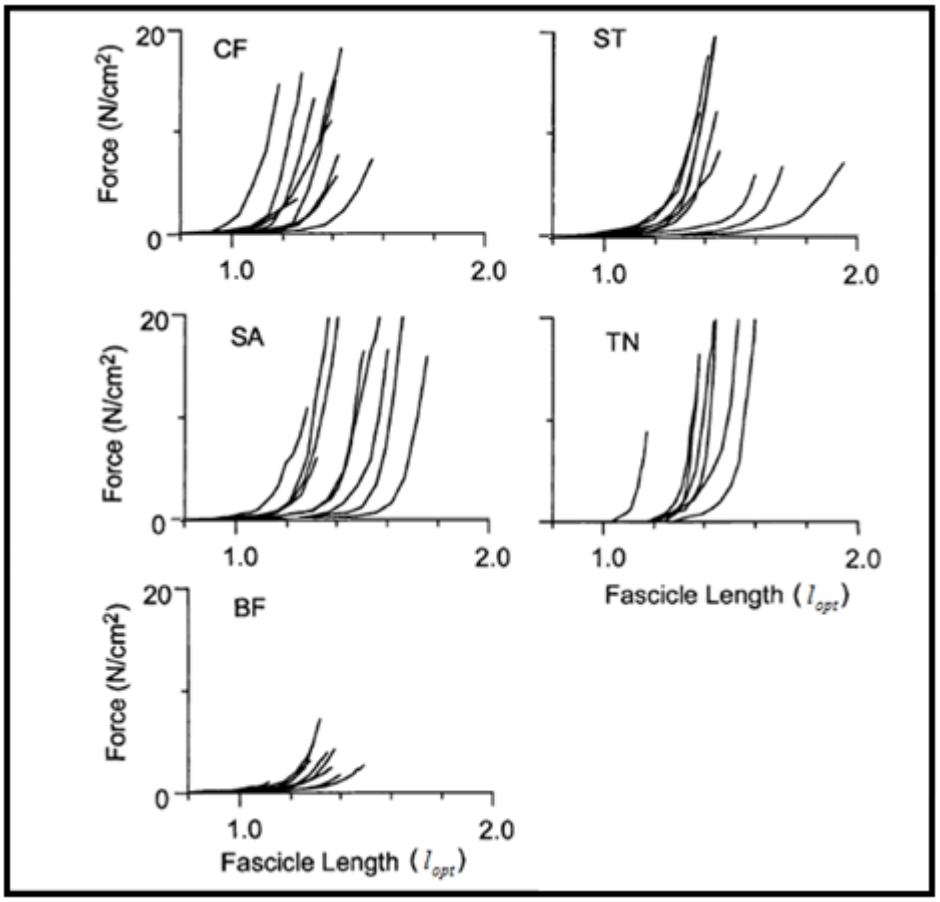

Figure 2.36: Passive elastic F-L curves for 43 muscles taken from different animals. Forces are normalized to PCSA and fascicle lengths to l_{opt} of muscle fibres. (From [158]).

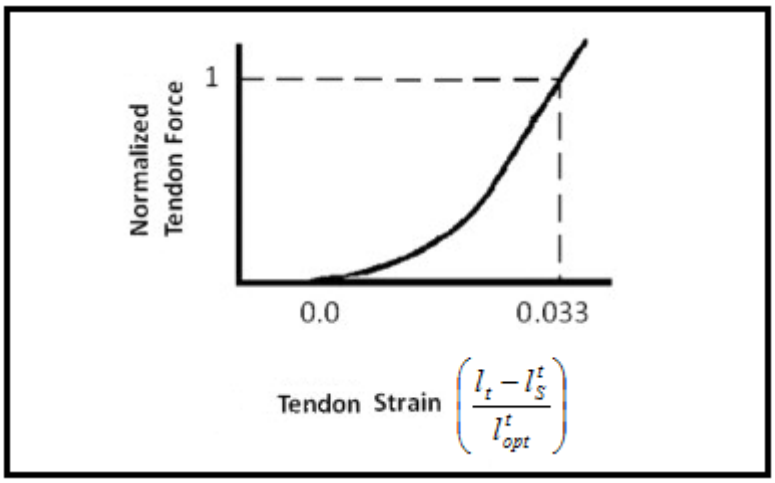

Figure 2.37: Typical tendon passive elastic F-L curve. Tendon strain=$\left[\frac{l_t - l_S^t}{l_{opt}^t}\right]$, unit-less.

(Adapted from [159]).

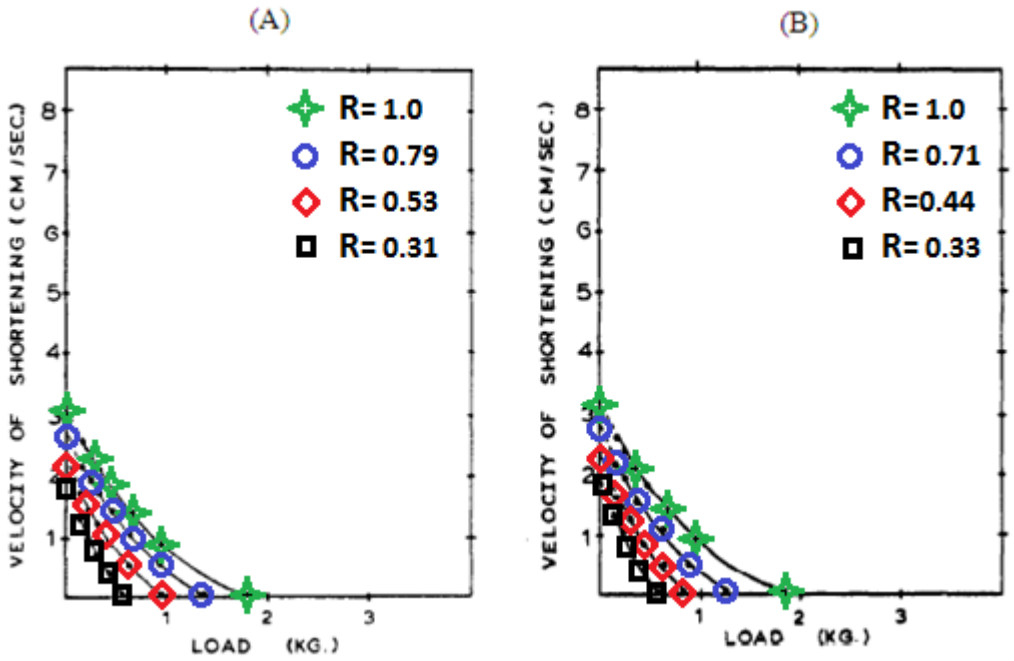

Figure 2.38: Force-velocity relationship for the soleus (SOL) at four levels of recruitment: (A) Physiological sequence, (B) Non-physiological sequence. (From [135]).

2.5.6.2. Summary of key passive elements sub-models

Alternative mathematical equations are used in different muscle models to mathematically represent the empirical data of the passive F-L and F-V relationships.

i) Herzog sub-model for muscle passive elements

The passive elastic forces of muscle belly f_{PE1} and tendon f_{SE} are modelled as linear functions (of linear springs) in Herzog model [18], the passive elements are arranged as in form (b) of Figure 2.11 in section 2.4.1.

$$f_{SE}(l_{SE}) = \begin{cases} k_s \times (l_{SE} - l_S^{SE}) & for: l_{SE} > l_S^{SE} \\ 0.00 & for: l_{SE} \le l_S^{SE} \end{cases}, \; l_S^{SE} = l_S^t \qquad (2.29)$$

$$f_{PE1}(l_{PE1}) = k_p \times (l_{PE1} - l_S^{PE1}), \; l_S^{PE1} = l_S^{mt} \qquad (2.30)$$

Note that ($f_{PE1} > 0$) for ($l_{PE1} > l_S^{PE1}$) and ($f_{PE1} < 0$) for ($l_{PE1} < l_S^{PE1}$). Since $PE1$ and SE of Herzog model are linear, the arrangement of passive elements can be changed to form (a) of Figure 2.11 using Fung equations given in [107] as follows:

($k_{S1} = k_{S2} + k_{P2}$) and ($k_{P2} = \frac{k_{S1} \times k_{P1}}{k_{S1} + k_{P1}}$).

k_{S1} and k_{P1} are the series and parallel elements of form (a), k_{S2} and k_{P2} are the series and parallel elements of form (b). Form (a) will be used as the standard form because of the following: it is more common in the literature, it was suggested by many researchers to be more accurate [103, 105, 106] and also this makes all models represented in this chapter to have the same arrangement of model elements.

ii) Brown sub-model for muscle passive elements

Brown muscle model is presented in different references [41, 82, 84, 100, 127]. All sub-models and constants' values were taken from the last update of Brown model given in [100]. Passive elements of Brown model are illustrated in Figure (2.39). The linear parallel viscous element *VE* was added in [127] for stability purposes during simulation.

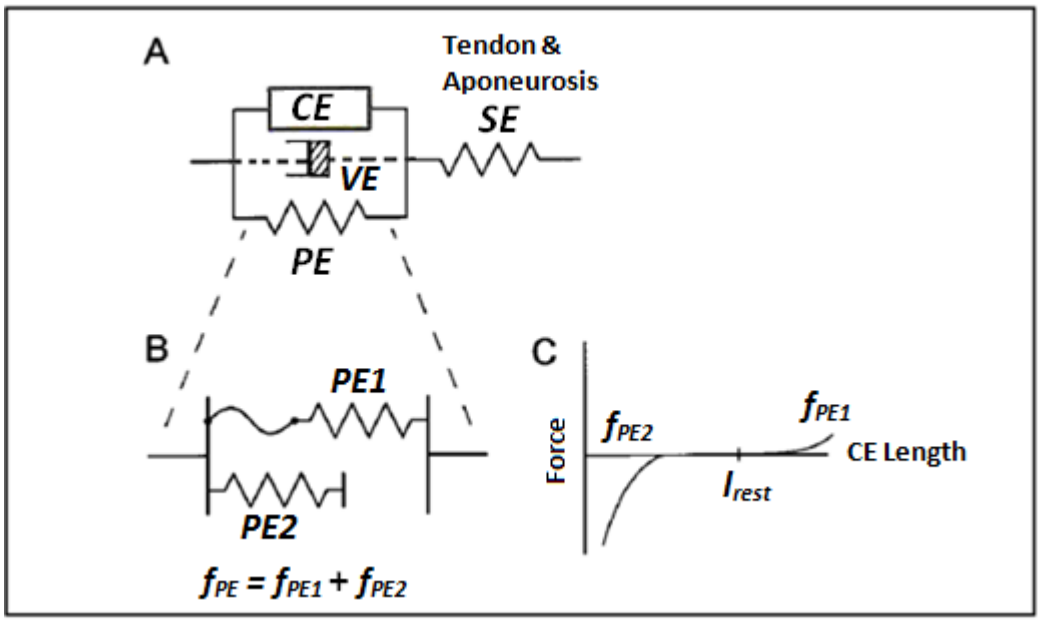

Figure 2.39: A) Representation of Brown muscle model using rheological elements structure. B) The two parts of the passive elastic element *PE*. C) The passive F-L curves of *PE1* and *PE2*. (Adapted from [82, 160]).

Series element passive F-L sub-model (f_{SE}):

The passive force of the series elastic element (represents the combined tendon and aponeurosis) is given as a non-linear function of its length l_{SE}:

$$f_{SE}(\bar{l}_{SE}) = 0.13066 \times \ln\left\{\exp\left[\frac{\bar{l}_{SE} - \bar{l}_S^t}{0.0047}\right] + 1\right\} \quad (2.31)$$

$\bar{l}_S^t = 0.964\ l_{opt}^t$.

Parallel element passive F-L sub-model (f_{PE1}):

The passive elastic force f_{PE1} as a function of $\bar{l}_{CE}$:

$$f_{PE1}(\bar{l}_{CE}) = 1.058 \times \ln\left\{\exp\left[\frac{(\bar{l}_{CE} / \bar{l}_{\max}) - 1.17}{0.046}\right] + 1\right\} \quad (2.32)$$

$l_{\max}$ was used in the "Virtual Muscle" because *PE*1 scales more appropriately with $l_{\max}$ [127].

Passive *PE2* F-L sub-model (f_{PE2}):

The passive elastic resistance to compression at short *CE* lengths ($l_{CE} < 0.7 \times l_{opt}$) is modelled by a non-linear function:

$$f_{PE2}(\bar{l}_{CE}) = -0.02 \times \{\exp[-21 \times (\bar{l}_{CE} - 0.7)] - 1\} \quad , \quad f_{PE2} \le 0 \quad (2.33)$$

Passive *VE* F-V sub-model (f_{VE}):

A small viscosity was added for stability purposes during simulation:

$$f_{VE} = 0.01 \times \bar{v}_{CE} \times \left(\frac{\left|v_{CE,\max}(l_{opt})\right|}{l_{opt}}\right) \quad (2.34)$$

For slow-twitch fibres (type-I):

$$f_{VE} = 0.01 \times \bar{v}_{CE} \times \left(\frac{\left|v_{CE,\max}(l_{opt})\right|}{l_{opt}}\right) = 0.01 \times \left(\frac{\left|-7.88 \times l_{opt}\right|}{l_{opt}}\right) \times \bar{v}_{CE} = 0.0788 \times \bar{v}_{CE}$$

For fast-twitch fibres (types IIa and IIb):

$$f_{VE} = 0.01 \times \bar{v}_{CE} \times \left(\frac{\left|v_{CE,\max}(l_{opt})\right|}{l_{opt}}\right) = 0.01 \times \left(\frac{\left|-9.15 \times l_{opt}\right|}{l_{opt}}\right) \times \bar{v}_{CE} = 0.0915 \times \bar{v}_{CE}$$

iii) Hawkins sub-model for muscle passive elements

Hawkins muscle model is presented in different references [101, 129, 130]. Passive elements of Hawkins model are illustrated in Figure (2.40).

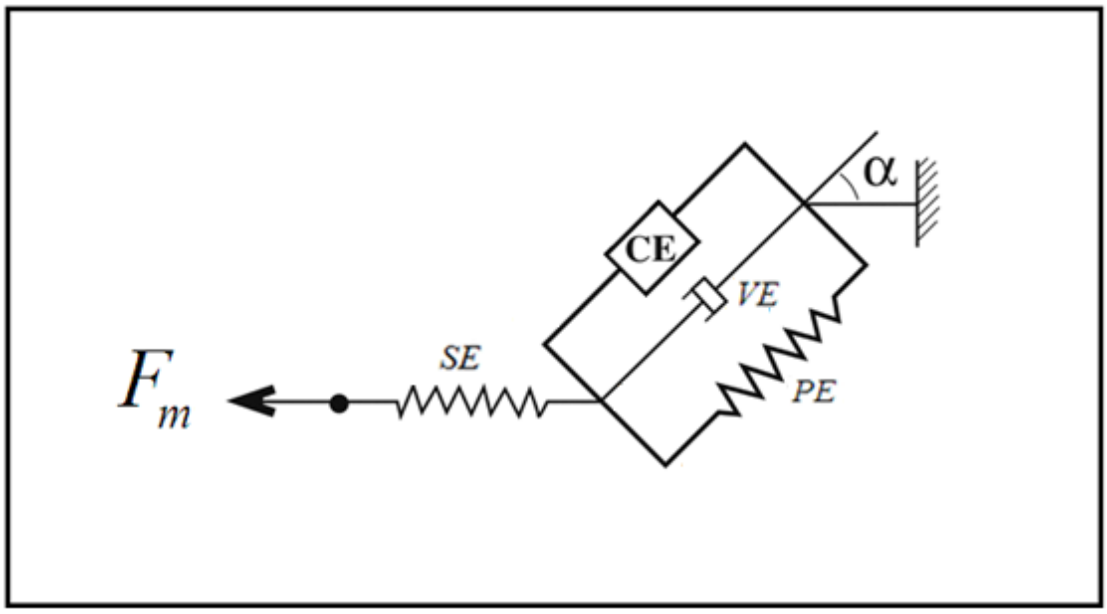

Figure 2.40: Representation of Hawkins muscle model [101, 129, 130] using rheological elements structure.

Series element passive F-L sub-model (f_{SE}):

The aponeurosis is assumed as a rigid structure, the tendon passive force is modelled as:

$$f_{SE}(l_{SE}) = 0.00504 \times \exp\left(147 \times (\bar{l}_{SE} - \bar{l}_S^t)\right) \quad (2.35)$$

Tendon length is normalised to the tendon optimal length l_{opt}^t.

Note that the curve of Hawkins *SE* sub-model is very similar to that of Hatze *SE* sub-model [161]: $f_{SE}(l_t) = c_1 \times \exp\left(c_2 \times (l_t - l_S^t) - 1\right)$. The curve of Hatze *SE* sub-model is almost exactly the same when using the following constants: ($c_1 = 0.314$, $c_2 = 60$) when simulated in Matlab.

Parallel element passive F-L sub-model (f_{PE1}):

$$f_{PE1}(\bar{l}_{CE}) = c_1 \times \exp\left\{10.3 \times (\bar{l}_{CE} - 1.6)\right\} \quad (2.36)$$

The rest length was assumed to be: ($l_{rest} = 1.6$)

$c_1 = 34257.78$

Passive *VE* F-V sub-model (f_{VE}):

For the i[th] fibre-type: $f_{VE,i} = c_i \times v_{CE} \times (1 - R_i)$ (2.37)

i : Fibre-type identifier; (1) for type-I, (2) for type-IIa, and (3) for type-IIb.

c_1, c_2, c_3 : are constants. $c_1 = 0.51585$, $c_2 = c_3 = 0.44195$.

The viscous drag "passive" force created by all non-recruited fibres in the whole muscle:

$$f_{VE} = \sum_{i=1}^{n} f_{VE,i} = f_{VE,1} + f_{VE,2} + f_{VE,3}$$

Units used for *CE* velocity: $v_{CE} = \left[\frac{m}{\sec}\right]$, f_{VE} is normalised with respect to $f_{iso,\max}$.

iv) LifeMOD sub-model for muscle passive elements

In the muscle model used in LifeMOD [137, 138], a two-element Hill-type model (*CE* and *PE*1) is used, see Figure (2.41).

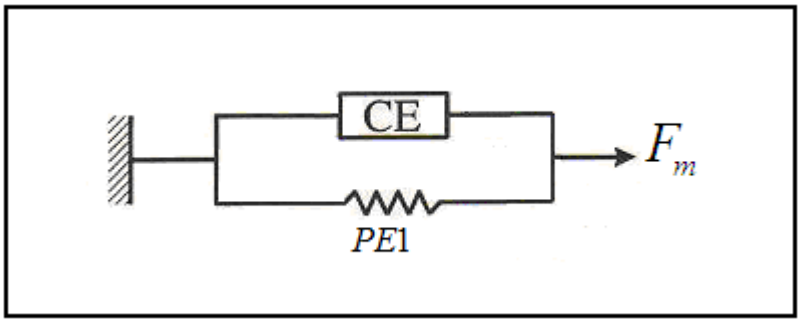

Figure 2.41: Representation of LifeMOD muscle model using rheological elements structure, *SE* is assumed rigid in LifeMOD muscle model [137, 138].

Parallel element passive F-L sub-model (f_{PE1}):

For lengths beyond ($\bar{l}_{rest} = 0.75$), f_{PE1} normalised with respect to $f_{\max}$ is given by:

$$f_{PE1}(\bar{l}_{CE}) = \left(\frac{\bar{l}_{CE} - 0.75}{1.5 - \bar{l}_{CE}}\right) \times c_L \qquad (2.38)$$

$$c_L = \frac{2.338 \times PCSA_m}{f_{iso,\max}},\ PCSA_m = [m^2]$$

$$c_L = \frac{2.338}{ST},\ PCSA_m = [m^2], \text{ the specific tension: } ST = \left[\frac{N}{m^2}\right].$$

2.5.6.3. Implications of the application of passive elements sub-models on the single motor-unit model

The passive elements of *PE1*, *PE2*, and *SE* are not affected by level of recruitment R. The viscous drag "passive" force created by non-recruited motor-units can be properly incorporated into the multiple motor-unit model. However, experimental data available in the literature does not show any difference between different fibre types in the viscous drag "passive" force created by non-recruited motor-units. Until detailed experimental data for different fibre types becomes available, both of the single motor-unit model and the multiple motor-unit model are equal regarding modelling passive elements.

2.5.7. Standard sub-models of the "General Model"

A standard form representing all alternative sub-models of any muscle property is possible. These standard forms can be used to represent any of the simplified alternative sub-models presented in this section or to build a new alternative sub-model at the required level of complexity for any muscle property.

The standard forms were developed in this study to represent each muscle property; description and details are provided in Chapter 6. A "General Model" that can be used to represent all relevant instances from the literature was developed; the topology of the standard forms of the general muscle model and how different sub-models are connected in the "General Model" are described in Chapter 6.

2.6. The need for a multiple motor-unit model for FES applications

As discussed in section 2.4.3, improvements to muscle model accuracy can help improve the performance of FES controllers. Because of the different characteristics of different types of motor-units; recruitment order will affect the calculated muscle force. Also, the properties of different fibre types cannot be incorporated into a single motor-unit model. FES simulations are usually based on single motor-unit models which cannot account for continuously varying recruitment as would usually be seen in closed loop FES control. Such simulations would result in an over- or under-estimation of muscle force and hence inaccurate assessment of the FES system's performance in the real world.

The multiple motor-unit modelling approach may improve model accuracy; since it properly accounts for the physiological properties specific to each fibre-type (i.e. recruitment order, F-L relationship, F-V relationship, and fatigue), and also can account for the continuously varying recruitment levels by modelling each motor-unit separately regarding its length at initial recruitment and time history of recruitment.

2.6.1. How can the multiple motor-unit modelling approach improve model accuracy?

Using this approach of modelling will make the muscle model more complex and will require more parameters to be estimated experimentally, but will increase model accuracy. During FES, the recruitment level can change in a continuous fashion such that different motor-units are recruited at different muscle lengths and at different times. Some muscle properties are highly affected by these changes such as fatigue and force enhancement & depression. Fatigue is highly affected by fibre-type and time history of recruitment, force enhancement/depression is highly affected by the change in *CE* length (displacement) during stretch/shortening, and isometric force is highly affected by the length at initial recruitment. Such properties should be modelled for each motor-unit separately, which can only be achieved by modelling at the motor-unit level.

Specifically, the multiple motor-unit modelling approach is able to properly account for the following properties:

- **i.** Motor-units in the muscle model are of different fibre types that have different contractile properties.
- **ii.** Appropriate non-physiological recruitment order depending on electrodes used.
- **iii.** Different F-L sub-models used with motor-units of different fibre-type.
- **iv.** Different F-V sub-models used with motor-units of different fibre-type.
- **v.** The length at which each motor-unit is initially recruited.
- **vi.** Time history of recruitment for each motor-unit.

These properties cannot be modelled nor be incorporated into a single motor-unit model. The multiple motor-unit model has many advantages over the single *CE* modelling approach. These advantages can be summarised as follows:

1. During FES, stimulation levels could be rapidly and continuously varying which results in different motor-units being recruited and de-recruited at different lengths and

different times. Obviously, this can only be modelled with multiple motor-units modelling approach.

2. During FES, non-physiological recruitment order happens when (the commonly used) surface electrodes are used, and this is the primary cause of fatigue when using FES. For electrically stimulated muscle, physiological recruitment order can only be achieved using special electrodes and special strategies. This case can only be modelled with the multiple motor-unit modelling approach.
3. The F-L relationship of different fibre types is different. Single motor-unit model cannot use more than one F-L relationship, but the multiple motor-unit model can use separate F-L sub-model for each individual motor-unit.
4. The F-V relationship of different fibre types has different curves, including different maximum shortening velocities. Single motor-unit model cannot use more than one relationship, but the multiple motor-unit model can use different F-V sub-model for each motor-unit.
5. Muscle fatigue depends on fibre-type and duration of activity (time history). When different motor-units are recruited and de-recruited at different times the single motor-unit model cannot account for these changes accurately. Only the multiple motor-units model can model each motor-unit separately and take into account the fatigue and recovery cycle for each motor-unit individually.
6. Force enhancement f_e and force depression f_d are length history-dependent. When different motor-units are recruited at different lengths, the only way to accurately model this situation is by the multiple motor-unit modelling approach. In the single CE model it is not possible to accurately model this situation.
7. Muscles of complex structure can be modelled with higher accuracy where different motor-units, even from the same type, can have different lengths and different pennation angles which change in different values during isometric and dynamic situations.

2.6.2. Multiple motor-unit models in the literature (by different authors)

Most muscle models in the literature use single motor-unit modelling approach where the *CE* is modelled as a single unit. Only a few multiple motor-unit models have been reported in the literature [30, 73, 101, 127, 162, 165] (different authors use different names, for example: multi motor-unit model, multi-fibre model, cellular-based model, etc.), none of these have

used initial length in the F-L relationship. Number of motor-units in the multiple motor-unit model does not correspond to real motor-units; it represents the force resolution, more motor-units will increase force resolution and vice versa. Muscle models found in the literature which use this approach include the following:

1. Brown model [81, 82, 83, 84] is a complex multiple motor-unit model. Despite its complex sub-models, some important properties like fatigue, and force enhancement & depression are not included. This model is used in the "Virtual Muscle" software package [127, 128]. Different sub-models of Brown model are summarised in section 2.5.1.
2. Hawkins model [101, 129, 130] is claimed to be a multiple fibre model. However, fibres are modelled in a superficial way, where the portion of each fibre-type is modelled separately not the fibre. The model is divided into three units only, one unit for each fibre-type and linear analogue recruitment is applied on each unit. Different sub-models of Hawkins model are summarised in section 2.5.1.
3. Riener-2 model [73] is a physiologically based model; the multiple motor-unit modelling approach was used to model the recruitment and activation under isometric conditions, two inputs stimulation intensity and stimulation frequency are allowed to vary in this model (frequency not constant). *CE* length is constant and hence this model is not for dynamic conditions. It can be used for FES control under isometric conditions but not dynamic protocols.
4. Liu et al [30] used multiple motor-unit approach only for the purpose of estimating fatigue under isometric conditions and MVC. Unrealistic motor-units are used in this model, where they are considered either fully recruited (100% recruitment), at rest state waiting to be recruited, or fully fatigued. Physiologically this is not true, where motor-units will fatigue and recover gradually as discussed earlier in section 2.5.4. Essential muscle properties (e.g. F-L and F-V relationships) are not considered in this model.
5. Xia and Frey Law [162] model is an improved version of Liu model, where the original Liu model was modified to include submaximal voluntary contraction and dynamic (non-isometric) conditions, but still uses the same principle of unrealistic motor-units.
6. Stojanovic et al. [163, 164, 165] model is a "multi units" model based on Hill's three-element model, the model includes different properties of different fibre types. The *CE* is divided into multi units; each of these units is modelled using finite element

method. However, this model is not considered since it was developed using finite element method which is beyond the scope of this study.

The only model that can be considered here as a good multiple motor-unit model is Brown model [81, 82, 83, 84] where this model was developed using large collection of experimental data for physiological properties of different fibre types. This model is used in the "Virtual Muscle" software package [127, 128]. Brown model was developed for voluntary contraction (not FES). The recent version of Virtual Muscle, VM4.0 [128], has one option for FES in which the stimulation frequency is kept constant and non-physiological recruitment order is applied where recruitment is weighted equally among all fibre types, the recruitment sub-model is summarised in section 2.5.1.2.1.

Brown model uses multiple motor-units approach with complex sub-models for recruitment, activation, F-L and F-V. Yet, important properties such as fatigue and force enhancement & depression are not included in the model. The complex activation sub-model is not needed in the case of FES since frequency is typically constant during FES and the effect of the activation sub-model in this case is negligible. Two fibre types (not three) are modelled.

Riener-2 model [73] accounts for different motor-units being recruited at different times for the fatigue sub-model; it can be used for FES control under isometric conditions only, but not dynamic protocols.

The author proposes a generic complex multiple motor-unit model that has 1000 motor-units and three fibre types, the physiological properties specific to each fibre-type can be modelled separately, the length at initial recruitment l_o and time of recruitment can also be included with each motor-unit to further increase the model accuracy. The modelling of l_o and time of recruitment/non-recruitment with each motor-unit separately has not been used in the literature. Development and details of the "General Model" are provided in Chapter 6.

2.7. Conclusions and overview of rest of the thesis

Skeletal muscle is a highly complex and nonlinear system. The response of electrically stimulated muscle is nonlinear, time varying, coupled, and often accompanied by unpredictable disturbance in SCI subjects. Computer simulations based on accurate mathematical models of the musculoskeletal system would help in the design and evaluation

of FES controllers. The multiple motor-unit modelling approach can improve the model accuracy; since it properly accounts for the physiological properties specific to each fibre-type (i.e. recruitment order, F-L relationship, F-V relationship, and fatigue), and can also account for the continuously varying recruitment levels by modelling each motor-unit separately regarding its length at initial recruitment and time history of recruitment.

In the rest of the thesis, the multiple motor-unit model is compared to the single motor-unit model for the realistic scenario when recruitment levels are rapidly and continuously varying which results in different motor-units being recruited and de-recruited at different lengths and different times.

Chapter 3 addresses the problem of muscle modelling for continuously varying R and hence different values of l_o for different motor-units. Open-loop simulation protocols are used with the multiple motor-unit model and the single motor-unit model using both the *CE* instantaneous length and the *CE* length at initial recruitment for the F-L relationship. Results are discussed at the end.

Chapter 4 addresses the problem of muscle modelling for muscle fatigue with continuously varying R at different times and hence different fatigue and recovery cycles for different motor-units. Open-loop simulation protocols are used with the multiple motor-unit model and the single motor-unit model using both the multiple motor-unit fatigue sub-model and single motor-unit fatigue sub-model. Results are discussed at the end.

Chapter 5 addresses the problem of muscle modelling for force enhancement/depression following active stretch/shortening with continuously varying R. Open-loop simulation protocols are used with the multiple motor-unit model and the single motor-unit model using both the multiple motor-unit force enhancement & depression sub-model and single motor-unit force enhancement & depression sub-model. Results are discussed at the end.

Chapter 6 addresses the development of a new "General model" using standard forms for different sub-models representing all muscle properties and the inter-connection of these sub-models (model topology). The "General Model" is capable of representing the alternative sub-models (for each muscle property), and hence all relevant models from the literature. Such a "General Model" could be used to study the effect of muscle model complexity on FES controller design.

Chapter 3: The Multiple Motor-Unit Muscle Model

3.1. Introduction

In normal human movement, it is reasonable to assume that the recruitment level R changes continuously. Similarly, in closed loop FES control applications R will usually vary with time. As discussed in sections 2.5.2 and 2.5.5 and Appendix 2, because the length of the contractile element *CE* at initial recruitment (l_o) is thought to be a key parameter influencing total muscle force F_m, via the muscle's F-L relationship, the use of a single value for l_o in a realistic scenario where R and l_{CE} are changing continuously would result in an over- or under-estimation of F_m. However, as almost all muscle models used in FES control studies treat the muscle as a single contractile element (i.e. one large motor-unit), there can only be one value for l_o despite the fact that in reality different motor-units are recruited at different lengths. In most previous work on FES control [1, 72, 74, 109, 113], a compromise is adopted whereby the instantaneous *CE* length is used rather than the initial length. However, this does not reflect the way in which the F-L relationship of a muscle (or muscle fibre) is believed to act as the input should be length at initial recruitment, not instantaneous length.

Therefore, this chapter addresses the problem of muscle modelling for continuously varying R and hence different values of l_o for different motor-units. A new multiple motor-unit model is developed which considers the muscle to comprise a large number (1000) of individual Hill-type virtual motor-units. These virtual motor-units are connected in parallel and can be either on or off, mimicking the structure and behaviour of physiological motor units. Details on the structure of skeletal muscles, together with the recruitment process are provided in section 2.2.

The Herzog model, a relatively simple Hill-type model, was chosen for its simplicity and also because it uses the *CE* length at initial recruitment (l_o). An overview of Hill-type models is provided in section 2.4.2 and the Herzog model is summarised in Appendix 3.

As the recruitment level $R(t)$ may vary during stimulation, these virtual motor-units are recruited at different times and each with its own initial length ($l_{o,j}$ for j=1 to 1000); thus

overcoming the problem described above. It should be noted that the virtual motor-units in the model do not correspond to real motor-units. Rather, the number of virtual motor-units used in the model is chosen to give the required force resolution. For example, if a resolution of 1% is required, then a model based on 100 motor-units would be used (this is calculated by dividing one by the required resolution, i.e. $\frac{1}{1\%} = \frac{1}{1/100} = 100$).

The multiple motor-unit model has been implemented in two ways. Firstly, by only using the 1000 virtual motor-units to model recruitment and calculate the isometric force (i.e. to apply the F-L relationship) and then treating the muscle as a single motor-unit (single *CE*) when applying the F-V relationship using one single value for the isometric force $f_{iso}(l_o)$. Secondly, by also applying the F-V relationship separately for each virtual motor-unit individually (different motor-units can have different values for $f_{iso}(l_o)$). The relative merits of these two approaches are discussed at the end of the chapter.

3.2. Effective isometric force model

In the original Herzog model, which incorporated a single *CE*, it was assumed that the muscle remembers the *CE* length l_0 at which it was initially recruited for as long as the recruitment remains (i.e. $R > 0$). This is acceptable if the recruitment remains constant, but it is not accurate if R changes during stimulation, as different motor-units are recruited or de-recruited at different lengths each time there is a change in R. To take account of the recruitment of motor-units at different lengths, the isometric force $f_{iso}(l_o)$ (using one initial length) was replaced by an effective isometric force ($Eff.f_{iso}$). The effective isometric force model is presented in Figure 3.1 and Figure 3.2 and is a "novel contribution" to the field. It is based on the multiple motor-unit principle, where every motor-unit (of index *j*) remembers the length ($l_{0,j}$) at which it was initially recruited.

As discussed in section 2.5.1, the instantaneous value of the analogue recruitment $R(t)$, shown in Figure 3.1, is used as a representation of the proportion of recruited motor-units. $R(t)$ has a value between 0 (no recruitment) and 1 (all motor-units are recruited), $0 \le R(t) \le 1$. An extension to the work presented here, to include modelling of recruitment of three different fibre-types is introduced in Chapter 6.

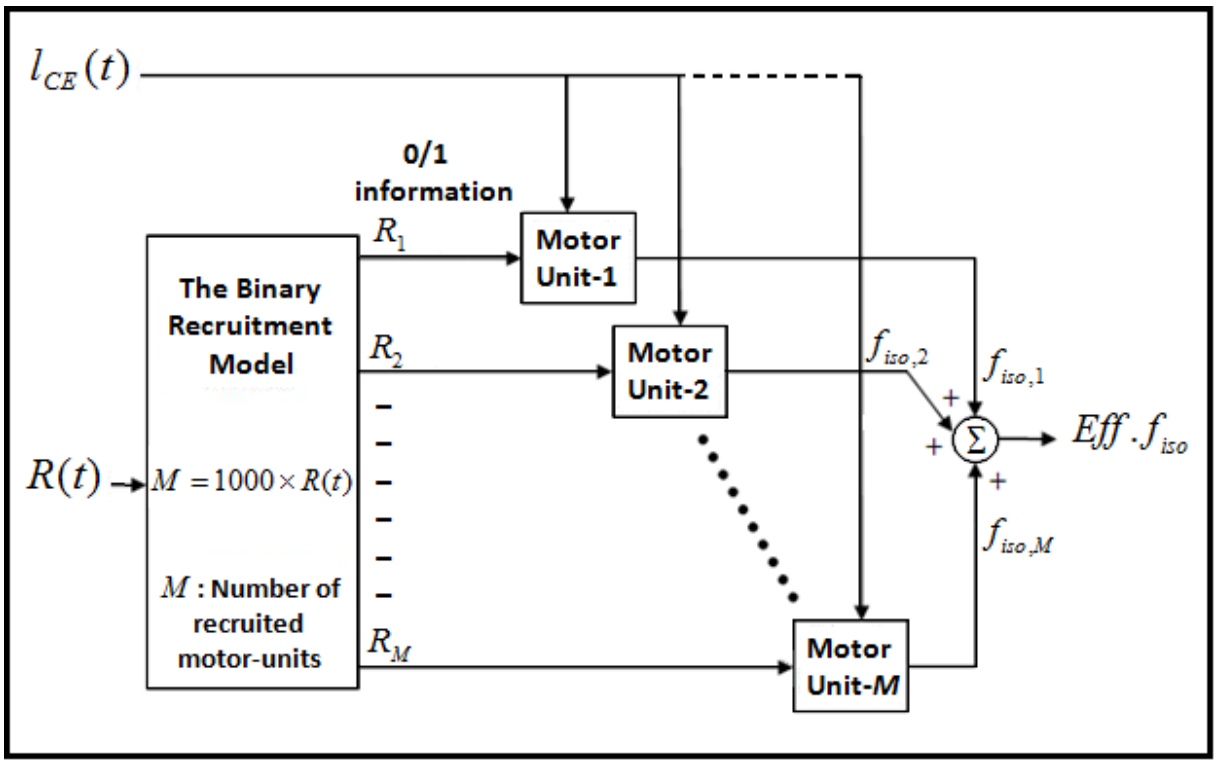

Figure 3.1: Effective isometric force model.

The binary recruitment sub-model calculates the number of recruited motor-units. The input to the binary recruitment sub-model is $R(t)$, where $R(t)$ is the output of the analogue recruitment sub-model (see section 2.5.1). In this example, the total number of virtual motor-units (m) is $m = 1000$, number of recruited motor-units (M) is $M = m \times R(t) = 1000 \times R(t)$. Every recruited motor-unit is treated as a separate fully recruited *CE* for the purposes of calculating the isometric force.

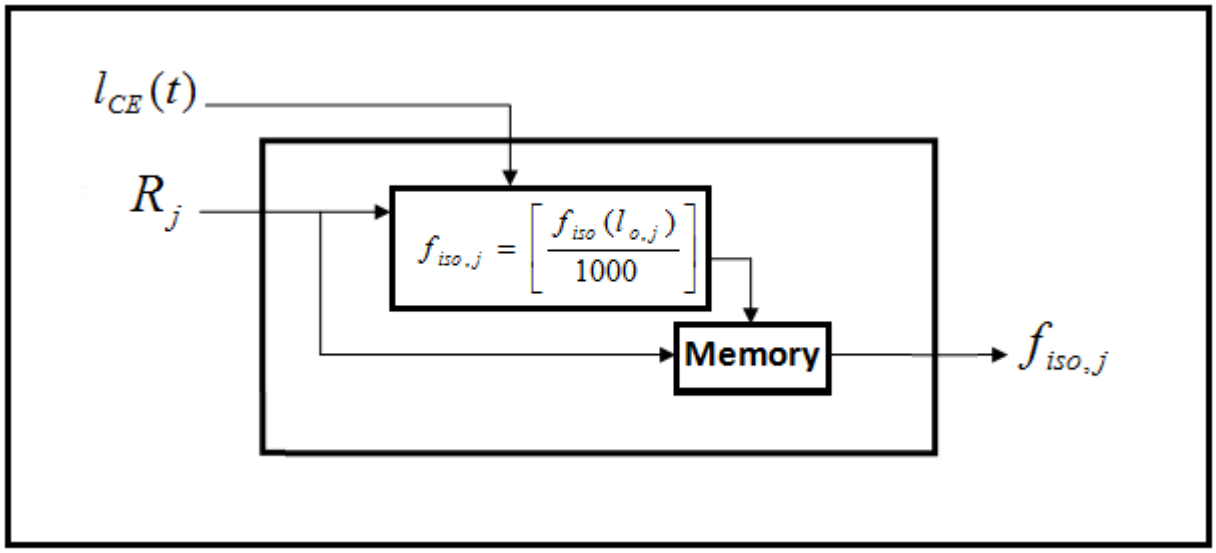

Figure 3.2: Isometric force of a single motor-unit.

In Figure 3.2, every recruited motor-unit remembers the length at which it was initially recruited. The isometric force of the whole muscle $f_{iso}(l_{o,j})$ is divided by the number of virtual motor-units used in the multiple motor-unit model (1000).

Input to the analogue recruitment sub-model is typically the pulse width (i.e. $R=PW/PW_{max}$, where PW_{max} is the pulse width that corresponds to maximum recruitment). Total "isometric" muscle force is controlled by the number of recruited motor-units M and the force produced by each recruited motor-unit. m is the total number of all motor-units in the model. The total number of motor-units in the model, m, is chosen by the user to give the required force resolution and does not correspond to the real number of motor-units.

In order to get a high resolution, the number of virtual motor-units m was chosen to be 1000, so the number of recruited motor-units is: $M = 1000 \times R(t)$, where $R(t)$ varies between 0 and 1 ($0 \le M \le 1000$). The value of M will be rounded to the nearest integer and, hence, the smallest detectable change in R is 0.001 ($\Delta M = 1$). A positive change in $R(t)$ means more motor-units are recruited and a negative change in $R(t)$ means some, or even all, motor-units will be de-recruited. If $R(t)$ is decreased (i.e. $\Delta R(t) < 0$) then a new M value will be calculated and the motor-units that were recruited last will be de-recruited first. This means that all motor-units of index (j) higher than the new M will be fully de-recruited.

Referring to Figure 3.2, every recruited motor-unit remembers the length at which it was initially recruited for as long as it is still recruited. Once the motor-unit is de-recruited that length will be erased from memory. The inputs to each motor-unit model are the binary recruitment R_j of the j^{th} motor-unit and the instantaneous *CE* length l_{CE}, where R_j can only be 0 or 1 (either 0% or 100% recruitment). Each motor-unit model only re-calculates its associated isometric force $f_{iso,j}$ when R_j changes from 0 to 1 and from 1 to 0. When R_j changes from 0 to 1, the j^{th} motor-unit is recruited, a new value of $f_{iso,j}$ is calculated from the F-L relationship for the *CE* length at that particular time, and this is stored in the j^{th} motor-unit's memory. When R_j changes from 1 to 0, the j^{th} motor-unit is de-recruited and its memory erased ($f_{iso,j} = 0$). Finally, the effective isometric force of the whole muscle is the sum of the individual forces $f_{iso,j}$ produced by all recruited motor-units.

In Herzog's single motor-unit muscle model [18], the normalised isometric muscle force is approximated by the positive values of a parabola as follows:

$$FL(l_o) = \frac{f_{iso}(l_o)}{f_{iso,\max}} = [-2.777(l_o / l_{opt})^2 + 5.554(l_o / l_{opt}) - 1.777] \qquad (3.1)$$

This parabola has positive values for "normalised" *CE* length values of: $0.4 < \bar{l}_{CE} < 1.6$.

Where $f_{iso}(l_o)$ is the isometric muscle force in Newton [N] as a function of *CE* length (l_o) at the moment of initial recruitment. $\bar{l}_{CE}$ is the instantaneous *CE* length normalized with respect to the optimal *CE* length, $\bar{l}_{CE} = \frac{l_{CE}}{l_{opt}}$.

Herzog's F-L sub-model [18] is relatively simple and, for this reason, it has been used in this first implementation of the multiple motor-unit model. With the muscle now represented by 1000 virtual motor-units, the force produced by a single motor-unit $f_{iso,j}$ will be one thousandth of the corresponding whole muscle isometric force if it was fully recruited at the same length as follows:

$$f_{iso,j} = \frac{f_{iso}(l_{o,j})}{1000} = \frac{f_{iso,\max}}{1000}.[-2.777(l_{o,j}/l_{opt})^2 + 5.554(l_{o,j}/l_{opt}) - 1.777] \quad (3.2)$$

Where $l_{o,j}$ is the *CE* length at the time of initial recruitment for the j^{th} motor-unit. $f_{iso}(l_{o,j})$ is the isometric force of the whole muscle at the length when the j^{th} motor-unit was initially recruited.

In equation 3.2, $f_{iso}(l_{o,j})$ is divided by (1000) because the multiple motor-unit model uses 1000 virtual motor-units. If a different number of virtual motor-units m is used then that number should be used in the equation. The effective isometric muscle force is the summation of the forces produced by all motor-units. Given that only the recruited motor-units produce force, it is also equal to the summation of the forces produced by just the recruited motor-units as follows:

$$Eff.f_{iso} = f_{iso,1} \times R_1 + f_{iso,2} \times R_2 + ... + f_{iso,1000} \times R_{1000} = \sum_{j=1}^{1000} f_{iso,j} \times R_j = \sum_{j=1}^{M} f_{iso,j} \quad (3.3)$$

The remainder of the original Herzog model (F-V relationship and passive elements) is not dependent on the *CE* length at initial recruitment. For this reason, this was implemented for the muscle as a whole rather than for the individual motor-units. Hence, this part of the model implementation is similar to that of Herzog [18] but with the isometric force $f_{iso}(l_o)$ of Herzog's single motor-unit model replaced by the effective isometric force $Eff.f_{iso}$, the calculation of which has been explained above.

As explained in Appendix 3, the author adapted Herzog's single motor-unit model to simplify its use in simulation. Replacing $[R \times f_{iso}(l_o)]$ by $Eff.f_{iso}$ in the derivation described below.

3.2.1. Derivation of $\dot{F}_m$ for Herzog's single motor-unit model

Using equations A3.3, A3.6 and A3.8 (see Appendix 3) and by substitution for v_{CE} in the formulas (of equation A3.3) and their conditions:

i) First Equation:

$$F_m - k_p \times \Delta l_{mt} = R \times 0 = 0$$

$$F_m = k_p \times \Delta l_{mt}$$

$$\dot{F}_m = k_p \times v_{mt} \quad for \quad v_{mt} \le \left(\frac{\dot{F}_m}{(k_p + k_s)} - \frac{b.f_{iso}(l_0)}{a.\left(1 + \frac{k_p}{k_s}\right)} \right) \tag{3.4A}$$

ii) Second Equation:

$$F_m - k_p \times \Delta l_{mt} = R \times \frac{f_{iso}(l_0)b + a.\left(\left(1 + \frac{k_p}{k_s}\right) \times v_{mt} - \frac{\dot{F}_m}{k_s}\right)}{b - .\left(\left(1 + \frac{k_p}{k_s}\right) \times v_{mt} - \frac{\dot{F}_m}{k_s}\right)} = \frac{R.b.f_{iso}(l_0) + R.a.\left(1 + \frac{k_p}{k_s}\right) \times v_{mt} - R.a.\frac{\dot{F}_m}{k_s}}{b - \left(1 + \frac{k_p}{k_s}\right) \times v_{mt} + \frac{\dot{F}_m}{k_s}}$$

$$\frac{\dot{F}_m}{k_s}(R.a + (F_m - k_p \times \Delta l_{mt})) =$$

$$b.R.f_{iso}(l_o) - b(F_m - k_p \times \Delta l_{mt}) + (F_m - k_p \times \Delta l_{mt}).\left(1 + \frac{k_p}{k_s}\right) \times v_{mt} + R.a.\left(1 + \frac{k_p}{k_s}\right) \times v_{mt}$$

$$\dot{F}_m = \frac{b(R.f_{iso}(l_o) - F_m + k_p \times \Delta l_{mt}) + \left(1 + \frac{k_p}{k_s}\right).(R.a + F_m - k_p \times \Delta l_{mt}) \times v_{mt}}{\frac{1}{k_s}(R.a + F_m - k_p \times \Delta l_{mt})}$$

$$for \quad \left(\frac{\dot{F}_m}{(k_p + k_s)} - \frac{b.f_{iso}(l_0)}{a.\left(1 + \frac{k_p}{k_s}\right)} \right) < v_{mt} \le \frac{\dot{F}_m}{(k_p + k_s)} \tag{3.4B}$$

iii) Third Equation:

$$F_m - k_p \times \Delta l_{mt} = 1.5R.f_{iso}(l_0) - 0.5R \frac{f_{iso}(l_0)b' - a'\left(\left(1 + \frac{k_p}{k_s}\right) \times v_{mt} - \frac{\dot{F}_m}{k_s}\right)}{\left(1 + \frac{k_p}{k_s}\right) \times v_{mt} - \frac{\dot{F}_m}{k_s} + b'}$$

$$2(F_m - k_p \times \Delta l_{mt}) - 3R.f_{iso}(l_0) = \frac{-R.f_{iso}(l_0)b' + R.a'\left(1+\frac{k_p}{k_s}\right)\times v_{mt} - R.a'\frac{\dot{F}_m}{k_s}}{\left(1+\frac{k_p}{k_s}\right)\times v_{mt} - \frac{\dot{F}_m}{k_s} + b'}$$

$$\left(2(F_m - k_p \times \Delta l_{mt}) - 3R.f_{iso}(l_0)\right)\times\left(1+\frac{k_p}{k_s}\right)\times v_{mt} - \frac{\dot{F}_m}{k_s}\left(2(F_m - k_p \times \Delta l_{mt}) - 3R.f_{iso}(l_0)\right)$$

$$+ b'\left(2(F_m - k_p \times \Delta l_{mt}) - 3R.f_{iso}(l_0)\right) = -R.f_{iso}(l_0)b' + R.a'\left(1+\frac{k_p}{k_s}\right)\times v_{mt} - R.a'\frac{\dot{F}_m}{k_s}$$

$$\frac{\dot{F}_m}{k_s}\left[3R.f_{iso}(l_0) - 2(F_m - k_p \times \Delta l_{mt}) + R.a'\right] =$$

$$b'\left[2R.f_{iso}(l_0) - 2(F_m - k_p \times \Delta l_{mt}) - R.f_{iso}(l_0)\right] + \left[3R.f_{iso}(l_0) - 2(F_m - k_p \times \Delta l_{mt}) + R.a'\right]\left(1+\frac{k_p}{k_s}\right)\times v_{mt}$$

$$\dot{F}_m = \frac{2b'\left[R.f_{iso}(l_o) - (F_m - k_p \times \Delta l_{mt})\right] + \left[R.(3f_{iso}(l_o) + a') - 2(F_m - k_p \times \Delta l_{mt})\right]\left(1+\frac{k_p}{k_s}\right)\times v_{mt}}{\frac{1}{k_s}\left[R.(3f_{iso}(l_o) + a') - 2(F_m - k_p \times \Delta l_{mt})\right]}$$

$$for \quad \frac{\dot{F}_m}{(k_p + k_s)} < v_{mt} \le \left(\frac{\dot{F}_m}{(k_p + k_s)} - \frac{b'.f_{iso}(l_0)}{a'.\left(1+\frac{k_p}{k_s}\right)}\right) \qquad (3.4C)$$

iv) Fourth Equation:

$$F_m - k_p \times \Delta l_{mt} = 1.5R.f_{iso}(l_0)$$

$$F_m = k_p \times \Delta l_{mt} + 1.5R.f_{iso}(l_0)$$

$$\dot{F}_m = k_p \times v_{mt} \quad for \quad \left(\frac{\dot{F}_m}{(k_p + k_s)} - \frac{b'.f_{iso}(l_0)}{a'.\left(1+\frac{k_p}{k_s}\right)}\right) < v_{mt} \qquad (3.4D)$$

The replacement of $\left[R\times f_{iso}(l_o)\right]$ by $Eff.f_{iso}$ leads to equation 3.5 below for the rate of change of total force $\dot{F}_m$ produced by the musculotendon complex.

$$\dot{F}_m = \begin{cases} k_p v_{mt} & for \quad v_{mt} \le \left(\dfrac{\dot{F}_m}{(k_p + k_s)} - \dfrac{bEff \,.\, f_{iso}}{Ra\left(1 + \dfrac{k_p}{k_s}\right)} \right) \\ \dfrac{b(Eff \,.\, f_{iso} - F_m + k_p \Delta l_{mt}) + \left(1 + \dfrac{k_p}{k_s}\right)(Ra + F_m - k_p \Delta l_{mt}) v_{mt}}{\dfrac{1}{k_s}(R.a + F_m - k_p \times \Delta l_{mt})} & for \quad \left(\dfrac{\dot{F}_m}{(k_p + k_s)} - \dfrac{bEff \,.\, f_{iso}}{Ra\left(1 + \dfrac{k_p}{k_s}\right)} \right) < v_{mt} \le \dfrac{\dot{F}_m}{(k_p + k_s)} \\ \dfrac{2b'\left[Eff \,.\, f_{iso} - (F_m - k_p \Delta l_{mt})\right] + \left[(3Eff \,.\, f_{iso} + Ra') - 2(F_m - k_p \Delta l_{mt})\right]\left(1 + \dfrac{k_p}{k_s}\right) v_{mt}}{\dfrac{1}{k_s}\left[(3Eff \,.\, f_{iso} + Ra') - 2(F_m - k_p \Delta l_{mt})\right]} & for \quad \dfrac{\dot{F}_m}{(k_p + k_s)} < v_{mt} \le \left(\dfrac{\dot{F}_m}{(k_p + k_s)} - \dfrac{b'Eff \,.\, f_{iso}}{Ra'\left(1 + \dfrac{k_p}{k_s}\right)} \right) \\ k_p v_{mt} & for \quad \left(\dfrac{\dot{F}_m}{(k_p + k_s)} - \dfrac{b'Eff \,.\, f_{iso}}{Ra'\left(1 + \dfrac{k_p}{k_s}\right)} \right) < v_{mt} \end{cases} \tag{3.5}$$

Then total musculotendon force is obtained by integration of $\dot{F}_m$ with respect to time.

$$F_m = \int \dot{F}_m \quad dt \tag{3.6}$$

In summary, Herzog's F-L sub-model has been replaced by the effective isometric force $Eff.f_{iso}$. Because the calculation of $Eff.f_{iso}$ is based on the length of each motor-unit when that motor-unit was recruited ($l_{o,j}$), the multiple motor-unit model properly accounts for continuously varying recruitment $R(t)$ as would usually be seen in closed loop FES control. Conversely, Herzog's single motor-unit model does not take into account the time history of muscle recruitment $R(t)$ because the isometric force $f_{iso}(l_o)$ is calculated using the length l_o at the moment of initial recruitment for the whole muscle (regardless of the dynamic variations in recruitment during simulation).

3.3. Effective *CE* force model

In the effective *CE* force ($Eff.f_{CE}$) model, each one of the muscle's 1000 motor-units is modelled using a separate Herzog single motor-unit model, including both the F-L and F-V sub-models. This served two purposes, firstly it allowed the incorporation of additional features that are best modelled using a multiple motor-unit approach (see chapters 4, 5 and 6) and, secondly, it served to validate the $Eff.f_{iso}$ model.

The effective *CE* force model is presented in Figure 3.3; the binary recruitment sub-model is the same as that of the effective isometric force model. The isometric force $f_{iso,j}$ of each recruited motor-unit is calculated separately using equation 3.2 in the same way as the effective isometric force model and as shown in Figure 3.2. Herzog's F-V sub-model is then used for each motor-unit separately, Herzog's muscle model is summarised in Appendix 3. The force of a single motor-unit is calculated as follows:

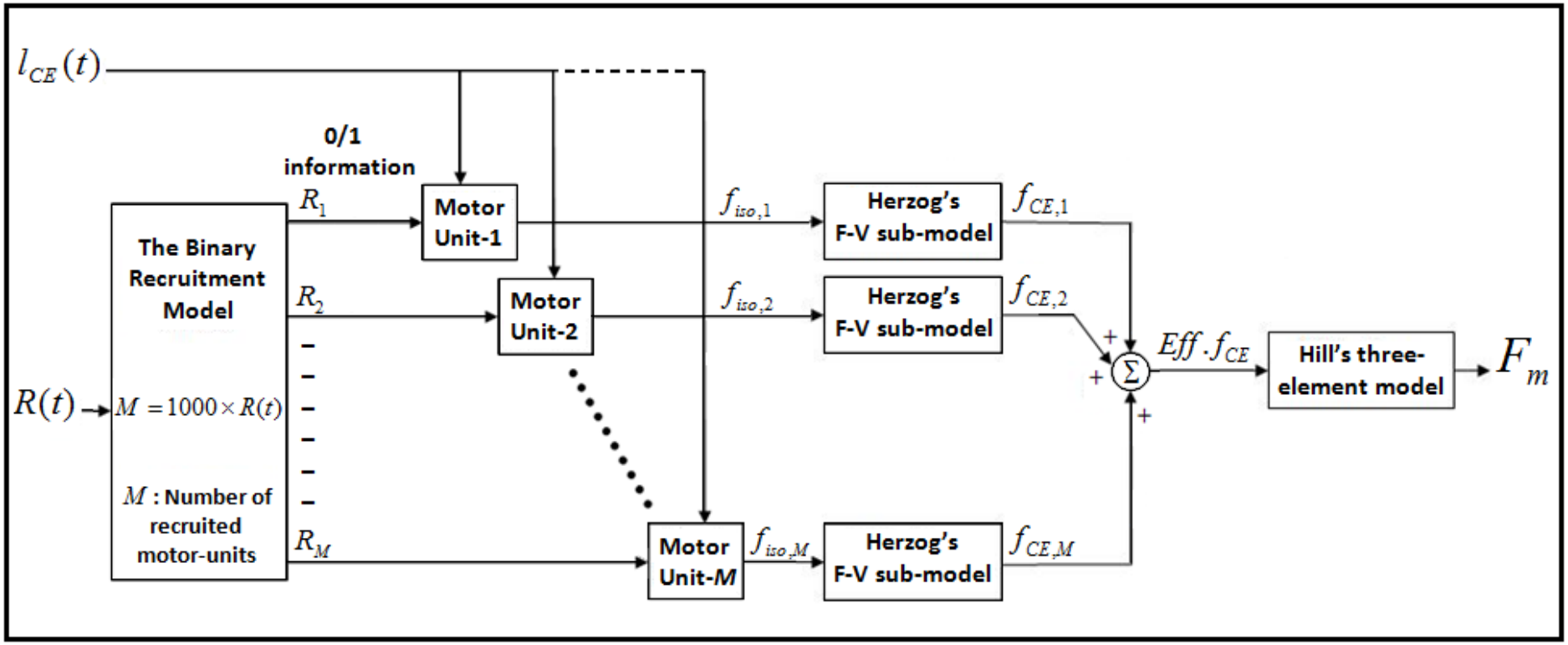

Figure 3.3: Effective *CE* force model. Every recruited motor-unit is treated as a separate fully recruited *CE* for the purposes of calculating the isometric and non-isometric forces for each motor-unit separately.

$$f_{CE,j} = f_{CE,j}(v_{CE}, l_{0,j}) = \left\{ \begin{array}{c} 0 \quad for \quad v_{CE} \le -f_{iso}(l_{0,j})\dfrac{b}{a} \\ \dfrac{f_{iso}(l_{0,j})b + av_{CE}}{-v_{CE} + b} \quad for \quad -f_{iso}(l_{0,j})\dfrac{b}{a} < v_{CE} \le 0 \\ 1.5 f_{iso}(l_{0,j}) - 0.5\dfrac{f_{iso}(l_{0,j})b' + a'v_{CE}}{v_{CE} + b'} \quad for \quad 0 < v_{CE} \le f_{iso}(l_{0,j})\dfrac{b'}{a'} \\ 1.5 f_{iso}(l_{0,j}) \quad for \quad v_{CE} > f_{iso}(l_{0,j})\dfrac{b}{a'}' \end{array} \right\} \tag{3.7}$$

The total *CE* force is the sum of all forces ($f_{CE,j}$) produced by all recruited motor-units:

$$Eff.f_{CE} = f_{CE,1} + f_{CE,2} + ... + f_{CE,M} = \sum_{j=1}^{M} f_{CE,j} \tag{3.8}$$

Non-recruited motor-units (of index higher than *M*) do not produce force. The simulation protocols used in this Chapter and in the subsequent chapters include cycles of stretch/shortening for the musculotendon complex. The equation for $\dot{F}_m$ (equation 3.5) cannot be used with the $Eff.f_{CE}$ model because in this equation the passive elements are assumed to apply to the muscle as a whole and cannot be split into multiple units, whereas the F-V sub-model need to be applied separately for each motor-unit in the $Eff.f_{CE}$ model using the same passive elements as in the single motor-unit model. In order to determine the present *CE* length, *CE* velocity, and *CE* force at any instant during the simulation, an iterative approach is used, this approach is summarised below.

Starting at ($t = t_o$), the algorithm steps through the inputs $l_{mt}(t)$ and $R(t)$. At any given time, t as the instantaneous forces of *CE* and *SE* (f_{CE} and f_{SE}) have to be equal (see Appendix 3), an iterative approach can be utilized to solve for the instantaneous lengths and velocities of both *CE* and *SE*. This approach can be used to approximate the lengths of *CE* and *SE* when simulating the responses to simulation protocols of a muscle model. When the muscle becomes recruited, previous *CE* length information (of previous time-increment ($t - h$), where h is a small time-increment) can be used in an iterative approach to determine

the present *CE* length, *CE* velocity, and *CE* force at that instant. At each iteration *CE* force is compared to the corresponding *SE* force for the *CE* and *SE* lengths specified. If the *CE* and *SE* forces are not equal, then a new *CE* length is assigned and the iterative process is repeated. These steps will be repeated until *CE* force and *SE* force are equal (within a small pre-specified tolerance band). At this point, the next time step in the simulation is initiated by reading in new values for l_{mt} and R.

The iterative approach is illustrated in the flow-chart shown in Figure 3.4, this flow-chart represents the algorithm implemented in the $Eff.f_{CE}$ Matlab code. A detailed description of the iterative approach for a recruited muscle with a single motor-unit (single *CE*) model is as follows:

i) At time ($t = t_o$), first guess ($i = 1$) for *CE* length: Assume: $l_{CE,i}(t) = l_{CE}(t-h)$.

ii) Calculate the first guess for *SE* length using *CE* length of previous step: $l_{SE,1} = l_{mt}(t) - l_{CE,i}(t)$.

iii) Calculate $f_{CE} = f_{CE}(v_{CE}, l_{CE})$ of Herzog F-V sub-model (equation A3.3 in Appendix 3), using $l_{CE,i}(t)$ of previous step and: $v_{CE,i}(t) = \dfrac{l_{CE,i}(t) - l_{CE}(t-h)}{h}$.

iv) Since *CE* and *SE* are connected in series, then: $f_{CE} = f_{SE}$, solve for the second guess for *SE* length $l_{SE,2}$: $f_{CE} = f_{SE} = k_S \times \Delta l_{SE} = k_S \times (l_{SE,2} - l_S^t)$, l_S^t: tendon slack length. The second guess for *SE* length is: $l_{SE,2} = \dfrac{f_{SE}}{k_S} + l_S^t$.

v) Compare $l_{SE,1}$ and $l_{SE,2}$, are they equal within pre-specified tolerance band ($l_{SE,1} \approx l_{SE,2}$) ?

vi) If step (v) is not satisfied then repeat steps (ii) (iii) (iv) and (v) using the following equation as the next guess for *CE* length: $l_{CE,i}(t) = l_{mt}(t) - \left(\dfrac{l_{SE,1} + l_{SE,2}}{2} \right)$.

vii) If step (v) is satisfied then use the last guess of *CE* length and *CE* velocity to calculate *CE* force: $f_{CE} = f_{CE}(v_{CE}, l_{CE})$, and then total muscle force: $F_m = (k_p \times \Delta l_{mt}) + f_{CE}$.

viii) Go to step (i) and do the first guess of *CE* length for next time increment. The algorithm will stop at ($t = T$).

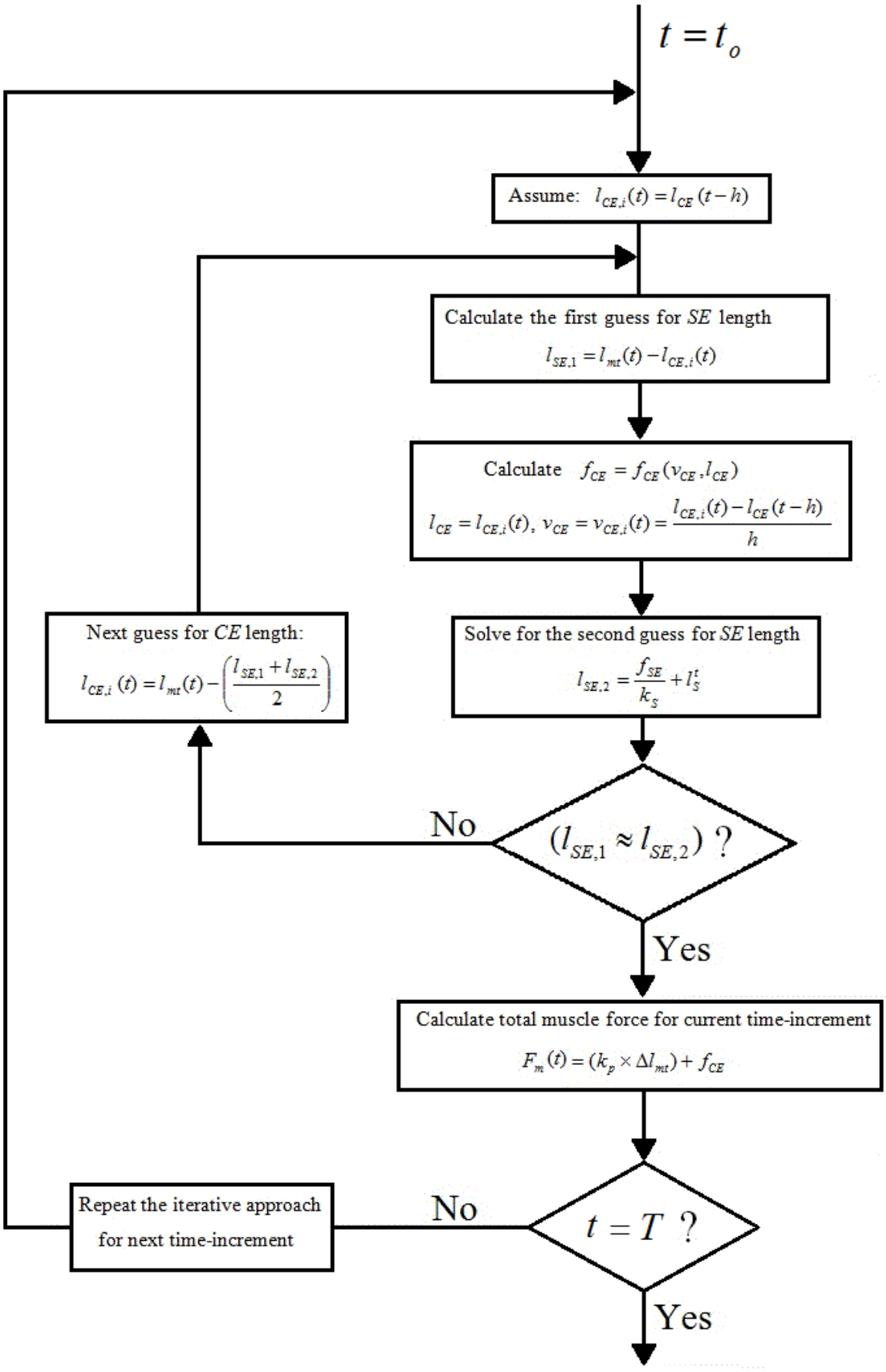

Figure 3.4: Flow-chart of the iterative approach for a recruited muscle with single motor-unit (single *CE*) model.

Finally, the effective *CE* force ($Eff.f_{CE}$) of all recruited motor-units is used to calculate the total muscle force F_m in a similar way as in the single motor-unit model (equation A3.8 in Appendix 3).

$$F_m = (k_p \times \Delta l_{mt}) + \sum_{j=1}^{M} f_{CE,j} = (k_p \times \Delta l_{mt}) + Eff.f_{CE} \qquad (3.9)$$

In summary, this is another version of the multiple motor-unit model and has been called the effective *CE* force model ($Eff.f_{CE}$). It is similar to the $Eff.f_{iso}$ model; the main difference is that the F-V sub-model is applied on each recruited motor-unit separately. As will be explained in Chapter 6, different fibre types can have different sub-models for the same muscle property (e.g. F-V sub-model). This is an advantage for the $Eff.f_{CE}$ model over the $Eff.f_{iso}$ model, since the $Eff.f_{CE}$ model allows the incorporation of additional features using the multiple motor-unit modelling approach.

3.4. Simulation results

Matlab codes were developed for simulating the responses to open-loop simulation protocols of three muscle models:

- The Herzog model (treating the muscle as a single motor-unit);
- The $Eff.f_{iso}$ multiple motor-unit model;
- The $Eff.f_{CE}$ multiple motor-unit model.

Additionally, in all three cases, the *CE* length used for the F-L relationship can be either the instantaneous length or the length at initial recruitment.

In the following sections; firstly, the two input protocols that have been used are defined. Then simulation results are presented to compare the alternative muscle models and, in particular, to demonstrate the potential errors introduced by: a) treating the muscle as a single motor-unit; and b) using instantaneous *CE* length instead of *CE* length at initial recruitment.

3.4.1. Input protocols

In order to demonstrate the need to use a multiple motor-unit modelling approach when R and l_{CE} vary with time, input protocols are required that involve changing both R and l_{CE}. Two suitable protocols that have previously been used by Herzog [18] were chosen as this allowed comparison with his simulation results for validation purposes (single motor-unit model only). Details of the two protocols are as follows:

Protocol-I (Figure 3.5):

(i) At $t = 0.0$ seconds: Full isometric recruitment at the unique resting state (i.e. at $l_{CE} = l_{rest} = 125 \quad mm,\ \Delta l_{mt} = 0$);

(ii) At $t = 1.0$ seconds: Stretch of 10 mm at speed of 10mm/sec for one second;

(iii) Between $t = 2.0$ and $t = 3.0$: No change in R nor in l_{mt};

(iv) At $t = 3.0$ seconds: Partial (50%) de-recruitment;

(v) At $t = 4.0$ seconds: Shortening of 10 mm (to $\Delta l_{mt} = 0$) at speed of 10mm/sec for one second;

(vi) At $t = 5.0$ seconds: Re-recruitment to 100% level.

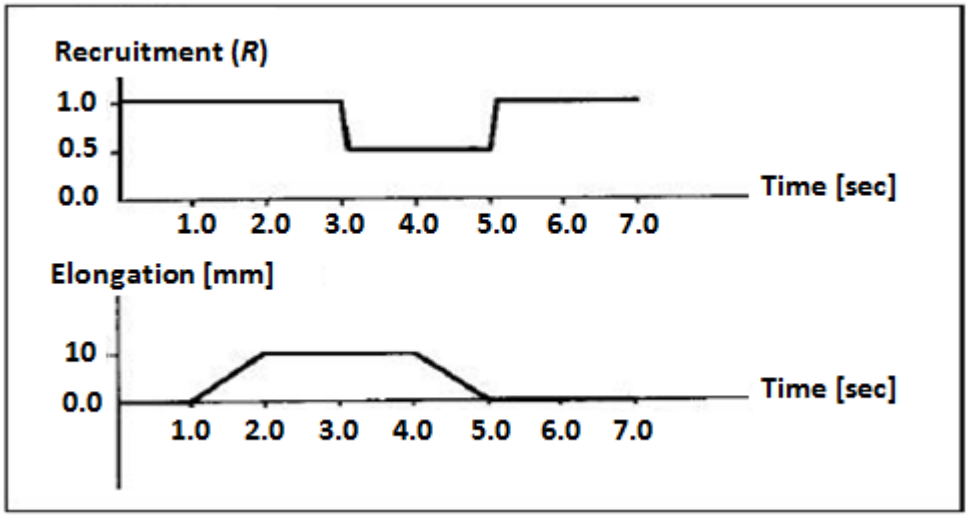

Figure 3.5: Protocol-I. (From [18]).

Protocol-II (Figure 3.6):

(i) At $t = 0.0$ seconds: Partial (50%) isometric recruitment at the unique resting state (i.e. at $l_{CE} = l_{rest} = 125 \quad mm,\ \Delta l_{mt} = 0$);

(ii) At $t = 1.0$ seconds: Stretch of 10 mm at speed of 10mm/sec for one second;

(iii) Between $t = 2.0$ and $t = 3.0$: No change in R nor in l_{mt};

(iv) At $t = 3.0$ seconds: Full (100%) recruitment;

(v) At $t = 4.0$ seconds: Shortening of 10 mm (to $\Delta l_{mt} = 0$) at speed of 10mm/sec for one second.

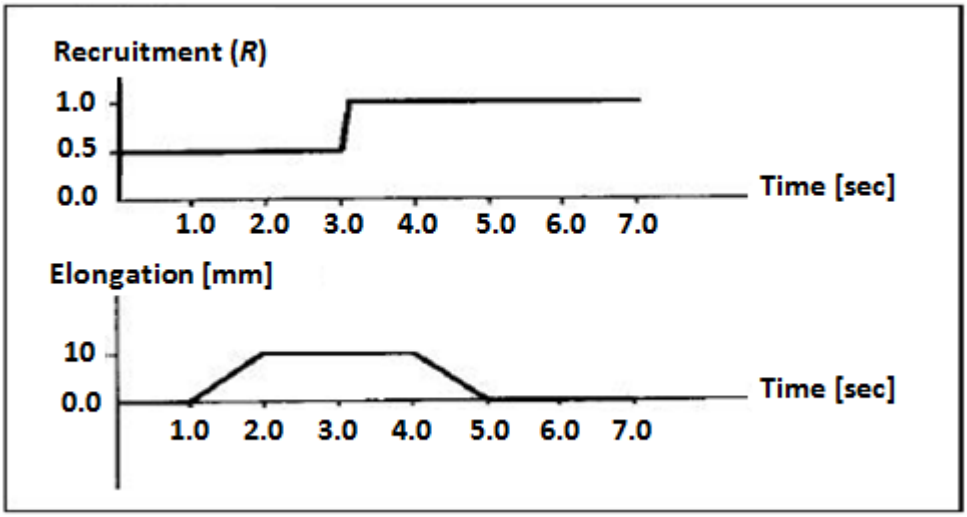

Figure 3.6: Protocol-II. (From [18]).

Although the two protocols have different recruitment cycles, both have the same stretch/shortening cycle and both end at full recruitment and zero elongation.

Typical values were used for the muscle parameters as provided in [18]: $f_{iso,\max} = 45 \quad N$; $k_S = 10 \quad N/mm$; $k_P = 1 \quad N/mm$; $l_{rest} = 125 \quad mm$; $l_{opt} = 100 \quad mm$. The constants of the Herzog model were: $a = 10 \quad N$; $b = 40 \quad mm/\sec$; $a' = 10 \quad N$; $b' = 30 \quad mm/\sec$. An extra study on the effect of *CE* resting length (l_{rest}) on force response is presented in Appendix 5.

When using these protocols, the author's Matlab implementation of the standard Herzog model produced the same force responses (shown in Figure 3.7) as those published by Herzog

[18]. In both protocols, although the muscle was recruited instantaneously, the force rises gradually to the full isometric force corresponding to that *CE* length. This is due to the velocity dependence of the Hill model (F-V relationship of the *CE* in series with the *SE*).

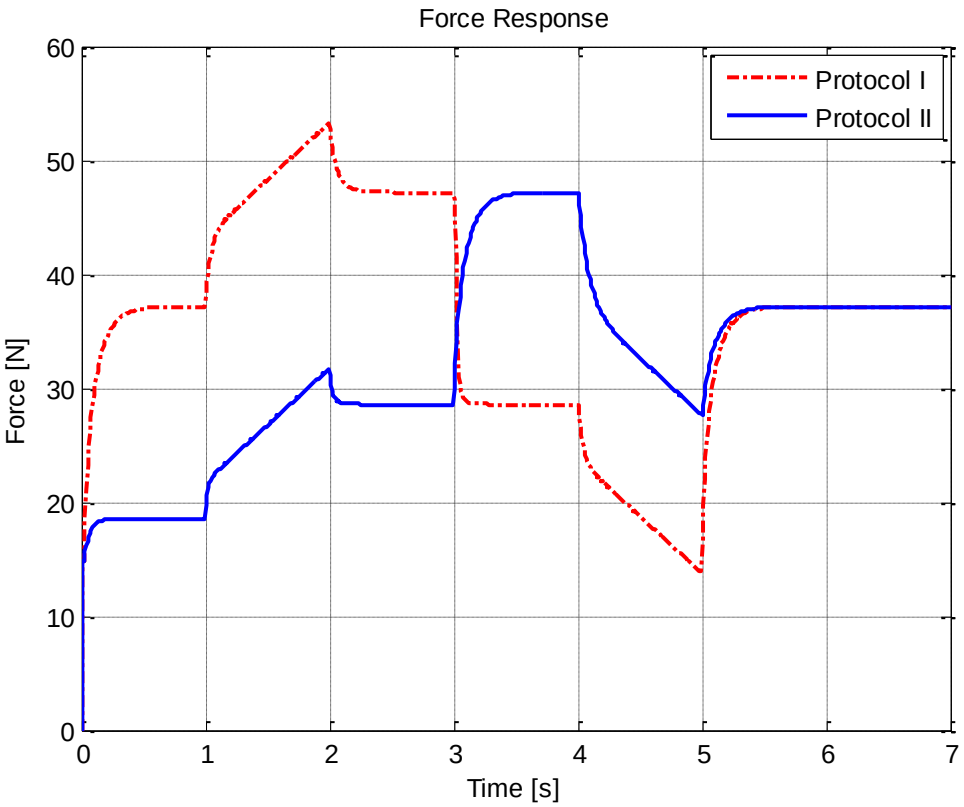

Figure 3.7: Force responses of Herzog's single motor-unit using protocol-I and protocol-II.

3.4.2. Comparison of the $Eff.f_{iso}$ and the $Eff.f_{CE}$ models

Two versions of the multiple motor-unit model were implemented. The aim was to verify that, for the simple Herzog model, only the F-L relationship needs to be applied in a multiple motor-unit manner (as in the $Eff.f_{iso}$ implementation). Therefore, the $Eff.f_{iso}$ model was compared with the $Eff.f_{CE}$ model.

Figure 3.8 and Figure 3.9 show the force responses for protocol-I and protocol-II, respectively. The force responses of the two models are identical. This suggests that, for the simple Herzog model, only the F-L relationship needs to be applied in a multiple motor-unit manner.

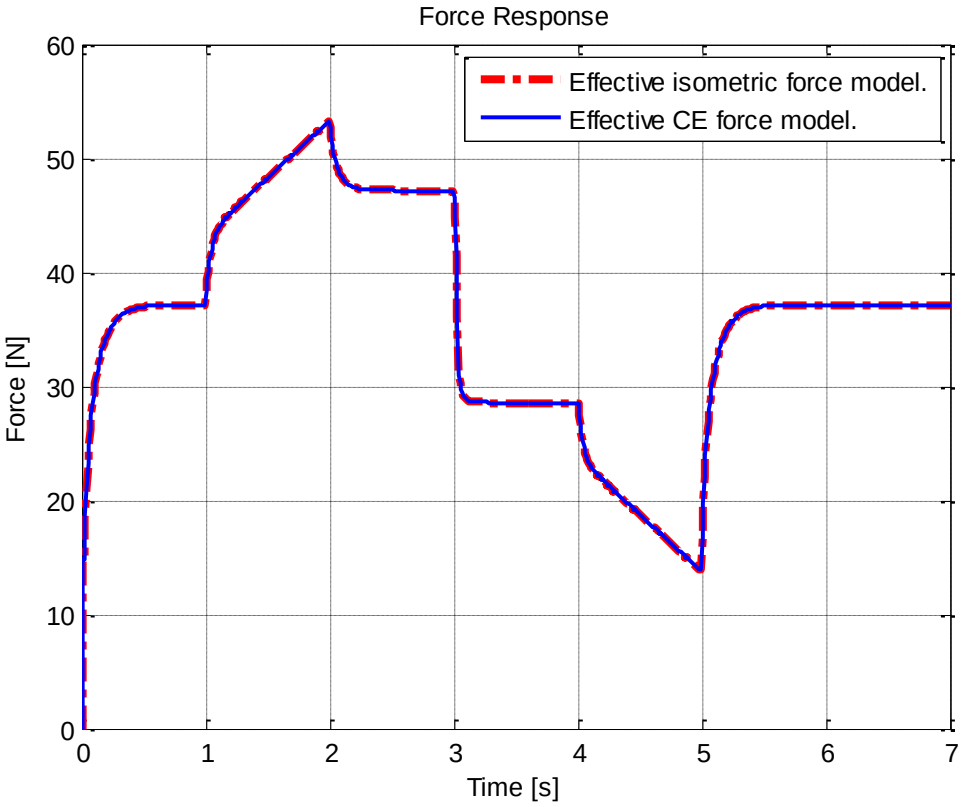

Figure 3.8: Force responses of the $Eff.f_{iso}$ and the $Eff.f_{CE}$ models, protocol-I.

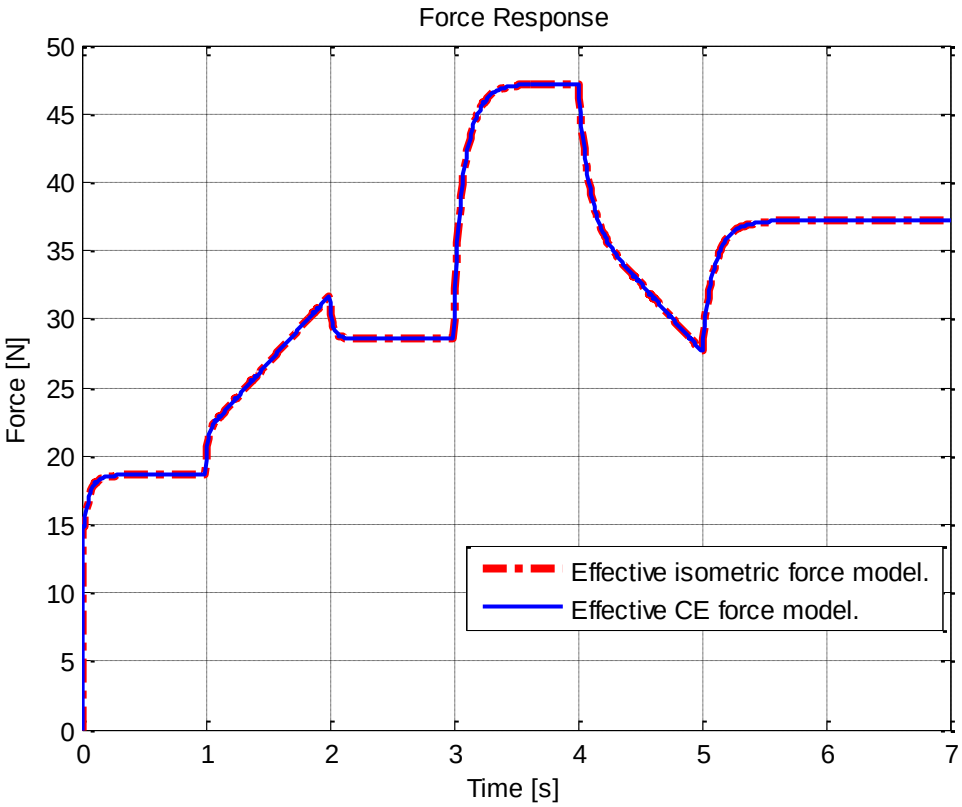

Figure 3.9: Force responses of the $Eff.f_{iso}$ and the $Eff.f_{CE}$ models, protocol-II.

3.4.3. Single versus multiple motor-unit

The simulation results using the $Eff.f_{iso}$ version of the multiple motor-unit model versus the single motor-unit model for protocol-I are plotted in Figure 3.10. When the two models are compared, the force response for protocol-I was observed to be virtually identical when using the $Eff.f_{iso}$ model and the original single CE model over the first 5 seconds. This can be explained by considering the recruitment profile (Figure 3.5). At time zero, full recruitment occurs and the corresponding initial recruitment length is 125mm. Then recruitment drops to 50% at 3 seconds. Hence, for all active motor-units, the initial recruitment length remains the same (125mm) throughout the first 5 seconds and, therefore, both models produce the same force profile.

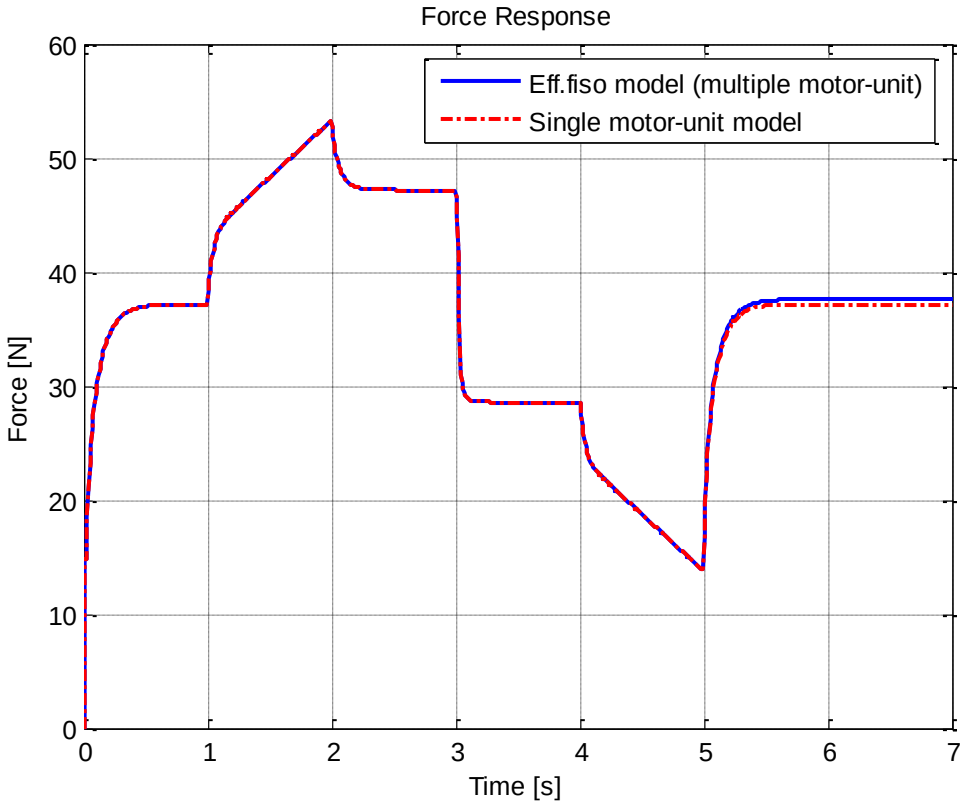

Figure 3.10: Force responses of the $Eff.f_{iso}$ model and the single motor-unit model, protocol-I.

At 5 seconds the recruitment rises again to 100%. For the single motor-unit model the initial length is still 125mm. But for the multiple motor-unit-model, the *CE* is already contracted and its length is less than 125mm which results in a higher isometric force for the remaining 50% of motor-units. The difference is small in this protocol because the *CE* length is only slightly different in the two cases. However, it should be emphasised that the single motor-unit model incorrectly uses the length at 0 seconds throughout.

Conversely, with protocol-II, after the rise to full recruitment at 3 seconds, the $Eff.f_{iso}$ model produced a significantly different force profile (Figure 3.11). This is a direct result of the fact that the initial *CE* recruitment length for the motor-units recruited at 3 seconds is not the same as the length at 0 seconds which is used throughout by the single motor-unit model. This clearly demonstrates the problem with using a single motor-unit model when both recruitment and *CE* length are changing continuously as discussed earlier.

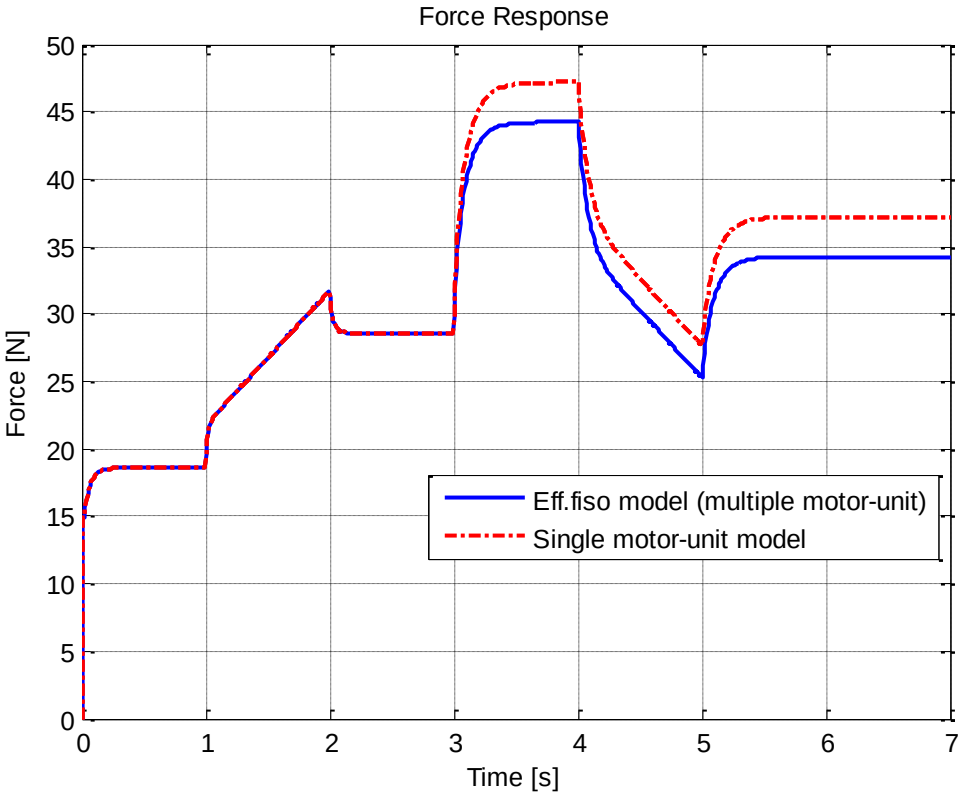

Figure 3.11: Force responses of the $Eff.f_{iso}$ model and the single motor-unit model, protocol-II.

3.4.4. Initial *CE* length versus instantaneous *CE* length

This section compares the simulation results using the *CE* length at initial recruitment (l_o) as the input to the F-L relationship with those using instantaneous *CE* length (l_{CE}) as the input. This is done with both the single motor-unit model and the multiple motor-unit model (i.e. the $Eff.f_{iso}$ model). The aim was to demonstrate the potential errors introduced by using the instantaneous length which is common in FES control studies.

3.4.4.1. Comparison using single motor-unit model (standard Herzog model)

In this section, the responses of two models are compared:

- The single motor-unit model using length at initial recruitment (l_o) in the F-L relationship;
- The single motor-unit model using instantaneous length (l_{CE}) in the F-L relationship.

Referring to the two recruitment protocols (Figure 3.5 and Figure 3.6) and muscle parameters given earlier in section 3.4.1, in both cases the muscle was at rest when recruitment started. Therefore the *CE* length at initial recruitment was $l_o = 125 \quad mm$ and this was used throughout the two protocols because the single motor-unit model effectively consists of only one large motor-unit (single *CE*) which is recruited immediately. Conversely the instantaneous *CE* length varies continuously throughout the two protocols.

Considering the first second of the force responses for the two protocols (Figure 3.12. and Figure 3.13) and referring to the F-L relationship and the three-element Herzog model (Figures A3.2 and A3.6 in Appendix 3), after initial recruitment but at constant musculotendon length, the *CE* shortens and the tendon (*SE*) lengthens until the isometric *CE* force (at $v_{CE} = 0$) and the tendon force are equal. This shortening occurs quite quickly and the force reaches its steady-state value. However, after *CE* shortening, the instantaneous length is different from the initial length; which explains why the force responses for the two cases are different during the first second despite the constant length of the musculotendon complex (no stretch in the first second, i.e. $\Delta l_{mt} = 0$). Similar differences in steady-state forces can be observed throughout the two protocols.

When the muscle is stretching (between 1 and 2 seconds), the stretch increases the force response because of the parallel element (*PE*) stiffness and also because a new equilibrium between the *CE* and the *SE* is established. This increase is less when using instantaneous length (because longer *CE* lengths produce less isometric *CE* force on the descending limb of the F-L relationship). Similarly, when the muscle shortens (between 4 and 5 seconds), the decrease in force is less when using instantaneous length (because shorter *CE* lengths produce more isometric *CE* force on the descending limb of the F-L relationship).

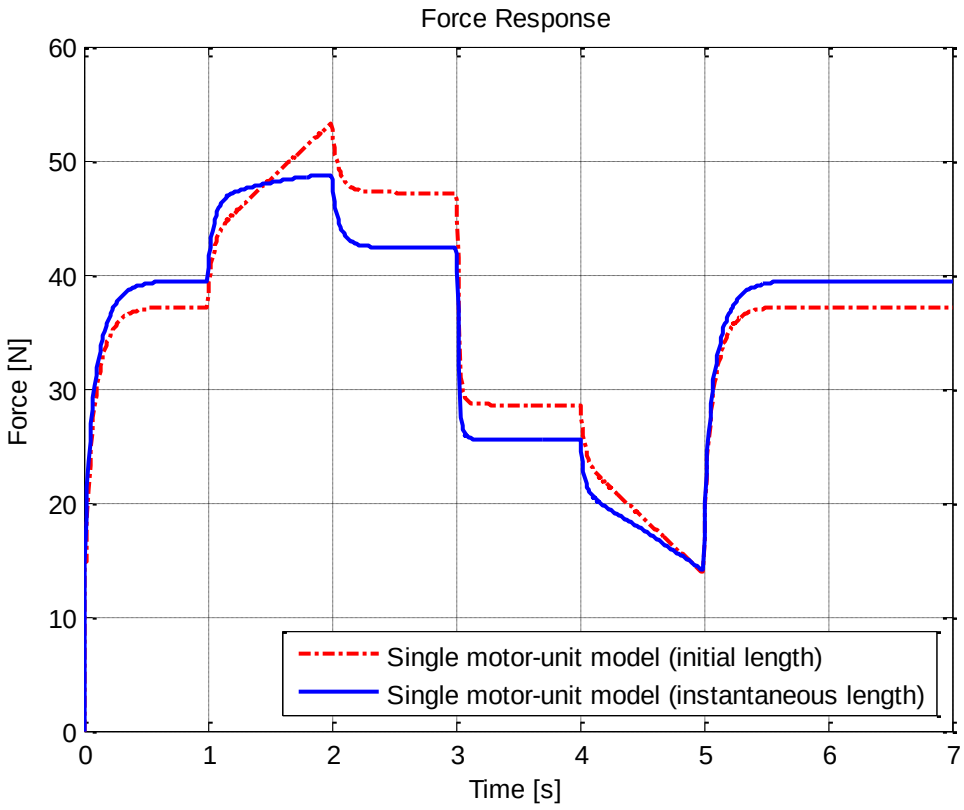

Figure 3.12: Force responses of Herzog's single motor-unit model, protocol-I: Using the initial and the instantaneous lengths.

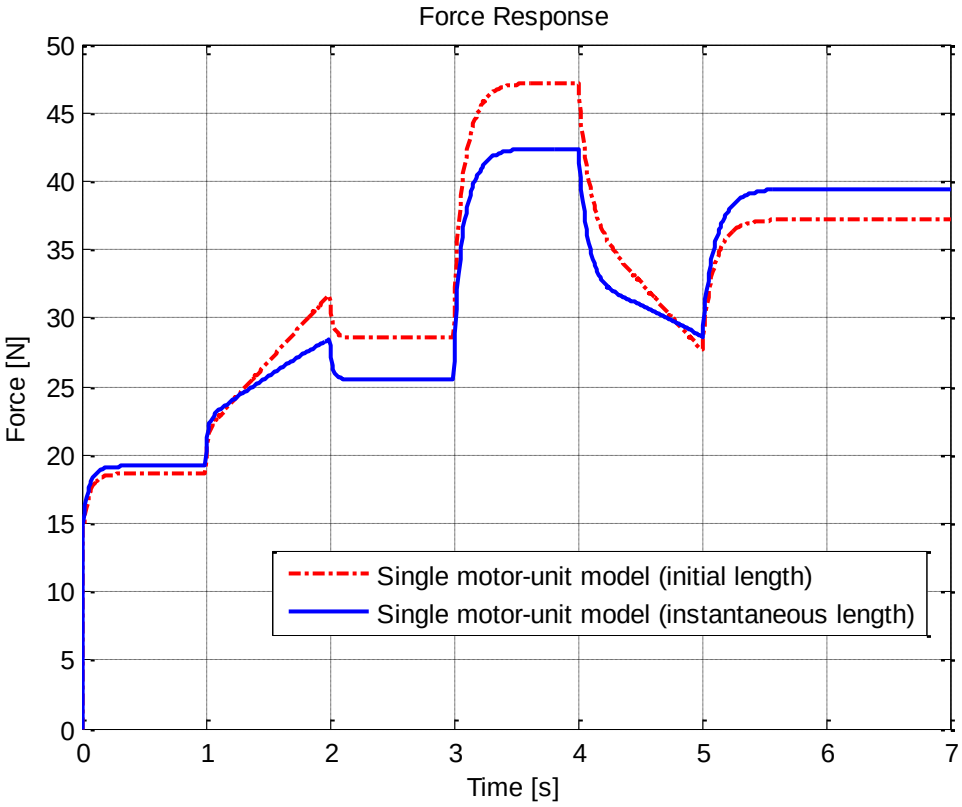

Figure 3.13: Force responses of Herzog's single motor-unit model, protocol-II: Using the initial and the instantaneous lengths.

3.4.4.2. Comparison using multiple motor-unit model

In this section, the responses of two models are compared:

- The multiple motor-unit model using length at initial recruitment;
- The multiple motor-unit model using instantaneous length.

Referring to Figure 3.14 and Figure 3.15, the differences between the two multiple motor-unit models (using alternative lengths) are similar to those seen between the corresponding single motor-unit models (Figure 3.12 and Figure 3.13). These differences largely arise for the reasons explained in the previous section. However, there are some additional noteworthy observations that are discussed below.

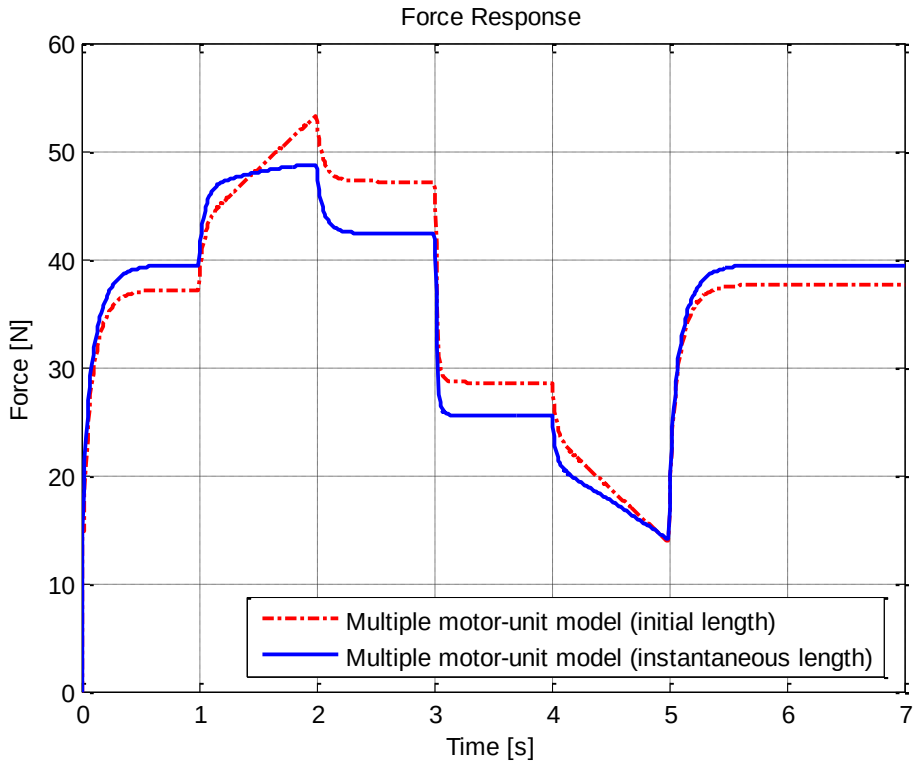

Figure 3.14: Force responses of the $Eff.f_{iso}$ multiple motor-unit model, protocol-I: Using the initial and the instantaneous lengths.

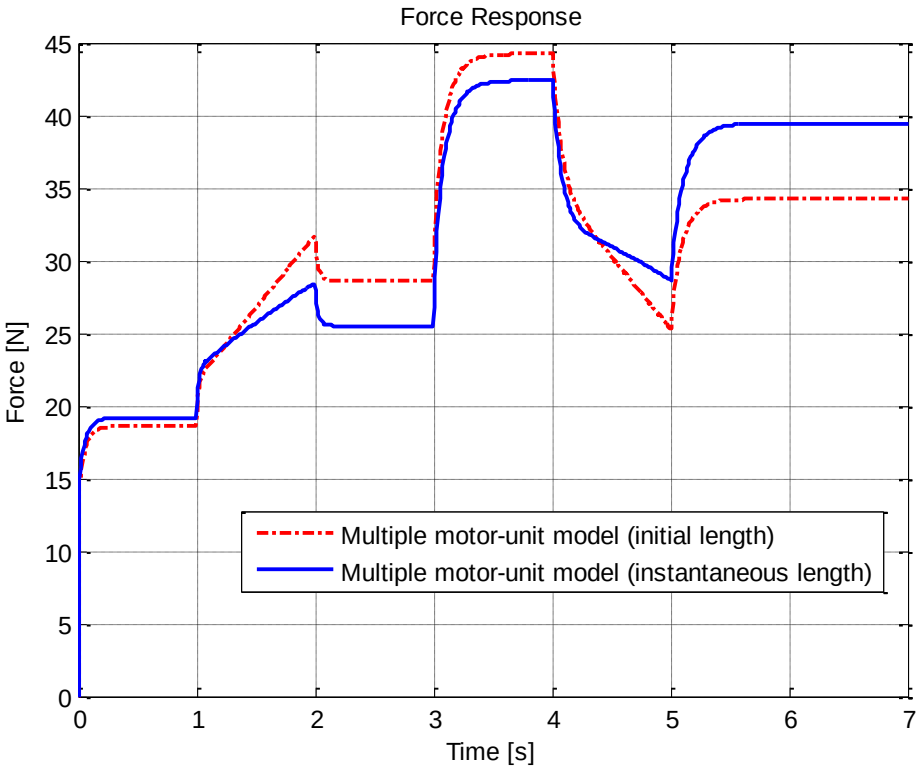

Figure 3.15: Force responses of the $Eff.f_{iso}$ multiple motor-unit model, protocol-II: Using the initial and the instantaneous lengths.

When instantaneous length is used, the results are exactly the same as those for the single motor-unit model when using instantaneous length (Figure 3.16 and Figure 3.17). This is because, in this case, there is no fundamental difference between the single motor-unit model and the multiple motor-unit model (they both use the same instantaneous length for the entire muscle at all times).

However, when using initial recruitment length, the results differ from those for the single motor-unit model because recruitment changes at different lengths (see Figure 3.6) and the multiple motor-unit model properly accounts for this (Figure 3.16 and Figure 3.17). In particular, the results diverge after recruitment rises from 50% to 100% at 5 seconds (Protocol-I) and at 3 seconds (Protocol-II) because the corresponding initial recruitment length for the remaining 50% of motor-units is different from that when the first 50% of motor-units were recruited at 0 seconds.

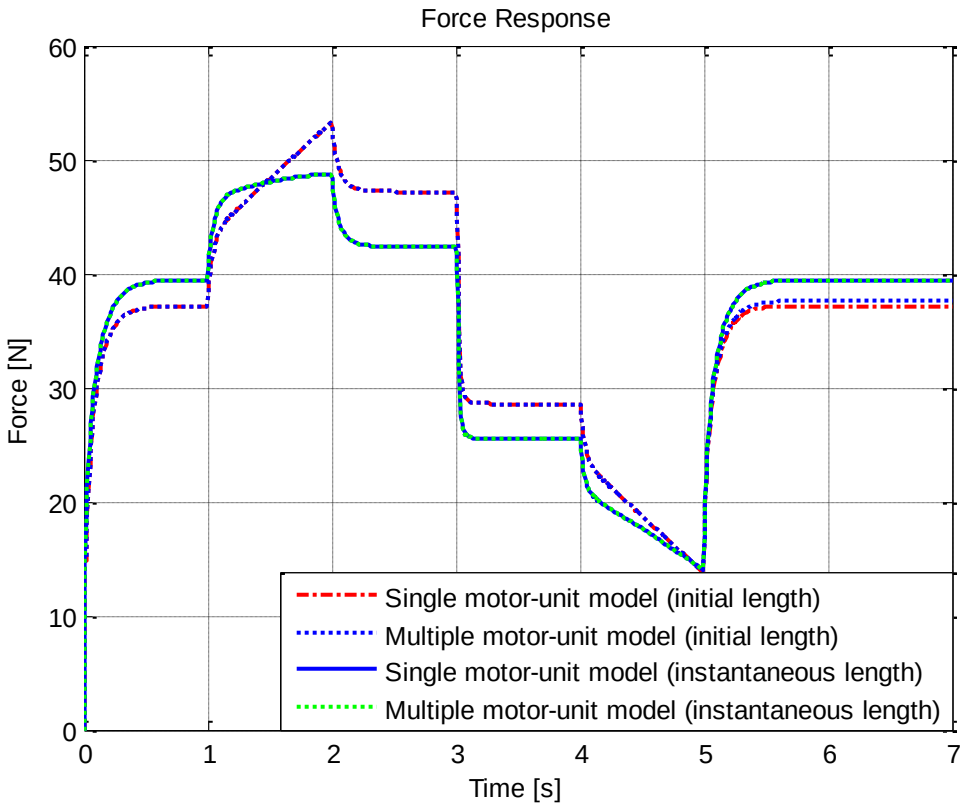

Figure 3.16: Force responses of all models, protocol-I: Single motor-unit model using initial length, single motor-unit model using instantaneous length, multiple motor-unit model using initial length, and multiple motor-unit model using instantaneous length.

In conclusion, when instantaneous length is used, the single motor-unit model and the multiple motor-unit model will give the same results for any protocol. But when initial recruitment length is used, the multiple motor-unit model produces different results if different motor-units are recruited at different lengths.

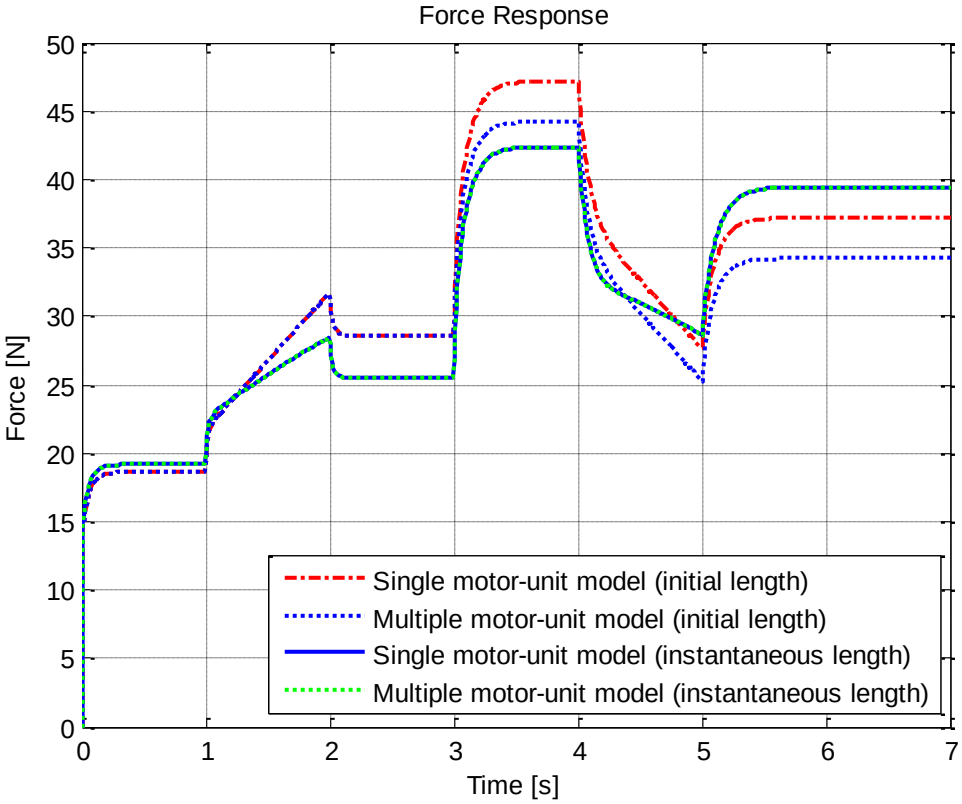

Figure 3.17: Force responses of all models, protocol-II: Single motor-unit model using initial length, single motor-unit model using instantaneous length, multiple motor-unit model using initial length, multiple motor-unit model using instantaneous length.

3.5. Comparison of different resolution models

In order to demonstrate the effects of different resolution models on force response, simulation results for 1, 10, 100 and 1000 motor-unit models are plotted and discussed here.

The simulation results for 1, 10, 100 and 1000 motor-unit models for protocol-I are plotted in Figure 3.18. When these models of different resolution are compared, the force responses for protocol-I were observed to be virtually identical over the first 5 seconds, during which time

recruitment was 100% for the first three seconds and 50% between $t = 3.0$ and $t = 5.0$ seconds. At 5 seconds the recruitment rises again to 100%, the force responses of the multiple motor-unit models are exactly the same. The number of recruited motor-units at 5 seconds is different for different multiple motor-unit models, but the same force is produced since half of the motor-units are recruited at the new length. For the single motor-unit model the initial length is still 125mm. But for the multiple motor-unit-models (10, 100 and 1000 motor-units), the *CE* is already contracted and its length is less than 125mm which results in a higher isometric force for the remaining 50% of motor-units. The difference is small in this protocol because the *CE* length is only slightly different in the two cases.

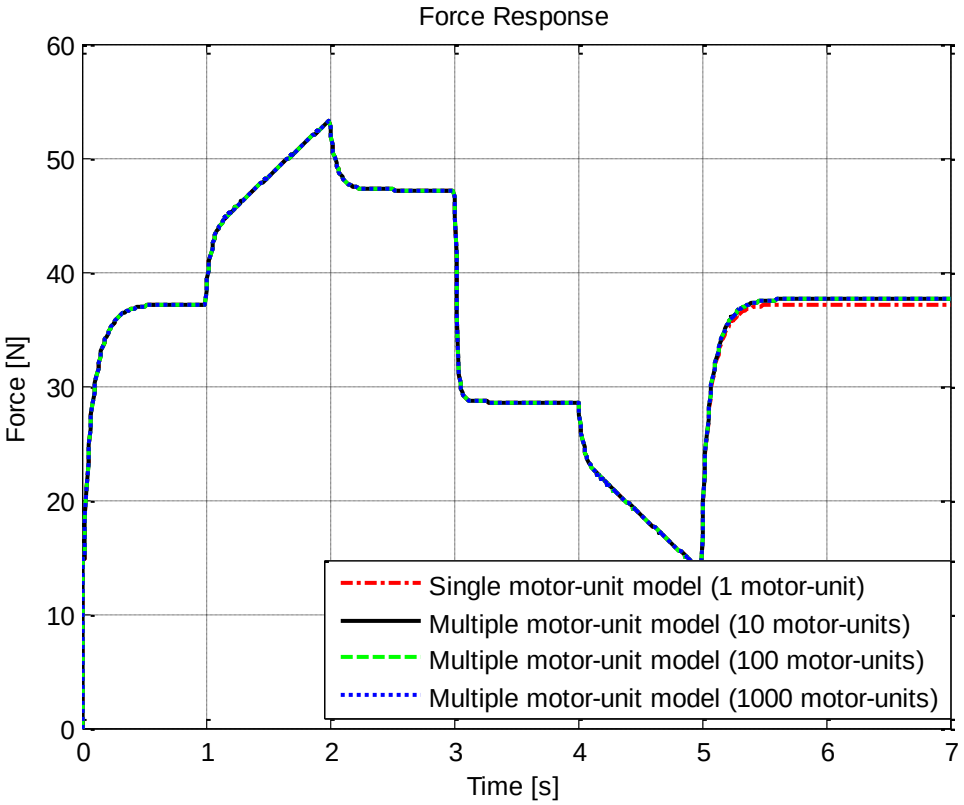

Figures 3.18: Force responses of the 1, 10, 100 and 1000 motor-unit models, protocol-I.

Similarly, with protocol-II, after the rise to full recruitment at 3 seconds, the force responses of the multiple motor-unit models are exactly the same (Figure 3.19). The number of recruited motor-units at 3 seconds is different for different multiple motor-unit models, but the same force is produced since half of the motor-units are recruited at the new length. After the rise to full recruitment at 3 seconds, the multiple motor-unit models (10, 100 and 1000 motor-units)

produced a significantly different force profile from the single motor-unit model. This is a direct result of the fact that the initial *CE* recruitment length for the motor-units recruited at 3 seconds is not the same as the length at 0 seconds which is used throughout by the single motor-unit model.

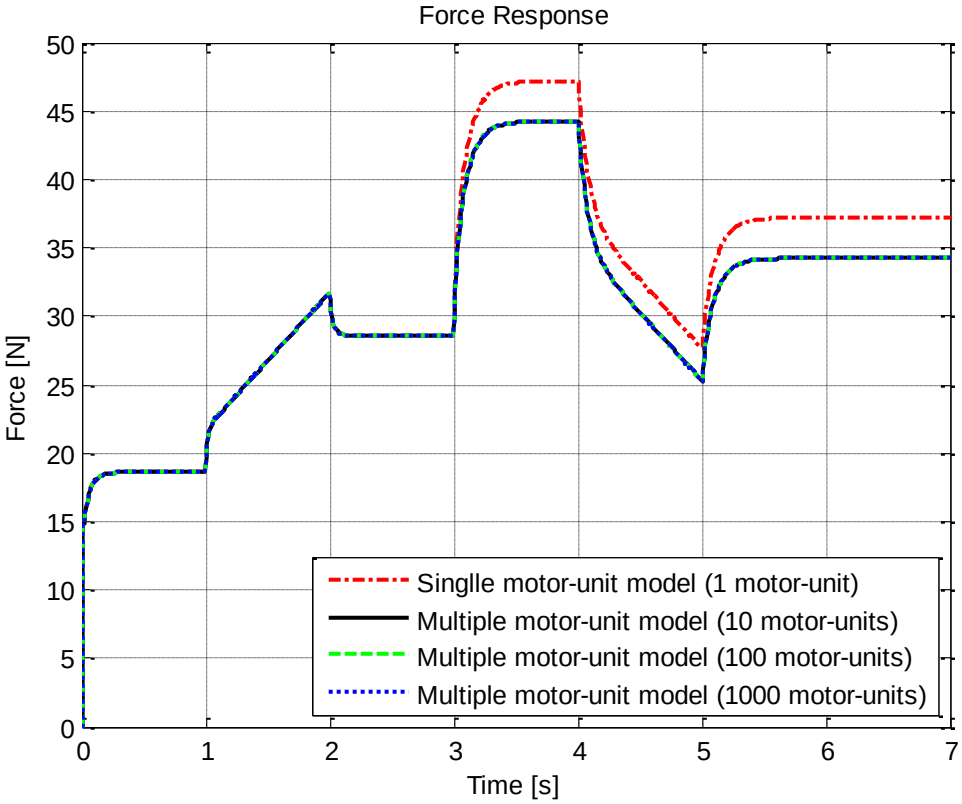

Figures 3.19: Force responses of the 1, 10, 100 and 1000 motor-unit models, protocol-II.

These results suggest that, since each motor-unit is modelled separately in the multiple motor-unit model; a higher resolution results in more accuracy. For protocol-I and protocol-II, the change in recruitment was 50% which can be detected by the three multiple motor-units used here (10, 100 and 1000 motor-units). But for a small change in the recruitment level, for example 0.1%, this will only be detected by the 1000 motor-unit model. If recruitment was changed by 1%, this will be detected by the 1000 motor-unit model and also the 100 motor-unit model, but not the 10 motor-unit model. The 10 motor-unit model will only detect changes in recruitment level of 10% or more. However, a resolution of 0.1% seems to be reasonably high and hence the number of virtual motor-units (m) was chosen as 1000 in the effective isometric force ($Eff.f_{iso}$) model and the effective *CE* force model ($Eff.f_{CE}$).

3.6. Conclusion

The accuracy of the standard Herzog model can be enhanced by the multiple motor-unit modelling approach using the *CE* length at initial recruitment. Because the calculation of isometric force in the $Eff.f_{iso}$ model is based on the length of each motor-unit when it was recruited, the multiple motor-unit model properly accounts for continuously varying recruitment as would usually be seen in closed loop FES control.

Another version of the multiple motor-unit model, the $Eff.f_{CE}$ model, was developed to allow for the incorporation of additional features that are best modelled using a multiple motor-unit approach such as fatigue. It also served to validate the $Eff.f_{iso}$ model.

Open-loop simulation protocols were used to study three muscle models using both the instantaneous *CE* length and the *CE* length at initial recruitment for the F-L relationship. The three models studied were: The standard Herzog model, the $Eff.f_{iso}$ model, and the $Eff.f_{CE}$ Model.

The comparison between the $Eff.f_{iso}$ model and the $Eff.f_{CE}$ model ascertained that the force responses of the two models are identical. This suggests that, for the simple Herzog model, only the F-L relationship needs to be applied in a multiple motor-unit manner.

When instantaneous length is used as the input to the F-L relationship, the single motor-unit model and the multiple motor-unit model will give the same results for any protocol. But when the length at initial recruitment is used as the input to the F-L relationship, the multiple motor-unit model produces different results if different motor-units are recruited at different lengths. These results demonstrate the potential errors introduced by using the instantaneous length which is common in FES control studies.

Chapter 4: The Multiple Motor-Unit Muscle Model with Fatigue

4.1. Introduction

The force response of electrically stimulated muscle decays nonlinearly as the muscle begins to fatigue [3]. Eventually, the muscle is not able to produce any force [141]. The main cause of fatigue in FES is the use of high stimulation frequency to produce smooth contractions [24, 142, 166]. Stimulation frequency has a great effect on muscle fatigue, higher frequency will produce higher force but also results in a faster fatigue rate, and vice versa [3, 47, 167]. Muscle fatigue is one of the major limitations of FES applications [1, 12, 47].

As discussed in section 3.1, in closed loop FES control applications R will usually vary with time. As almost all muscle models used in FES control studies treat the muscle as a one large motor-unit, there can only be one value for the muscle's fatigue condition despite the fact that in reality different motor-units are recruited at different times and hence fatigue and recovery cycles of different motor-units will be different. Moreover, different fibre-types have different fatigue characteristics. The use of a fatigue sub-model incorporated into a single motor-unit (SMU) model in a realistic scenario where R is changing continuously would result in an over- or under-estimation of muscle force.

Therefore, this chapter addresses the problem of muscle modelling for continuously varying R, hence different cycles of fatigue and recovery for different motor-units. A model for fatigue and recovery is used in the open-loop simulation protocols of single and multiple motor-unit (MMU) models. The results are discussed at the end of the chapter.

4.2. Effective *CE* force model with fatigue

As discussed in section 2.2, skeletal muscles are composed of one or more of the three fibre-types. Fatigue resistance depends on the percentage of each fibre-type in the muscle. For simplicity and in order to demonstrate the potential errors introduced by ignoring fatigue or by incorporating fatigue into a single motor-unit model, the virtual motor-units of the multiple motor-unit model are assumed of the same fibre-type (i.e. the same fatigue sub-model is used for all motor-units).

Muscle fatigue can be experimentally measured and modelled as index of fatigue (*IF*) which is defined as "force of the fatigued muscle normalised to force of the same un-fatigued muscle under same conditions". *IF* is incorporated in the muscle model by multiplying it with the force produced by the muscle.

In the review of published fatigue sub-models (section 2.5.4), many fatigue sub-models are available in the literature, one of the most cited fatigue sub-models was developed by Riener [72]. This model was chosen because its inputs are stimulation frequency *freq* and recruitment R. Hence, fatigue of partially recruited muscle can be calculated using this model and the results of the single and the multiple motor-unit models can be compared.

Riener-1 fatigue sub-model [72] is a modified and simplified version, of the more complex, Giat fatigue sub-model [143, 144, 145, 146], where in Riener fatigue sub-model, only one equation is used for fatigue and recovery. This model was developed first in [55] as a general approach then effects of recruitment and frequency were modelled and incorporated in [72]. Fatigue and/or recovery rate at any time is given by the following first-order equation:

$$\frac{d}{dt}(IF) = \frac{(IF_{\min} - IF(t)) \times [R \times A_{freq} \times \lambda]}{T_{fat}} + \frac{(1 - IF(t)) \times (1 - [R \times A_{freq} \times \lambda])}{T_{rec}} \qquad (4.1)$$

$$A_{freq}(freq) = \left(\frac{(freq)^2}{100 + (freq)^2} \right) \qquad for: freq < 100Hz$$

$$\lambda(freq) = 0.4 + \left[0.6 \times \left(\frac{freq}{100} \right)^2 \right] \qquad for: freq < 100Hz$$

R: Recruitment of the whole muscle.

A_{freq}: Muscle activation due to stimulation frequency only without the effect of other parameters (i.e. without yield, sag, effective length and effective frequency).

λ: This term is used to model the effect of stimulation frequency on fatigue rate.

$IF_{\min}$: The minimum fitness of the muscle at which fatigue rate = 0 of the fully recruited muscle (i.e. the minimum value for the index of fatigue).

T_{fat}: Time constant for fatigue, it can have largely different values for different muscles and different fibre types.

T_{rec}: Time constant for recovery, estimated in [72] as ($T_{rec} = 30$ [sec]) for all muscles.

Riener-1 fatigue sub-model (equation 4.1) can be used for the whole muscle, or for a single motor-unit assuming full recruitment ($R_j = 1$) when recruited and full recovery at zero recruitment ($R_j = 0$) providing that appropriate values for model parameters are used.

$IF_{\min}$ and T_{fat} are estimated experimentally, they can have largely different values for different muscles depending of fibre-type. Parameters of Riener-1 fatigue sub-model are given in [72] for five muscle groups (Mono-articular hip flexors, Mono-articular hip extensors, Rectus femoris, Vasti, and Gastrocnemius) as: $IF_{\min} = 0$, $T_{fat} = 18$ [sec], and $T_{rec} = 30$ [sec] (T_{rec} value is for any muscle). These parameters will be used in equation 4.1.

At stimulation frequency ($freq = 30$ Hz), the fatigue curve of equation 4.1 for fully recruited muscle ($R = 1$) is shown in Figure 4.1. Note that the fatigue curve will reach zero only when the stimulation frequency is maximum (i.e. $freq = 100$ Hz) and full recruitment ($R = 1$). The recovery curve of equation 4.1 for fatigued muscle at zero recruitment ($R = 0$) is shown in Figure 4.2.

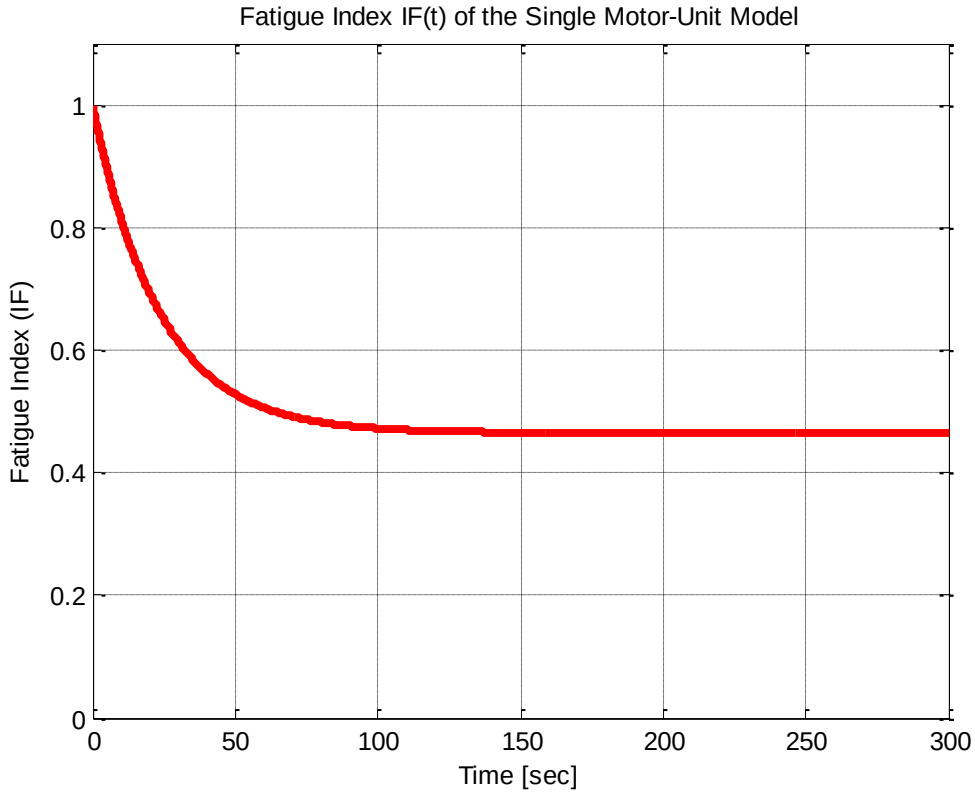

Figure 4.1: Fatigue curve of Riener fatigue sub-model. Model parameter values were taken from [72].

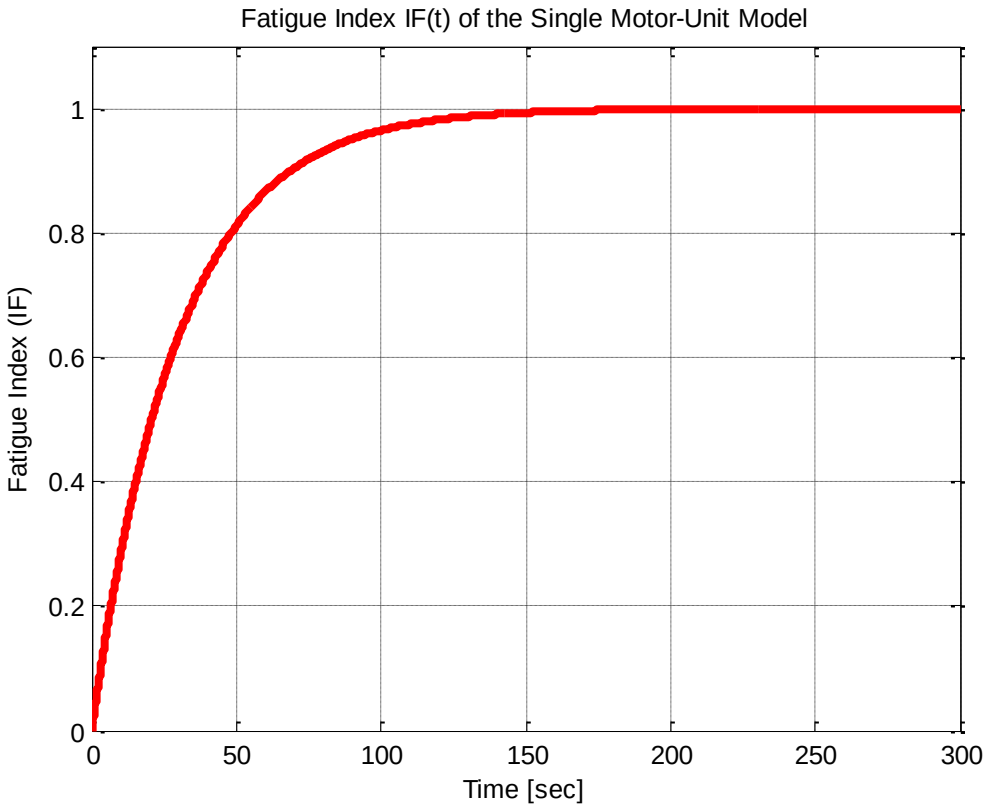

Figure 4.2: Recovery curve of Riener fatigue sub-model. Model parameter values were taken from [72].

The effective *CE* force model with fatigue sub-model is presented in Figure 4.3. The effective *CE* force of the entire muscle, including fatigue and recovery of every motor unit, is the sum of the individual motor unit forces as follows:

$$IF \times Eff.f_{CE} = \left[IF_1 \times f_{CE,1}\right] + \left[IF_2 \times f_{CE,2}\right] + ... + \left[IF_M \times f_{CE,M}\right] = \sum_{j=1}^{M} \left[IF_j \times f_{CE,j}\right] \quad (4.2)$$

Finally, the effective *CE* force ($Eff.f_{CE}$) with fatigue of all recruited motor-units is used to calculate the total muscle force F_m as follows:

$$F_m = \left(k_p \times \Delta l_{mt}\right) + \sum_{j=1}^{M} \left[IF_j \times f_{CE,j}\right] \quad (4.2A)$$

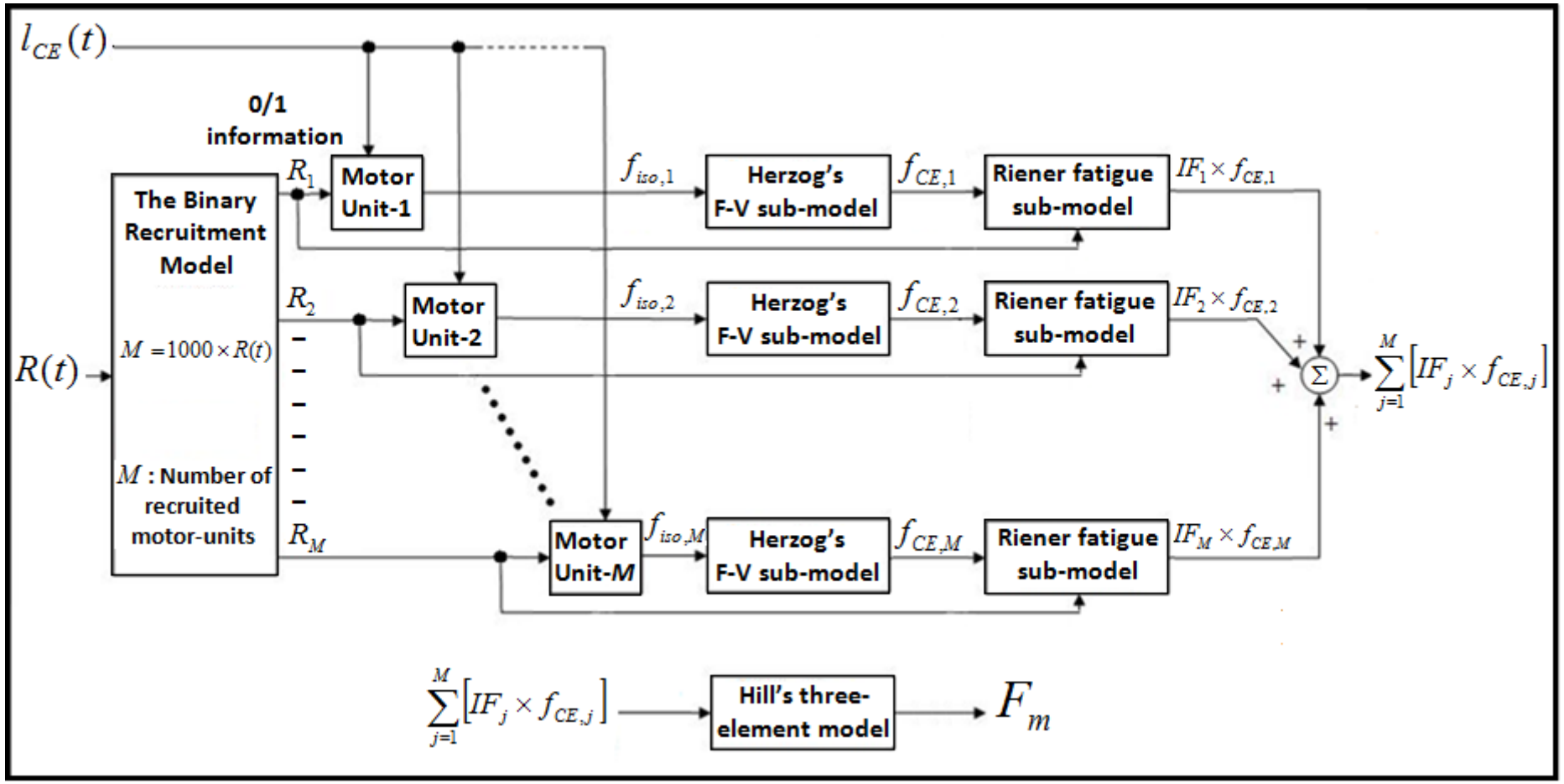

Figure 4.3: Fatigue sub-model incorporated into the effective *CE* force model $Eff.f_{CE}$. Fatigue and recovery of every motor-unit is modelled separately.

4.3. Simulation results

Matlab codes were developed for simulating the responses to open-loop simulation protocols of two muscle models:

- The Herzog model (treating the muscle as a single motor-unit);
- The $Eff.f_{CE}$ multiple motor-unit model.

In both cases, fatigue can be ignored or incorporated into the model.

In the following sections, firstly, the three input protocols that have been used are defined. Then simulation results are presented to compare the alternative muscle models and, in particular, to demonstrate the potential errors introduced by: a) ignoring fatigue; and b) incorporating fatigue sub-model into single motor-unit model instead of the multiple motor-unit model.

4.3.1. Input protocols

In order to demonstrate the need to use a multiple motor-unit modelling approach to model fatigue when R varies with time, input protocols are required that involve changing R at different times and for different periods of time. Three suitable protocols were chosen, details of the three protocols are as follows:

Protocol-III (Figure 4.4):

(i) At $t = 0.0$ seconds: Full isometric recruitment at the unique resting state (i.e. at $l_{CE} = l_{rest} = 125 \quad mm$, $\Delta l_{mt} = 0$), at *IF*=1 (fully recovered muscle);

(ii) At $t = t_1$: Partial (50%) de-recruitment;

(iii) At $t = t_2$: Re-recruitment to 100% level.

t_1: The time at which muscle force is minimal because of fatigue (recruited motor-units are fully fatigued).

t_2: The time at which fatigued motor-units are fully recovered (after being not recruited for some time that is enough for full recovery).

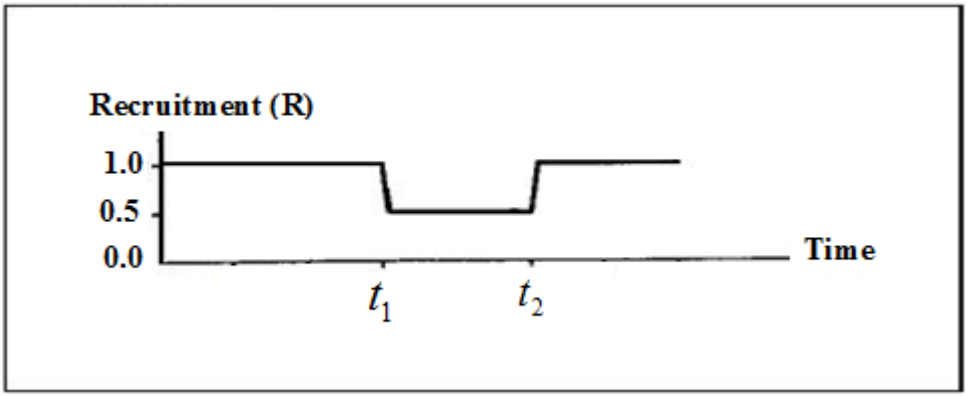

Figure 4.4: Protocol-III.

Protocol-IV (Figure 4.5):

(i) At $t = 0.0$ seconds: Partial (50%) isometric recruitment at the unique resting state (i.e. at $l_{CE} = l_{rest} = 125 \quad mm$, $\Delta l_{mt} = 0$), at *IF*=1 (i.e. fully recovered muscle);

(ii) At $t = t_1$: Full (100%) recruitment.

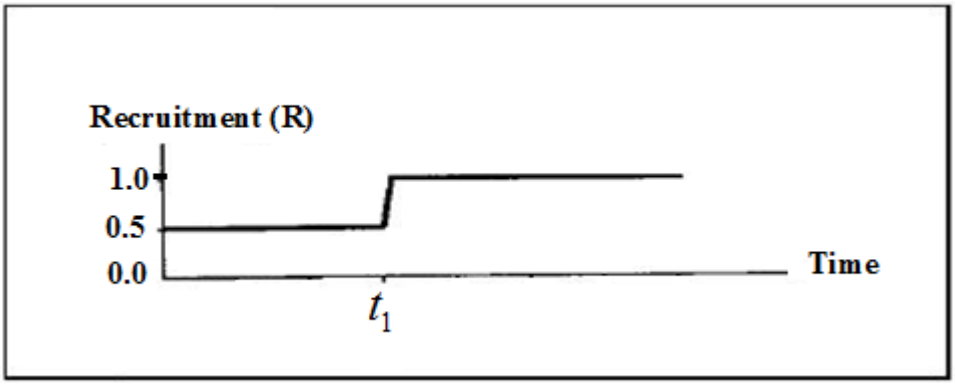

Figure 4.5: Protocol-IV.

Protocol-V (Figure 4.6):

(i) At $t = 0.0$ seconds: Partial (50%) isometric recruitment at the unique resting state (i.e. at $l_{CE} = l_{rest} = 125 \quad mm$, $\Delta l_{mt} = 0$), at *IF*=1 (fully recovered muscle);

(ii) At $t = t_3$: Constant rate of recruitment up to full (100%) recruitment, at recruitment rate = 0.1667% per second.

t_3: The time at which recruited motor-units start to fatigue. In Riener fatigue sub-model it is assumed that: $t_3 = 0$, (in Hawkins fatigue sub-model: $t_3 > 0$ for all fibre types).

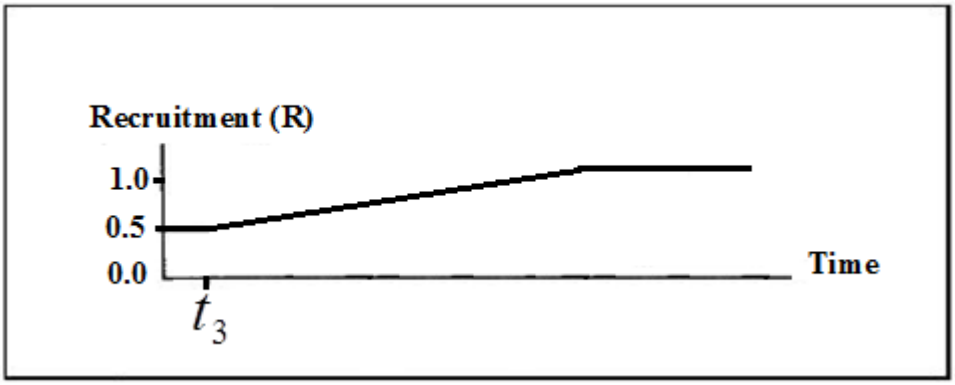

Figure 4.6: Protocol-V.

In protocol-V; R starts at 50% isometric recruitment. Once fatigue starts R is increased to compensate for the force loss (due to fatigue) by recruiting more motor-units. This can be considered as mimicking a closed-loop FES control realistic scenario, where the FES controller will increase stimulation input in order to maintain the output muscle force at the required level thus compensating for fatigue by recruiting more un-fatigued motor-units.

Isometric contractions are applied in all protocols, there is no stretch nor shortening since this has no effect on Riener-1 fatigue sub-model (equation 4.1). For simplicity, constant recruitment level at the unique resting state ($l_o = l_{rest}$, $\Delta l_{mt} = 0$) is assumed in all protocols. However, in a realistic scenarios FES is usually intermittent. The muscle is able to recover and restore some of its capacity while FES is off. Intermittent FES may delay fatigue but will not prevent it.

Rigid tendon is assumed in all protocols (i.e. $k_S = \infty$), and hence $\Delta l_{mt} = \Delta l_{CE} = 0$. This assumption was made so that the *CE* and *SE* lengths do not change when *CE* force changes because of changes in recruitment level R and hence different l_o for different motor-units in the multiple motor-unit model (if the tendon is not rigid then *CE* length will be shorter after recruitment because of tendon compliance). In this way all differences in force responses of different models are due to fatigue only.

4.3.2. Comparison of the single and multiple motor-unit models without fatigue

The simulation results using the multiple motor-unit model versus the single motor-unit model for protocol-III, protocol-IV and protocol-V are plotted in Figure 4.7, Figure 4.8 and Figure 4.9, respectively. The aim was to confirm that, for the chosen protocols, the force responses of the two models (SMU model and MMU model) are identical. The force responses of the two models in protocol-III, protocol-IV and protocol V are calculated using the length at the same initial length (l_o). In all protocols, all or part of motor-units is recruited first and then the rest is recruited at different time. The isometric forces of all motor-units are all calculated at the same initial length in the Herzog F-L sub-model since the tendon is assumed rigid and the *CE* length is the same at all times in all protocols. For this reason the two force responses are identical.

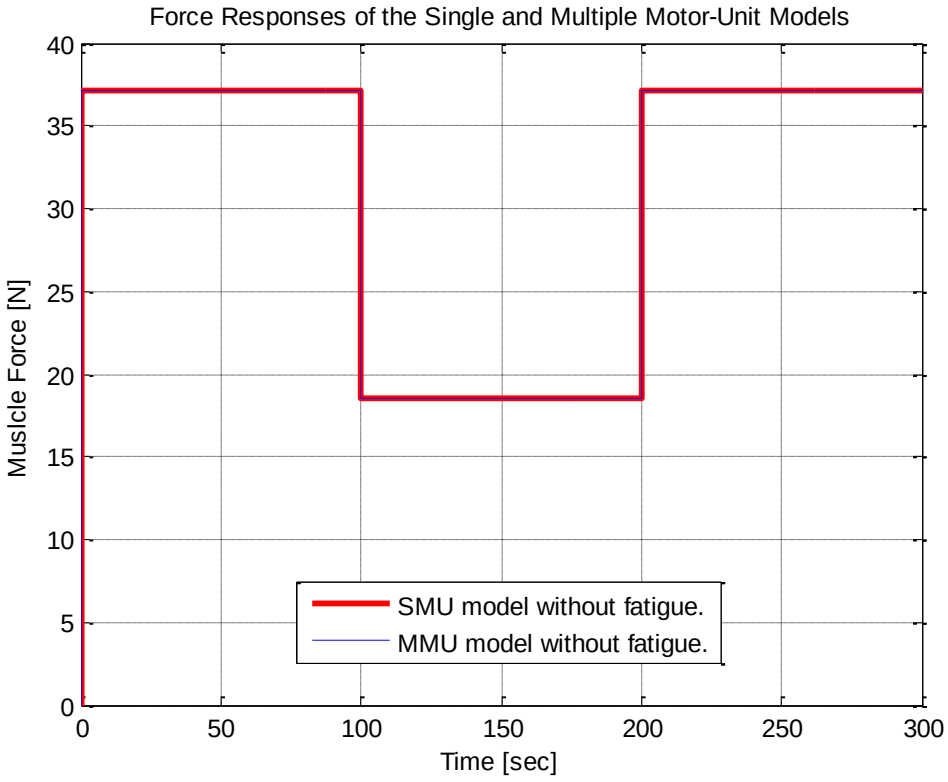

Figure 4.7: Identical force responses of the single and multiple motor-unit models without fatigue sub-model, protocol-III.

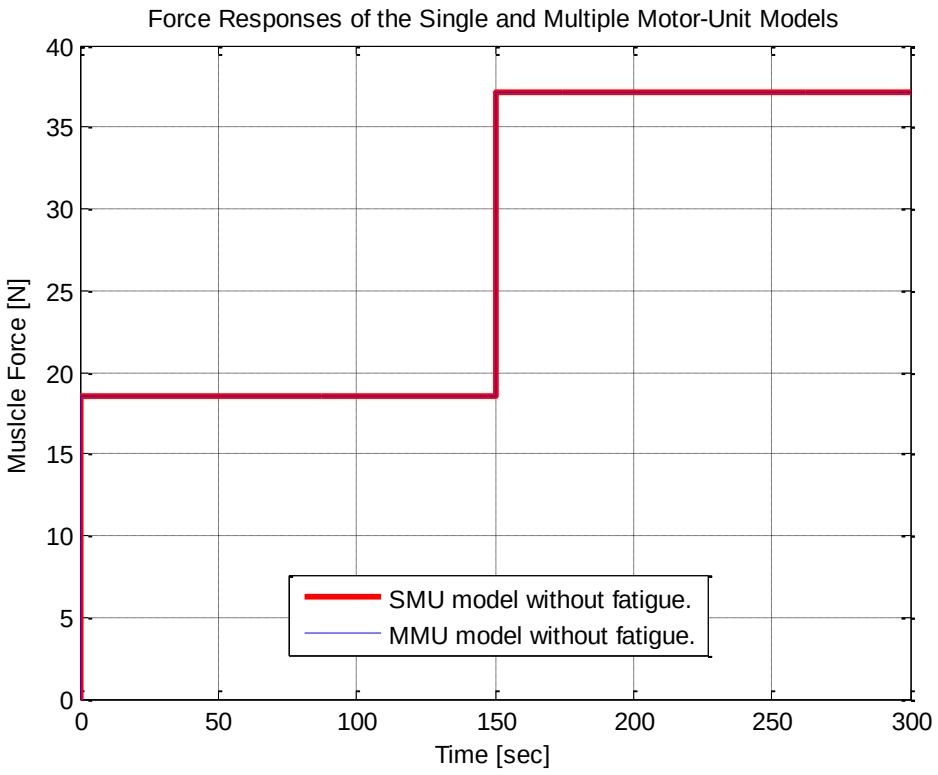

Figure 4.8: Identical force responses of the single and multiple motor-unit models without fatigue sub-model, protocol-IV.

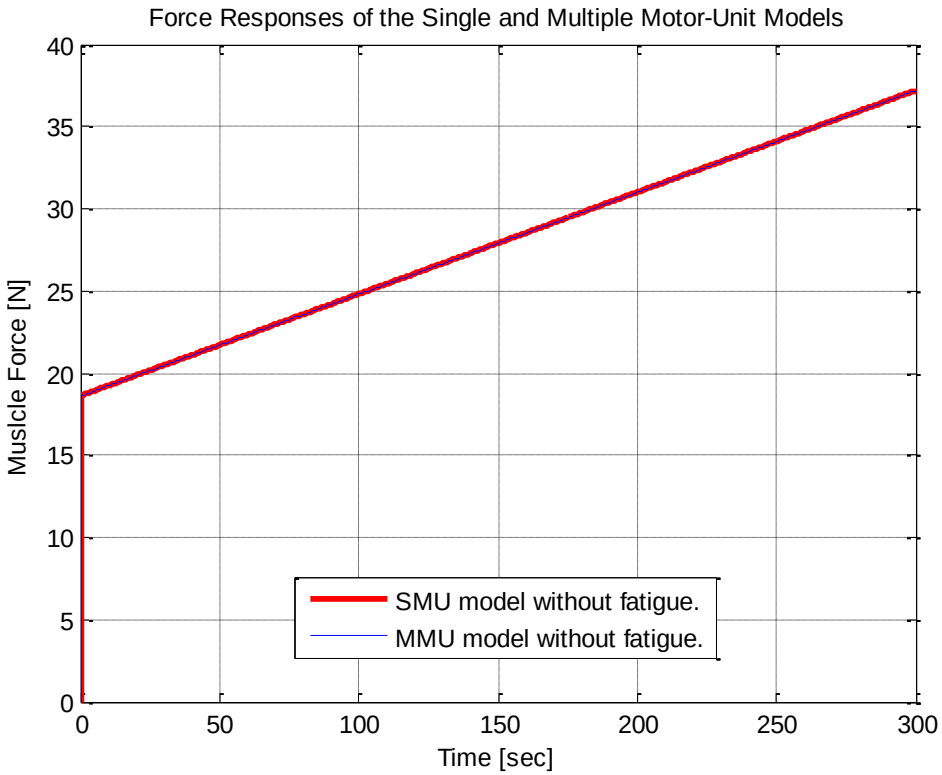

Figure 4.9: Identical force responses of the single and multiple motor-unit models without fatigue sub-model, protocol-V.

4.3.3. Comparison of models with and without fatigue

This section compares the simulation results using the same model with and without fatigue. This is done with both the single motor-unit model and the multiple motor-unit model. The aim was to demonstrate the potential errors introduced by ignoring fatigue which is quite common in FES control studies.

4.3.3.1. Comparison using single motor-unit model (standard Herzog model)

In this section, the responses of two models are compared:

- The single motor-unit model without fatigue;
- The single motor-unit model with fatigue (using Riener fatigue sub-model for whole muscle with variable recruitment).

Indices of fatigue are calculated using equation 4.1. For all next simulations, indices of fatigue are plotted for comparison with corresponding force responses.

Referring to the recruitment protocol-III, the fatigue index, and the force response of the single motor-unit model with fatigue (Figure 4.4, Figure 4.10 and Figure 4.11), in the first 100 seconds the muscle force decreases exponentially until the partial de-recruitment at 100 seconds. During the partial recruitment (between 100 and 200 seconds) the index of fatigue increases causing the force to increase, which is unrealistic (see section 2.2). The recruited part of the muscle is already fully fatigued and cannot make any recovery while still recruited, and only the non-recruited part can make recovery. The full recruitment on 200 seconds increases the force instantly and starts to decay again because of fatigue.

Referring to the recruitment protocol-IV, the fatigue index, and the force response of the single motor-unit model with fatigue (Figure 4.5, Figure 4.12 and Figure 4.13), for the first 150 seconds the fatigue rate of the 50% recruited muscle is less than the fatigue rate when the muscle is fully recruited (in protocol-III). The fatigue rate in Figure 4.13 when the muscle is 50% recruited is slow when compared with the fully recruited muscle in the first 100 seconds of Figure 4.11. Again, this behaviour is also unrealistic.

Referring to the recruitment protocol-V, the fatigue index, and the force response of the single motor-unit model with fatigue (Figure 4.6, Figure 4.14 and Figure 4.15), the force response was roughly maintained at constant level. The gradual increase in R recruits more fresh motor-units to compensate for the decrease in the force produced by those recruited motor-units because of fatigue.

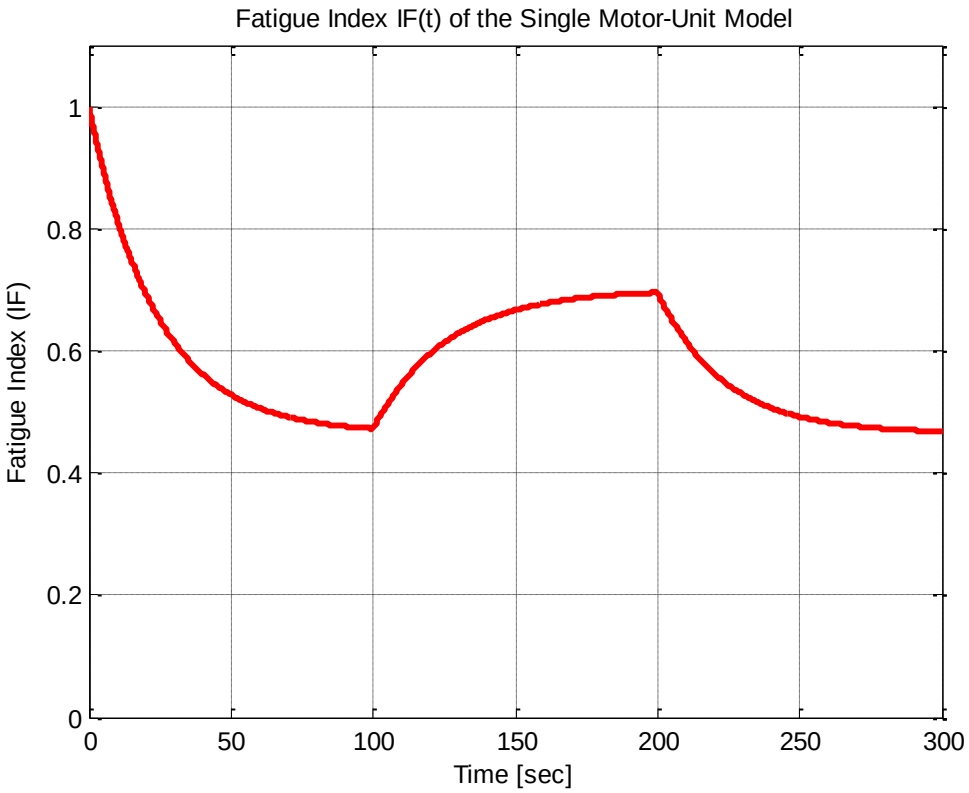

Figure 4.10: Index of fatigue for the single motor-unit model, protocol-III.

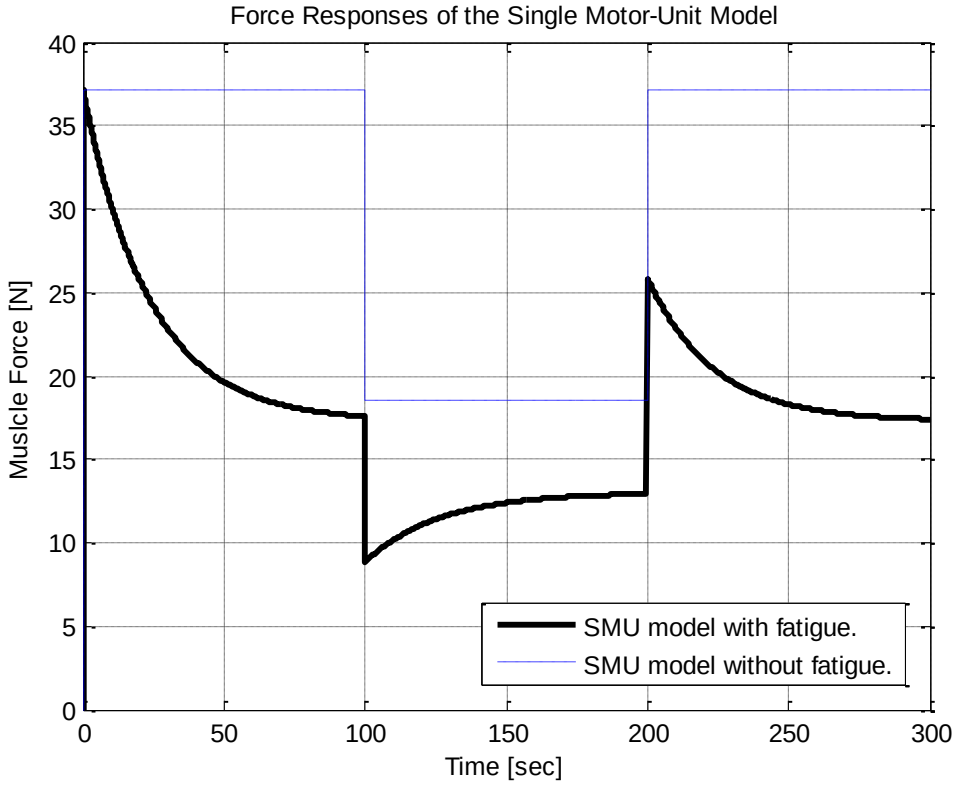

Figure 4.11: Force responses of the single-motor-unit model, protocol-III: ignoring and including fatigue sub-model.

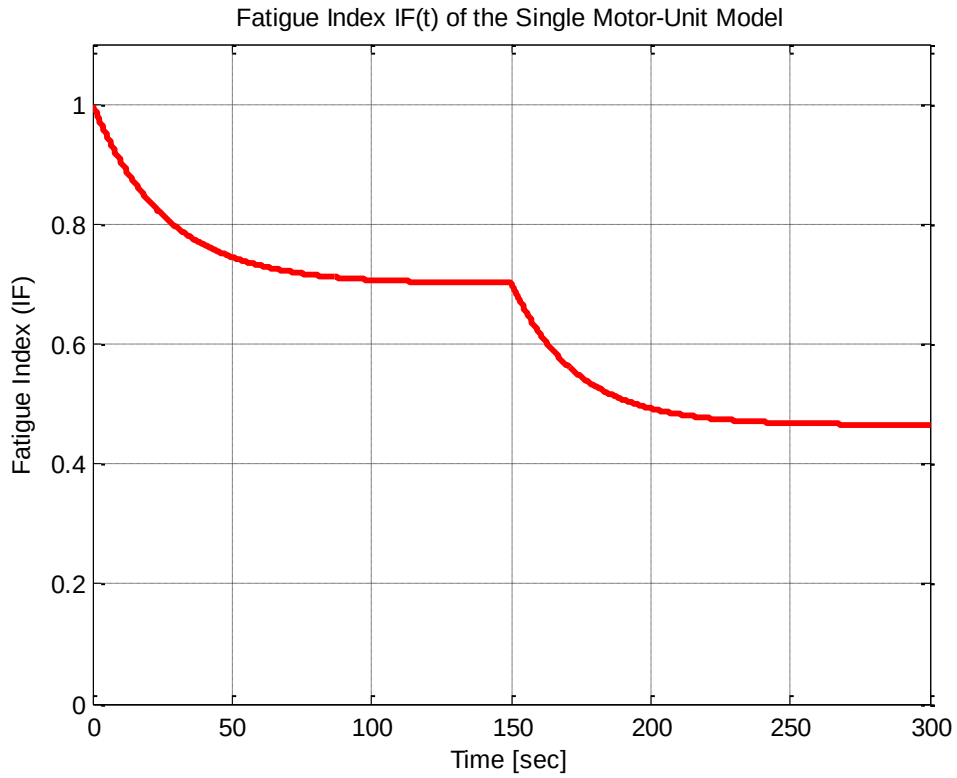

Figure 4.12: Index of fatigue for the single motor-unit model, protocol-IV.

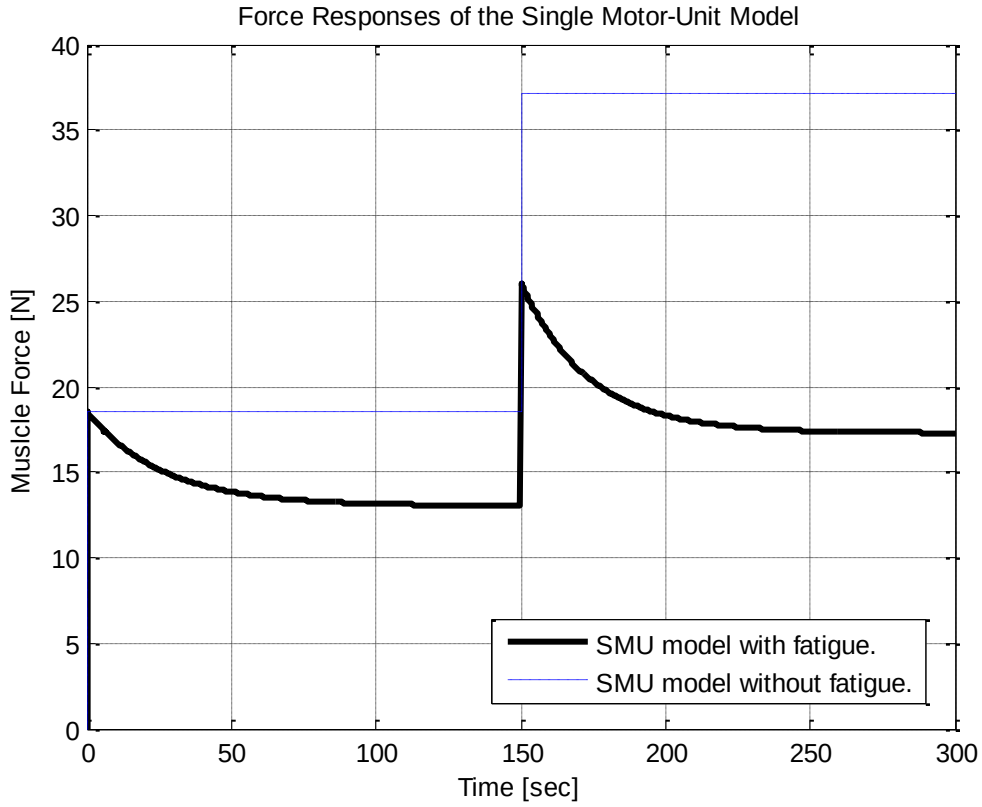

Figure 4.13: Force responses of the single-motor-unit model, protocol-IV: ignoring and including fatigue sub-model.

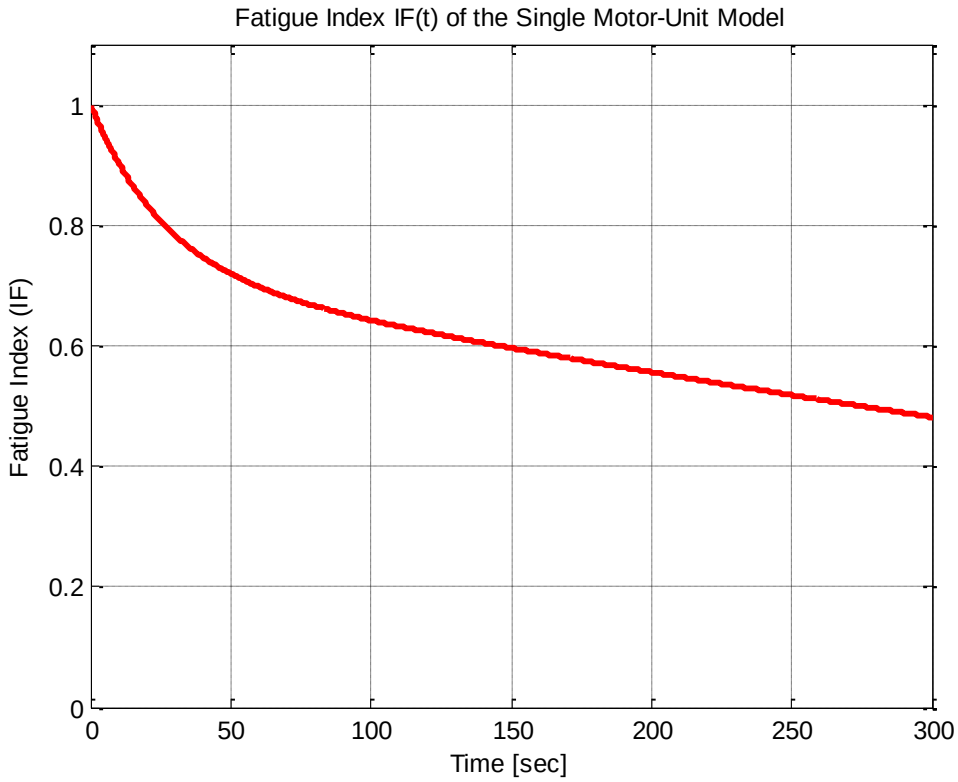

Figure 4.14: Index of fatigue for the single motor-unit model, protocol-V.

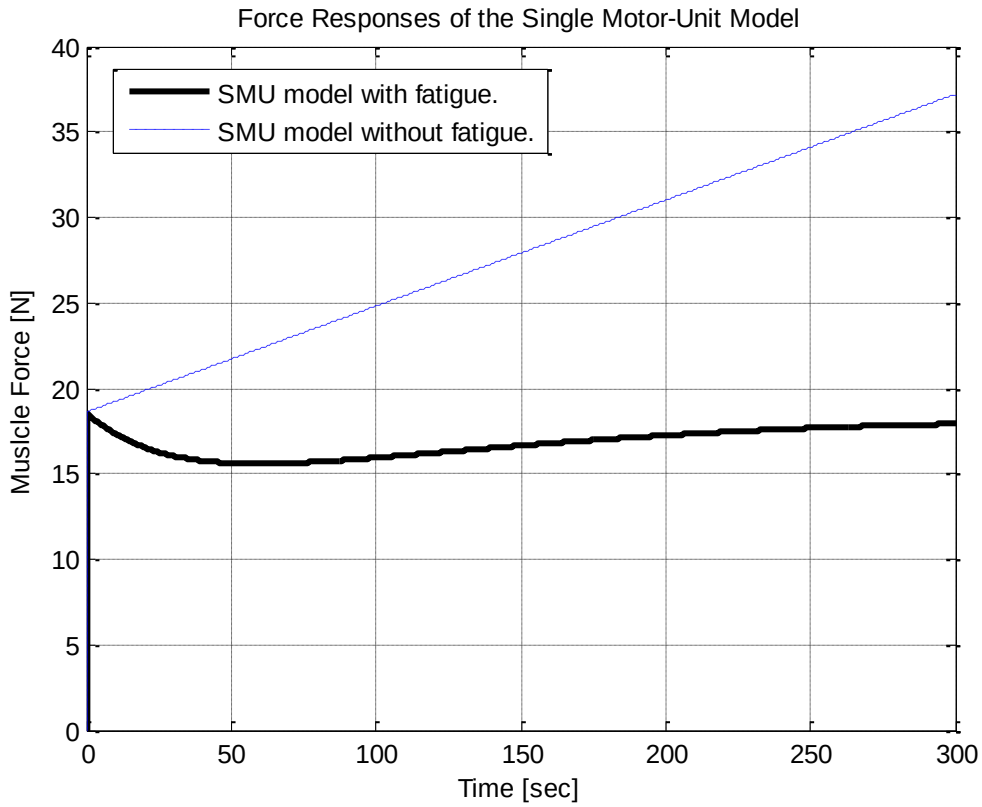

Figure 4.15: Force responses of the single-motor-unit model, protocol-V: ignoring and including fatigue sub-model.

4.3.3.2. Comparison using the multiple motor-unit model

In this section, the responses of two models are compared:

- The multiple motor-unit model without fatigue;
- The multiple motor-unit model with fatigue (using separate Riener fatigue sub-model with every motor-unit).

For each motor-unit, the fatigue curve when recruited and the recovery curve when not recruited are similar to a fully recruited muscle as described earlier in this chapter (Figure 4.1 and Figure 4.2). However, for comparison purposes, the average fatigue index of the MMU model for all of the 1000 motor units is shown for each protocol (equals *IF* of SMU model).

Referring to the recruitment protocol-III, the average index of fatigue, and the force response of the MMU model with fatigue (Figure 4.4, Figure 4.16 and Figure 4.17), in the first 100 seconds the muscle force decreases exponentially until the partial de-recruitment at 100 seconds. During the partial recruitment (between 100 and 200 seconds) the force response of the MMU model with fatigue is virtually constant because the recruited part of the muscle is already fatigued at its lowest level; the other non-recruited part of the muscle is already making recovery. The full recruitment on 200 seconds increases the force at high level because the newly recruited motor-units have been fully recovered, and the fatigue cycle starts again for the newly recruited motor-units. Figure 4.17 shows the force responses of the SMU and MMU models with and without fatigue for protocol-III.

Referring to the recruitment protocol-IV, the average index of fatigue, and the force response of the MMU model with fatigue (Figure 4.5, Figure 4.18 and Figure 4.19), for the first 150 seconds the fatigue rate of the 50% recruited muscle is virtually the same as that of the fully recruited muscle (in protocol-III). In Figures 4.17 and 4.19, both forces gradually fatigue to a value just below 50% of its value at start of protocol, but average indexes of fatigue for the MMU model are different as shown in Figures 4.16 and 4.18. Figure 4.19 shows the force responses of the SMU and MMU models with and without fatigue for protocol-IV.

Referring to the recruitment protocol-V, the average index of fatigue, and the force response of the MMU model with fatigue (Figure 4.6, Figure 4.20 and Figure 4.21), the force response decreases exponentially in the first 50 seconds then starts to increase at about constant rate; this is largely different than the force response of the single motor-unit model. Figure 4.21 shows the force responses of the SMU and MMU models with and without fatigue for protocol-V.

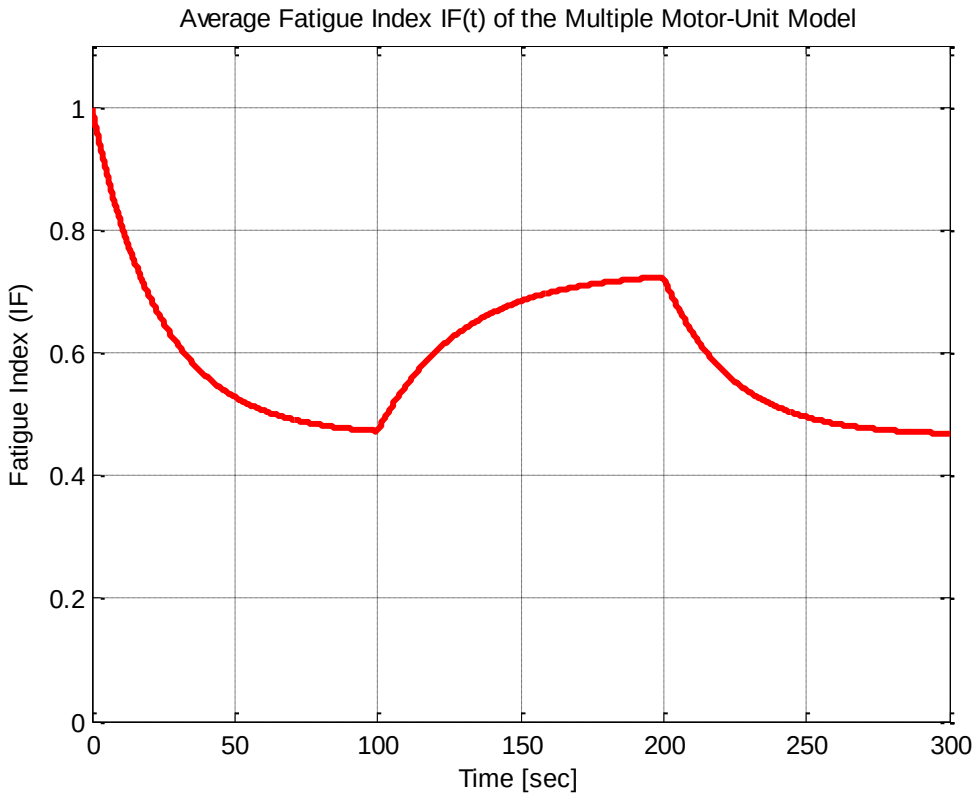

Figure 4.16: Average index of fatigue for the multiple motor-unit model, protocol-III.

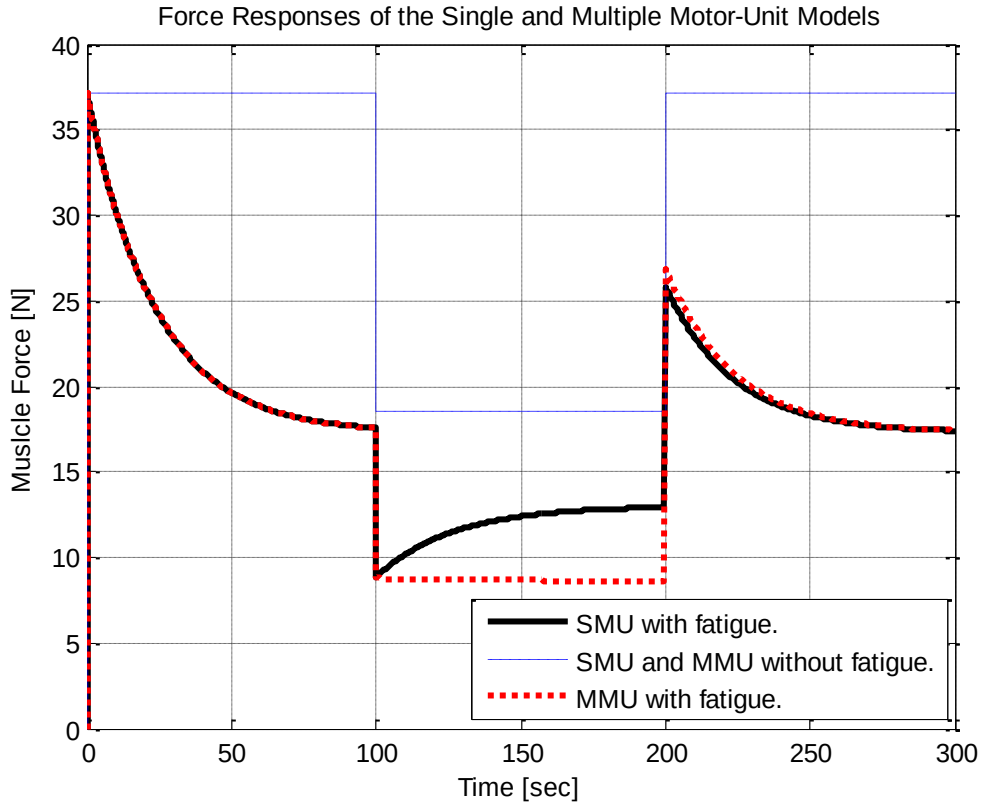

Figure 4.17: Force responses of the single and multiple motor-unit models, protocol-III: ignoring and including fatigue sub-model.

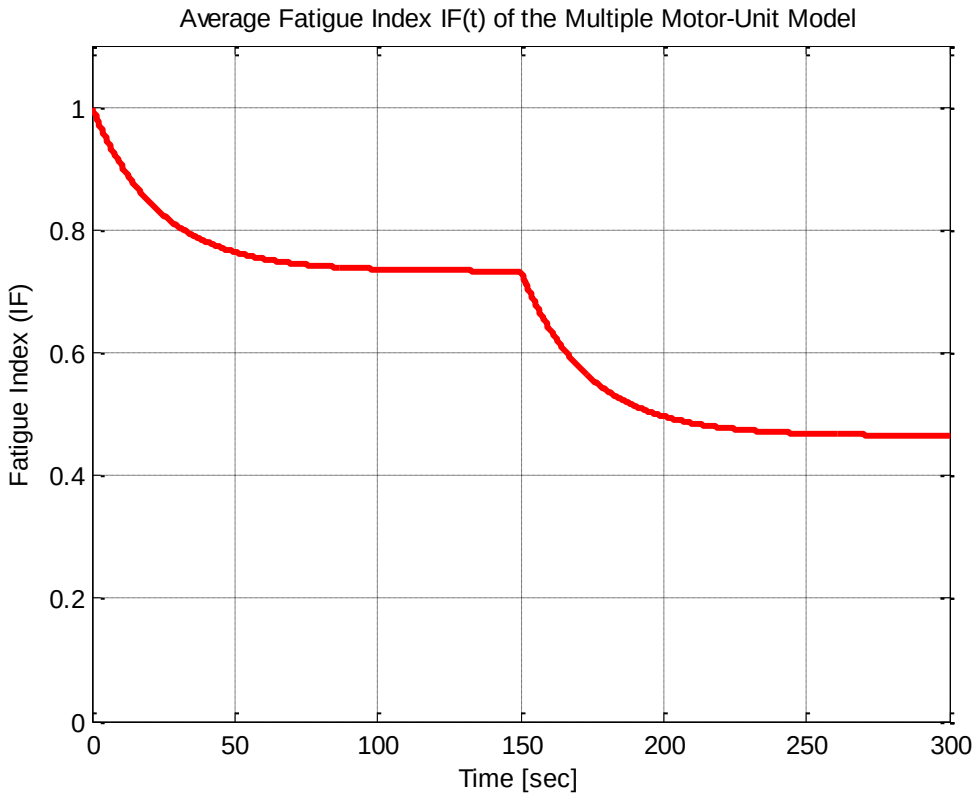

Figure 4.18: Average index of fatigue for the multiple motor-unit model, protocol-IV.

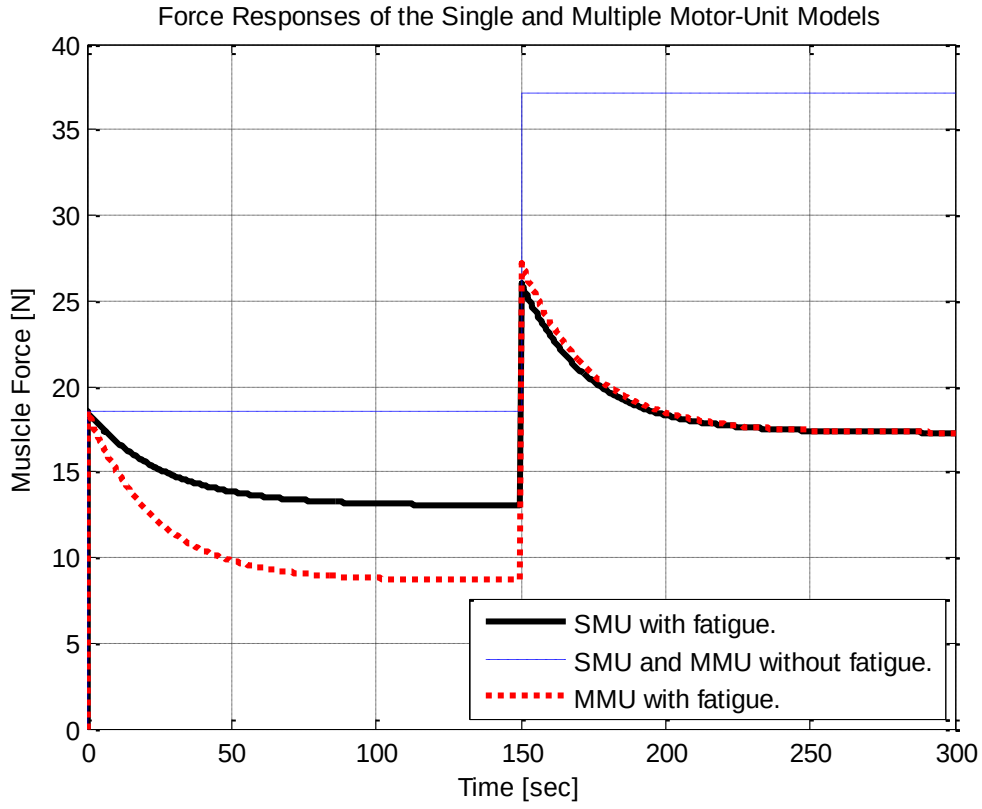

Figure 4.19: Force responses of the single and multiple motor-unit models, protocol-IV: ignoring and including fatigue sub-model.

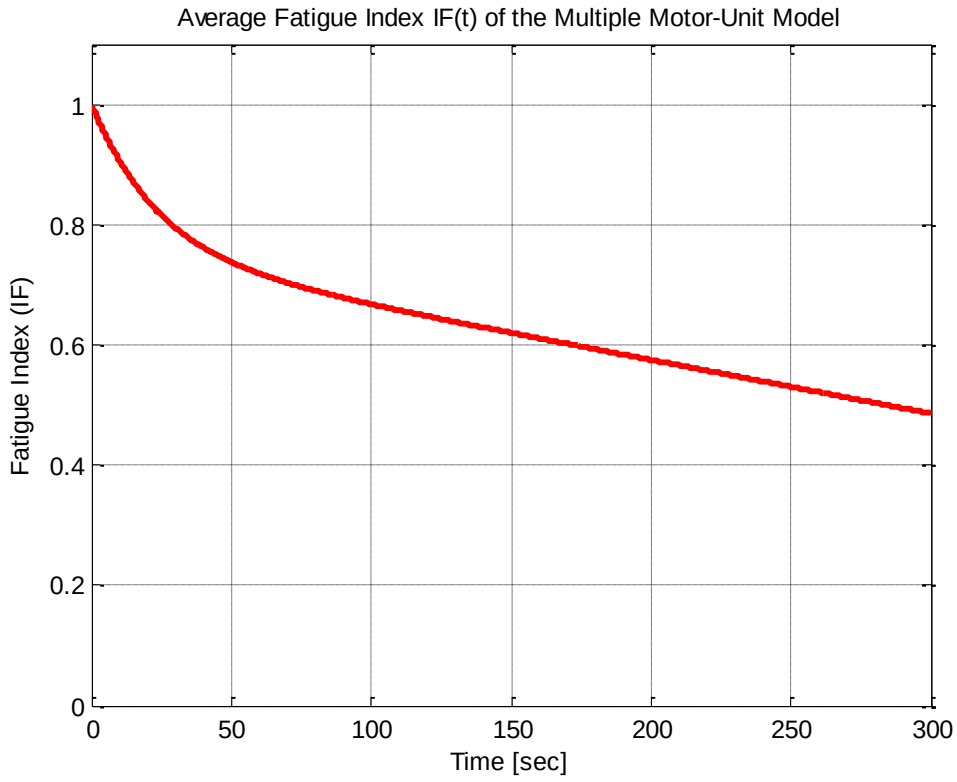

Figure 4.20: Average index of fatigue for the multiple motor-unit model, protocol-V.

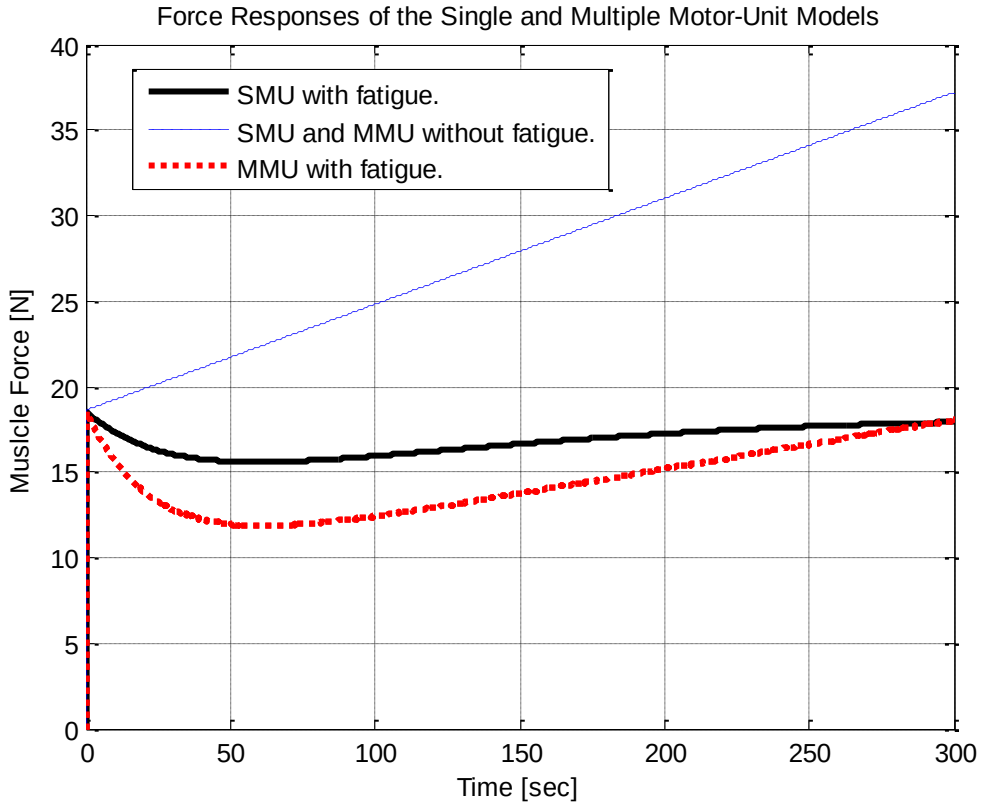

Figure 4.21: Force responses of the single and multiple motor-unit models, protocol-V: ignoring and including fatigue sub-model.

4.4. Conclusion

The fatigue sub-model was incorporated into the multiple motor-unit muscle model, further improving the way in which the recruitment-history is accounted for. The accuracy of the standard Herzog model can be enhanced by incorporation of the fatigue sub-model into the multiple motor-unit model. In the MMU model with fatigue, each motor-unit has its own fatigue and recovery cycles independent from other motor-units. This also takes account of the fact that muscle fatigue is highly affected by fibre-type and time elapsed since onset of recruitment. Such property should be modelled for each motor-unit separately, which can be achieved by using the multiple motor-unit modelling approach. The multiple motor-unit model is able to properly account for continuously varying recruitment as would usually be seen in closed loop FES control.

Effect of recruitment on fatigue and recovery in Riener fatigue sub-model (when incorporated into the SMU model) contradicts the empirical experiments. Empirical experiments show that partial recruitment increases muscle capacity by allowing non-recruited motor-units to recover, but recruited motor-units cannot recover when they are still recruited (electrically stimulated by FES).

Open-loop simulation protocols were used in this chapter to study two muscle models (SMU and MMU models) with and without fatigue. The two models studied were: The standard Herzog model and the $Eff.f_{CE}$ Model.

When fatigue is incorporated using Riener fatigue sub-model, the multiple motor-unit model produces different results (than those of the single motor-unit model) for different levels of recruitment and when different motor-units are recruited at different times because every motor-unit is modelled separately in the multiple motor-unit model with fatigue.

These results demonstrate the potential errors introduced by ignoring fatigue or by using single motor-unit (even if the fatigue sub-model is incorporated into the model) which are quite common in FES control studies. By correctly modelling the effects of continuously changing recruitment, by means of the multiple motor-unit model with fatigue sub-model, it is hoped that better FES controllers can be designed.

Chapter 5: The Multiple Motor-Unit Model with Force Enhancement & Depression

5.1. Introduction

Skeletal muscle force production is history dependent, yet this aspect of muscle modelling has received little attention in FES control studies [13]. Force depression following shortening and force enhancement following stretch can reach values of up to almost 50% of the corresponding isometric muscle force [13]. Therefore, if not properly accounted for during the design, it is reasonable to assume that this effect may adversely influence the performance of FES controllers. To the best of the author's knowledge, this length-history dependence has yet to be incorporated in muscle models in the context of FES control.

As discussed in section 2.5.5, force enhancement/depression is affected by magnitude of stretch/shortening, length at initial recruitment, recruitment level, velocity, and stimulation frequency during stretch/shortening, but is mainly affected by magnitude of stretch/shortening [13, 150, 151, 152, 153, 154, 155, 156, 157].

As discussed in section 3.1, it is reasonable to assume that the recruitment level (R) changes continuously. Similarly, in closed loop FES control applications R will usually vary with time. However, as almost all muscle models used in FES control studies treat the muscle as a one large motor-unit, there can only be one value for the force enhancement or depression despite the fact that in reality different motor-units are recruited at different lengths and hence magnitude of stretch/shortening will be different. The use of a force enhancement & depression sub-model incorporated into a single motor-unit (SMU) model in a realistic scenario where R and l_{CE} are changing continuously would result in an over- or under-estimation of force enhancement and depression.

Therefore, this chapter addresses the problem of muscle modelling for continuously varying R and l_o, hence different initial lengths and magnitude of stretch and/or shortening for different motor-units. For simplicity, the focus in this chapter will be on the steady-state force enhancement and depression after end of stretch and/or shortening (i.e. effects of force enhancement/depression during stretch/shortening are ignored here).

As discussed in section 2.5.5, only a few models for force enhancement & depression are available in the literature, and they do not include all the length-history properties as observed experimentally, see experimental data in Appendix 2. A standard and new complex sub-model for force enhancement & depression was developed during this research that incorporates most of the length-history properties (more complex than Hawkins and Forcinito *IE & ID* sub-models). The empirical data used to develop this sub-model were collected from the literature. Details of the standard force enhancement & depression sub-model are given in Chapter 6.

A simple model for force enhancement & depression that models the steady-state effects of force enhancement/depression following stretch/shortening is used in the open-loop simulation protocols of single and multiple motor-units models. The results are discussed at the end of the chapter.

5.2. Effective *CE* force ($Eff.f_{CE}$) model with force enhancement & depression

The effective *CE* force model (developed in Chapter 3) is extended by incorporating the model of force enhancement & depression proposed by Forcinito and colleagues [156, 157] for a fully recruited muscle treated as a single motor-unit. Based on their model, an elastic rack has been included in parallel with each motor-unit (Figure 5.1). When a motor-unit is recruited, its elastic rack is engaged and thus, if there is any change in the *CE* length after recruitment of this motor-unit, then the length of the elastic rack ($l_{ER,j}$) will also change by the same magnitude. The passive force produced by that motor-unit will be a function of the change in the elastic rack length $\Delta l_{ER,j}$. Instantaneous length of the elastic rack (l_{ER}) is the same as the instantaneous *CE* length (i.e. $l_{ER} = l_{CE}$). Force enhancement or depression for a single motor-unit of index (*j*) is given by:

$$(f_e / f_d)_j = \left(\frac{E.A}{\bar{l}_{ER,j,o}} \times \Delta \bar{l}_{ER,j} \right) \qquad (5.1)$$

E: is the modulus of elasticity of the elastic rack.

A: is the cross-sectional area of the elastic rack.

$\bar{l}_{ER,j,o}$: is the elastic rack length at initial recruitment (normalised with respect to l_{opt}).

$\Delta\bar{l}_{ER}$: is the total displacement of the elastic rack after end of stretch/shortening (normalised with respect to l_{opt}).

IE: Index of force enhancement following stretch of recruited muscle.

ID: Index of force depression following shortening of recruited muscle.

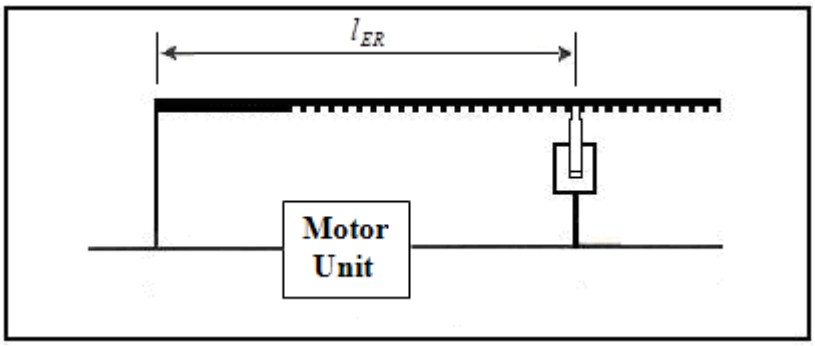

Figure 5.1: Motor-unit with parallel elastic rack. Force enhancement & depression is modelled by an elastic rack in parallel with each motor-unit.

Forcinito elastic rack models only the steady-state force enhancement of depression. The complete Forcinito *IE & ID* sub-model includes also the transient response during stretch/shortening, Forcinito *IE & ID* sub-model is summarised in Appendix 8.

Force enhancement following stretch is modelled by the index of enhancement *IE*. Force depression following shortening is modelled by the index of depression *ID*, for topology of different models see appendix 1. The index of enhancement & depression *IE & ID* is represented by:

$$IE = 1 + \left(\frac{E.A}{\bar{l}_{ER,j,o}} \times \Delta\bar{l}_{ER,j} \right) \quad , \quad \Delta\bar{l}_{ER,j} > 0 \tag{5.2}$$

$$ID = 1 + \left(\frac{E.A}{\bar{l}_{ER,j,o}} \times \Delta\bar{l}_{ER,j} \right) \quad , \quad \Delta\bar{l}_{ER,j} < 0 \tag{5.3}$$

Both of *IE* and *ID* have the same equation but ($\Delta \bar{l}_{ER}$) will be positive in case of stretch and negative in case of shortening.

The effective *CE* force model with force enhancement & depression is presented in Figure 5.2. The effective *CE* force of the entire muscle, including force enhancement and depression for each motor unit recruited, is the sum of the individual motor unit forces as follows:

$$\begin{aligned} Eff.f_{CE} + (f_e / f_d) &= \lfloor f_{CE,1} + (f_{e,1} / f_{d,1}) \rfloor + \lfloor f_{CE,2} + (f_{e,2} / f_{d,2}) \rfloor + ... + \lfloor f_{CE,M} + (f_{e,M} / f_{d,M}) \rfloor \\ &= \sum_{j=1}^{M} \left[f_{CE,j} + (f_{e,j} / f_{d,j}) \right] \end{aligned} \tag{5.4}$$

Finally, the effective *CE* force ($Eff.f_{CE}$) with force enhancement & depression of all recruited motor-units is used to calculate the total muscle force F_m as follows:

$$F_m = \left(k_p \times \Delta l_{mt} \right) + \sum_{j=1}^{M} \left[f_{CE,j} + (f_{e,j} / f_{d,j}) \right] \tag{5.4A}$$

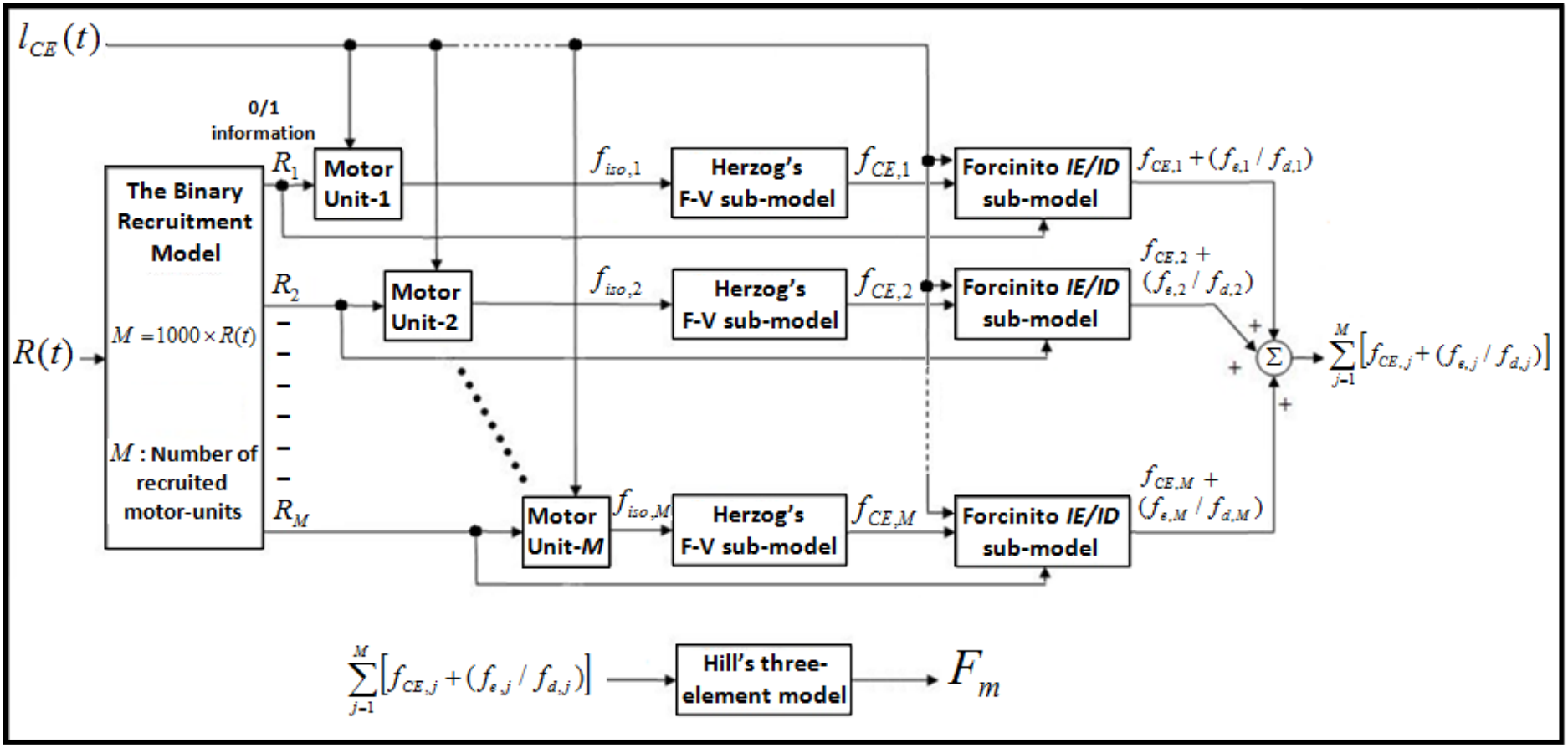

Figure 5.2: Force enhancement & depression incorporated into the effective *CE* force model.

5.3. Simulation results

Matlab codes were developed for simulating the responses to open-loop simulation protocols of two muscle models:

- The Herzog model (treating the muscle as a single motor-unit);
- The $Eff.f_{CE}$ multiple motor-unit model.

In both cases, the force enhancement & depression can be neglected or incorporated into the model.

In the following sections, firstly, the two input protocols that have been used are defined. Then simulation results are presented to compare the alternative muscle models and, in particular, to demonstrate the potential errors introduced by: a) ignoring the force enhancement & depression; and b) incorporating force enhancement & depression sub-model into a single motor-unit model instead of multiple motor-unit (MMU) model.

5.3.1. Input protocols

In order to demonstrate the need to use a multiple motor-unit modelling approach to model force enhancement & depression when R and l_{CE} vary with time, input protocols are required that involve changing R, l_{CE}, and magnitude of stretch/shortening. Two suitable protocols were chosen, details of which are as follows:

Protocol-VI (Figure 5.3):

(i) At $t = 0.0$ seconds: Partial (50%) isometric recruitment at the unique resting state (i.e. at $l_o = l_{rest} = 125 \quad mm,\ \Delta l_{mt} = 0$);

(ii) At $t = 1.0$ seconds: Shortening of 50 mm (to $\Delta l_{mt} = -50\,\text{mm}$) at speed of 25mm/sec for two seconds;

(iii) Between $t = 3.0$ and $t = 4.0$: No change in R nor in l_{mt}.

(iv) At $t = 4.0$ seconds: Full (100%) recruitment;

(v) Between $t = 4.0$ and $t = 5.0$: No change in R nor in l_{mt}.

(vi) At $t = 5.0$ seconds: Stretch of 50 mm (to $\Delta l_{mt} = 0$) at speed of 25mm/sec for two seconds.

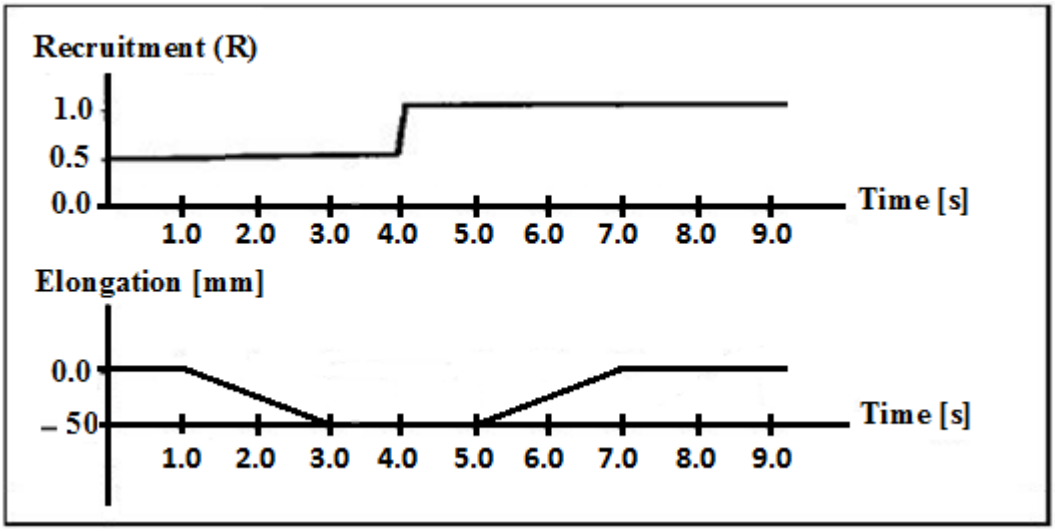

Figure 5.3: Protocol-VI.

Protocol-VII (Figure 5.4):

(i) At $t = 0.0$ seconds: Partial (50%) isometric recruitment at $\Delta l_{mt} = -50\,\text{mm}$;

(ii) At $t = 1.0$ seconds: Stretch of 50 mm (to $\Delta l_{mt} = 0$) at speed of 25mm/sec for two seconds;

(iii) Between $t = 3.0$ and $t = 4.0$: No change in R nor in l_{mt}.

(iv) At $t = 4.0$ seconds: Full (100%) recruitment;

(v) Between $t = 4.0$ and $t = 5.0$: No change in R nor in l_{mt}.

(vi) At $t = 5.0$ seconds: Shortening of 50 mm (to $\Delta l_{mt} = -50\,\text{mm}$) at speed of 25mm/sec for two seconds.

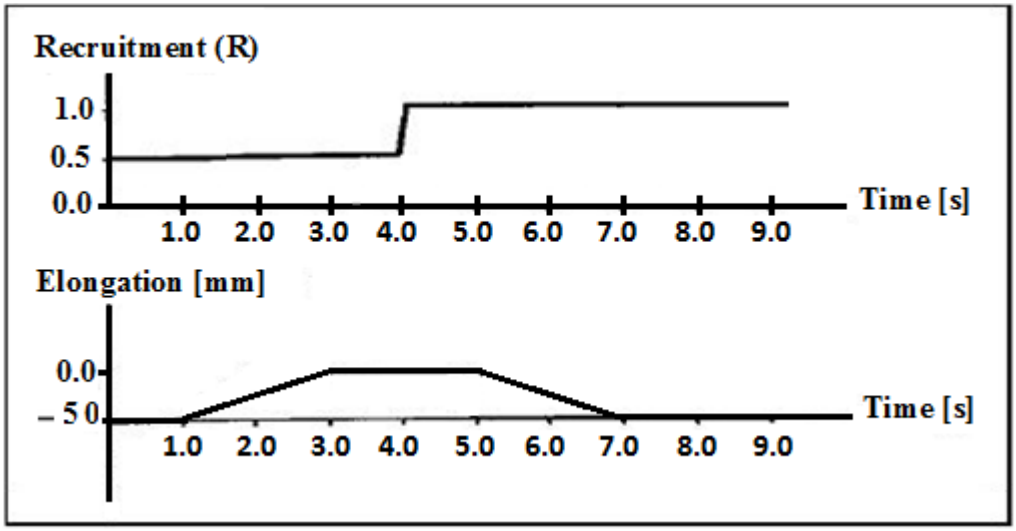

Figure 5.4: Protocol-VII.

Although the two protocols have different stretch/shortening cycles, both have the same recruitment cycle and both end at full recruitment. Another important point, since the length at initial recruitment is used, the corresponding isometric forces of the start and end *CE* lengths of both protocols are the same in the Herzog force-length sub-model (i.e. $f_{iso}(0.75l_{opt}) = f_{iso}(1.25l_{opt})$), hence there is no effect of the initial length in these two protocols (the problem addressed in chapter 3) and no difference (in the steady-state) if the instantaneous or the initial length was used, see Figure 5.5 (the transient-state is different in this case). This means any difference in the simulation results is only because of the force enhancement & depression sub-model.

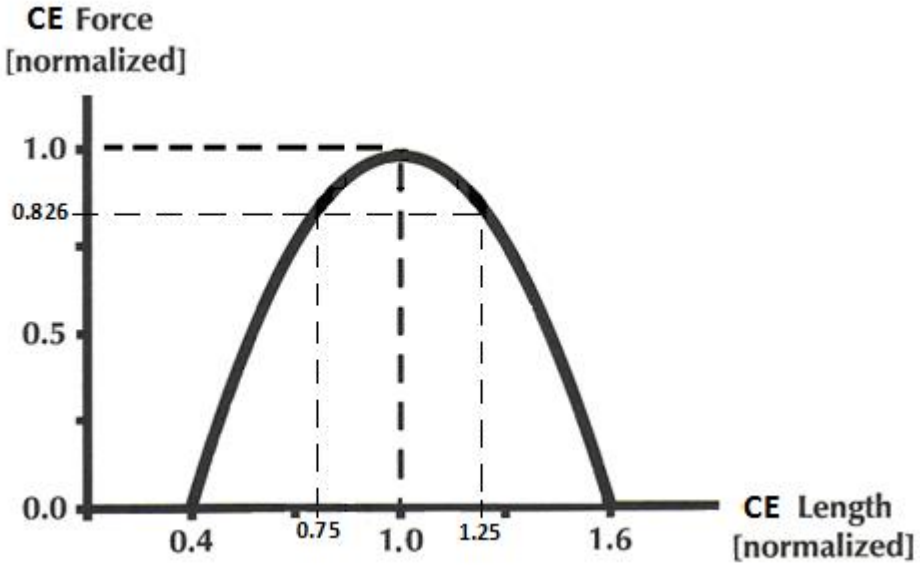

Figure 5.5: The corresponding isometric forces of the start and end *CE* lengths of protocol-VI and protocol-VII are equal in Herzog F-L sub-model. $f_{iso}(0.75l_{opt}) = f_{iso}(1.25l_{opt})$.

The typical values for the muscle parameters used in Chapter 3 are used in this chapter as well. The parameters of force enhancement & depression sub-model (equation 5.1) were roughly estimated using the experimental data in Appendix 2. However, the aim was not to make an exact estimation for the parameters of equation 5.1, the aim was to demonstrate the potential errors introduced by ignoring the force enhancement & depression or using the single motor-unit model instead of the multiple motor-unit model.

Rigid tendon is assumed in both protocols (i.e. $k_S = \infty$). The rigid tendon is assumed so that the *CE* length does not change when *CE* force changes because of changes in recruitment level R and hence different l_o for different motor-units in the multiple motor-unit model. Based on this assumption: $\Delta l_{mt} = \Delta l_{CE}$, i.e. changes in *CE* length are always the same as the changes in the length of the musculotendon complex (the whole muscle lenght). In this way all differences in force response are due to force enhancement and/or depression only. It is also assumed that *PE* force (f_{PE}) is zero for lengths less than l_{rest} (i.e. $f_{PE} = 0 \quad for \quad l_{CE} \le l_{rest}$).

5.3.2. Comparison of the single and multiple motor-unit models without force enhancement & depression

Simulation results using the multiple motor-unit model versus the single motor-unit model for protocol-VI and protocol-VII are plotted in Figure 5.6 and Figure 5.7. The aim was to confirm that, for the chosen protocols, the force responses of the two models are identical. The force responses of the two models, in protocol-VI and protocol VII, are calculated using the length at initial recruitment (l_o). In both protocols, half of motor-units is recruited at ($l_o = 0.75 l_{opt}$) and the other half is recruited at ($l_o = 1.25 l_{opt}$). The corresponding isometric forces of both initial lengths are the same in the Herzog F-L sub-model since $f_{iso}(0.75 l_{opt}) = f_{iso}(1.25 l_{opt})$ as illustrated in Figure 5.5. For this reason the two force responses are identical.

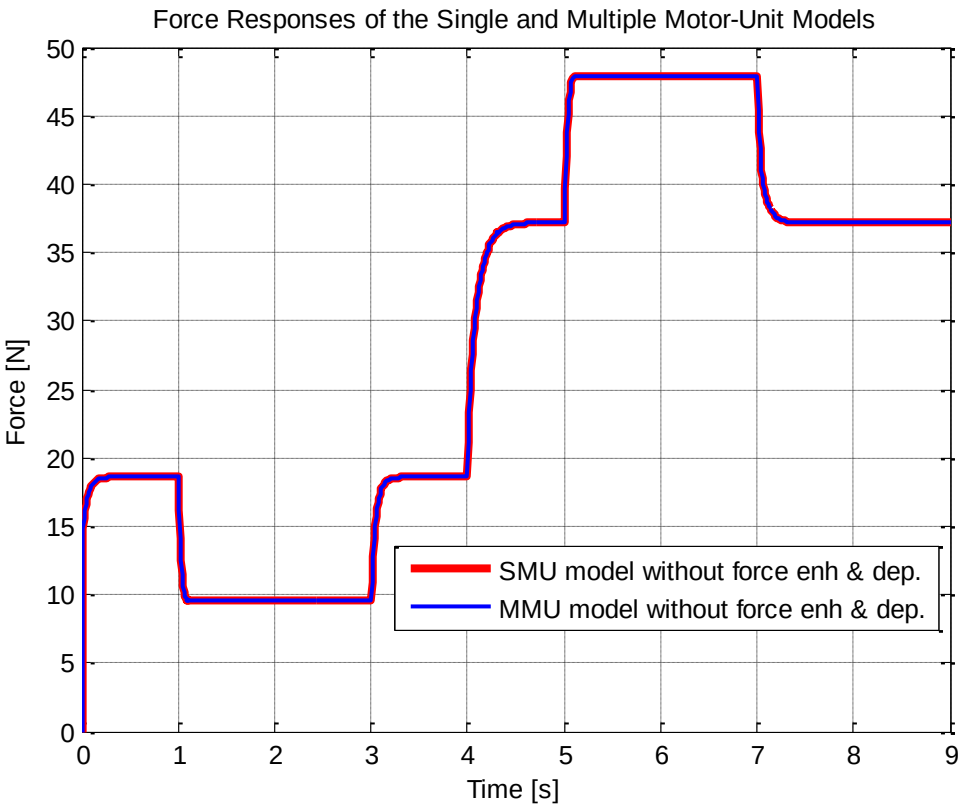

Figure 5.6: Identical force responses of the single and multiple motor-unit models without force enhancement & depression sub-model, protocol-VI.

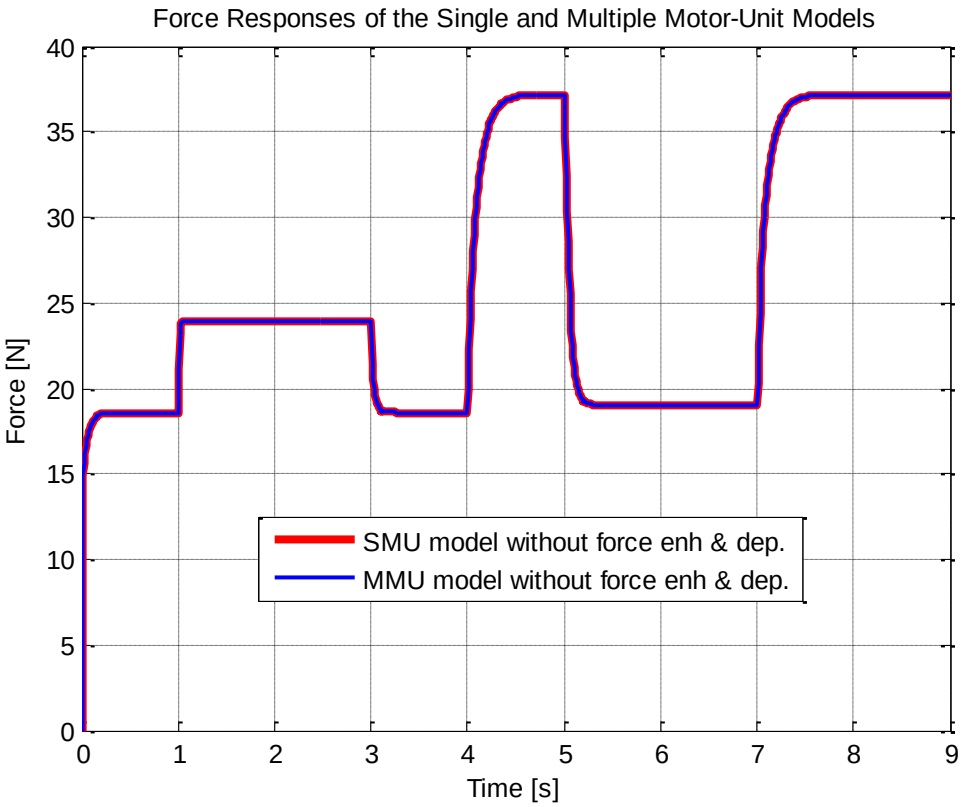

Figure 5.7: Identical force responses of the single and multiple motor-unit models without force enhancement & depression sub-model, protocol-VII.

5.3.3. Comparison of models with and without force enhancement & depression

This section compares the simulation results using the same model with and without force enhancement & depression. This is done with both the single motor-unit model and the multiple motor-unit model. The aim was to demonstrate the potential errors introduced by ignoring force enhancement & depression which is common in FES control studies.

5.3.3.1. Comparison using single motor-unit model (standard Herzog model)

In this section, the responses of two models are compared:

- The single motor-unit model without force enhancement & depression;
- The single motor-unit model with force enhancement & depression (using one single elastic rack).

Referring to the two recruitment protocols; protocol-VI (Figure 5.3) and protocol-VII (Figure 5.4), the force responses of the SMU models (Figure 5.8 and Figure 5.9) and the force enhancement & depression sub-model (equations 5.2 and 5.3), in both cases the isometric forces corresponding to the *CE* length at initial recruitment (at 0 seconds) are equal. Although the initial *CE* lengths, in the two protocols, are on different limbs of the F-L curve when recruitment started, the corresponding isometric forces are equal, see Figure 5.5. The *CE* length at initial recruitment is used throughout the two protocols since the single motor-unit model effectively consists of only one single *CE* and can have only one initial length as long as it is still recruited at any level of recruitment (details are illustrated in Appendix 3).

In Figure 5.8, when the muscle is shortening (between 1 and 3 seconds) the shortening decreases the force response of the model with elastic rack and continues to decrease until the end of shortening while the force response of the other model is constant. After end of shortening, the elastic rack is still engaged and thus the passive force which was produced during shortening will not disappear after end of shortening since the elastic rack is still engaged. After the rise to full recruitment at 4 seconds, the force responses of both models increase with the same amount since the elastic rack is not affected by recruitment variations when *CE* length in constant. When the muscle is stretching (between 5 and 7 seconds), the force response of the model with the elastic rack starts to increase until the force responses of both models are equal at the end of stretch. The elastic rack is still engaged but because it stretches back to the initial length when it was first engaged, the passive force produced by the elastic rack continues to decrease until it disappears at 7 seconds (at the length it was initially engaged at).

Conversely, with protocol-VII, the elastic rack increases the force response during stretch (between 1 and 3 seconds) and retains it (Figure 5.9). When the muscle is shortening (between 5 and 7 seconds), the elastic rack starts to lose its force until the force responses of both models are equal at the end of shortening.

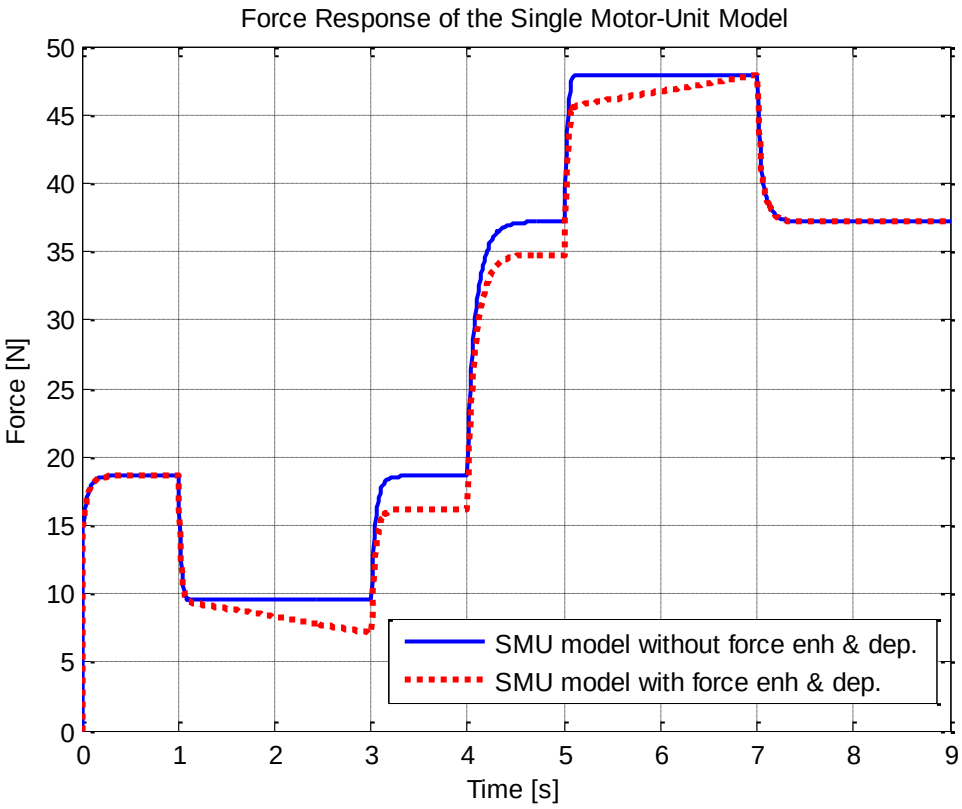

Figure 5.8: Force response of the single-motor-unit model, protocol-VI: ignoring and including force enhancement & depression.

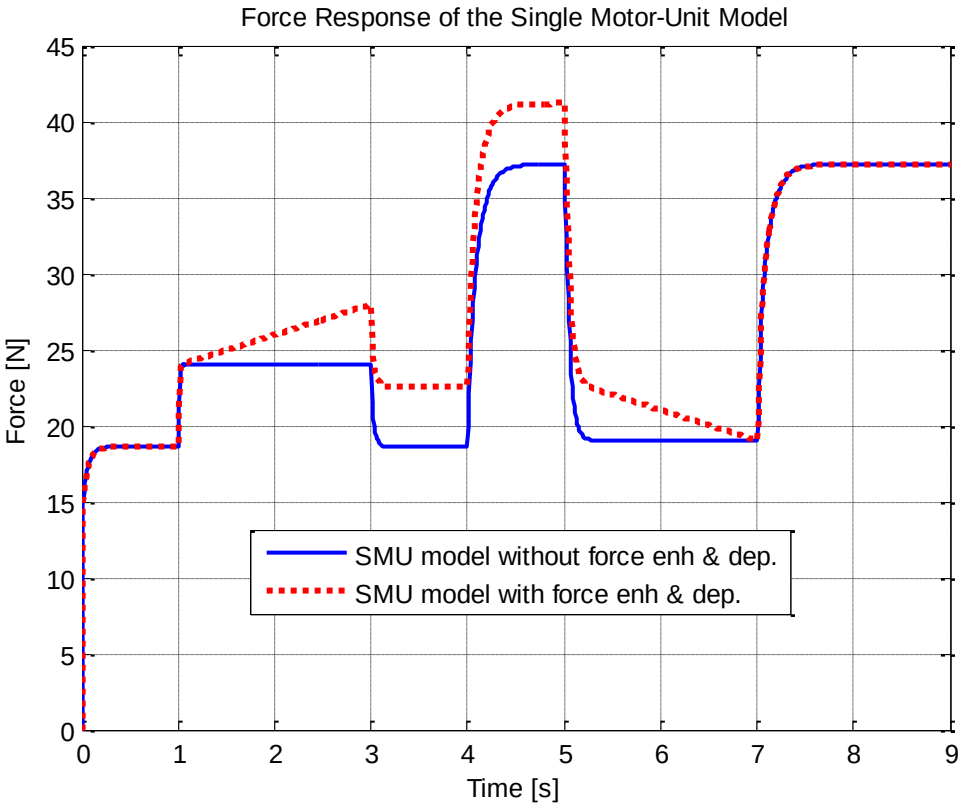

Figure 5.9: Force response of the single-motor-unit model, protocol-VII: ignoring and including force enhancement & depression.

5.3.3.2. Comparison using the multiple motor-unit model

In this section, the responses of two models are compared:

- The multiple motor-unit model without force enhancement & depression;
- The multiple motor-unit model with force enhancement & depression (using 1000 elastic racks).

Referring to the force responses of the MMU model with and without force enhancement & depression sub-model (Figure 5.10 and Figure 5.11), the differences between the two multiple motor-unit models (with and without elastic racks) are similar to those seen between the corresponding single motor-unit models (Figure 5.8 and Figure 5.9). These differences largely arise for the reasons explained in the previous section. However, there are some additional noteworthy observations that are discussed below.

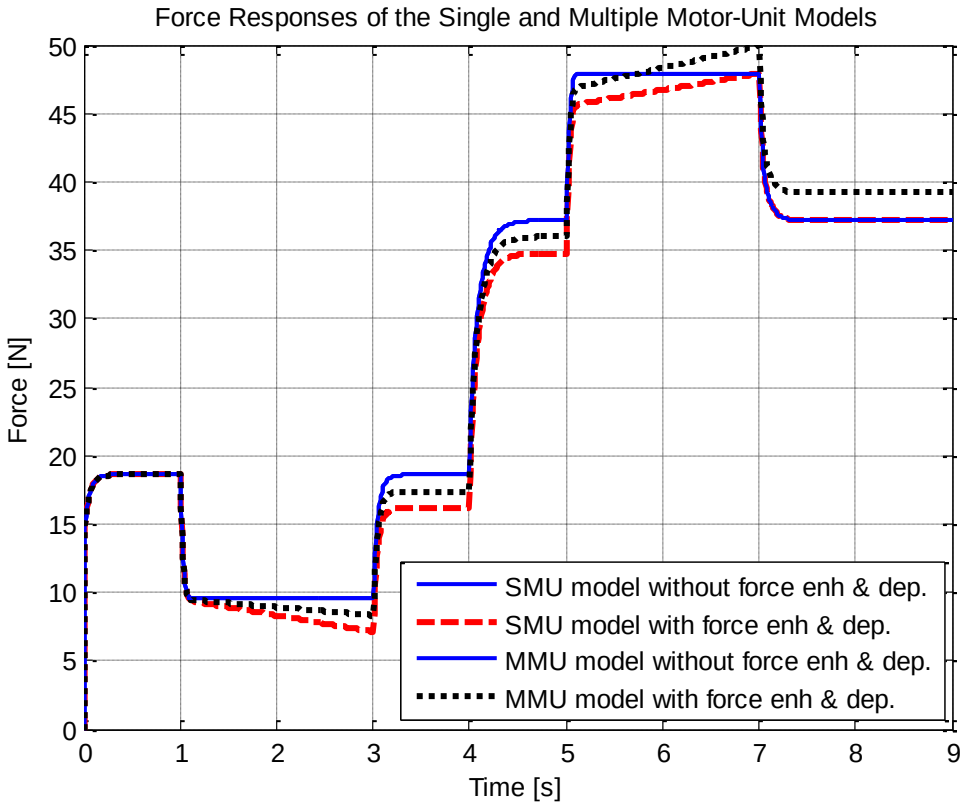

Figure 5.10: Force responses of all models, protocol-VI: SMU model without force enhancement & depression sub-model, SMU model with force enhancement & depression sub-model, MMU model without force enhancement & depression sub-model, and MMU model with force enhancement & depression sub-model.

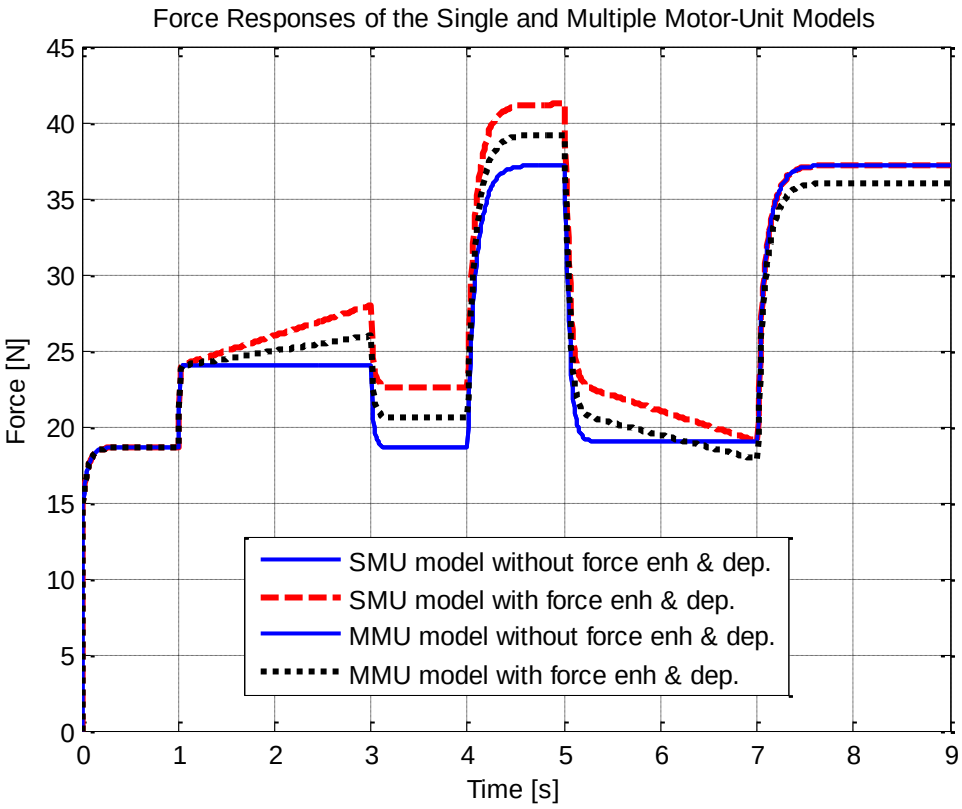

Figure 5.11: Force responses of all models, protocol-VII: SMU model without force enhancement & depression sub-model, SMU model with force enhancement & depression sub-model, MMU model without force enhancement & depression sub-model, and MMU model with force enhancement & depression sub-model.

When force enhancement & depression sub-model is ignored, the results are similar to those for the single motor-unit model when ignoring force enhancement & depression sub-model, all models are plotted together in Figures 5.10 and 5.11. This is because, for these particular protocols, the isometric forces of all initial *CE* lengths for both protocols are equal (as discussed earlier). The rise to full recruitment at 4 seconds, in both protocols, was on a *CE* length on the other limb of the F-L curve but the corresponding isometric force is the same as that corresponding to the *CE* length at 0 seconds.

However, when including force enhancement & depression, the results differ from those for the single motor-unit model because recruitment changes at different lengths and hence the elastic racks of the multiple motor-unit model are engaged at different lengths and different magnitudes of stretch or shortening (see Figure 5.3 and Figure 5.4) and the multiple motor-unit model is able to properly account for varying recruitment level at different *CE* lengths (Figure 5.10 and Figure 5.11).

Referring to the multiple motor-unit model with force enhancement & depression sub-model (Figure 5.10), when the muscle is shortening (between 1 and 3 seconds) 50% of the elastic racks are engaged and the shortening decreases the force response of this model (MMU model with elastic racks) and continue to decrease until the end of shortening while the force response of the other model (MMU model without elastic racks) is constant. After end of shortening, 50% of the elastic racks are still engaged and thus the passive forces produced during shortening will not disappear. After the rise to full recruitment at 4 seconds, the force responses of both models (MMU models with and without elastic racks) increase by the same magnitude since the elastic racks are not affected by the increase in recruitment level. The rise of recruitment to 100% at 4 seconds will also engage the remaining 50% of elastic racks at different length (for the MMU model with elastic racks). When the muscle is stretching (between 5 and 7 seconds), the passive forces of the elastic racks engaged first (at $l_{CE} = l_{rest}$) start to decrease because they stretch back to the initial length where they were first engaged, and the passive forces of the lately engaged elastic racks start to increase until the end of stretch (at $l_{CE} = l_{rest}$). At the end of the protocol, the force magnitudes of the two MMU models are different because there are 50% of elastic racks still engaged and produce passive force in the MMU model with elastic racks. The other 50% of elastic racks are still engaged but at the same initial length where they were engaged first, and hence will produce no force.

In Figure 5.11, force enhancement and force depression are modelled in a similar way as described above. Note that the amount of force enhancement or depression produced at shorter initial length is more than that produced at longer initial length (Figure 5.10 and Figure 5.11), this is because force enhancement or depression is divided by the initial length $\left(\bar{l}_{ER,j,o}\right)$ in equations 5.2 and 5.3.

The single and the multiple motor-unit models without force enhancement & depression are plotted together in the same figure, but their force responses are exactly the same for the two protocols (Figure 5.10 and Figure 5.11).

5.4. Conclusion

The force enhancement & depression sub-model was incorporated into the multiple motor-unit muscle model, further improving the way in which the recruitment-history and length-history are accounted for. The accuracy of the standard Herzog model can be enhanced by the

force enhancement & depression sub-model incorporated into the multiple motor-unit model. Since the force enhancement & depression sub-model is based on the magnitude of stretch and/or shortening and the length of each motor-unit when it was initially recruited, the multiple motor-unit model is able to properly account for continuously varying recruitment levels at different *CE* lengths as would usually be seen in closed loop FES control.

Open-loop simulation protocols were used to study two muscle models (SMU and MMU models) with and without force enhancement & depression sub-model. The two models which have been studied in this chapter are the standard Herzog model (with SMU) and the $Eff.f_{CE}$ Model.

When force enhancement and/or depression are ignored in the muscle model, the single motor-unit model and the multiple motor-unit model do not show any force enhancement or depression because this is not modelled in the standard Hill model (or any other standard Hill-based model). When force enhancement & depression are modelled using Forcinito elastic rack, the multiple motor-unit model produces different results if different motor-units are recruited at different lengths because the elastic racks engage at different lengths and stretch/shorten at different magnitudes.

These results demonstrate the potential errors introduced by ignoring the force enhancement & depression sub-model or by using the single motor-unit model (even if the force enhancement & depression sub-model is incorporated) which are common in muscle models used in FES control studies. By correctly modelling the effects of continuously changing recruitment levels and *CE* length (during dynamic contractions), by means of the multiple motor-unit model with force enhancement & depression sub-model, it is hoped that better FES controllers can be designed.

Chapter 6: Towards a General Model

6.1. Introduction

A general model, capable of representing the alternative sub-models (for each muscle property) presented in section 2.5 and the inter-connection of these sub-models (model topology), could be used to represent any of the alternative muscle models presented in Chapter 2 or to build new models at different levels of complexity. Such a "General Model" could be used to study the effect of muscle model complexity on FES controller design so that appropriate trade-offs between model complexity and model accuracy could be determined. Therefore a "General Model" that can be used to represent all relevant models from the literature was developed.

The topology of the "General Model" is presented in section 6.2 showing the arrangement of sub-models and the interlinking model variables, i.e. the inputs and outputs of the various sub-models. The arrangement of the passive elements is also presented. Section 6.3 presents the proposed general forms for the sub-models required in muscle modelling for FES controller design.

6.2. Topology of the "General Model"

A standard topology for the "General Model" is presented here with a description of how it can be adapted to represent the topologies of other models presented in the literature. The topologies of some of the important published muscle models are presented in Appendix 1.

The full topology of the "General Model" is too large to be represented in one diagram. Therefore it is broken into parts and represented in separate figures, which are discussed under the following sub-headings.

6.2.1 Recruitment model topology

Figure 6.1 shows the FES recruitment model, which assumes stimulation frequency is constant and pulse width (or pulse amplitude) determines recruitment R_i, which can be

different for different fibre-types (*i* indicating the fibre type). A model of calcium dynamics is included before the recruitment model.

Referring to Figure 6.2, the natural stimulation sub-model includes a model of the relationship between natural stimulation input U and both recruitment and stimulation frequency for each fibre-type. The input is the natural stimulation input U and the outputs are U_{eff} and $freq_i$. These two outputs can be used in the same way as used with FES (i.e. the same recruitment sub-model can be used with both FES and natural stimulation). U_{eff} was introduced in VM 4.0 [128] to model the rise and fall effects of calcium dynamics, which represents the activation transient-state.

As discussed in sections 2.2.1, 2.3.3 and 2.5.1; at onset and termination of FES (or natural voluntary contraction) there is a transient-state of activation, this can be modelled by the rise and fall time U_{eff} sub-model as in Brown model (details are provided in [128], summary in Appendix 1) or the "calcium dynamics + time delay" sub-model as in Riener-1 model (details are provided in [72], summary in Appendix 1). These two alternative sub-models (or any other alternative) can be incorporated into the "General Model" as shown in Figures 6.1 and 6.2.

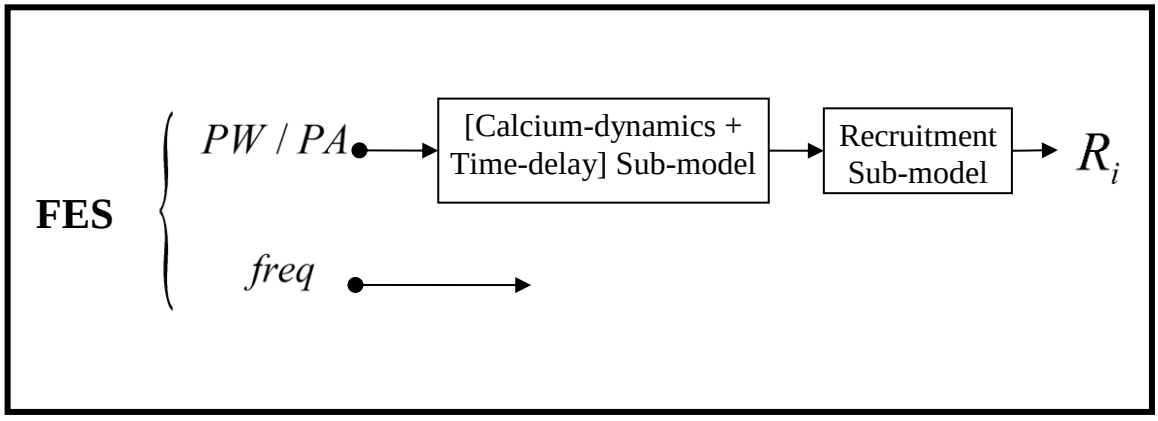

Figure 6.1: Topology of the "General Model" for FES input.

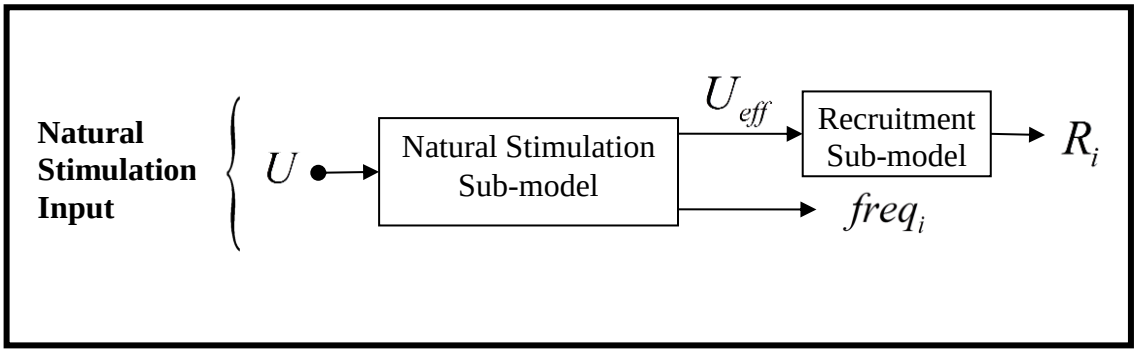

Figure 6.2: Topology of the "General Model" for natural stimulation input.

6.2.2 Muscle model topology

Stimulation frequency is assumed constant during FES. In some special cases, during intermittent FES, the stimulation frequency can be changed when FES is off in order to increase the force produced by the muscle, in this case the frequency will be assumed adjustable, but not a real-time variable (i.e. ignoring dynamic changes in frequency). At constant stimulation frequency, the frequency dependent activation A_i is constant and hence it is omitted from the model (A_i=1 for all fibre types). The topology of the "General Model" for analogue recruitment input (fibre-type level) assuming constant stimulation frequency $(A_i = 1)$ is shown in Figure 6.3.

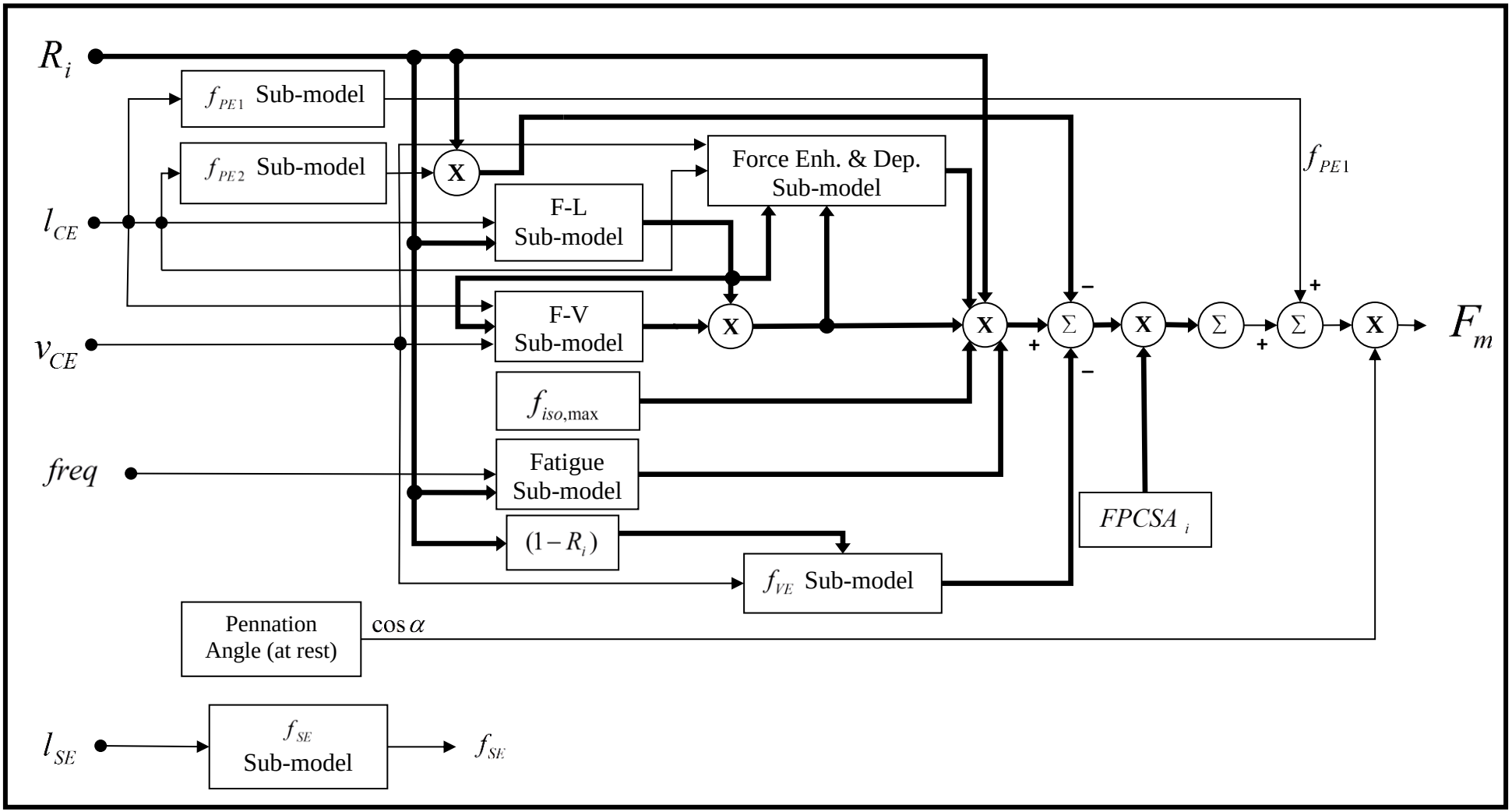

Figure 6.3: Topology the "General Model" for analogue recruitment input (fibre-type level) for FES, assuming constant stimulation frequency ($A_i = 1$). Thick arrows denote variables of multiple values (for i = 1, 2, and 3) and thin arrows denote single variables.

The total muscle force for the "General Model" at the fibre-type level (which represents the topology of the "General Model") is given by:

$$F_m = \cos\alpha \times \left[f_{PE1} + \sum_{i=1}^{n} \left\{ FPCSA_i \times \left[R_i \times \left[(f_{iso,\max} \times FL_i \times FV_i \times IF_i \times [IE_i / ID_i]) - f_{PE2,i} \right] - f_{VE,i} \right] \right\} \right] \quad (6.1)$$

F_m: Total muscle force including all active and passive forces of the musculotendon complex.

Note that for equation (6.1) the following points have to be considered:

- The term $[IE_i / ID_i]$ is used to indicate either (IE_i or ID_i) not (IE_i divided by ID_i).
- Series element passive force (f_{SE}) is not included in this equation, f_{SE} effect on v_{CE} will be calculated separately (SE is assumed as a pure series elastic element), $f_{SE} = F_m$.
- SE has no effect on F_m under isometric conditions. Indirect effect of SE on F_m under non-isometric conditions is because the stiffness of SE affects the instantaneous v_{CE} which affects f_{CE} and consequently F_m.
- Sub-models of ($f_{iso,\max}$, f_{PE1}, f_{PE2}, and $[IE_i / ID_i]$) produce their outputs for the whole muscle (not for the fibre-type), the contribution of each fibre-type for these sub-models will be calculated by multiplying with recruitment level R_i and $FPCSA_i$ for each fibre-type.
- The output of f_{VE} sub-model is multiplied by the percentage of non-recruited motor-units $(1 - R_i)$ in Hawkins model topology (see Appendix 1). In the "General Model" topology this can be incorporated into f_{VE} sub-model equation, see section 6.3.6.5.

The topology of the "General Model" for binary recruitment input (motor-unit level) is shown in Figure 6.4.

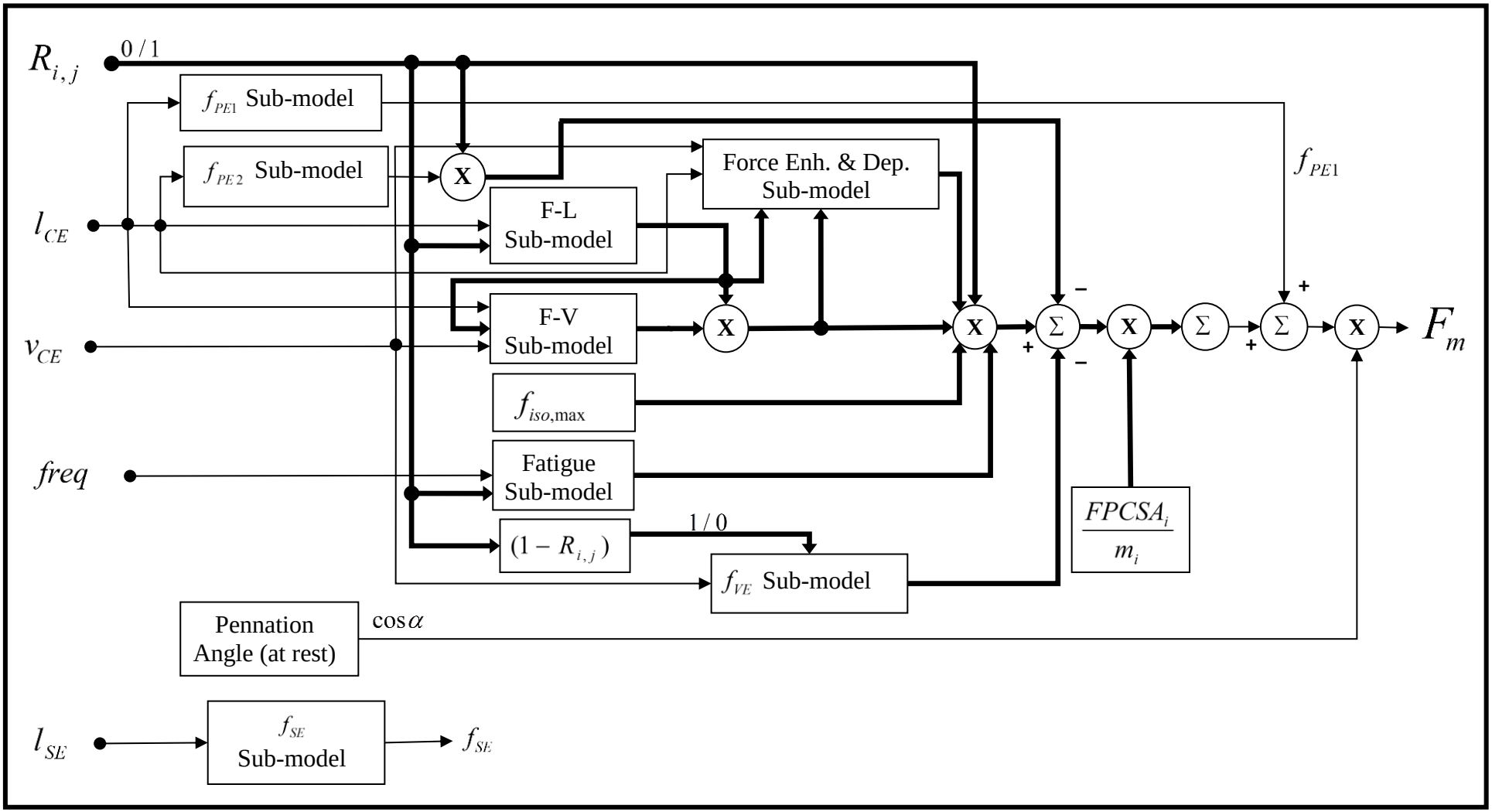

Figure 6.4: Topology of the "General Model" for binary recruitment input (motor-unit level). Thick arrows denote variables of multiple values (i = 1, 2, and 3) and thin arrows denote single variables.

The total muscle force for the "General Model" at the motor-unit level (which represents the topology of the "General Model") is given by:

$$F_m = \cos\alpha \times \left[f_{PE1} + \sum_{i=1}^{n} \left\{ \sum_{j=1}^{mi} \left[\left(\frac{FPCSA_i}{m_i} \right) \times \left[R_{i,j} \times \left[(f_{iso,\max} \times FL_i \times FV_i \times IF_i \times IE_i) - f_{PE2,i} \right] - f_{VE,i,j} \right] \right] \right\} \right] \quad (6.2)$$

Equation 6.2 is similar to that for the fibre-type level, but here each individual motor-unit will be modelled separately. The advantage of converting to binary recruitment is to increase model accuracy by calculating fatigue, force enhancement & depression, and effect of initial length (l_o) separately for each motor-unit.

Note that *CE* represents muscle belly when pennation angle is not modelled (pennation angle assumed zero, i.e. $\cos\alpha = \cos 0^o = 1$) as in most models in the literature. When pennation angle is modelled, as in except Hawkins model, *CE* represents muscle fibres in this case.

The standard topologies shown in Figures 6.3 and 6.4 can represent all topologies of the published muscle models presented in Appendix 1. Any redundant sub-models can be excluded by using values of (1) for those which are multiplied and (0) for those which are added. The following sub-sections describe how each of the published models can be represented by the standard topology.

Herzog model:

The "calcium dynamics + time delay" sub-model will not be used (i.e. input = output). Recruitment is not modelled in Herzog model; therefore any recruitment sub-model can be used.

Fatigue ($IF_i = 1$), force enhancement & depression ($[IE_i \,\&\, ID_i] = 1$), *PE2* ($f_{PE2} = 0$), *FV* ($f_{VE} = 0$). ($FPCSA_i = 1$, $\cos\alpha = \cos 0^o = 1$).

Riener-1 model:

Force enhancement & depression ($[IE_i \,\&\, ID_i] = 1$), *FV* ($f_{VE} = 0$).

($FPCSA_i = 1, \cos\alpha = \cos 0^o = 1$).

(f_{SE}, f_{PE1} and f_{PE2}) are not be modelled in Riener muscle model, but they are modelled with the joint model; therefore any sub-model can be used for them. Note that frequency is assumed constant during FES; therefore the force-frequency sub-model will be cancelled. However, since the value of $f_{iso,\max}$ provided by Riener in [72] is for high frequency of $freq = 100[Hz]$. Therefore, this value of $f_{iso,\max}$ should be adjusted to the used frequency during FES. The new value can be calculated by multiplying $f_{iso,\max}$ by: $\left[\frac{(0.1\times freq)^2}{1+(0.1\times freq)^2}\right]$.

As an example, this will be (80%) for ($freq = 20[Hz]$) and (90%) for ($freq = 30[Hz]$).

Hawkins model:

Natural stimulation input will not be considered as an input, only FES.
The "calcium dynamics + time delay" sub-model will not be used (i.e. input = output).
PE2 sub-model can be excluded using ($f_{PE2} = 0$).

Brown model:

Natural stimulation input will not be considered as an input, only FES, and the activation sub-model is already removed from the "General Model" topology.
The "calcium dynamics + time delay" sub-model will not be used (i.e. input = output).
Fatigue ($IF_i = 1$), Force enhancement & depression $([IE_i \,\&\, ID_i] = 1)$, FV ($f_{VE} = 0$), $(\cos\alpha = 1)$.

6.2.3 Arrangement of passive elements in the "General model"

The standard form for the muscle model using rheological elements structure is represented in Figure 6.5, where the parallel element $PE1$ is parallel on CE only (this form is a modified version of Brown Model by adding the pennation angle α). Another more general standard model structure (was developed during this study) is represented in Figure 6.6, models in which $PE1$ is parallel on both CE and SE can be represented by this form. However, the parallel element will be assumed always parallel on CE only. Therefore the form shown in Figure 6.5 will be used as the standard form for the proposed "General Model".

The form for rheological elements structure shown in Figure 6.5 can represent all other models' structure as follows:

Herzog model (the new form): $\alpha = 0$, $PE2 = 0$ ($k_{PE2} = 0$), $VE = 0$, ($k_{VE} = 0$), *PE1* can be made parallel on *CE* (*CE* only not *CE* and *SE*) by using Fung equations [107], this equation is summarised in section 2.5.6.2.

Hawkins model: $PE2 = 0$.

Brown model: $\cos\alpha = \cos(0^o) = 1$.

The alternative standard form shown in Figure 6.6 can be used to represent the all previous models in addition to the original form of Herzog model given in [18], the original form of Herzog model can be represented by using the following values: $SE1 = \infty$, $\alpha = 0$, $PE2 = 0$, and $VE = 0$.

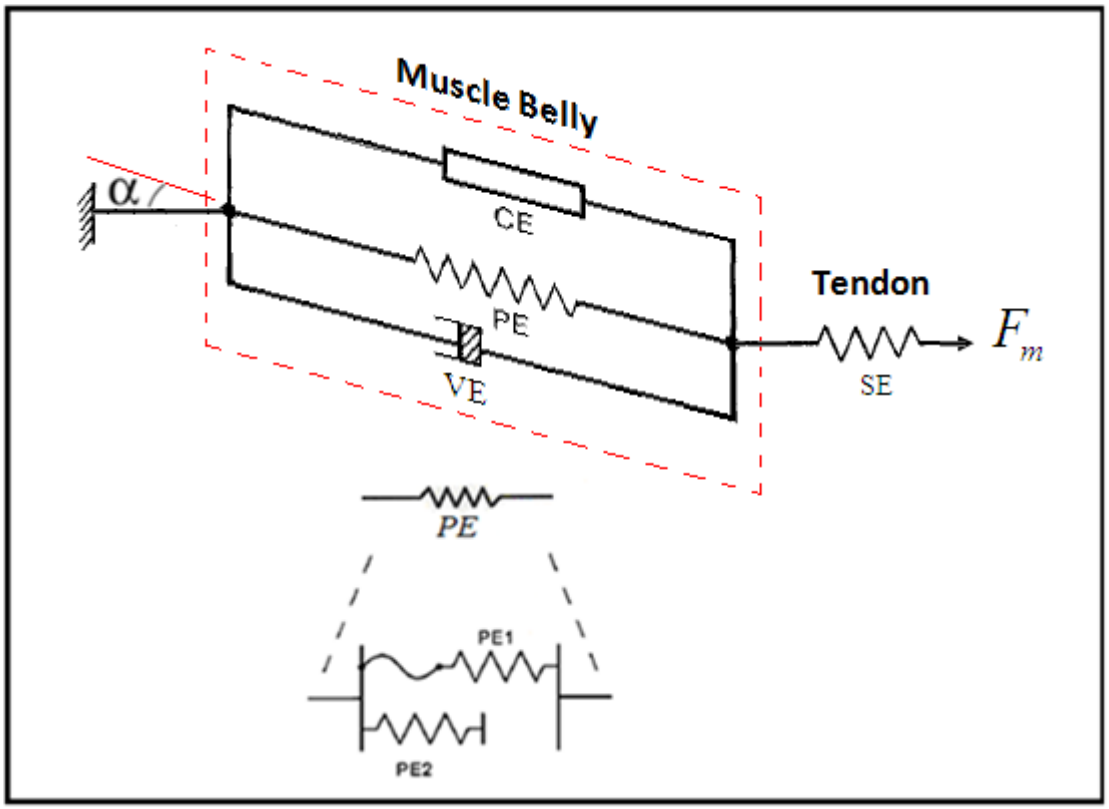

Figure 6.5: Representation of the standard form muscle model using rheological elements structure. *PE1* is parallel on *CE* only, ($f_{PE} = f_{PE1} + f_{PE2}$), ($l_{CE} = l_{PE1} = l_{PE2}$).

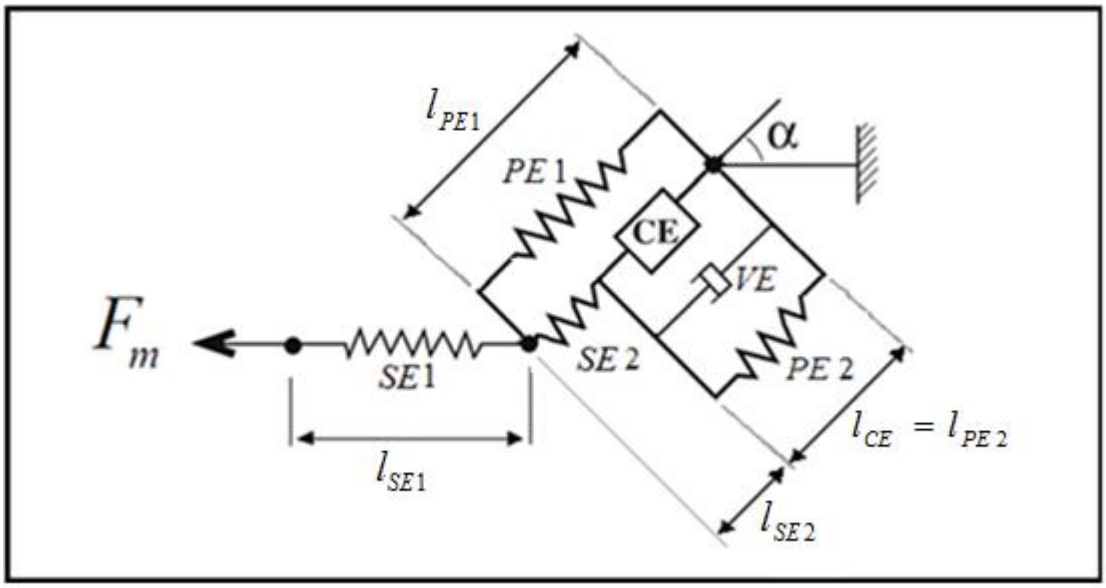

Figure 6.6: Another alternative standard muscle model structure. The original form of Herzog model can be represented (with *PE* parallel on both *CE* and *SE*) by making *SE1* rigid and using *SE2* to represent the tendon together with $\alpha = 0$, $PE2 = 0$ and $VE = 0$.

6.3. Standard sub-models for the "General Model"

In this section, standard sub-models are proposed for the various components of the "General Model". These can be used to produce consistent, interchangeable alternatives for all sub-models of the "General Model" that can be used to represent all relevant instances from the literature. They can also be adapted to allow for multiple motor-units to be represented. The different alternatives for each sub-model are described using the same set of variables.

Five standard sub-models representing "active" muscle properties and four standard sub-models representing "passive" muscle properties are summarised in this section. Each sub-model represents one of the muscle's main properties, which are: recruitment of motor-units; the contractile element *CE* active force-length relationship; the *CE* active force-velocity relationship; muscle fatigue; force enhancement following active stretch and force depression following active shortening; and finally the muscle's passive properties.

6.3.1 The standard recruitment sub-model

As discussed in section 2.5.1, the mechanism of motor-unit recruitment is complex and difficult to measure. Many recruitment sub-models are available in the literature, see section 2.5.1.2. However, here a standard recruitment sub-model is proposed which can be used with any Hill-type model. This sub-model is able to account for the different properties of different fibre-types and can be used with either FES or natural contraction. This standard form can be used to represent all alternative recruitment sub-models introduced in Chapter 2. The standard form can also be used to build new recruitment sub-model at the required complexity level.

The standard recruitment sub-model developed in this research has three fibre-types and one thousand motor-units. Each fibre-type is recruited with an analogue recruitment (can be linear or non-linear). The input to the recruitment sub-model can be the natural stimulation input U or the pulse width/amplitude (PW / PA) of the electrical stimulation.

The standard recruitment sub-model is shown in Figure 6.7. The input U is used for natural contraction, and the input PW is used for FES. Either input will yield the same output (R_i). U_{eff} models the calcium dynamics for natural stimulation, U_{eff} and the calcium dynamics sub-models are separate from the recruitment sub-model and can be placed before or after the recruitment sub-model (in reality, it is after recruitment). Frequency is assumed constant for FES.

Recruitment order can be arranged to be in physiological or non-physiological order. Input to the F-L sub-model can be either the length at initial recruitment or the instantaneous length. The number of virtual motor-units used in the model was chosen as ($m = 1000$) to give high force resolution.

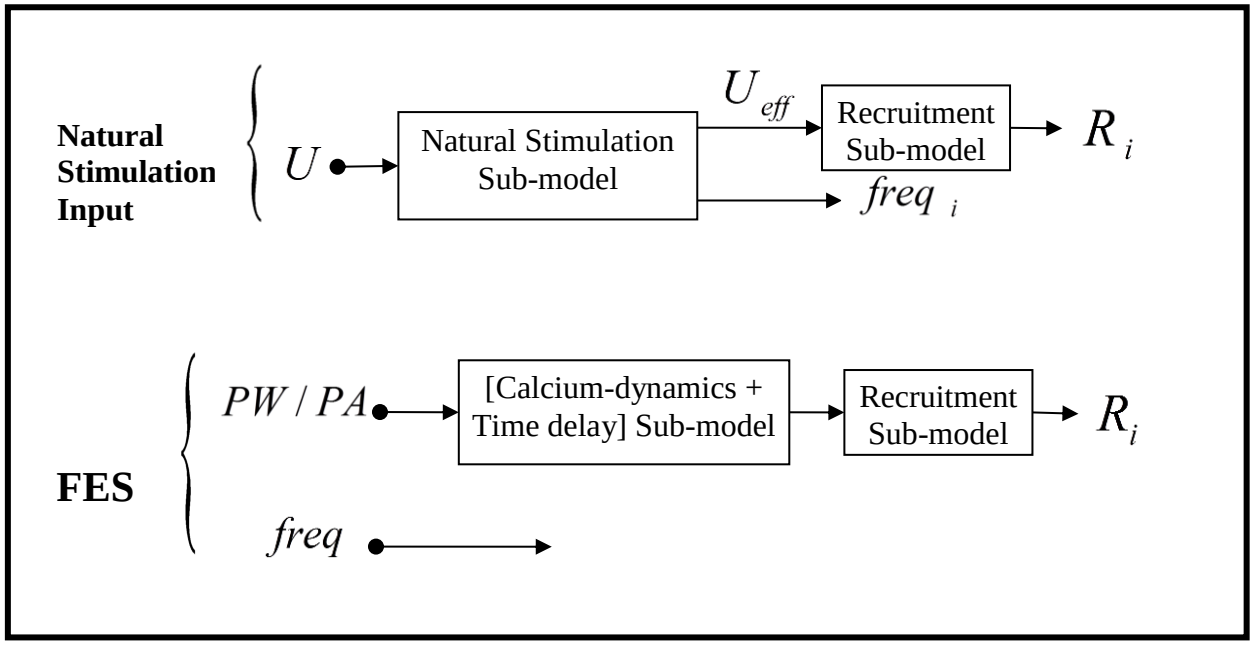

Figure 6.7: The standard recruitment sub-model.

i) The Analogue Recruitment of fibre types:

The analogue recruitment of the i^{th} fibre-type (R_i) in the standard recruitment sub-model is shown in Figure 6.8 and presented mathematically in the following structure:

$$R_i = \begin{cases} 0 & , \quad pw < pw_i^{thr} \\ R_i(pw) & , \quad pw_i^{thr} \le pw \le pw_i^{sat} \\ 1 & , \quad pw > pw_i^{sat} \end{cases} \qquad (6.3)$$

Below the threshold level pw_i^{thr} there is no recruitment, above the saturation level pw_i^{sat} the recruitment is maximum. Between these two levels the recruitment can be controlled by adjusting PW. The recruitment equation of Riener-1 model [72] is used for the analogue recruitment:

$$R_i(pw) = c_2 + c_1\left\{(pw - pw_i^{thr})\arctan\left[c_{thr}(pw - pw_i^{thr})\right] - (pw - pw_i^{sat})\arctan\left[c_{sat}(pw - pw_i^{sat})\right]\right\} \qquad (6.4)$$

The constants (c_{thr}, and c_{sat}) can be adjusted to get a straight line with a very sharp curvature at pw_i^{thr} and pw_i^{sat}. The recruitment of fibre-type is always analogue, it can be linear or non-

linear. The recruitment sequence of different fibre-types can be moved at will making the sequence at any order with or without overlapping. In figure 6.9, adjusting PW or PA will change the number of recruited motor-units, modulating the stimulation frequency will change the muscle force but will not affect the number of recruited motor-units..

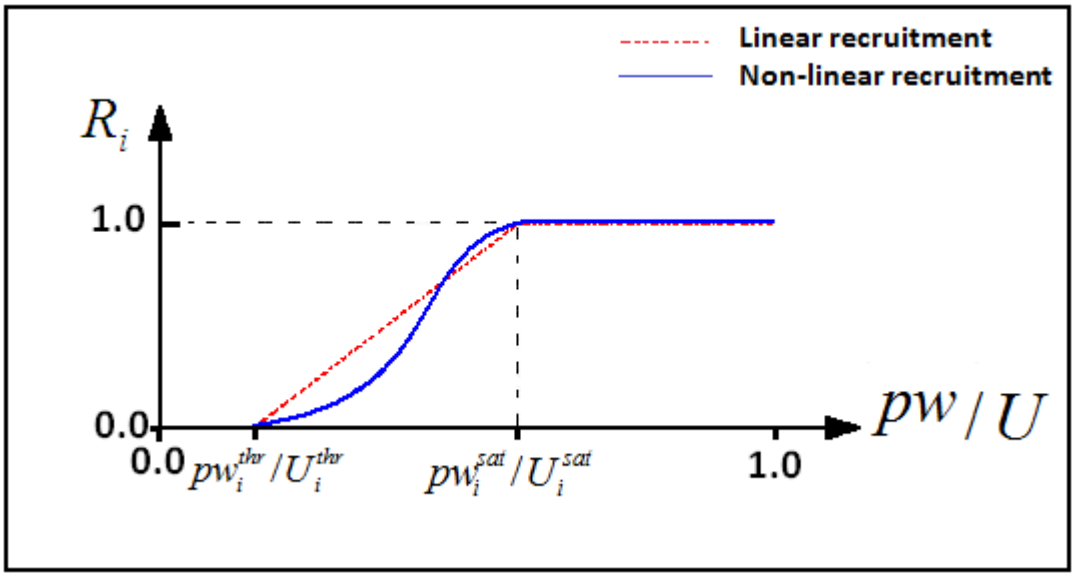

Figure 6.8: The analogue recruitment can be linear or non-linear. ($U_1^{thr} = U_{thr}$) and similarly ($pw_1^{thr} = pw_{thr}$). ($U_n^{sat} = U_{sat}$) and similarly ($pw_n^{sat} = pw_{sat}$).

The normalised values for pw and U will be used, assuming that when all "real" motor-units in the whole muscle are recruited: ($pw_{sat} = U_{sat} = 1.0$). The pw is normalised to pw_{sat} and U is normalised to U_{sat}. This assumption will make it possible to use the same recruitment sub-model with both FES and natural contractions (i.e. pw and U are interchangeable in equation 6.3)

For ($pw_i^{thr} \le pw \le pw_i^{sat}$), R_i is a function of pw $\{R_i(pw)\}$. The values of pw_i^{thr} and pw_i^{sat}, and the recruitment sequence can be different for different recruitment sub-models.

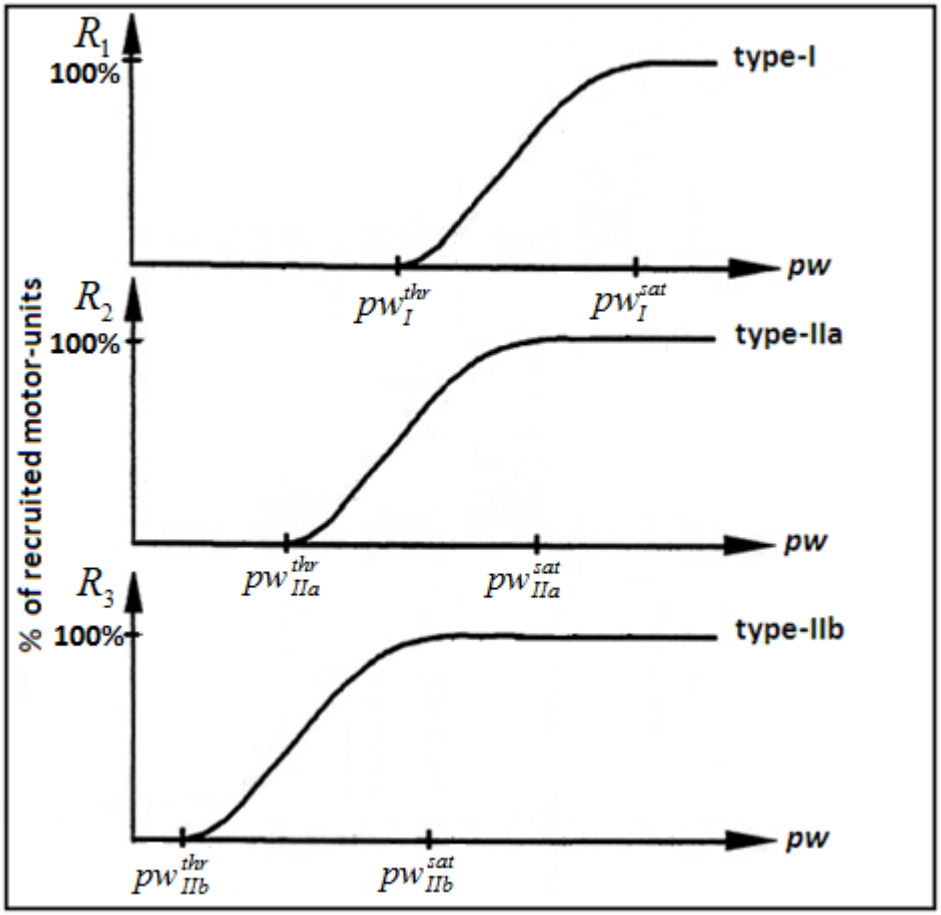

Figure 6.9: Analogue recruitment of different fibre-types for electrically stimulated "heterogeneous" muscle. The recruitment curves are non-linear and overlapping.

ii) The Extension of Binary Recruitment:

Recruitment of motor-units is incorporated as an extension to the analogue recruitment. The analogue recruitment of fibre type-i is converted to binary recruitment (Figure 6.10), the motor-unit j of fibre type i can only be 100% recruited or not recruited at all (either 0 or 1), see Figure 6.11. This is represented mathematically as follows:

$$R_{i,j} = \begin{cases} 0 & , R_i \le \left(\dfrac{j-1}{m_i} \right) \\ 1 & , R_i > \left(\dfrac{j-1}{m_i} \right) \end{cases} \qquad (6.5)$$

The threshold level of the j^{th} motor-unit of the i^{th} fibre-type is: $\left(\frac{j-1}{m_i}\right)$. Once R_i exceeds this threshold level, the j^{th} motor-unit of fibre type-i becomes recruited (i.e. $R_{i,j}=1$).

The threshold level $pw_{i,j}^{thr}$ for the j^{th} motor-unit of fibre-type i is the value of pw that makes $R_i=\left(\frac{j-1}{m_i}\right)$.

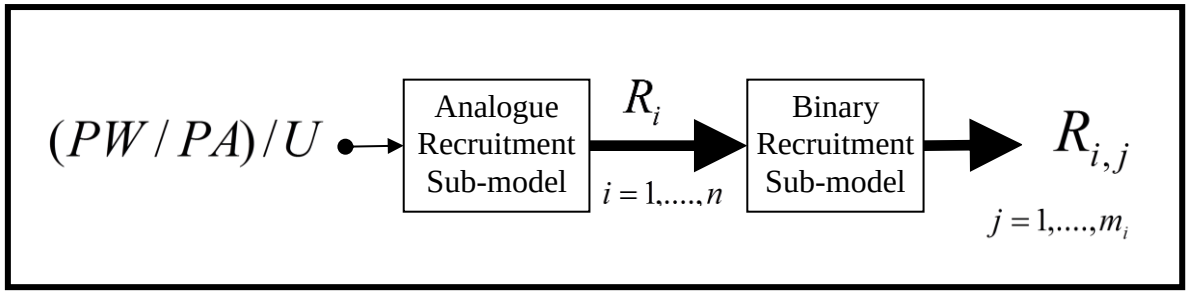

Figure 6.10: The recruitment of different fibre types is analogue. Conversion to binary is added as an extension in order to model the recruitment of motor-units, $R_{i,j}=0$ *or* 1. Thin arrow indicates single variable input/output, thick arrows indicate multi-variable inputs/outputs.

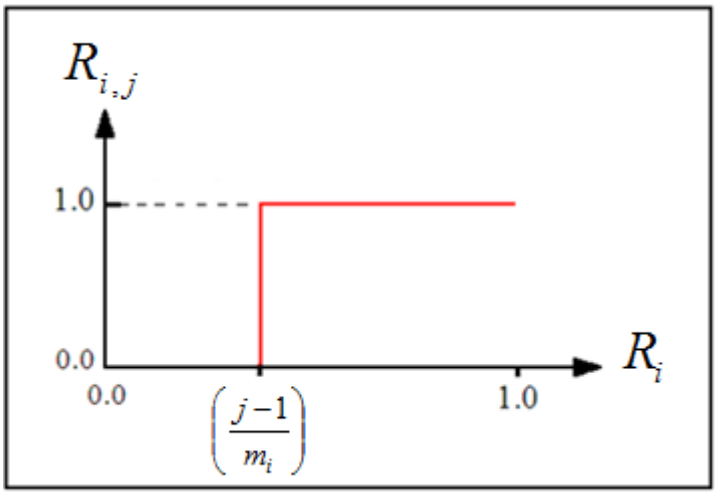

Figure 6.11: Recruitment of the motor-unit j of fibre-type i. $R_{i,j}$ has a binary value (0 or 1).

The standard recruitment sub-model can incorporate up to three fibre-types $(1 \le n \le 3)$, and up to one thousand motor-units $(1 \le m \le 1000,\ m = m_1 + ... + m_n)$. Modelling of muscle recruitment is done in two steps; analogue recruitment for each fibre-type is done first, followed by conversion to binary recruitment for each motor-unit ($R_{i,j} = 0$ *or* 1), see Figure 6.12.

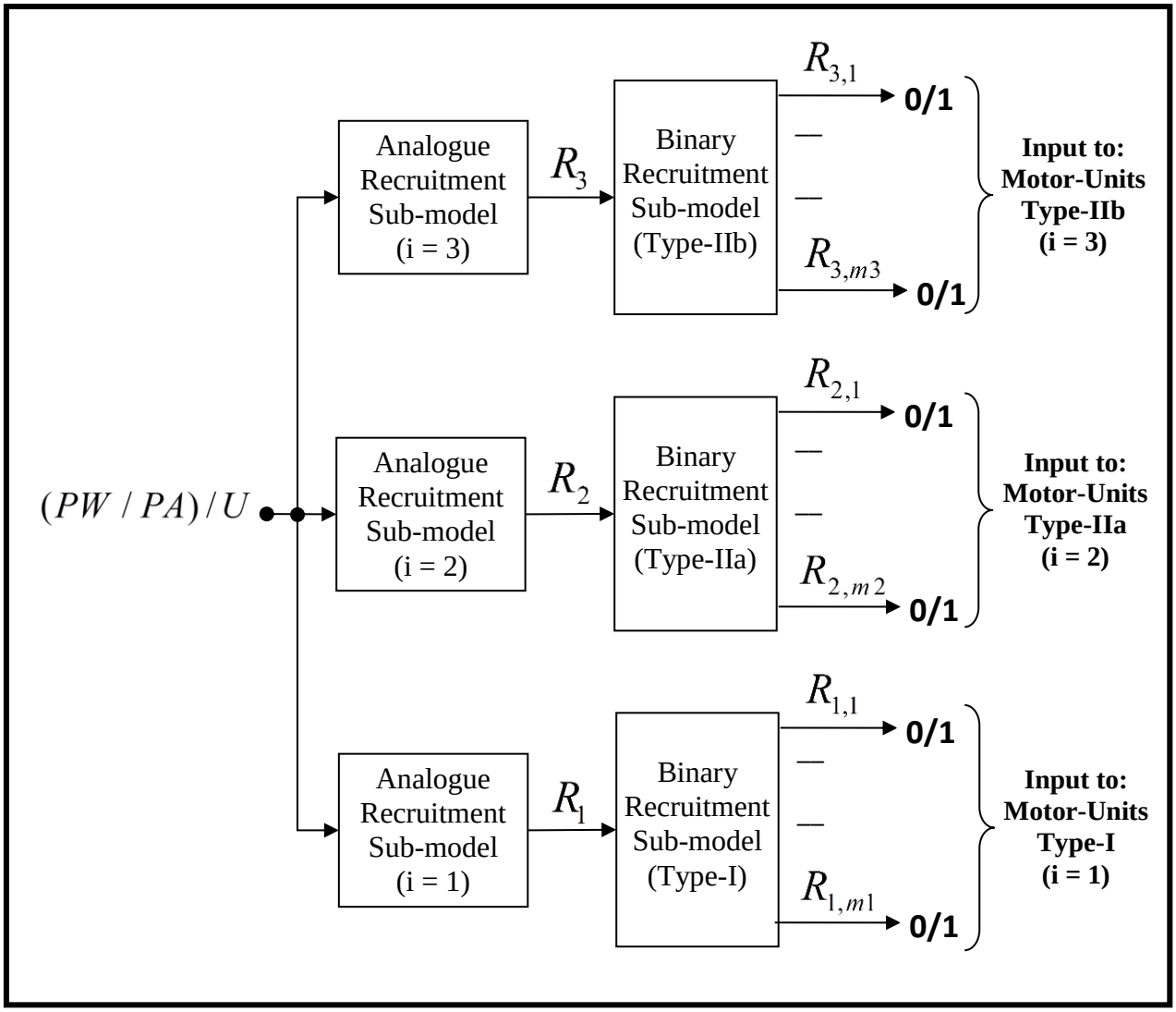

Figure 6.12: The standard recruitment sub-model for the "General Model" with ($i = 3$, $m = m_1 + m_2 + m_3$). The input can be FES (PW / PA) or natural stimulation input U.

For natural contraction (natural stimulation input not FES), the input to the recruitment sub-model is the natural stimulation input U . The threshold level is modelled as:

$$U_i^{thr} = \frac{(i-1)}{n} \times U_{sat}, \quad U_{sat} < 1 \quad , i = 1,..., n \tag{6.6}$$

Linear and analogue recruitment is assumed for all motor-units (of any fibre-type):

$$R_i = \left\{ \begin{array}{ccc} 0 & , & U < U_i^{thr} \\ \left(\dfrac{U - U_i^{thr}}{U_{i+1}^{thr} - U_i^{thr}} \right) & , & U_i^{thr} \le U \le U_{i+1}^{thr} \\ 1 & , & U > U_{i+1}^{thr} \end{array} \right\}, \quad U_{n+1}^{thr} = U_{sat} \tag{6.7}$$

$$U_{i+1}^{thr} - U_i^{thr} = \frac{U_{sat}}{n}$$

$$U_{i+1}^{thr} = U_i^{sat}$$

Threshold levels for different motor-unit under natural contraction are described in section 2.5.1.2. Stimulation frequency of recruited units will be modulated by U as shown in Figure 6.13. This represented mathematically as:

$$freq_i = freq_i^{\min} + c_{fi} \times (U - U_i^{thr}), \text{ for any input } (U \ge U_i^{thr}). \tag{6.8}$$

$$\text{Slope} = c_{fi} = \frac{freq_i^{\max} - freq_i^{\min}}{1 - U_i^{thr}} \tag{6.9}$$

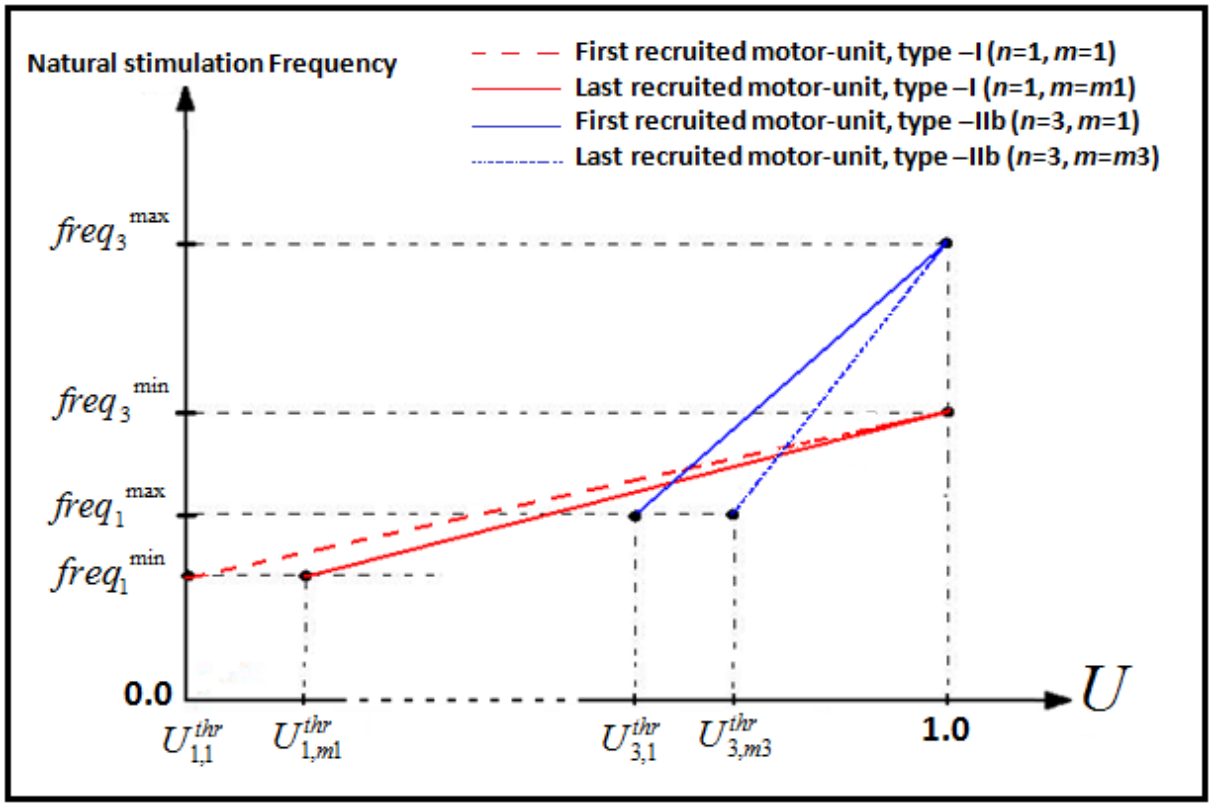

Figure 6.13: The relationship between stimulation frequency and natural stimulation input U. The stimulation frequency of recruited motor-units increases linearly with U.

All alternative recruitment sub-models can be exactly constructed (or a close match achieved) using the standard recruitment sub-model. Each alternative recruitment sub-model can be built using the FES recruitment sequence of that sub-model and proper values for: n, m, pw_{thr}, pw_{sat}, c_1, c_2, c_{thr}, and c_{sat}. Some sub-models will have the binary recruitment extension.

6.3.2 The standard F-L sub-model

As discussed in section 2.5.2, different F-L relationships are observed experimentally because muscle architecture and fibre orientations can vary widely in different muscles. Various modelling approaches at different levels of complexity are used in the literature to model this complex property and hence alternative sub-models are reported in the literature. A standard form for all alternative F-L sub-models is possible. The standard form proposed here can be used to represent all alternative F-L sub-models introduced in Chapter 2. The standard form can also be used to build new F-L sub-models at the required complexity level.

The F-L standard form was first developed using Otten F-L sub-model and the multi-compartment approach used by Garies. Riener and Brown F-L sub-models can be constructed directly from Otten F-L sub-model, but Herzog and Hawkins F-L sub-models cannot be constructed using Otten or Garies F-L sub-models, the main difference is at extreme lengths away from the optimal length. The logic behind the development of the F-L standard form is explained step by step as follows:

1. Starting form Garies F-L sub-model (eq. 2.12), this is the most complex F-L sub-model. The "exact equation for all sub-models that are based on Otten can be achieved (i.e. Otten, Kaufman, Riener, Brown, and Garies) by making: (*N*=1) to get one single optimal length ($\bar{l}_m = l_m / l_{opt}$) and ($c_i = c_1 = 1$), then using the same values for (c_S , c_R , and c_W) as the original of each sub-model. Garies equation was given by:

$$FL(l_m) = \sum_{i=1}^{n} c_i \times \exp\left(- abs \left| \frac{(\bar{l}_{m,i})^{c_{S,i}} - 1}{c_{W,i}} \right|^{c_{R,i}} \right) \qquad (6.10)$$

N: number of compartments in the F-L sub-model, c_i : scaling factor representing the effective influence of the i^{th} compartment on the overall model.

2. The variable l_{CE} will be used instead of (l_m and l_f), this is a general symbol and can be used to represent (l_m or l_f). Note that: l_f is used when pennation angle α is modelled (as in Hawkins model). l_m is muscle length and l_f is fibre length which are only equal if (α = 0).

3. In order to get better fit to experimental data, different constants' values will be used for each of the ascending and descending limbs (still the same equation but different values for constants). This is an improvement over Garies F-L sub-model (which is the most complex and the most accurate model found in the literature). The empirical data for ascending and descending limbs in many muscles are not symmetrical. Changing the value of the skewness parameter c_S is not enough to fit the empirical data, hence two different curves for each limb will give better fit. Note that the two curves (of the ascending and descending limbs) are continuous at peak since the value of each curve = 1.0 at ($l_{CE} = l_{opt}$).

4. Hawkins (eq. 2.10) and Herzog (eq. 2.11) F-L sub-models are of different structure, only the positive values of the F-L curve are considered and this makes discontinuity at extreme lengths which is clearly different from the empirical data. A close match (not exact) can be achieved at lengths not far from the optimal length by using Otten (eq. 2.8) or Garies (eq. 2.12) F-L sub-models. But at extreme lengths the two curves are differen.

5. A very close match (almost 100%) can be achieved for Hawkins (eq. 2.10) and Herzog (eq. 2.11) F-L sub-models by using the following technique:

- Using a positive constant (c_{oi}) added to unity, the value $(1+c_{oi})$ is multiplied by each side of the F-L curve, and then deducting (c_{oi}) from the product.
- This operation produces a new curve whose maximum value is unity and minimum value is ($-c_{oi}$), a very close match to Hawkins F-L sub-model was achieved by using ($c_{o1} = 0.8$, $c_S = 1$, $c_R = 2.4$, $c_W = 0.44$,) for the ascending limb and ($c_{o2} = 1.2$, $c_S = 0.2$, $c_R = 1.65$, $c_W = 0.152$) for the descending limb.
- By taking the positive values of the curve, a very close match to either Hawkins or Herzog F-L sub-models can be achieved.
- Using this technique makes it possible to control the shape of the curve (using the least squares method) until the peak of the new curve is very close to the curve to be matched, either Hawkins (eq. 2.10) or Herzog (eq. 2.11).
- The constant c_{oi} was used in order to get better fit at extreme lengths.
- Herzog F-L sub-model has symmetrical limbs and hence ($c_{o1} = c_{o2}$), while Hawkins F-L sub-model has non- symmetrical limbs and hence ($c_{o1} \neq c_{o2}$).

6. For other sub-models (other than Hawkins and Herzog), c_{oi} is cancelled by making $c_{oi} = 0$. This brings us back to Garies F-L sub-model but with different curves for each side (they can be the same if the constants' values are the same).

The equation of the standard F-L sub-model is given as the positive values of:

$$FL(l_{CE}) = \begin{cases} (1+c_{o1}) \times \left[\sum_{i=1}^{N} c_i \times \exp\left(-abs \left| \frac{\left(\frac{\bar{l}_{CE}}{\bar{l}_{opt,i}} \right)^{c_{S1,i}} - 1}{c_{W1,i}} \right|^{c_{R1,i}} \right) \right] - c_{o1} & for \quad l_{CE} \le l_{opt,i} \\ (1+c_{o2}) \times \left[\sum_{i=1}^{N} c_i \times \exp\left(-abs \left| \frac{\left(\frac{\bar{l}_{CE}}{\bar{l}_{opt,i}} \right)^{c_{S2,i}} - 1}{c_{W2,i}} \right|^{c_{R2,i}} \right) \right] - c_{o2} & for \quad l_{CE} > l_{opt,i} \end{cases} \tag{6.11}$$

For the negative values: $FL(l_{CE}) = 0$.

l_{CE} represents either l_m or l_f depending on the muscle model.

N: Number of compartments in the F-L sub-model.

c_i: Scaling factor representing the effective influence of the i^{th} compartment on the overall model.

$\bar{l}_{opt,i}$: Optimal length of the i^{th} compartment (not real) normalised with respect to the optimal length (the real optimal length of muscle belly).

c_{o1}, c_{o2}: constants, used to shape the F-L curve at extreme lengths (i.e. to mimic Herzog and Hawkins F-L sub-models).

The values of the curve shaping parameters (c_S, c_R, c_W) can be different in each compartment, and also in the two sides of the F-L curve (the ascending and descending limbs). This depends on the experimental data need to be fitted, or any F-L sub-model needed.

The standard F-L sub-model can represent all alternative F-L sub-models presented in this document. It can easily represent Otten, Riener, and Brown F-L sub-models by using the following: ($c_{o1} = c_{o2} = 0,\ N = 1,\ c_i = 1$) and the same shaping parameters for both sides of the F-L curve (i.e. same equation for the ascending and descending limbs) as given in those F-L sub-models. The standard F-L sub-model can represent all other F-L sub-models presented in section 2.5.2.2 as follows:

For Garies F-L sub-model:

$c_{o1} = c_{o2} = 0$, and the same shaping parameters for the ascending and descending limbs of the F-L curve (i.e. same equation for all lengths).

For Herzog F-L sub-model:

$N = 1,\ c_i = 1,\ c_{o1} = c_{o2}$, and the same shaping parameters for the ascending and descending limbs of the F-L curve. The standard F-L sub-model can represent Herzog F-L sub-model very well. The positive values of the following equation can be used for muscle-1:

$c_{S1} = c_{S2} = 1,\ c_{R1} = c_{R2} = 2.4,\ c_{W1} = c_{W2} = 0.44,\ c_{o1} = c_{o2} = 0.8$

$$FL(l_{CE}) = (1+0.8) \times \left[\exp\left(-abs\left| \frac{(\bar{l}_{CE})^1 - 1}{0.44} \right|^{2.4} \right) \right] - 0.8, \quad for \quad positive \quad values$$

For muscle-2: ($c_{S1} = c_{S2} = 1,\ c_{R1} = c_{R2} = 2.3,\ c_{W1} = c_{W2} = 0.75,\ c_{o1} = c_{o2} = 1.2$).

For Hawkins F-L sub-model:

$l_{CE} = l_f,\ N = 1$, and $c_i = 1$. The standard F-L sub-model can represent Hawkins F-L sub-model very well. The positive values of the following equation are used:

For the ascending limb: ($c_{S1} = 1,\ c_{R1} = 2.4,\ c_{W1} = 0.44,\ c_{o1} = 0.8$).

For the descending limb: ($c_{S2} = 0.2,\ c_{R2} = 1.65,\ c_{W2} = 0.152,\ c_{o2} = 1.2$).

$$FL(l_{CE}) = \left\{ \begin{array}{ll} (1+0.8) \times \left[\exp\left(-abs\left| \frac{(\bar{l}_{CE})^{1} - 1}{0.44} \right|^{2.4} \right) \right] - 0.8 & for \quad l_{CE} \le l_{opt} \\ (1+1.2) \times \left[\exp\left(-abs\left| \frac{(\bar{l}_{CE})^{0.2} - 1}{0.152} \right|^{1.65} \right) \right] - 1.2 & for \quad l_{CE} > l_{opt} \end{array} \right\}, \quad for \quad positive \quad values$$

$$FL(l_{CE}) = 0, \quad for \quad negative \quad values.$$

By choosing appropriate values for the shaping parameters (c_S, c_R, c_W) and other constants in the standard F-L sub-model, it is possible to fit any experimental data with high accuracy better than all alternative sub-models listed here because of the extra advantage the standard F-L sub-model has, where each limb of the F-L curve being modelled by separate curve (using the same equation but with different constants' values).

6.3.3 The standard F-V sub-model

As discussed in section 2.5.3, the F-V relationship is affected by different factors (fibre-type, muscle architecture, recruitment level, recruitment order, "instantaneous" fibre length and stimulation frequency), and hence different F-V relationships are observed experimentally. Various modelling approaches at different levels of complexity are used to model this complex property and hence alternative sub-models are reported in the literature. A standard form for all alternative F-V sub-models is possible. The standard form proposed here can be used to represent all alternative F-V sub-models introduced in Chapter 2 (and almost all alternative Hill-based F-V sub-models in the literature). The standard form can also be used to build new F-V sub-models at the required complexity level.

To develop the F-V standard form, the start was with Brown F-V sub-model because it is the most complex. Then more formulas and constants were added in order to match all other sub-models. The logic behind the development of the F-V standard form is explained step by step as follows:

1. All sub-models have to be reformulated in order to make all of them in the same form.

2. Riener F-V sub-model (eq. 2.13) is the only sub-model that was difficult to reformulate. Therefore, least squares method was used to find the best fit that will make a close matching curve.

3. Brown F-V sub-model (eq. 2.14) has only two formulas, one for ($\bar{v}_{CE} \le 0$) and the other for ($\bar{v}_{CE} > 0$). Other two formulas are required for ($\bar{v}_{CE} \le -1$) and ($\bar{v}_{CE} > \bar{v}^{str}_{CE,\max}$) since some alternative F-V sub-models have constant values at these velocities.

4. For ($\bar{v}_{CE} \le -1$): The first formula of Brown (eq. 2.14) is used but will be multiplied by a constant (b_{v1}) which will have the value ($b_{v1} = 1$) for Brown and ($b_{v1} = 0$) for other models which have [$FV = 0 \quad for: \quad \bar{v}_{CE} \le -1$]. This makes "exactly" the same equation of all F-V sub-models (except Riener).

5. For ($-1 < \bar{v}_{CE} \le 0$): The first formula of Brown (eq. 2.14) is used as it is, constants can have different values to get other sub-models. This makes "exactly" the same equation of all F-V sub-models (except Riener).

6. For ($0 < \bar{v}_{CE} \le \bar{v}^{str}_{CE,\max}$): The second formula of Brown (eq. 2.14) is used but will be multiplied by a constant (b_{v3}) and added to another constant (b_{v2}), these two constants will have the values $b_{v2} = 0$ and $b_{v3} = 1$ for Brown. (b_{v3} and b_{v2}) where added in order to get the same form as Hawkins (eq. 2.15) and Herzog (eq. 2.18) F-V sub-models. This makes "exactly" the same equation of all F-V sub-models (except Riener).

7. For ($\bar{v}_{CE} > \bar{v}^{str}_{CE,\max}$): The second formula of Brown (eq. 2.14) is used but will be multiplied by a constant (b_{v7}) and added to another constant (b_{v2}), b_{v2} has the same value as in the previous formula for all sub-models, and $b_{v7} = 1$ for Brown. (b_{v2} and b_{v7}) where added in order to get the same form as Hawkins (eq. 2.15) and Herzog (eq. 2.18) F-V sub-models.

8. A very close match of Riener F-V sub-model was achieved using the standard form.

9. The "exact" equations of all other F-V sub-models represented in section 2.5.3.2 were achieved using the standard form. Constants' values for each alternative F-V sub-model are given below.

The equation of the standard F-V sub-model is given as:

$$FV(v_{CE}, l_{CE}) = \left\{ \begin{array}{lll} b_{v1} \times \left[(1+\bar{v}_{CE}) / (1-(c_{v0}+c_{v1}\bar{l}_{CE})\bar{v}_{CE}) \right] & for & \bar{v}_{CE} \le -1 \\ (1+\bar{v}_{CE}) / (1-(c_{v0}+c_{v1}\bar{l}_{CE})\bar{v}_{CE}) & for & -1 < \bar{v}_{CE} \le 0 \\ b_{v2} + b_{v3} \times \left[(b_{v4} - (a_{v0} + a_{v1}\bar{l}_{CE} + a_{v2}\bar{l}_{CE}{}^2)\bar{v}_{CE}) / (b_{v5} + b_{v6}\bar{v}_{CE}) \right] & for & 0 < \bar{v}_{CE} \le \bar{v}_{CE,\max}^{str} \\ b_{v2} + b_{v7} \times \left[(b_{v4} - (a_{v0} + a_{v1}\bar{l}_{CE} + a_{v2}\bar{l}_{CE}{}^2)\bar{v}_{CE}) / (b_{v5} + b_{v6}\bar{v}_{CE}) \right] & for & \bar{v}_{CE} > \bar{v}_{CE,\max}^{str} \end{array} \right\} \quad (6.12)$$

v_{CE} will be used in the standard F-V sub-model to represent the velocity of either muscle belly or muscle fibres depending on the F-V sub-model needed.

All alternative F-V sub-models can be exactly represented using the standard F-V sub-model by changing the constants values (except Riener F-V sub-model which was very close but not exactly the same). The standard F-V sub-model can represent all F-V sub-models referenced in this thesis as follows:

For Brown F-V sub-model:

The following constants' values can be used to get "exactly" Brown F-V sub-model.

c_{v0}, c_{v1}, b_{v4}, b_{v5}, a_{v0}, a_{v1}, a_{v2}: as provided by Brown in [100]. The values of these constants are also provided by Brown in other references with slightly different values, as in [41, 82, 127]. ($b_{v2}=0$), ($b_{v1}=b_{v3}=b_{v6}=b_{v7}=1$), ($V^{str}_{CE,\max}$ = any value > 0).

For Hawkins F-V sub-model:

The following constants' values can be used to get "exactly" Hawkins F-V sub-model.

($b_{v1}=b_{v6}=b_{v7}=a_{v1}=a_{v2}=c_{v1}=0$), ($b_{v4}=b_{v5}=1$).

Other constants as given in the new formulation presented in this document, originally taken from Hawkins [101, 129, 130]: $c_{v0}=\frac{1}{k}$, $a_{v0}=\left(\frac{1}{\bar{v}^{str}_{f,\max}}\right)$, $b_{v2}=1.3$, $b_{v3}=-0.3$.

For AnyBody F-V sub-model:

The following constants' values can be used to get "exactly" AnyBody F-V sub-model.

($b_{v1}=b_{v3}=b_{v4}=b_{v5}=b_{v7}=1$), ($b_{v2}=b_{v6}=c_{v0}=c_{v1}=a_{v1}=a_{v2}=0$), ($a_{v0}=-1$),

($V^{str}_{CE,\max}$ = any value > 0).

For LifeMOD F-V sub-model:

The following constants' values can be used to get "exactly" LifeMOD F-V sub-model.

($b_{v1}=b_{v2}=c_{v1}=a_{v1}=a_{v2}=0$), ($b_{v3}=b_{v4}=b_{v5}=b_{v7}=1$), ($V^{str}_{CE,\max}$ = any value > 0).

Other constants as given in [137, 138]: $c_{v0}=4$, $a_{v0}=-2$, $b_{v6}=1.5$.

For Herzog F-V sub-model:

The following constants' values can be used to get "exactly" Herzog F-V sub-model.

$(b_{v1} = b_{v7} = c_{v1} = a_{v1} = a_{v2} = 0)$, $(b_{v4} = b_{v5} = 1)$

Other constants are the same as those in the new form of Herzog F-V sub-model presented in this document, the values of these constants are derived from the original Herzog model presented in [18]: $c_{v0} = \left(\frac{1}{b}\right)$, $b_{v2} = 1.5$, $b_{v3} = -0.5$, $a_{v0} = \left(\frac{1}{\bar{v}^{str}_{CE,\max}}\right)$, $b_{v6} = \left(\frac{1}{b'}\right)$,

$v_{CE,\max} = -FL(l_o)\frac{b}{a}$, $V^{str}_{CE,\max} = \left(\frac{b' \times a}{a' \times b}\right)$.

For Riener F-V sub-model:

Although the standard model cannot achieve an exact match with the Riener F-V sub-model, a very close match was achieved as shown in Figure 6.14.

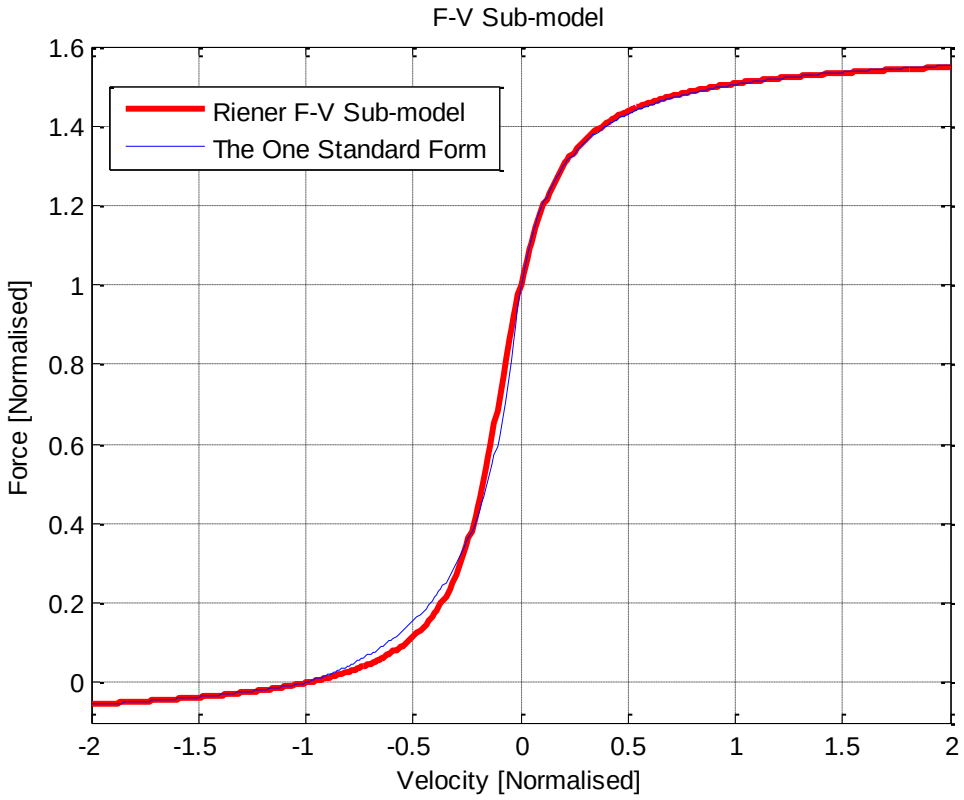

Figure 6.14: The standard F-V sub-model is used to represent Riener F-V sub-model using constants' values: $(b_{v1} = 0.55,\ c_{v0} = 4.5,\ b_{v4} = b_{v5} = 0.21,\ a_{v0} = -1.61,$ $(c_{v1} = b_{v2} = a_{v1} = a_{v2} = 0),\ (b_{v3} = b_{v6} = b_{v7} = 1),\ V^{str}_{CE,\max}$ = any value > 0).

6.3.4 The standard fatigue sub-model

As discussed in section 2.5.4, the mechanism of fatigue is complex and difficult to measure. Various modelling approaches at different levels of complexity are used in the literature to represent the fatigue effect on muscle force and hence alternative sub-models are reported in the literature. The standard form for fatigue proposed here can be used to represent all alternative sub-models introduced in Chapter 2 (and almost any alternative fatigue sub-models in the literature). The standard form can also be used to build new fatigue sub-models at the required accuracy and complexity level.

The focus is on the index of fatigue which represents force decay during FES and force capacity recovery when FES is off, pH level and all other physiological details will be ignored. The prediction of fatigue can be improved by using the multiple motor-unit modelling approach, where fatigue of every individual motor-unit will be modelled separately. The standard fatigue sub-model is given by:

$$\frac{d}{dt}(IF)=\begin{cases}0 & , \quad t<T_{end}\\ \left[C_{fat}\times(IF_{\min}-IF(t))\right]+\left[C_{rec}\times(1-IF(t))\right] & , \quad t\geq T_{end}\end{cases} \tag{6.13}$$

Assuming: $IF=1 \quad at \quad t=0$.

Previous equation can be used with a single motor-unit model, three fibre-types model, or the multiple motor-unit model. The standard fatigue sub-model can represent all fatigue sub-models represented in section 2.5.4.2 as follows:

For Riener-1 fatigue sub-model:

$$T_{end}=0,\ C_{fat}=\frac{R\times A_{freq}\times\lambda}{T_{fat}},\ C_{rec}=\frac{1-(R\times A_{freq}\times\lambda)}{T_{rec}}.$$

For Hawkins fatigue sub-model:

For type-I and type-IIa fibres: $T_{end}=6,\ C_{fat}=\frac{0.00097}{IF(t)},\ C_{rec}=0,\ IF_{\min}=0.$

For type-IIb fibres: $T_{end}=23,\ C_{fat}=\frac{0.0333}{IF(t)},\ C_{rec}=0,\ IF_{\min}=0.$

For Freund & Takala fatigue sub-model:

$T_{end} = 0$, $IF_{\min} = 0$, $C_{fat} = \frac{\beta \times R}{IF(t)}$, $C_{rec} = \alpha$.

For Ma fatigue sub-model:

$T_{end} = 0$, $IF_{\min} = 0$, $C_{fat} = k \times R$, $C_{rec} = r$.

For Giat fatigue sub-model:

The pH level has not be considered. Constants values need to be determined by empirical experiments for each muscle. Hence, constants' values of the standard sub-model can be adjusted to fit the fatigue experimental data of any muscle. Using this procedure any fatigue sub-model can be constructed exactly, or at least to get a very close match.

6.3.5 The standard force enhancement & depression sub-model

As discussed in section 2.5.5, only few force enhancement & depression sub-models are available in the literature. A new and more complex force enhancement & depression sub-model was developed in this research because those available in the literature are relatively simple compared with observed empirical data. The empirical data used to develop this sub-model were collected from the literature, see Appendix 2. Details of the new and the standard force enhancement & depression sub-models are given below.

6.3.5.1. A new force enhancement & depression sub-model

As discussed in section 2.5.5.1, force enhancement following stretch and force depression following shortening are affected by different factors (magnitude of stretch/shortening, velocity, recruitment level, and stimulation frequency) during stretch/shortening. The new sub-model proposed here can be used with any Hill-type model which uses the instantaneous length. Most of the length-history properties are accounted for (more complex than Hawkins and Forcinito *IE & ID* sub-models). In this sub-model, the effect of enhancement and/or depression starts immediately after the end of stretch/shortening. The force will decay (after stretch) or increase (after shortening) exponentially until the steady-state force is reached after 4.0 seconds. The experimental data used to develop this sub-model include those presented in Appendix 2 in addition to the data presented in [152, 154, 155, 168, 169, 170, 171, 172, 173].

Index of Enhancement (*IE*):

The index of enhancement is given by:

$$IE(t) = \begin{Bmatrix} IE_{\infty} + \left[(IE_{\max} - IE_{\infty}) \times \exp(c_{TS} \times t)\right] & for \quad t \le 4 \\ IE_{SS} & for \quad t > 4 \end{Bmatrix} \tag{6.14}$$

$$IE_{\max} = \frac{\text{maximum muscle force during stretch}}{\text{isometric force corresponding to the length at end of stretch}} \tag{6.15}$$

The plateau level of IE (IE_{∞}) after very large value of time ($t \to \infty$) is a function of the initial length ($l_{ER,o}$) just before the start of stretch, stretch magnitude (Δl_{ER}), and velocity of stretch (v_{CE}).

$$IE_{\infty} = 1 + \left[(c_1 \times \bar{l}_{ER,o}) + (c_2 \times \Delta\bar{l}_{ER}) + (c_3 \times \bar{v}_{CE})\right] \tag{6.16}$$

c_1, c_2 and c_3 are constants which can be adjusted to fit experimental data, a separate constant was multiplied with each variable in order to make the model more accurate. The effect of $\Delta\bar{l}_{ER}$ is clear from the experimental data shown in Appendix 2 (e.g. Figure A2.7), longer displacements produce more enhancement, and vice versa. Similarly stretches happen at longer length $\bar{l}_{ER,o}$ result in more enhancements, and vice versa. The effect of velocity is included in the model since it has an effect on IE_{∞} as can be observed from experimental data (e.g. Figure 2.33 in Chapter 2).

The time (t = 4.0 seconds) was chosen (similar to that of Hawkins) because it was found to be a good approximation to the decay time following stretch observed experimentally (see experimental data in Appendix 2).

$$IE_{SS} = IE(t = 4) = IE_{\infty} + \left[(IE_{\max} - IE_{\infty}) \times \exp(c_{TS} \times 4)\right] \tag{6.17}$$

The transient-state constant: $c_{TS} = \dfrac{-0.3}{(IE_{\max} - IE_{\infty})}$ (6.18)

t: Time from end of stretch.

Index of Depression (*ID*):

The index of depression is given by:

$$ID(t) = \begin{cases} ID_{\infty} + \left[(ID_{\min} - ID_{\infty}) \times \exp(c_{TS} \times t)\right] & for \quad t \le 4 \\ ID_{SS} & for \quad t > 4 \end{cases} \qquad (6.19)$$

$$ID_{\min} = \frac{\text{minimum muscle force during shortening}}{\text{isometric force corresponding to the length at end of shortening}} \qquad (6.20)$$

The plateau level of ID (ID_{∞}) after very large value of time ($t \to \infty$) is a function of the initial length $l_{ER,o}$ just before the start of shortening, shortening magnitude Δl_{ER}, and minimum force during shortening ($ID_{\min}$ is used in this sub-model which is a function of the minimum force during shortening).

$$ID_{\infty} = 1 - \left[(c_1 \times \bar{l}_{ER,o}) + (c_2 \times \Delta\bar{l}_{ER}) + (c_3 \times ID_{\min})\right] \qquad (6.21)$$

c_1, c_2 and c_3 are constants which can be adjusted to fit experimental data, a separate constant was multiplied with each variable in order to make the model more accurate. The effect of $\Delta\bar{l}_{ER}$ is clear from the experimental data as shown in Appendix 2 (e.g. Figure A2.8), longer displacements produce more depression, and vice versa. Similarly shortenings happen at longer $\bar{l}_{ER,o}$ result in more depression, and vice versa. The effect of $ID_{\min}$ is included since it has an effect on IE_{∞} as can be observed from experimental data (e.g. Figure 2.33 in Chapter 2).

The time (t = 4.0 seconds) was chosen (similar to that of Hawkins) because it was found to be a good approximation to the rise time following shortening observed experimentally (see experimental data in Appendix 2).

$$ID_{SS} = ID(t = 4) = ID_{\infty} + \left[(ID_{\min} - ID_{\infty}) \times \exp(c_{TS} \times 4)\right] \qquad (6.22)$$

The transient-state constant: $c_{TS} = \dfrac{-1}{(ID_{\infty} - ID_{\min})}$ (6.23)

t: Time from end of shortening.

6.3.5.2. The standard force enhancement & depression sub-model

The standard *IE & ID* sub-model proposed here was developed using the alternative *IE & ID* sub-models available in the literature (see section 2.5.5.2) and the new *IE & ID* sub-model. The standard form can also be used to build new *IE & ID* sub-models at the required accuracy and complexity level.

Index of enhancement (*IE*):

$$IE(t) = \begin{cases} IE_{\infty} + \left[(IE_{\max} - IE_{\infty}) \times \exp(c_{TS} \times t)\right] & for \quad t \le 4 \\ IE_{SS} & for \quad t > 4 \end{cases} \tag{6.24}$$

$$IE_{SS} = IE(t=4) = IE_{\infty} + \left[(IE_{\max} - IE_{\infty}) \times \exp(c_{TS} \times 4)\right] \tag{6.25}$$

$$IE_{\max} = \frac{\text{maximum muscle force during stretch}}{\text{isometric force corresponding to the length at end of stretch}} \tag{6.26}$$

Index of depression of (*ID*):

$$ID(t) = \begin{cases} ID_{\infty} + \left[(ID_{\min} - ID_{\infty}) \times \exp(c_{TS} \times t)\right] & for \quad t \le 4 \\ ID_{SS} & for \quad t > 4 \end{cases} \tag{6.27}$$

$$ID_{SS} = ID(t=4) = ID_{\infty} + \left[(ID_{\min} - ID_{\infty}) \times \exp(c_{TS} \times 4)\right] \tag{6.28}$$

$$ID_{\min} = \frac{\text{minimum muscle force during shortening}}{\text{isometric force corresponding to the length at end of shortening}} \tag{6.29}$$

Previous equations can be used with a single motor-unit model, multiple (two/three) fibre-type model, or multiple motor-unit model. The standard *IE & ID* sub-model can represent all IE and ID sub-models summarised in Chapter 2 of this thesis (and almost all alternative sub-models in the literature) as follows:

For Hawkins *IE* sub-model:

$$IE_{\infty} = \begin{cases} 0.505(IE_{\max}) + 0.403 & for: IE_{\max} \ge 1.2 \\ 1.0 & for: IE_{\max} < 1.2 \end{cases}$$

$$c_{TS} = -0.301/(IE_{\max} - IE_{\infty})$$

ID is not modelled by Hawkins.

For Forcinito *IE & ID* sub-model:

Forcinito force enhancement & depression sub-model was modified in order to be used in the "General Model", details are provided in Appendix 9. The initial length is used [$f_{CE} = f_{iso}(l_o)$], this has to be taken into account when using this sub-model. In the formulated Forcinito *IE & ID* sub-models; time starts after the end of stretch/shortening.

$$IE_{\infty} = 1 + \left(\frac{E.A}{\bar{l}_{ER,o}} \times \Delta \bar{l}_{ER} \right), \ (E.A = 1.575, \text{ for stretch}).$$

$$ID_{\infty} = 1 + \left(\frac{E.A}{\bar{l}_{ER,o}} \times \Delta \bar{l}_{ER} \right), \ (E.A = 0.675, \text{ for shortening}).$$

$$c_{TS} = -(\frac{k}{c}) = -\frac{0.7}{0.757} = -0.925$$

For the new *IE & ID* sub-model:

$$IE_{\infty} = 1 + \left[c_e \times \bar{l}_{ER,o} \times \Delta \bar{l}_{ER} \times \exp(-2 * \bar{v}_{CE}) \right],$$

$$c_{TS} = \frac{-0.3}{(IE_{\max} - IE_{\infty})}, \text{ (for stretch).}$$

$$ID_{\infty} = 1 - \left[c_d \times \bar{l}_{ER,o} \times \Delta \bar{l}_{ER} \times ID_{\min} \right]$$

$$c_{TS} = \frac{-1}{(ID_{\infty} - ID_{\min})}, \text{ (for shortening}$$

6.3.6 The standard sub-models for muscle passive elements

As discussed in section 2.5.6.1, skeletal muscles have complex passive viscoelastic structure which can vary among different muscles. Various modelling approaches at different levels of complexity are used in the literature and hence alternative sub-models are reported at different complexity levels. Standard forms for all alternative sub-models of the passive elements are possible. The standard forms proposed here can be used to represent all alternative passive elements sub-models introduced in Chapter 2 (and almost all alternative passive elements sub-models in the literature). The standard forms can also be used to build new passive element sub-models at the required complexity level.

The standard sub-models for passive elements are given in the following sub-sections. The standard arrangement of the model elements is shown earlier in this chapter (Figure 6.7), this

form consists of an elastic element (*SE*) representing the tendon along with a combination of *CE*, parallel elastic element *PE* and viscous element *VE* representing the muscle belly. All passive elements in this model can be linear or nonlinear elements. α represents pennation angle of muscle fibres, ($PE = PE1 + PE2$).

6.3.6.1. Arrangement of passive elements

All Hill-type models introduced in Chapter 2 of this thesis can be constructed using the standard form shown in Figure 6.5 as follows:

For Herzog model: $\alpha = 0$, *PE2*=0 ($f_{PE2} = 0$), *VE*=0 ($f_{VE} = 0$).

The form of Herzog model can be changed to the standard form using Fung equations given in [107].

For Hawkins model: *PE2*=0 ($f_{PE2} = 0$).

For Brown model: $\alpha = 0$.

For LifeMOD model: $\alpha = 0$, *VE*=0 ($f_{VE} = 0$), *PE2*=0 ($f_{PE2} = 0$), $SE = \infty$ (rigid tendon).

6.3.6.2. The standard sub-model for (f_{SE})

Brown *SE* sub-model was modified by adding an extra constant c_3 which allows for the slack length $\bar{l}_S^t$ to be shifted along the X-axis (this will shift the whole curve).

$$f_{SE}(\bar{l}_t) = c_1 \times \ln\left\{\exp\left[\frac{\bar{l}_{SE} - (\bar{l}_S^t + c_3)}{c_2}\right] + 1\right\} \qquad (6.30)$$

c_1, c_2, c_3: constants.

The following constants' values can be used to represent each *SE* sub-model introduced in Chapter 2:

For Herzog model: The following constants' values can be used to get "almost exactly" the linear curve of Herzog *SE* sub-model: ($c_1 = 0.00167$, $c_2 = 0.00006$, $c_3 = 0$).

For Brown model: The following constants' values can be used to get "exactly" Brown *SE* sub-model: ($c_1 = 0.13066$, $c_2 = 0.0047$, $c_3 = 0$).

For Hawkins model: A very similar curve was obtained by using the following constants' values: ($c_1 = 0.518$, $c_2 = 0.0045$, $c_3 = 0.028$).

6.3.6.3. The standard sub-model for (f_{PE1})

Brown *PE1* sub-model was chosen exactly as it is to be the standard form:

$$f_{PE1}(\bar{l}_{CE}) = c_1 \times \ln\left\{\exp\left[\frac{(\bar{l}_{CE} / \bar{l}_{\max}) - \bar{l}_{rest}}{c_2}\right] + 1\right\} \qquad (6.31)$$

c_1, c_2: constants.

The following constants' values can be used to represent each *SE* sub-model introduced in Chapter 2:

For Herzog model: The following constants' values can be used to get "almost exactly" the linear curve of Herzog *SE* sub-model: ($c_1 = 0.003$, $c_2 = 0.00108$, $l_{\max} = 1$, $l_{rest} = 1.25$).

For Brown model: The following constants' values can be used to get "exactly" Brown *PE1* sub-model: ($c_1 = 1.058$, $c_2 = 0.046$, $l_{\max} = 1.3$, $l_{rest} = 1.17$).

For Hawkins model: A very similar curve was obtained by using the following constants' values:
($c_1 = 12$, $c_2 = 0.08$, $l_{\max} = 1.2$, $l_{rest} = 1.6$).).

For LifeMOD model: A similar curve was obtained by using the following constants' values:
($c_1 = 12$, $c_2 = 0.08$, $l_{\max} = 1.2$, $l_{rest} = 1.6$).

6.3.6.4. The standard sub-model for (f_{PE2})

f_{PE2} was only modelled in Brown muscle model. Therefore, Brown *PE2* sub-model will be used as the standard sub-model. Note that if f_{PE2} model is used then the F-L sub-model has to be modified accordingly. Only Brown F-L sub-model is ready to be used with f_{PE2} sub-model. Vice versa, if Brown F-L sub-model was to be used without the f_{PE2} sub-model, then it has to be modified by removing f_{PE2} from the F-L sub-model.

$$f_{PE2}(\bar{l}_{CE}) = c_1 \times \left[-0.02 \times \{\exp[-21 \times (\bar{l}_{CE} - l_{r2})] - 1\}\right] \ , \quad f_{PE2} \le 0 \qquad (6.32)$$

$$l_{r2} = 0.7$$

For Brown model: ($c_1 = 1$ **).**

For other sub-models: ($c_1 = 0$ **).**

6.3.6.5. The standard sub-model for (f_{VE})

Linear viscous element is used, only Brown and Hawkins have used the passive viscous element f_{VE} sub-model.

$$f_{VE} = b \times \bar{v}_{CE} \qquad (6.33)$$

For Brown model: $b = 0.0788$ (slow-twitch fibres), $b = 0.0915$ (fast-twitch fibres).
Note that each fibre-type (slow and fast) has different values for: ($\left|v_{CE,\max}\right|$).

For Hawkins model: $b = c_i \times (1 - R_i)$

Each fibre-type has different values for c_i: $c_1 = 0.51585$, $c_2 = c_3 = 0.44195$.

For other models: ($b = 0$ **).**

Chapter 7: Discussion and Conclusions

7.1. Discussion

Skeletal muscle is a highly complex and nonlinear system. The response of electrically stimulated muscle is nonlinear, time varying, coupled, and often accompanied by unpredictable disturbance. Computer simulations based on accurate mathematical models of the musculoskeletal system can help in the design and evaluation of complex closed-loop control algorithms for FES systems. The commonly used single motor-unit muscle model (in FES control studies) with the instantaneous *CE* length as input to the force-length relationship cannot properly model the continuously varying partially recruited muscles, nor it can account for physiological properties specific to each fibre-type.

Multiple motor-unit models can properly account for continuously varying recruitment as would usually be seen in closed-loop FES control. Every virtual motor-unit in the multiple motor-unit model is modelled separately; in this way the effects of length at initial recruitment, fatigue and recovery, force enhancement & depression are calculated individually for each motor-unit. Moreover, the physiological properties specific to each fibre-type (i.e. recruitment order, F-L relationship, F-V relationship, and fatigue) can be incorporated into the multiple motor-unit model to further increase its accuracy.

The main goal of this study was to develop a multiple motor-unit model that can account for continuously varying recruitment levels at different muscle lengths and different times. Different aspects of muscle modelling have been investigated in this study using single and multiple motor-unit models. The results demonstrate the potential errors introduced by using the single motor-unit model and the instantaneous length which are common in FES control studies.

7.2. Conclusions

A new multiple motor-unit model has been developed which considers the muscle to comprise a large number (1000) individual Hill-type virtual motor-units. As the recruitment

level $R(t)$ varies over time and at different *CE* lengths, these virtual motor-units are recruited at different times and each with its own initial length; thus overcoming the problem described above.

The simulation results obtained in chapters 3, 4 and 5 demonstrate the differences and potential errors introduced by using single motor-unit models in FES control studies. By correctly modelling the effects of continuously changing recruitment and length, as seen during FES control, it is hoped that better FES controllers can be designed.

In addition to the improvements to the model accuracy, multiple motor-unit models can also provide clear and deep understanding of the highly complex and non-linear response of the paralysed muscle including the internal muscle dynamics. A better understanding of the muscle's physiological properties can help in the design of FES controllers that optimize the produced muscle force and hence the generated movement.

For the multiple motor-unit models presented in chapters 3, 4 and 5; higher accuracy can be achieved using the same number of model parameters, which is an advantage over the single motor-unit model. However, if high level of complexity is required when using the "General Model" presented in Chapter 6, the main limitation is the large number of model parameters. Hence more parameters need to be estimated experimentally.

7.3. Future work

Although this study has covered many modelling issues regarding multiple motor-unit models, there are many other issues that can be studied and investigated. Suggestions for future work that can be done to further improve the performance of multiple motor-unit models are given below:

- In this study, one fibre-type was assumed when simulating the responses of open-loop simulation protocols in chapters 3, 4 and 5. The new recruitment sub-model (presented in section 6.3.1.1) with three different fibre-types can be used in open-loop simulation protocols.

- In this study, the simulation was made for the responses of open-loop simulation protocols in chapters 3, 4 and 5. It is suggested to do more simulations and simulate the responses of closed-loop simulation protocols.
- The following complexities can be incorporated to further improve the accuracy of the multiple motor-unit model and also the "General model":
    - Pennation angle of muscle fibres.
    - Different F-L sub-models for different fibre-types.
    - Different F-V sub-models for different fibre-types.
    - Different fatigue sub-models for different fibre-types.
    - The same *IE & ID* and passive F-V sub-models (of non-recruited fibres) can be used with all fibre-types unless opposing experimental evidence was found.

  For simplicity and to demonstrate the potential errors introduced by using instantaneous *CE* length instead of *CE* length at initial recruitment, the *CE* length before recruitment was used in chapters 3 and 5. The *CE* length, before and after recruitment, is different due to the tendon compliance [196]. The use of length at initial recruitment can be further improved by using the *CE* length after onset of recruitment. Experimental force-length relationship (before and after recruitment) and some ankle joint parameters are given in appendix 6.

- The performance of the "General model" can be compared using different sets of sub-models at different levels of complexity. Then the results from this comparison can be analysed to identify the key effects (e.g. recruitment and fatigue sub-models) that require modelling and should be included in a muscle model, and at which level of complexity, to provide a simulation environment for developing FES controllers.

In this study, theoretical background and published experimental data from the literature were used to build new muscle models using the multiple motor-unit modelling approach. Open-loop simulation protocols were made on the single and multiple motor-unit models to demonstrate the differences and potential errors introduced by using the instantaneous length, ignoring certain sub-models or by using the single motor-unit modelling approach.

In order to build confidence in the multiple motor-unit modelling approach, appropriate experimental data are required. However, almost all experimental data available in the literature are for fully recruited muscles. Published data for partially recruited muscle are very little and do not include the main requirement of having different recruitment levels at different *CE* lengths. The experimental data required to validate the multiple motor-unit modelling approach and the *CE* length at initial recruitment have to be for dynamic contractions using different levels of recruitment at different values of *CE* lengths and using different muscles that comprise different fibre-types. The data should also include protocols of stretch and shortening on both limbs (the ascending and descending limbs) of the force-length relationship.

Closed-loop simulation protocols can also be tested on the single and multiple motor-unit models to demonstrate the differences and potential errors introduced by ignoring certain sub-models or by using the single motor-unit model during the design, development and evaluation of FES controllers.

Appendix 1: Topology of Published Muscle Models

This appendix describes the topologies of published models. Topologies of different models from the literature are presented first; a common standard topology for the "General Model" is presented in Chapter 6 with a description on how it can be adapted to represent topologies of other models described here (and almost all other alternative sub-models in the literature). Details of the various components (sub-models) of the "General Model" are provided in Chapter 6.

The original topology and arrangement of passive elements of Herzog model are formulated in order to make it similar to other models and then it can be reconstructed for the common standard topology. The activation sub-model of Brown model and Riener model are not included since the stimulation frequency is constant during FES, this step reduced a lot of un-necessary complexity for models of electrically stimulated muscles (for naturally contracted muscles, cancellation of the activation sub-model can affect the model accuracy since the stimulation frequency changes with the natural stimulation input).

Various components in the standard topology of the "General Model" are explained in Chapter 2 and Chapter 6 of this thesis. Alternative sub-models of different complexity levels can be used; it is also possible to represent different fibre-types and the multiple motor-units.

The topologies of Riener-1 and Riener-2 models are the only topologies which are provided in their related references. All other topologies were developed in this research using the models' equations and text provided in related references.

A1.1. Herzog Model

Topology of Herzog model [18] is shown in Figure A1.1. A three-element model is used with the form shown in Figure A1.2. Herzog model is the only model found in the literature that uses the length at initial recruitment (l_o). Topology of the original Herzog model given in [18] was formulated in order to make it possible to be represented in the standard topology form (given at the end of this chapter).

The position of PE can be changed and made parallel on CE only, the new equivalent values for the linear stiffness (k_p and k_s) can be calculated using Fung equations given in [107]. The topology shown in Figure A1.1 will not be affected by this change; the only change is in f_{PE1} which will be calculated as a function of l_{CE} not l_{mt}.

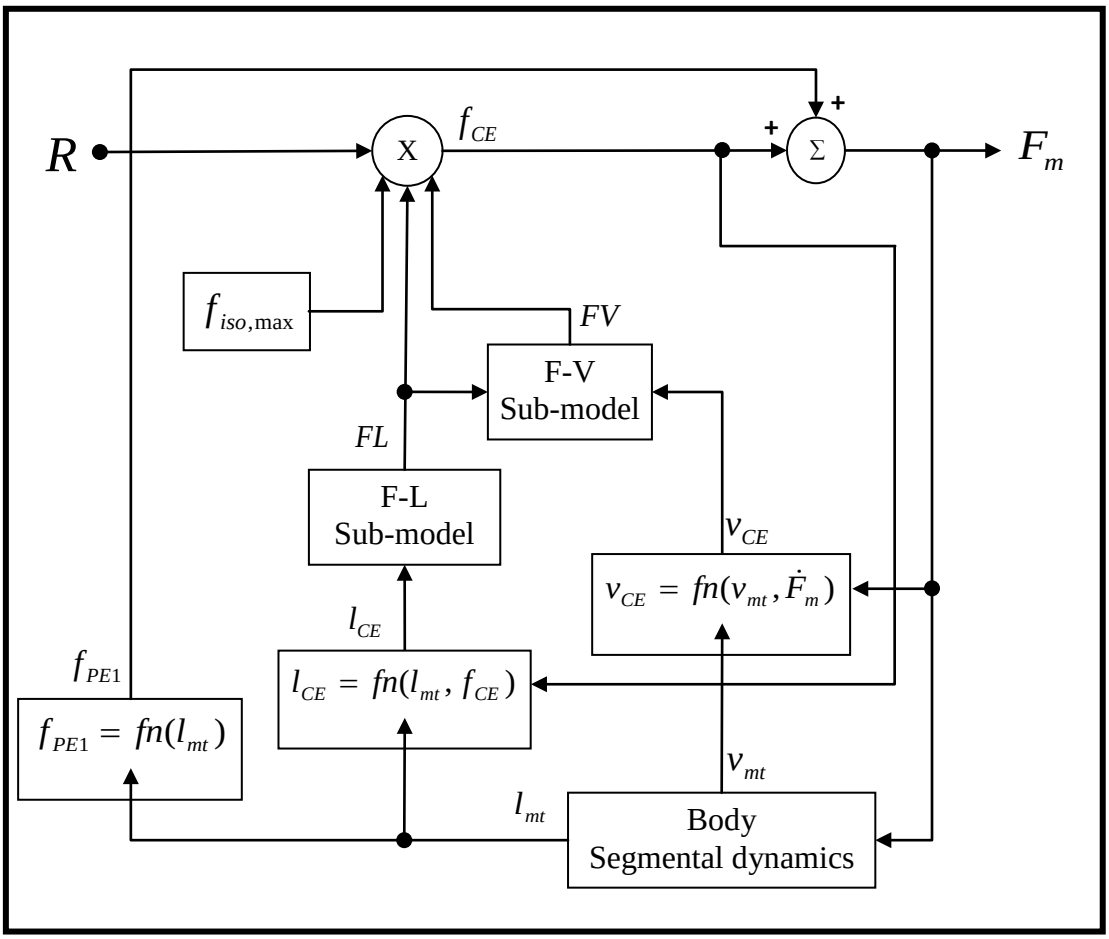

Figure A1.1: The "formulated" topology of Herzog model.

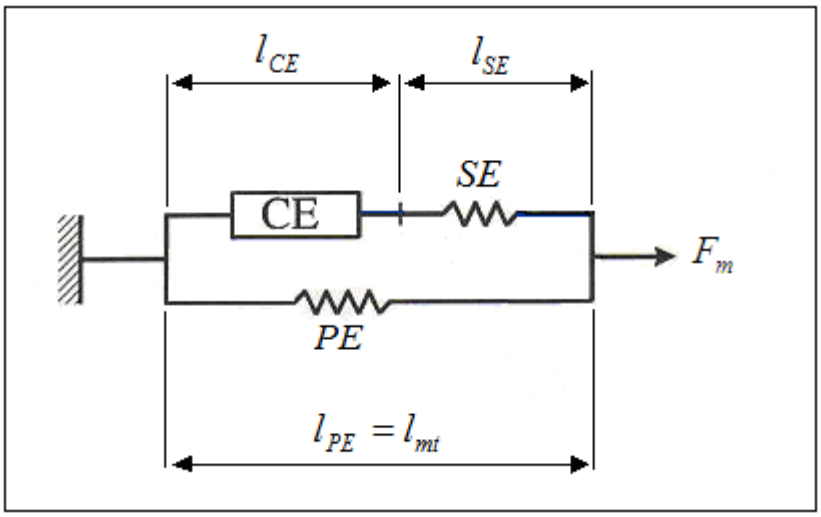

Figure A1.2: Representation of Herzog muscle model using rheological elements structure.

A1.2. Riener-1 Model

In Riener-1 model [72], only the active part of the muscle (CE) is modelled, muscle passive elements are not modelled in the muscle model but rather in the passive torque model of the joint, Riener-1 model is illustrated in Figure A1.3. Passive torque caused by passive forces of all muscles which span the same joint are modelled together as functions of joint angle and joint angular velocity, details are provided in [72, 174].

Muscle length (l_{CE}) and muscle velocity (v_{CE}) are estimated directly from joint angle and joint angular velocity.

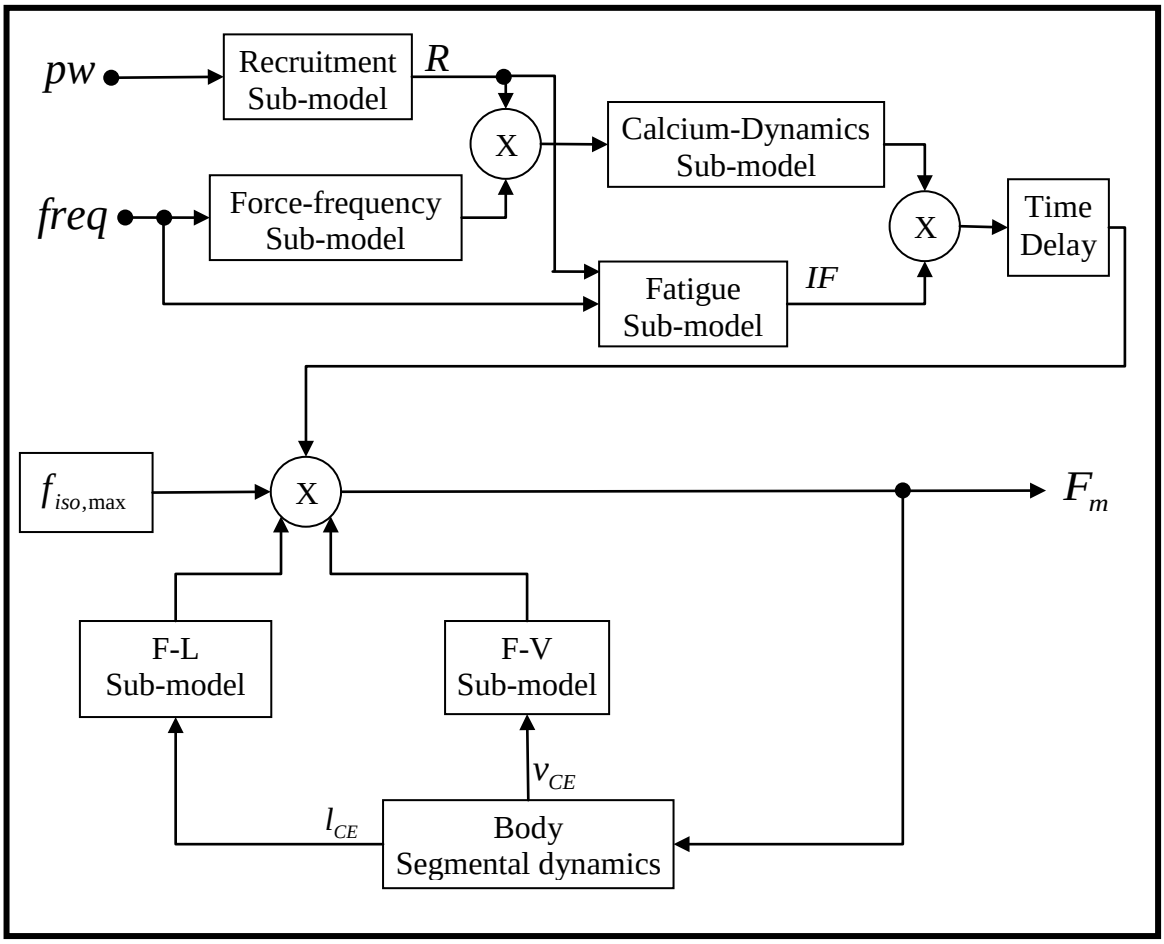

Figure A1.3: Topology of Riener-1 model.

Riener calcium dynamics sub-model:

The calcium (Ca^{2+}) dynamics describe the phenomenon of calcium ion released from sarcoplasmic reticulum. It is modelled by two first order transfer functions in series (time constant T_{Ca}), the model is represented as:

$$a(S) = \left(\frac{1}{T_{Ca}S+1}\right)\left(\frac{1}{T_{Ca}S+1}\right)a_p(S) = \frac{1}{{T_{Ca}}^2S^2 + 2T_{Ca}S + 1}a_p(S)$$

A1.3. Riener-2 Model

In Riener-2 model [73], the muscle is divided into 100 motor-units of slow-twitch (type-I) and fast-twitch (Types IIb and IIa together). Riener-2 model is a physiologically based model, where the output is the normalised isometric muscle force (under isometric conditions), passive elements are not modelled.

The recruitment sub-model is shown in Figure A1.4, the fatigue and calcium dynamics are similar to those in Riener-1 model. The biophysical processes underlying excitation and activation are also modelled for the isometric contraction only. The focus of this research is on the effect of different muscle properties on muscle force not the details of the biochemical and biophysical processes which happen during muscle contraction. Therefore, sub-models for the biophysical processes are not considered. The focus here is on the binary recruitment of motor-units.

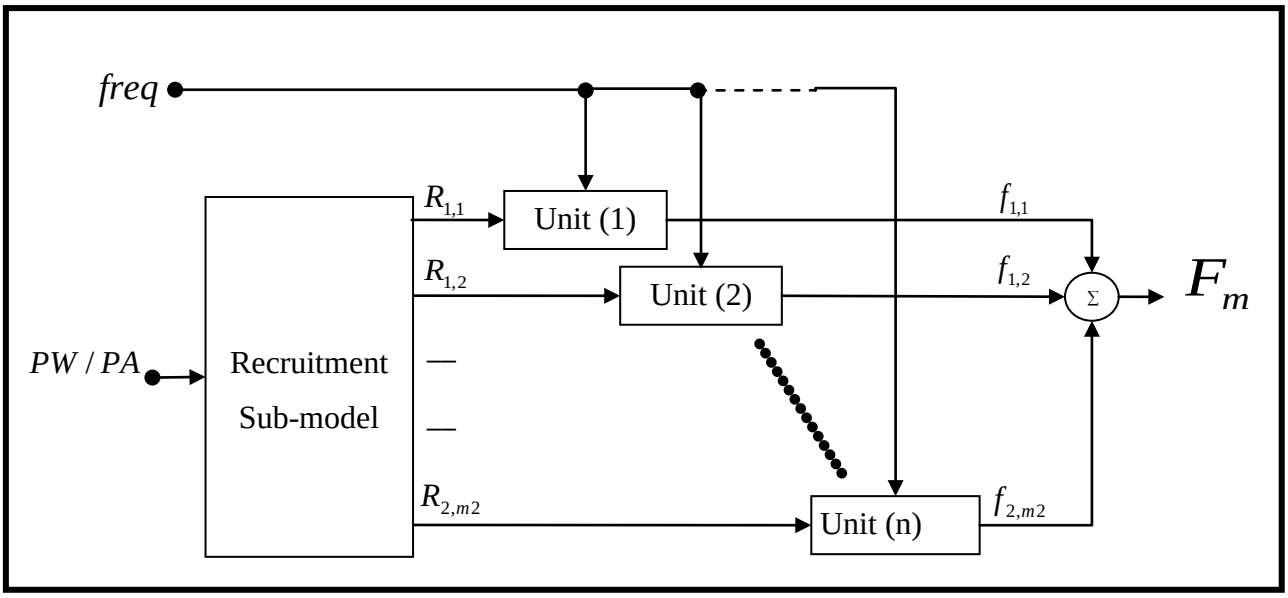

Figure A1.4: Topology of Riener-2 model.

A1.4. Brown Model

Topology of Brown model [41, 82, 84, 127] (including alternative variants of Brown models in the Virtual Muscle modelling package [128]) is shown in Figures A1.5 and A1.6. Although fatigue and force enhancement & depression are not included, Brown model is one of the most complex models reported in the literature. The arrangement of passive elements is represented in Figure A1.7. The linear parallel viscous element was added in virtual muscle modelling package [77] for stability purposes during simulation (incorporated into f_{PE1} sub-model)

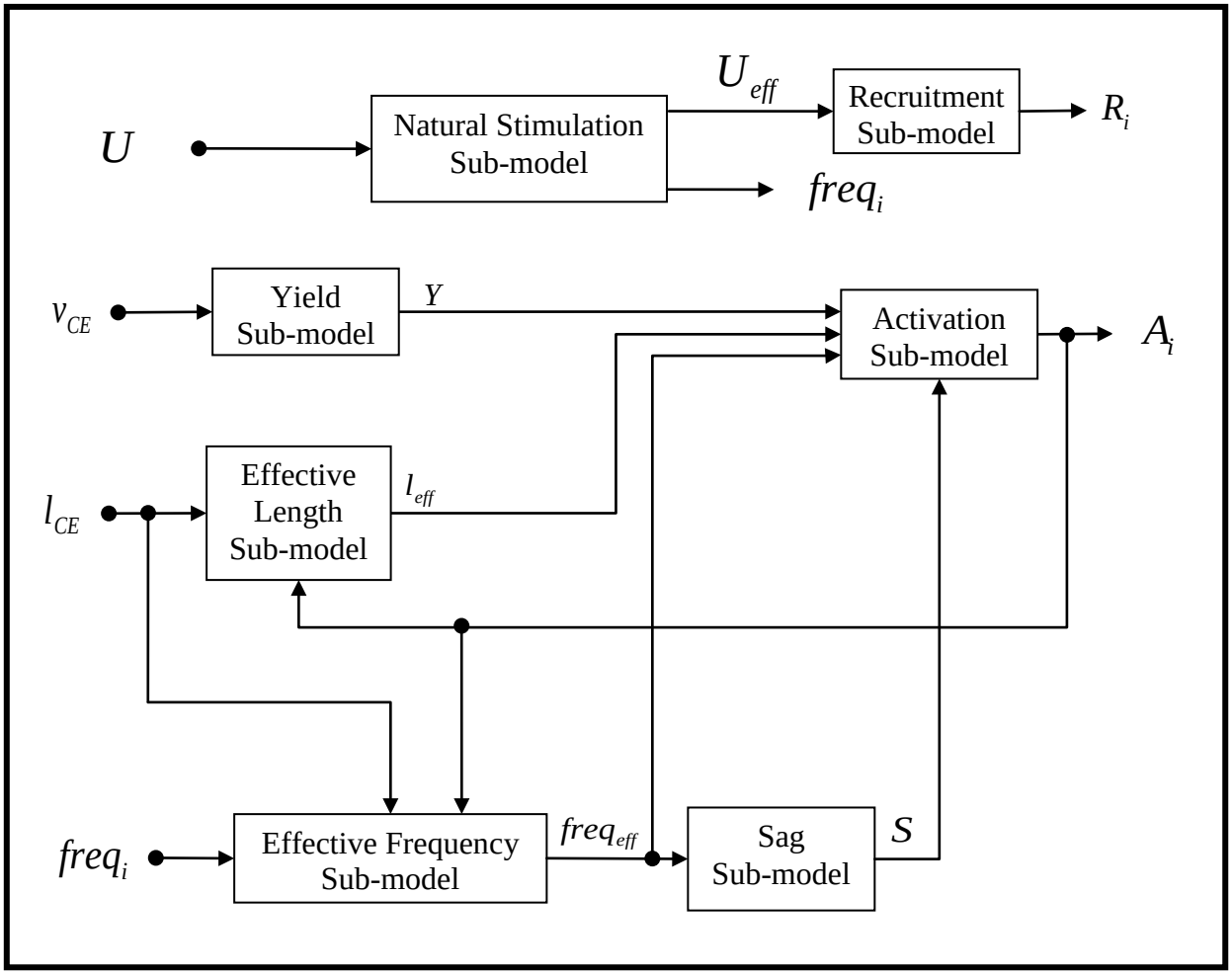

Figure A1.5: Topology of Brown model and other alternative models in Virtual Muscle software package.

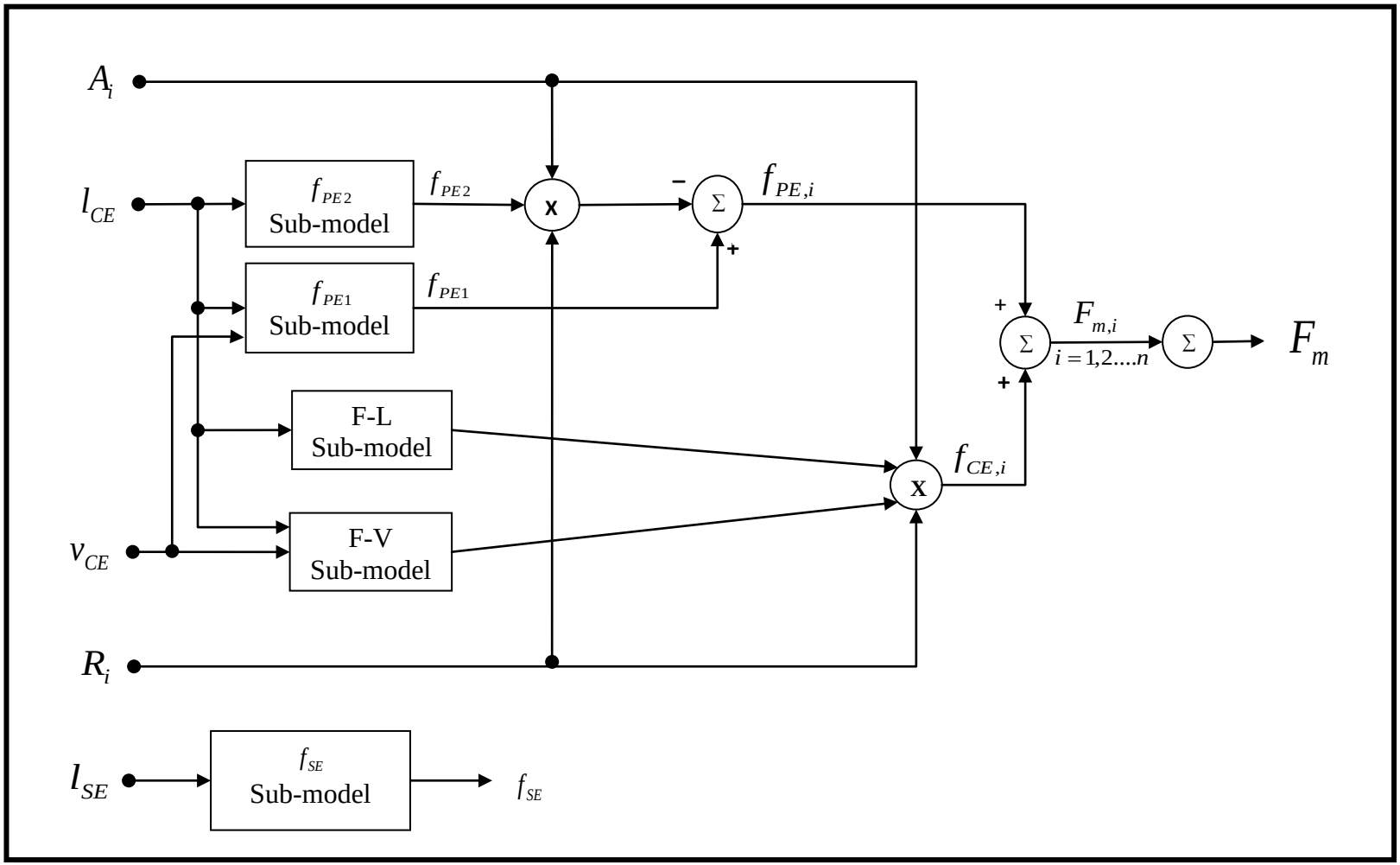

Figure A1.6: Topology of Brown model and other alternative models in Virtual Muscle software package.

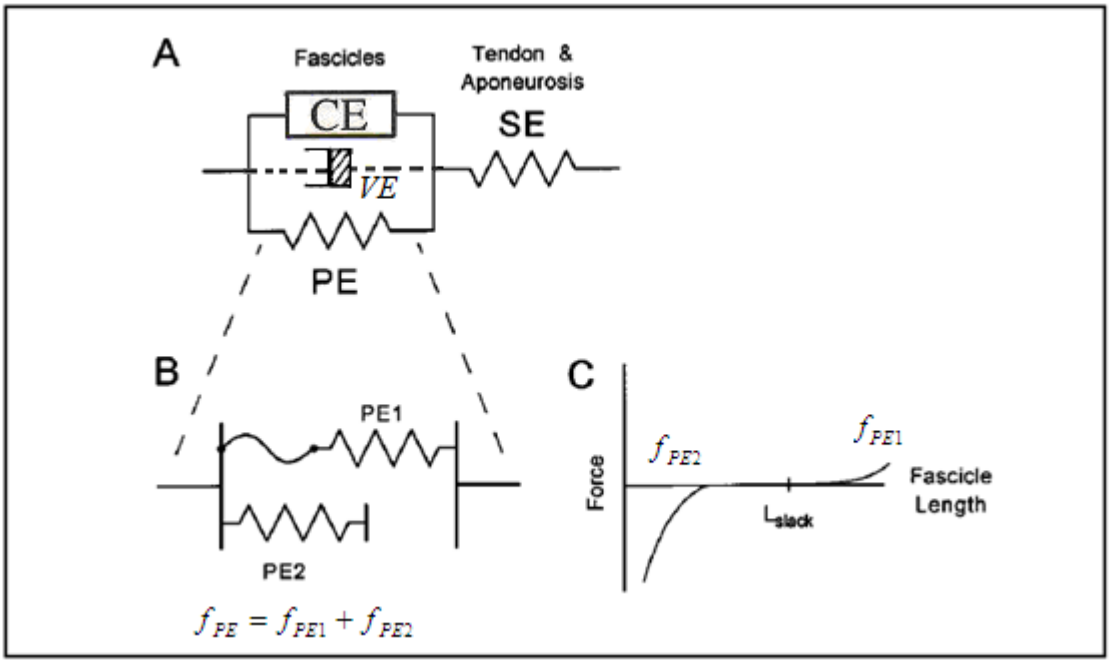

Figure A1.7: A) Representation of Brown muscle model using rheological elements structure, ($l_{CE} = l_{PE1} = l_{PE2}$). B) The two parts of the passive elastic element PE. C) The passive F-L curves of $PE1$ and $PE2$. (Adapted from [82, 160]).

The rise and fall time (U_{eff}) sub-model:

The rise and fall time sub- model U_{eff} (presented in[128]) is an intermediate natural stimulation input that models the rise and fall effect of calcium dynamics when there is a change in the level of U. Note that: U_{eff} is different from the "total muscle effective activation" mentioned in [127], which is used in this thesis.

$$\dot{U}_{eff} = \frac{U - U_{eff}}{t_U} \qquad t_U = \begin{cases} 0.03(\text{sec}) & U \geq U_{eff} \\ 0.15(\text{sec}) & U < U_{eff} \end{cases}$$

The effective natural stimulation input U_{eff} models the transient-state when there is a change in the natural stimulation input U, the steady-state of the effective natural stimulation input U_{eff} will be the new value of natural stimulation input U (i.e. models rise and fall times only). Note that the rise and fall times due to change in stimulation frequency are modelled separately in Brown activation sub-model.

A1.5. Hawkins Model

In Hawkins model [101, 129, 130], the pennation angle is modelled, and hence the fibres length is used in the F-L sub-model ($l_{CE} = l_f$). Isometric force produced by muscle fibres is multiplied by ($\cos\alpha$) in order to get the force of the muscle fibres in the direction of tendon line of action (which represents muscle belly). The passive forces due to muscle fibres (f_{VE}, f_{BE1}, and f_{BE2}) will also be multiplied by $\cos\alpha$.

Topology of Hawkins model is represented in Figure A1.8, the thick arrows denote variables of multiple values (for i = 1, 2, and 3) and thin arrow denote single variables. The arrangement of passive elements is shown in Figure A1.9.

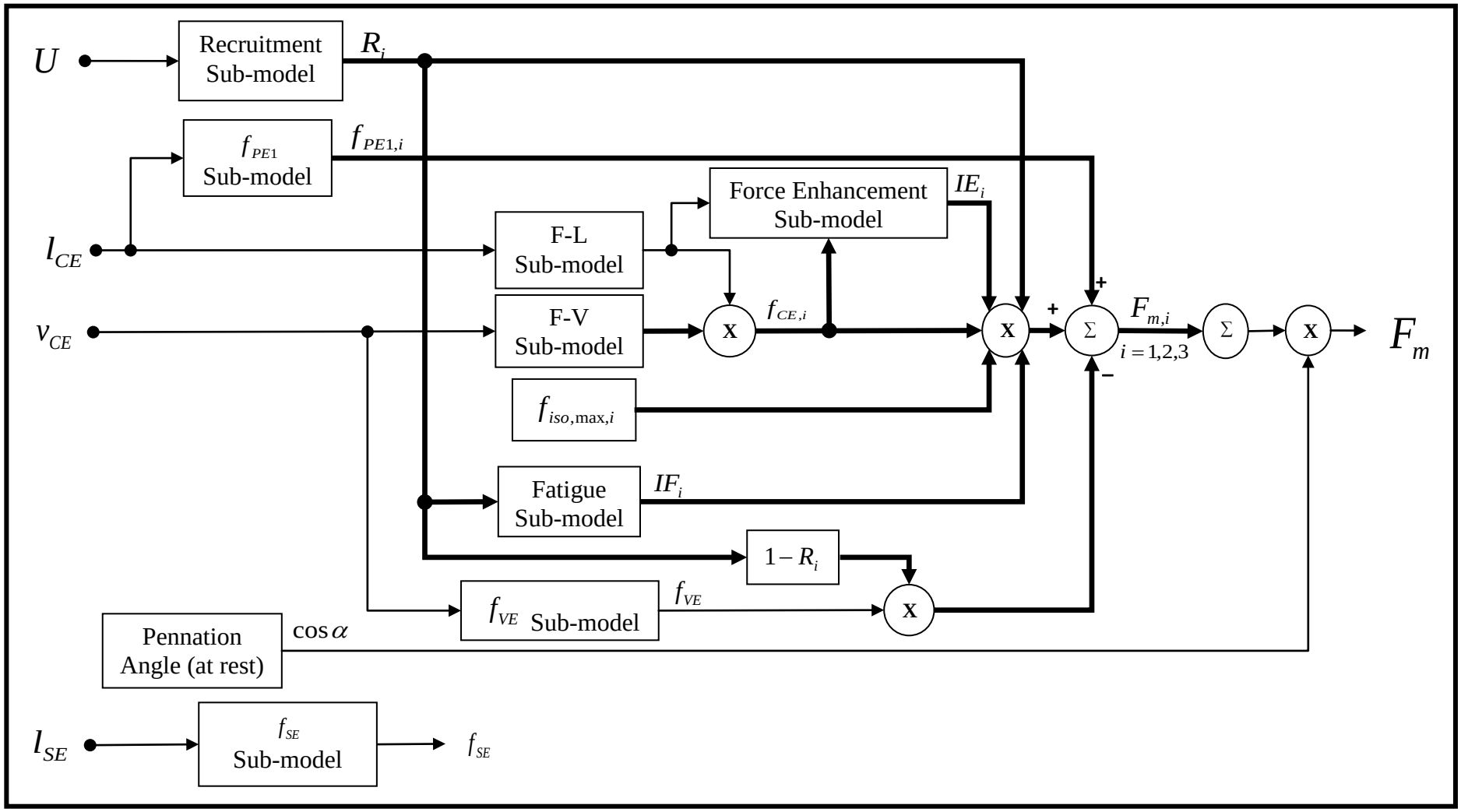

Figure A1.8: Topology of Hawkins model.

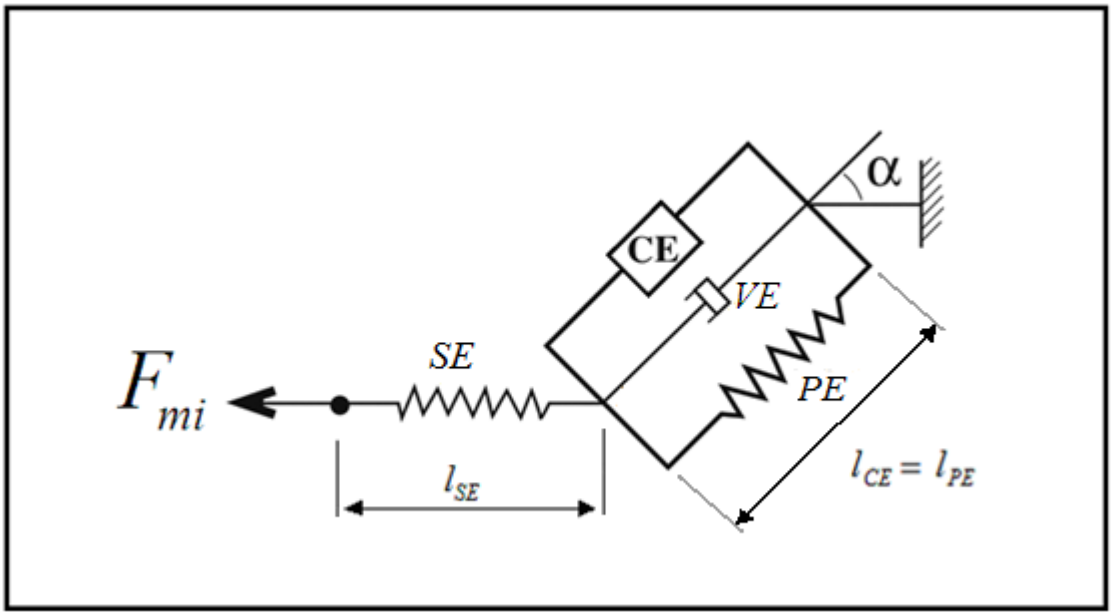

Figure A1.9: Representation of Hawkins muscle model using rheological elements structure.

Note that:

The viscous drag "passive" force created by all non-recruited fibres in the whole muscle:

$$f_{VE} = \sum_{i=1}^{n} f_{VE,i} = f_{VE,1} + f_{VE,2} + f_{VE,3}, \quad f_{VE,i} = c_i \times FPCSA_i \times (1 - R_i) \times v_{CE}$$

In the standard topology (topology of the "General Model"), all forces (except f_{PE1}) are multiplied by $PCSA_i$, and hence $PCSA_i$ was removed from the standard equation provided in section 6.3.6.5.

$$f_{VE} = \sum_{i=1}^{n} f_{VE,i} = c_1 \times \bar{v}_{CE} \times (1 - R_1) + c_2 \times \bar{v}_{CE} \times (1 - R_2) + c_3 \times \bar{v}_{CE} \times (1 - R_3)$$

$\bar{v}_{CE} = \dfrac{v_{CE}}{|v_{CE,\max}|}$, f_{VE} is normalised to $f_{iso,\max}$.

A1.6. Incorporation of activation sub-model into the "General Model"

In order to model muscle activation more accurately; an activation sub-model can be incorporated into the "General Model" proposed in Chapter 6. To the author's knowledge, Brown activation sub-model (Figure A1.5) which represents the steady-state activation, is the most complex activation sub-model reported in the literature.

The effective length sub-model L_{eff} models the time lag between changes in length and the effect of length on the activation sub-model (not F-L sub-model).

The effective frequency $freq_{eff}$ sub-model models the rise and fall times (effect of calcium dynamics) which happens after any change in stimulation frequency during FES (i.e. the time lag between changes in stimulation frequency and muscle activation).

Topology of the "General Model" for analogue recruitment input (fibre-type level), including activation (A_i) is shown in Figure A1.10, note that the hick arrows denote variables of multiple values (for i = 1, 2, and 3) and thin arrow denote single variables.

Sag is unique to fast-twitch fibres and becomes less at higher frequency and also at longer lengths. Sag happens during isometric and constant frequency, where the muscle force typically reaches a peak shortly after onset, after which there is a slow decline in force during the next few hundred milli-seconds [ms], this is not to be confused with fatigue.

Yield (Y) is the effect of stimulus frequency on sub-tetanic (at frequency lower than the maximum natural frequency) FV properties. Yielding behaviour is unique to slow-twitch fibres (fast-twitch fibres do not yield). Y is defined to be equal to 1 during the isometric condition and to be less than 1 during length changes.

Modelling the transient-state of activation

As discussed in Chapter 2; at onset and termination of FES (or natural voluntary contraction) there is a transient-state of activation, this can be modelled by the rise and fall time (U_{eff}) sub-model (proposed in Brown model, details are provided in [128] and summary in section A1.4) or the "calcium dynamics + time delay" sub-model proposed in Riener-1 model (details are provided in [72], summary in section A1.2). These two alternative sub-models (or any other alternative) can be incorporated into the "General Model".

More details about the activation sub-model and its components (effective length, effective frequency, Sag and yield) are provided in [81, 82, 84, 100, 127, 175, 176]. However, since frequency is typically constant during FES; the activation sub-model is not included and the activation has been assumed as constant at the value ($A_i = 1$).

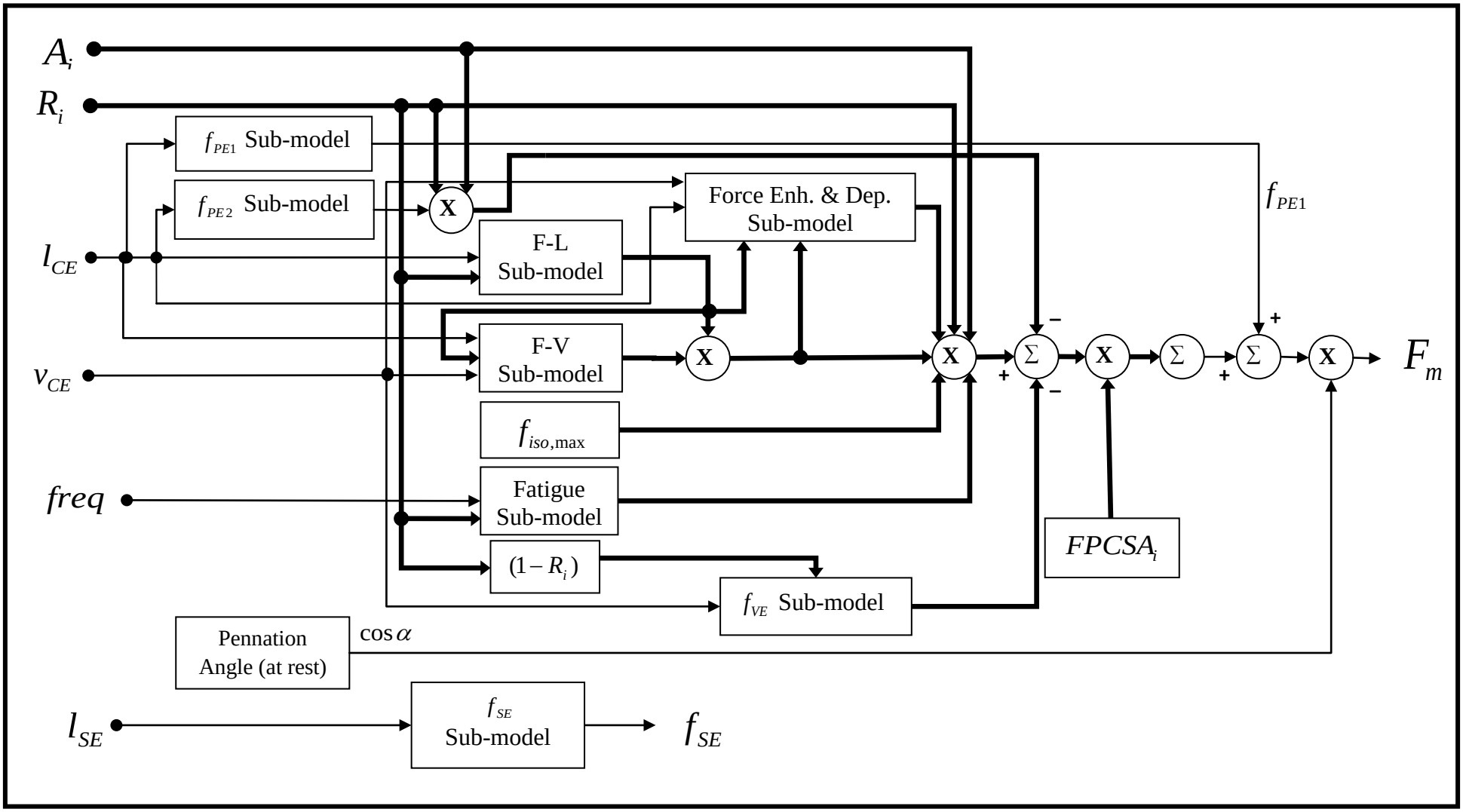

Figure A1.10: Topology of the "General Model" for analogue recruitment input (fibre-type level), including activation (A_i) as an extra input.

Thick arrows denote variables of multiple values (for i = 1, 2, and 3) and thin arrows denote single variables.

Discussion on why the activation A_i is assumed constant for in the "General Model":

Stimulation frequency is assumed constant during FES. In some special cases, during intermittent FES, the stimulation frequency can be changed when FES is off in order to increase the force produced by the muscle, in this case the frequency will be assumed adjustable, but not a real-time variable (i.e. ignoring dynamic changes in frequency).

At constant stimulation frequency: Yield and $freq_{eff}$ sub-models have no effect if the used sub-models of (F-L, F-V, and f_{PE2}) are adjusted for the used stimulation frequency (i.e. frequency can be assumed as hidden constant parameter). There is a very little effect from l_{eff} sub-model (reported in [128] to be less than 1%). Finally, since the effect of sag sub-model lasts for very short time at onset of stimulation, and its value is decreased at higher frequencies about or over 30 Hz (which is commonly used in FES), hence the effect of sag is negligible.

Therefore, for simplicity the activation sub-model will not be included in FES control because its effect on the output force is very little. Brown sub-models for (F-L, F-V, and f_{PE2}) should be modified to fit the used frequency in order to preserve the accuracy of these sub-models. The removal of the activation sub-model form the "General Model" is considered reasonable approximation; detailed reasons are given in the following points:

- In Brown model, all sub-models are developed for tetanic frequency (maximum natural frequency) and they need to be multiplied by A_i in order to model the effect of frequency on them. Brown defined tetanic frequency as the frequency at which muscle force is maximum (experimentally, he found it to be around 120 Hz). Force does not increase at frequencies higher than the tetanic frequency, but decreases at lower frequencies (Brown calls them sub-tetanic frequencies). Tetanic frequency is considered as "saturation frequency", not to be confused with the frequency required to get tetanic (smooth) contraction (i.e. fused contraction).
- Since frequency is constant, hence no need for the $freq_{eff}$ sub-model to model the calcium dynamics when there is a change in the stimulation frequency. Note that, the $freq_{eff}$ sub-model will model the change of frequency during FES, not at onset of stimulation. The calcium dynamics sub-model will model the change of both frequency and stimulation level (PW / PA) at onset of stimulation (since both start

from zero to the value wanted). Any further change in the stimulation level (PW / PA) will be modelled again by the calcium dynamics sub-model.

- The $freq_{eff}$ sub-model has another function which is to correct the curve of the F-L sub-model (modify it to fit the frequency used), but this effect can also be ignored if the F-L sub-model was developed for the used frequency not for tetanic frequency.
- Yield effect is not zero at constant frequency, but it only makes the F-V curve (at sub-tetanic frequency) different from that at tetanic frequency. So, yield sub-model can be ignored when frequency is constant and if the used F-V sub-model is for the frequency in use not for tetanic frequency. Yield affects only slow-twitch fibres.
- The F-V and F-L sub-models are usually developed and fitted using experimental data at constant frequency. Therefore, the effect of the activation sub-model on The F-V and F-L sub-models is similar to the effect of constant properties (such as muscle structure and percentage of fibre types) which are constant and do not change in real-time (different frequencies will alter the shape of the F-L and F-V curves but if constant frequency is used then there will be no change during FES). Therefore, the frequency can be assumed as a hidden parameter.
- The previous points also mean that, in Brown model, the F-L, F-V and f_{PE2} sub-models have to be modified to fit the used frequency. A simple way to do this is to use a Matlab code to modify brown sub-model for F-L, F-V and f_{PE2} to the frequency used during FES simulations (since they are already adjusted for the tetanic frequency).
- The effective length (l_{eff}) sub-model has negligible effect, less than 1%, see [128] for more details.
- Sag has a dynamic effect even at constant frequency. The effect of Sag lasts for a short period (few hundred milli-seconds) after onset of stimulation, so it has a little and very short effect. Sag affects only fast-twitch fibres.

Appendix 2: Instantaneous Length versus Initial Length

A2.1 Introduction

Skeletal muscle models are used for FES control applications. Many FES controllers have been developed using a simulation approach. The performance of these controllers depends on the muscle model accuracy [6, 55, 72, 73, 74, 76, 77]. In these models the instantaneous *CE* length (l_{CE}) is commonly used in the literature to calculate the corresponding muscle force following stretch and/or shortening. However, in addition to the instability problem on the descending limb (discussed in section A2.4) the isometric force-length curve is a poor estimator of the force-length curve during "non-isometric" dynamic contractions of skeletal muscle [177, 178]. Force enhancement following stretch f_e following stretch and force depression following shortening f_d can reach values of almost 50% of the isometric force corresponding to the instantaneous *CE* length after stretch/shortening [13].

During and after dynamic contractions, the force-length curve was found to be very different from the traditional isometric force-length curve [177, 178]. The maximum velocity of shortening ($v_{\max}$) was reported to be dependent on the initial *CE* length [179, 180, 181, 182, 183]. The isometric steady-state muscle force after stretch/shortening depends on some factors including the initial *CE* length [13, 177, 178]. Herzog [18] used the initial length (l_o) as input to the muscle model as long as the recruitment remains on, where both the F-L and F-V relationships are dependent on the initial *CE* length.

For protocols of skeletal muscle contraction including shortening and/or stretch, either *CE* length can be used for the calculation of force-length relationship, but which one is more accurate? Is it accurate to use the instantaneous *CE* length? Or should the initial *CE* length be used instead? These questions will be discussed and answered using experimental data taken from the literature to examine systematically which *CE* length is more appropriate to be used in predicting the steady-state muscle force following stretch/shortening.

In this study, the focus will be on the isometric steady-state muscle force after end of stretch/shortening. Related experimental data taken from the literature are shown (including recruitment plots and protocols of stretch/shortening). The collected data cover many possible protocols of stretch/shortening on the ascending and descending limbs of the force-length curve. The "active" force before stretch/shortening and the isometric steady-state "active"

force after stretch/shortening are calculated (estimated manually) from graphs and then compared with the purely isometric "active" muscle force (the traditional isometric force-length curve) at the corresponding muscle length after stretch/shortening (i.e. using the instantaneous *CE* length).

A2.2 Definitions

In this study; the term "instantaneous length" (l_{CE}) is defined as the muscle belly (*CE*) length or the muscle fibres length after stretch/shortening ends (generally, it is the *CE* length at any time), the term "initial length" or "length at initial recruitment" (l_o) is defined as the muscle belly (*CE*) length or the muscle fibres length just before stretch/shortening commences. These two lengths are used to calculate the corresponding isometric "active" muscle force from the traditional force-length curve. These two lengths will be compared against the experimental isometric steady-state force following stretch/shortening. The term "traditional isometric force-length curve" is used for the isometric force-length curve estimated experimentally without preceding stretch/shortening. The focus of this study will be on the changes of the "active" isometric steady-state force produced by the contractile element of the muscle. Passive force enhancement following "active" stretch and the transient-state force during stretch/shortening are not included in this study.

Stretch induced force enhancement f_e is defined as the increase of the isometric steady-state force (when compared with the corresponding isometric force of the instantaneous length), at a given level of recruitment, caused by stretching of a recruited muscle. Force enhancement f_e is also called "residual force enhancement", as in [154]. Shortening induced force depressions f_d is defined as the decrease of the isometric steady-state force (when compared with the corresponding isometric force of the instantaneous length), at a given level of recruitment, caused by shortening of a recruited muscle. Force depression f_d is also called "residual force depression", as in [184].

The increase/decrease in the isometric steady-state force after end of stretch/shortening is typically calculated relative to the force produced by a purely isometric contraction [13, 152, 154, 155, 168, 169, 170, 171, 172, 173] at the corresponding instantaneous length at the same condition. The reference force-length curve of a purely isometric contraction must be taken at

the same conditions of recruitment and activation, for FES applications this means same levels of stimulation voltage (PW and PA) and frequency.

A2.3 Experimental data from the literature

Vast majority of the experimental data available in the literature are for fully-recruited muscles (where all motor-units are recruited), a single fibre, or a single myofibril. Most of the experimental data used here are for fully-recruited muscles. Experimental data for partially recruited muscles available in the literature are only during stretch/shortening. For the best of my knowledge, protocols of stretch/shortening at different levels of recruitment are not available in the literature. Therefore, the behaviour of a recruited single motor-unit in a partially recruited muscle will be assumed similar to a fully recruited muscle.

The force-length curve consists of three parts; ascending limb, plateau region and descending limb. On the plateau region the corresponding isometric force is almost the same, so changes in length makes only little difference between forces corresponding to the two lengths (l_{CE} and l_o). On the ascending and descending limbs, the isometric force after stretch/shortening on each limb is of different characteristics; therefore each limb of the force-length curve will be studied separately. Dynamic contractions on the descending limb will be studied first.

A2.3.1. Dynamic contractions on the descending limb of the F-L curve

Dynamic movements on the descending limb can be pure shortening (concentric contraction), pure stretch (eccentric contraction), shortening followed by stretch, or stretch followed by shortening.

A2.3.1.1. Pure shortening

Figure A2.1 shows a protocol of shortening on the descending limb of the force-length curve. Isometric reference contraction was performed at the final length of the dynamic contraction after shortening. Force depression (f_d) was determined 4.5 seconds following the end of the shortening contraction.

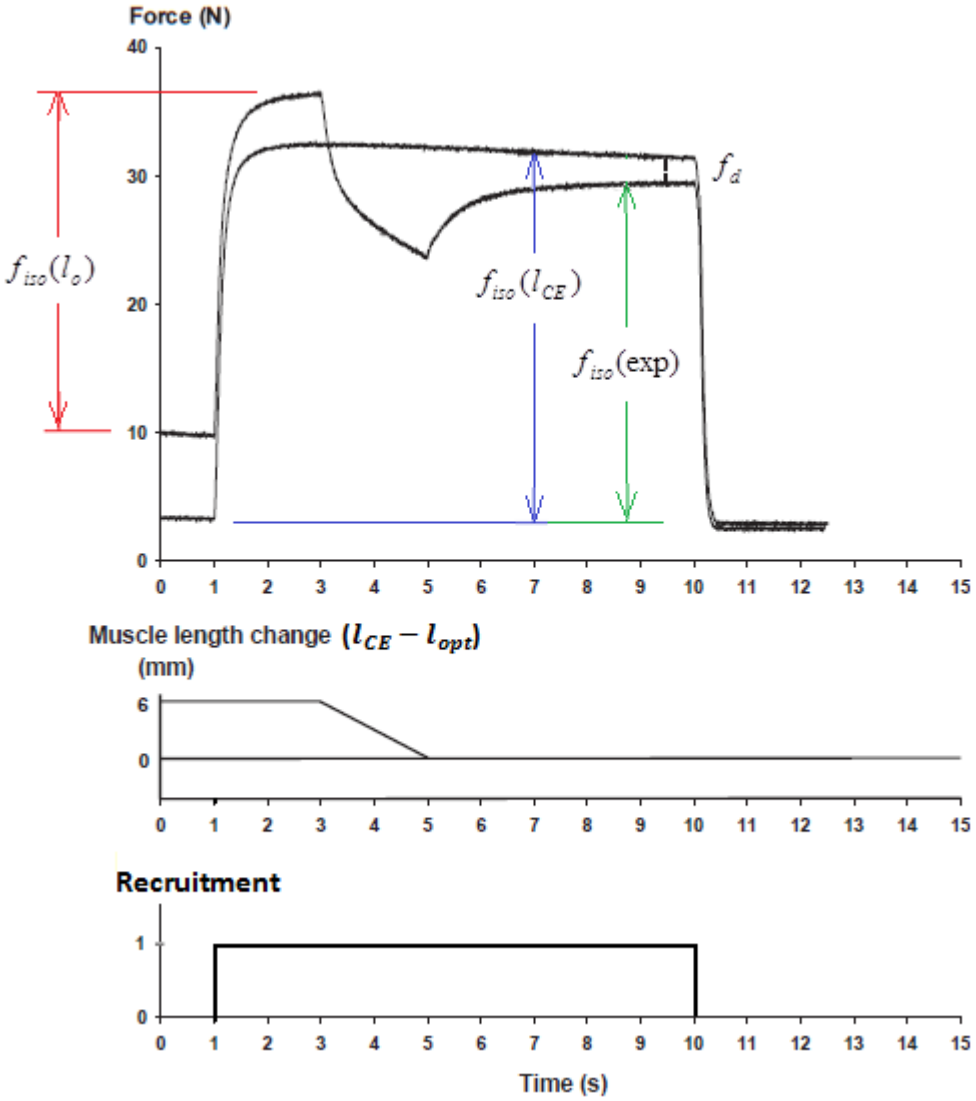

Figure A2.1: Force-time history for active shortening of 6 mm amplitude (about 18% of the muscle fibre optimal length) from 6 to 0 mm at a constant speed of 3 mm/s (about 9% fibre length per second). (From [152]).

The purely isometric force produced by contraction of muscle fibres $f_{iso}(l)$ at any length (l) can be calculated as follows:

$$f_{iso}(l) = f_{total} - f_p$$

f_{total} : Total isometric force including "active" and "passive" forces.

f_p : Pure "passive" isometric force of muscle belly.

The isometric force at initial length $f_{iso}(l_o)$, the purely isometric force corresponding to instantaneous length after shortening $f_{iso}(l_{CE})$, and the "experimental" isometric steady-state force after stretch $f_{iso}(\text{exp})$ were estimated manually from Figure A2.1 (see Table A2.1).

Table A2.1: Isometric "active" muscle forces estimated manually from Figure A2.1.

$f_{iso}(l_o)$	$f_{iso}(l_{CE})$	$f_{iso}(\text{exp})$
36.5-10=26.5 [N]	31.5-3=28.5 [N]	29-3=26 [N]

Observation: The isometric force at initial length $f_{iso}(l_o)$ is more accurate than the isometric force at the instantaneous length $f_{iso}(l_{CE})$, the initial length (l_o) is much more accurate.

A2.3.1.2. Pure stretch

Figure A2.2 shows a protocol of stretch on the descending limb of the force-length curve. The isometric reference contractions were performed at the initial and final lengths of the dynamic contraction, before and after the experimental stretch test. Passive force enhancement Δf_P following stretch of recruited muscle was greater than the corresponding passive force following isometric contraction (the muscle was stretched when not recruited).

The isometric force at initial length $f_{iso}(l_o)$, the purely isometric force corresponding to instantaneous length after shortening $f_{iso}(l_{CE})$, and the "experimental" isometric steady-state force after stretch $f_{iso}(\text{exp})$ were estimated manually from Figure A2.2 (see Table A2.2).

Table A2.2: Isometric "active" muscle forces estimated manually from Figure A2.2.

$f_{iso}(l_o)$	$f_{iso}(l_{CE})$	$f_{iso}(\text{exp})$
33-4=29 [N]	38-12=26 [N]	41-12=29 [N]

Observation: The isometric force of initial length $f_{iso}(l_o)$ is more accurate than the isometric force of the instantaneous length $f_{iso}(l_{CE})$, the initial length (l_o) is much more accurate.

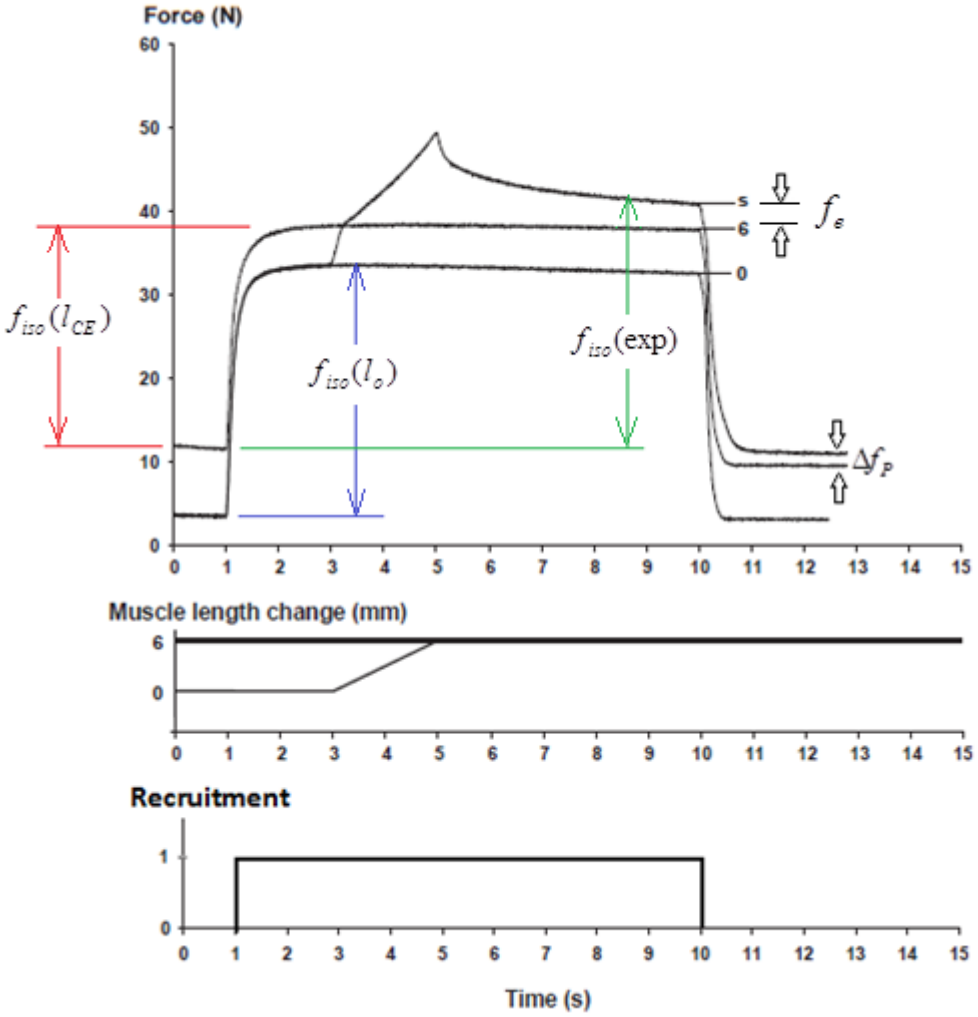

Figure A2.2: Force–time history for active stretch of 6 mm amplitude (about 18% of the muscle fibre optimal length) from 0 to 6 mm at a constant speed of 3 mm/s (about 9% fibre length per second). (From [168]).

A2.3.1.3. Shortening followed by stretch

Figure A2.3 shows a protocol of shortening followed by stretch on the descending limb of the force-length curve. The isometric reference contraction " i " was performed at the final length of the dynamic contraction (at +9mm). Note that increasing the amount of shortening makes the total and the passive force enhancement to decrease to a similar magnitude.

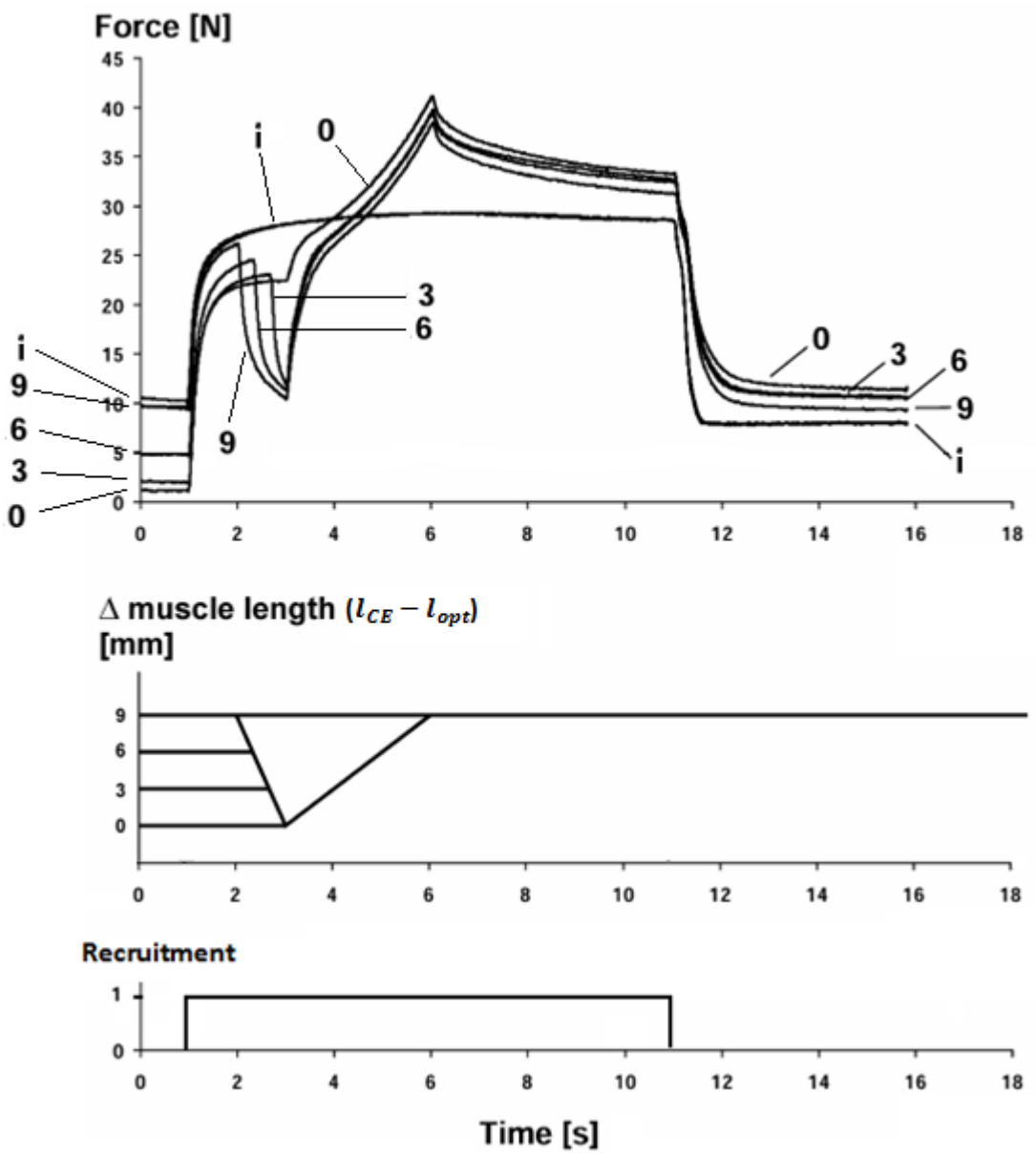

Figure A2.3: Force-time histories of four experimental active shortening of 0, 3, 6, and 9 mm (at speed of 3 mm/s) followed by active stretch contractions (0 to +9 mm at 3 mm/s). (From [169]).

The isometric force at initial length $f_{iso}(l_o)$, the purely isometric force corresponding to instantaneous length after shortening $f_{iso}(l_{CE})$, and the "experimental" isometric steady-state force after stretch were estimated manually from Figure A2.3 for both the 0 and the 9 force traces (see Table A2.3).

Table A2.3: Isometric “active” muscle forces estimated manually from Figure A2.3.

Force Trace	$f_{iso}(l_o)$	$f_{iso}(l_{CE})$	$f_{iso}(\exp)$
(0)	22.5-1=21.5 [N]	29-10=19 [N]	33-10=23 [N]
(9)	29-10=19 [N]	29-10=19 [N]	31.5-10=21.5 [N]

Observation: For a protocol of active shortening followed by active stretch of the same magnitude (force trace 9), this means that the isometric force at initial length and the isometric force at the instantaneous length after stretch are the same: $f_{iso}(l_{CE}) = f_{iso}(l_o)$. However, the isometric steady-state force was the same as that of length 0 (i.e. the length at end of shortening and before stretch). Decreasing the magnitude of shortening (making it shorter than stretch) further increases the isometric steady-state force making it maximum at zero shortening (i.e. pure stretch).

A2.3.1.4. Stretch followed by shortening

Figure A2.4 shows a protocol of active stretch followed by shortening on the descending limb of the force-length curve. This data is for intact, single fibres dissected from the lumbrical muscles of the frog, as presented in [171].

Observation: For a protocol of active stretch followed by shortening of the same magnitude, means that the isometric force at initial length and the isometric force at the instantaneous length after stretch are the same: $f_{iso}(l_{CE}) = f_{iso}(l_o)$. However, the isometric steady-state force was just slightly larger.

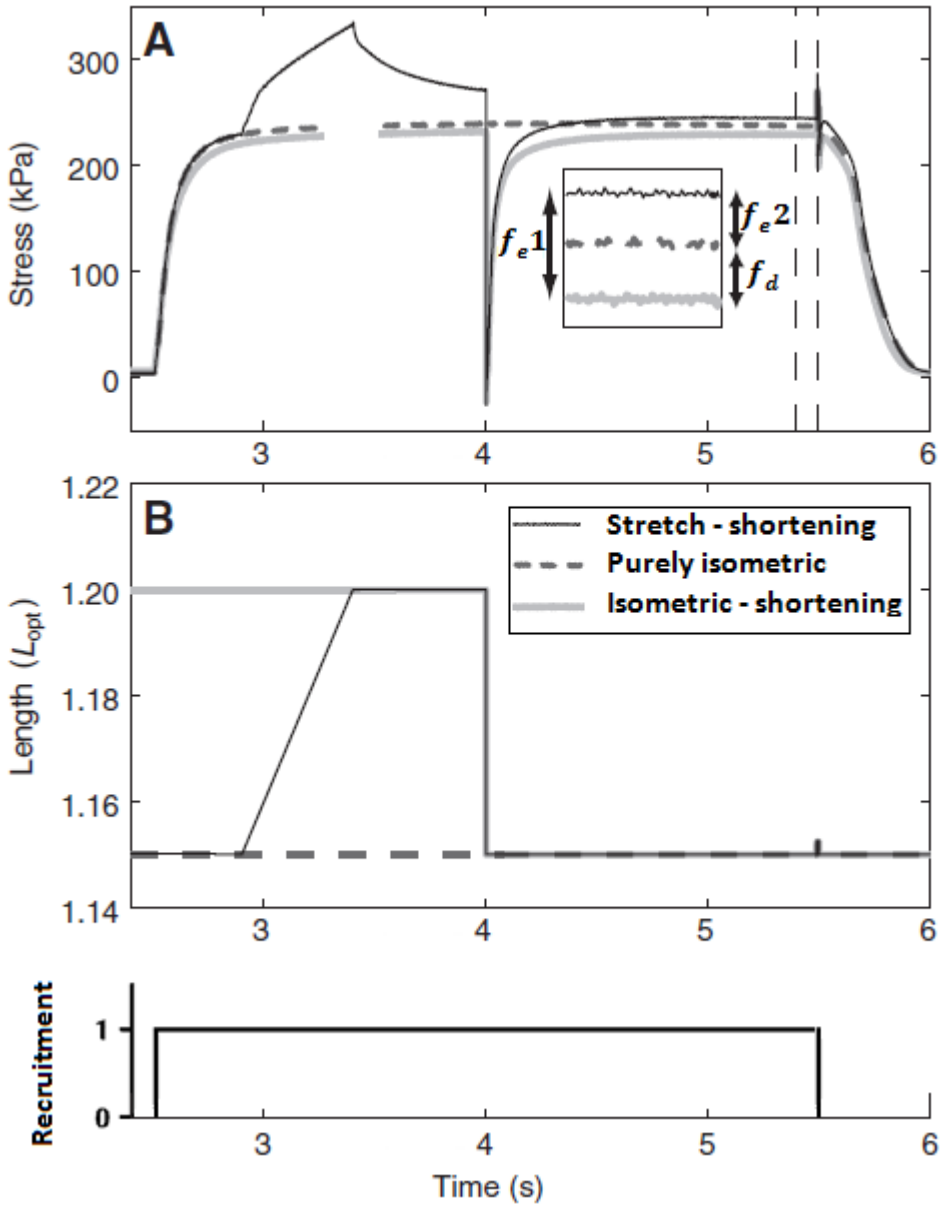

Figure A2.4: Force against time (A) and length against time (B) for one set of three contractions with a shortening of the same distance as stretch; isometric-shortening contraction (The thick, solid, light-grey), purely isometric contraction (The thick, broken, dark-grey line), and stretch followed by shortening contraction (The thin, solid, black line). Inset shows the force enhancement (f_e2) for the protocol of interest (stretch followed by shortening contraction). (From [171]).

A2.3.2. Dynamic contractions on the ascending limb of the F-L curve

Dynamic movements on the ascending limb can be pure shortening (concentric contraction), pure stretch (eccentric contraction), shortening followed by stretch, or stretch followed by shortening.

A2.3.2.1. Pure stretch and pure shortening

Figure A2.5 shows separate protocols of pure stretch and pure shortening on the ascending limb of the force-length curve (except for the top left plot which shows pure shortening on the descending limb and pure stretch on the ascending limb). The zero-reference cat soleus muscle length corresponds to 80^o ankle angle [152]. In this figure, the force enhancements following stretch and force depressions following shortening were less at shorter muscle lengths. Also, force enhancements and force depressions were less at higher speeds.

Observation: It is clear from the force traces that using the instantaneous length l_{CE} is more accurate than the initial length l_o, this is more obvious at shorter lengths and also at faster speeds of stretch/shortening. Speed of stretch/shortening has an effect on f_e and f_d as can be seen clearly in Figure A2.5, however this will not be considered here.

A2.3.2.2. Shortening followed by stretch and stretch followed by shortening

Figure A2.6 shows three protocols on the ascending limb of the force-length curve: an isometric reference contraction, a stretch followed by shortening of equal magnitude, and a shortening followed by stretch of equal magnitude. The zero-reference cat soleus muscle length corresponds to 80^o ankle angle on the upper part of the ascending limb [172].

i) Shortening followed by stretch:

Another experimental study in [185] found that a protocol of shortening followed by stretch of equal magnitude will cause slight enhancement, the measured force enhancement was 1.2 %, 1.4 % and 1.6 % for 4, 16 and 64 mm/s stretch speeds, respectively, it was also found in the same study (in [185]) that protocols of shortening followed by stretch at varying speeds produced very similar results as in Figure A2.6 but the speed of shortening has some little effect.

Protocols of shortening followed by stretch with varying magnitudes resulted in slightly different isometric steady-state forces $f_{iso}(\exp)$, shortening less that stretch causes larger force enhancement [172, 185]. Repeated cycles of shortening-stretch did not affect the isometric steady-state force [172, 185].

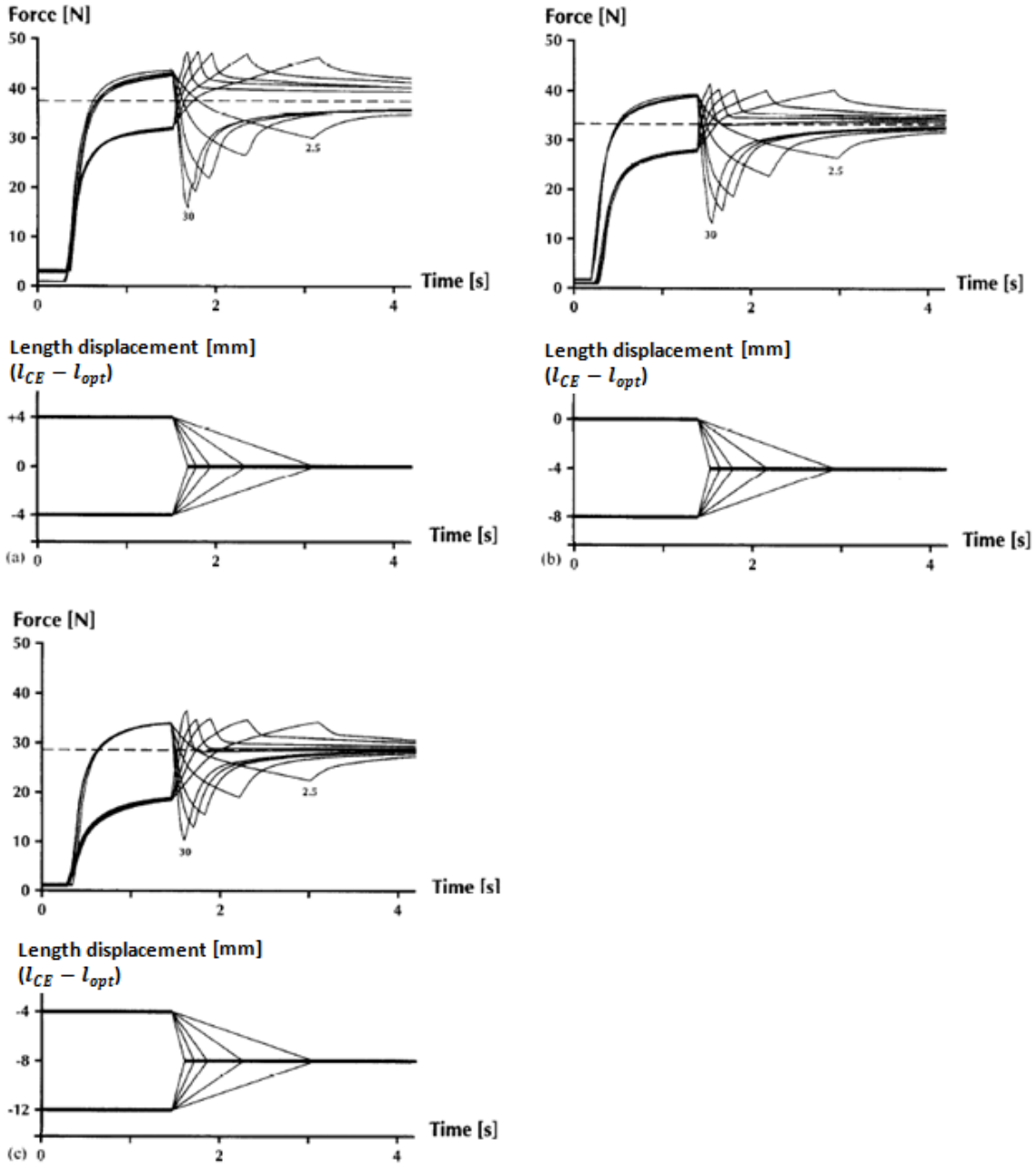

Figure A2.5: Force-time histories of three shortening and three stretch contractions, at speeds ranging from 2.5 to 30 [mm/s]. The isometric steady-state force of the muscle at the final length is indicated by horizontal broken line. Length represents displacement from optimal length ($l_{CE} - l_{opt}$). The final length was 0, - 4, and - 8 mm in (a), (b), and (c) respectively. (From [152]).

ii) Stretch followed by shortening:

Force-time histories for an isometric reference contraction and a stretch followed by shortening of equal magnitude and a shortening followed by stretch of equal magnitude are shown in Figure A2.6. The isometric steady-state forces after the shortening followed by

stretch $f_{iso}(\exp)$ were always (n=8) very similar as those obtained for purely isometric contractions [i.e. $f_{iso}(l_{CE})$]. The isometric steady-state forces after stretch followed by shortening $f_{iso}(\exp)$ were always (n=8) below the corresponding purely isometric forces $f_{iso}(l_{CE})$.

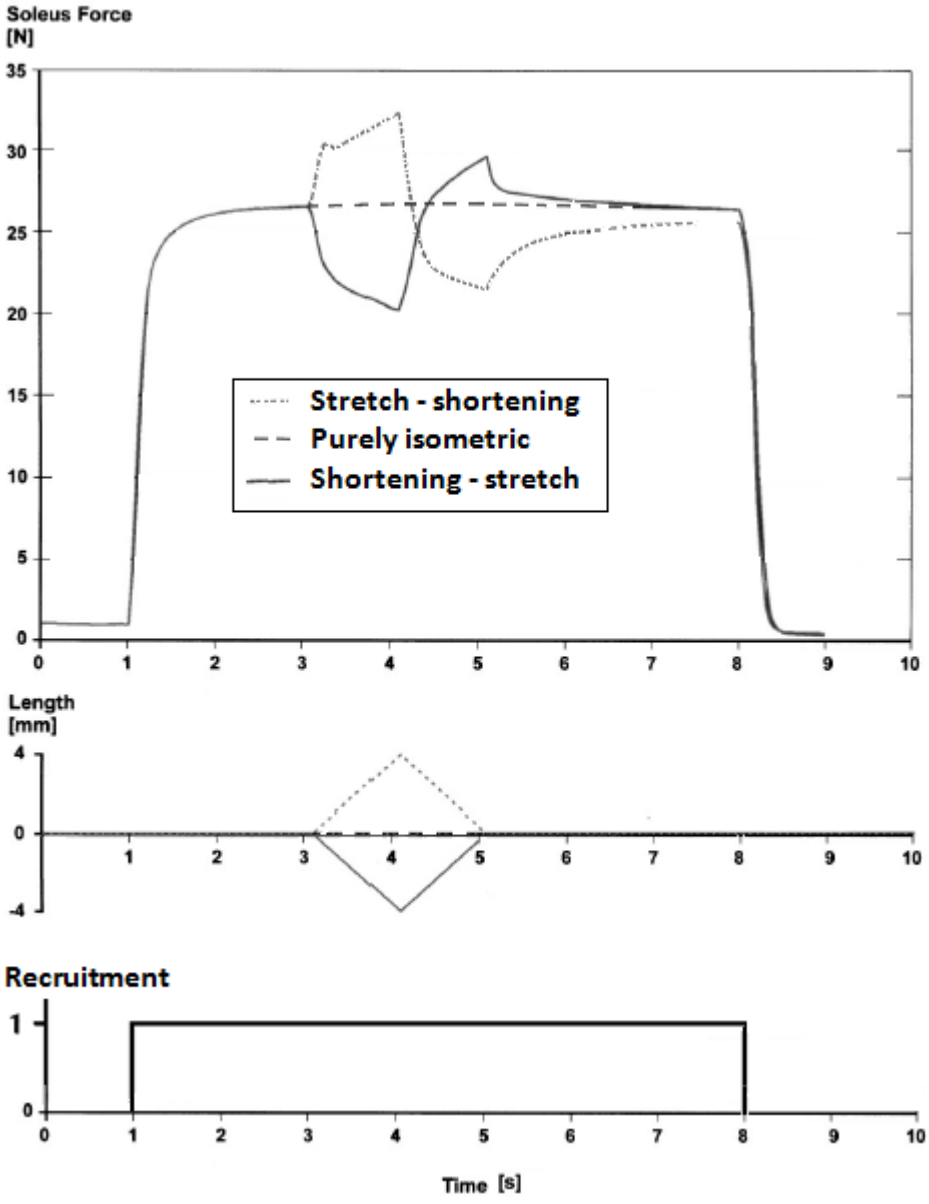

Figure A2.6: Force-time histories for an isometric reference contraction (0 mm) and a stretch followed by shortening of equal magnitude (± 4 mm) and a shortening followed by stretch of equal magnitude (± 4mm). (From [172]).

Protocols of stretch followed by shortening at varying speeds, and protocols of stretch followed by shortening with varying magnitudes (and equal speeds) resulted in little force depression (similar result as that in Figure A2.6). These results indicate that f_e and f_d are not affected by speed of stretch followed by shortening or the magnitude of stretch/shortening, details are provided in [172, 185]. Repeated cycles of stretch-shortening results in cumulative effect (i.e. more cycles results in a slightly smaller steady-state force) [172, 185].

Observation: For a protocol of shortening followed by stretch of equal magnitude, the isometric force at initial length and the isometric force at the instantaneous length after stretch are of similar values: $f_{iso}(l_{CE}) \approx f_{iso}(l_o)$. This means that using either length (initial or instantaneous) will produce similar results. However, both lengths are not accurate in the other case (stretch followed by shortening).

A2.3.3. Dynamic contractions on both limbs of the F-L curve

Dynamic movements on both of the ascending and descending limbs of the F-L curve can be either a pure stretch starts on the ascending limb and ends on the descending limb, or a pure shortening starts on the descending limb and ends on the ascending limb.

A2.3.3.1. Stretch starts on the ascending limb

Figure A2.7 shows protocols of stretch, a reference contraction at the final length +9mm length (9mm longer than optimal length) and a series of stretch contractions of various magnitudes. The protocol of interest is the protocol which starts on the ascending limb (at -12mm) and ends on the descending limb of the force-length curve (at +9mm). The zero-length corresponds to optimal length. Speed of stretch is 12mm/s, final isometric contractions lasting at least 5 s.

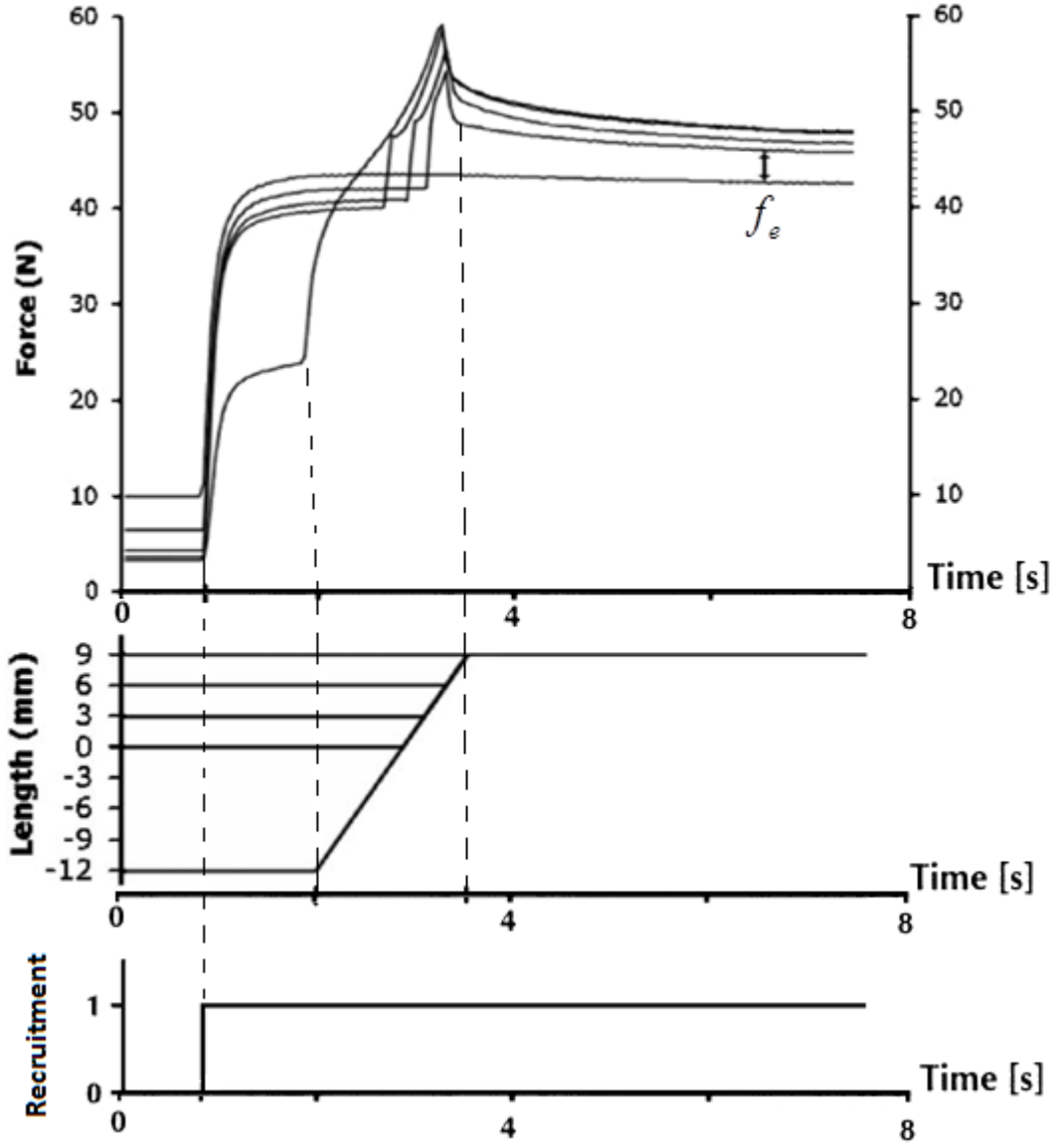

Figure A2.7: Force–time history for a muscle performing stretch protocols for magnitudes of 3, 6, 9, and 21 mm. The total force enhancement shown is between the 3 mm stretch trial and the isometric reference. (From [154]).

Observation: For the protocol of interest which starts on the ascending limb (at -12mm) and ends on the descending limb of the force-length curve (at +9mm) in Figure A2.7, the steady-state force $f_{iso}(\exp)$ is even larger than that which started at the optimal length (i.e. greater than maximum isometric force $f_{iso,\max}$). This indicates that instantaneous length (l_o) is more appropriate in this case.

A2.3.3.2. Shortening starts on the descending limb

Figure A2.8 shows protocols of shortening, a reference contraction at the final length (at -4mm), and a series of stretch contractions of various magnitudes. The protocol of interest is the protocol which starts on the descending limb (at +6mm) and ends on the ascending limb of the force-length curve (at -4mm). The zero-reference cat soleus muscle length corresponds to 80^o ankle angle [185]. Speed of stretch is 4mm/s.

The isometric force at initial length $f_{iso}(l_o)$, the purely isometric force corresponding to instantaneous length $f_{iso}(l_{CE})$ after shortening and the "experimental" isometric steady-state force after stretch were estimated manually from Figure A2.8 for all force traces (a, b, c, d, and e), as given in Table A2.4. From this Table, it is clear that, at least, traces (a) and (b) are on the descending limb. The purely isometric force reference (f) has a value of 22 [N] at length (-4 mm).

Table A2.4: Isometric "active" muscle forces estimated manually from Figure A2.8.

Force Trace	$f_{iso}(l_o)$	$f_{iso}(l_{CE})$	f_{iso}(exp)
a (+6 mm)	26.5-5=21.5 [N]	22 [N]	19.5 [N]
b (+4 mm)	25-3=22 [N]	22 [N]	20 [N]
c (+2 mm)	24-1.5=22.5 [N]	22 [N]	20.5 [N]
d (0 mm)	23.5-1=22.5 [N]	22 [N]	21 [N]
e (-2 mm)	22-0=22 [N]	22 [N]	21.5 [N]

Observations: Both lengths (l_o and l_{CE}) have a noticeable percentage of error when compared with experimental results reported in the literature; initial length is slightly better estimator for force trace (a), both lengths are similar for force traces (b) and (e), instantaneous length is better estimator for force trace (c) and (d). All forces were depressed. Traces (a), (b) and (c) were depressed by the same amount of about 2 [N] when compared with $f_{iso}(l_o)$, even they were shortened by different magnitudes of shortening. Traces (d) and (e) were depressed by 1.5 [N] and 0.5 [N].

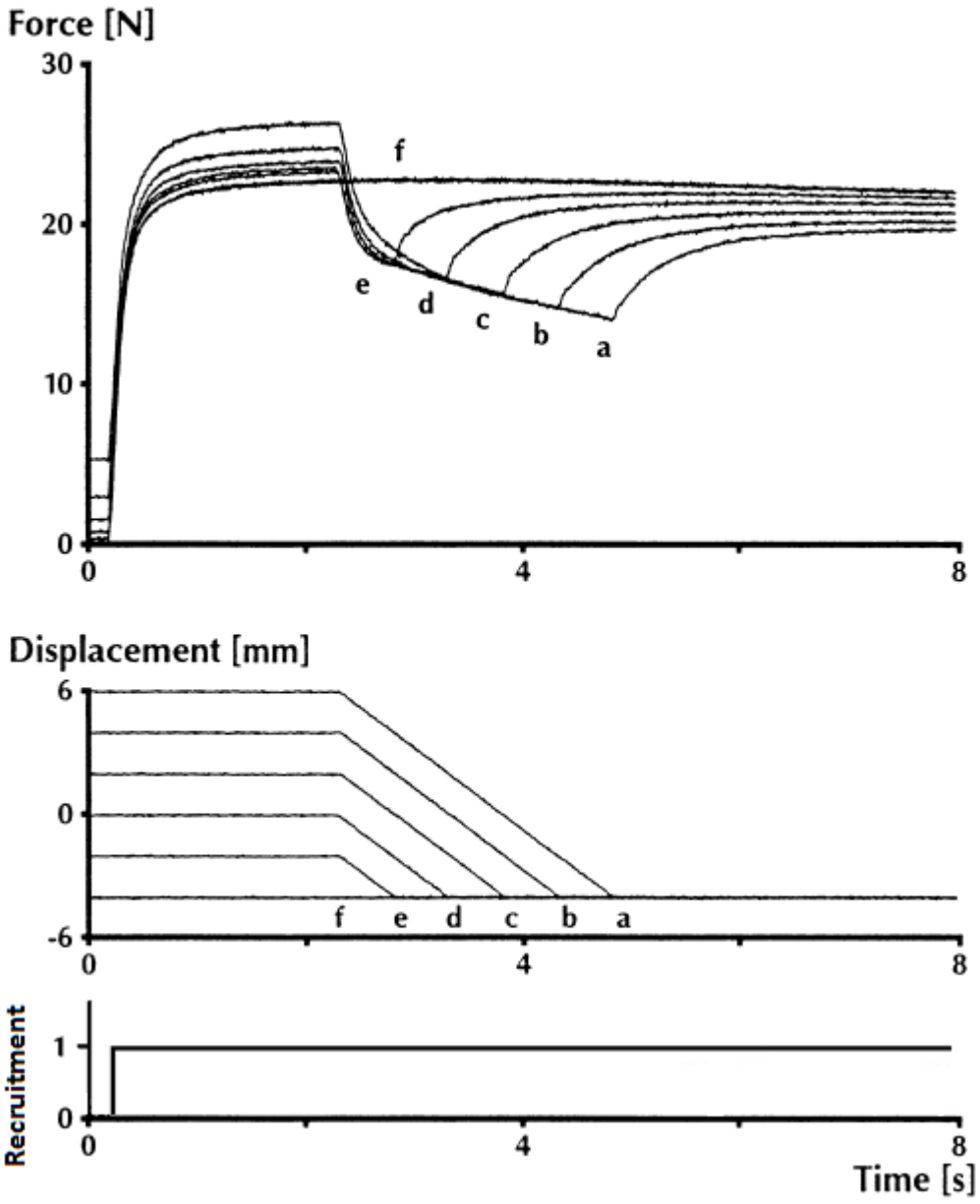

Figure A2.8: Force–time history for a muscle performing shortening protocols for magnitudes of 2, 4, 6, 8, and 10 mm. The isometric reference contraction at muscle length -4 mm. Shortening speed of 4 mm/s and maximal recruitment were kept constant. (From [155]).

A2.3.4. Effect of varying recruitment level during and after stretch/shortening

Modelling of skeletal muscle force production can be very complicated. The isometric steady-state force following stretch and/or shortening is affected by many factors; one of these factors is the level of recruitment during stretch/shortening which can change the shortening forces as shown in Figure A2.9, A2.10 and A2.11. Altering stimulation frequency has similar results as varying recruitment level, see Figure A2.12. If muscle recruitment was interrupted (decreased suddenly to zero level) during shortening, the isometric steady-state force will be affected depending on the time period of de-recruitment, see Figures A2.13, (A2.14) and (A2.15).

In Figure A2.9, no stretch/shortening was performed during this process. There was no force depression (associated with the change in recruitment levels) upon full re-recruitment.

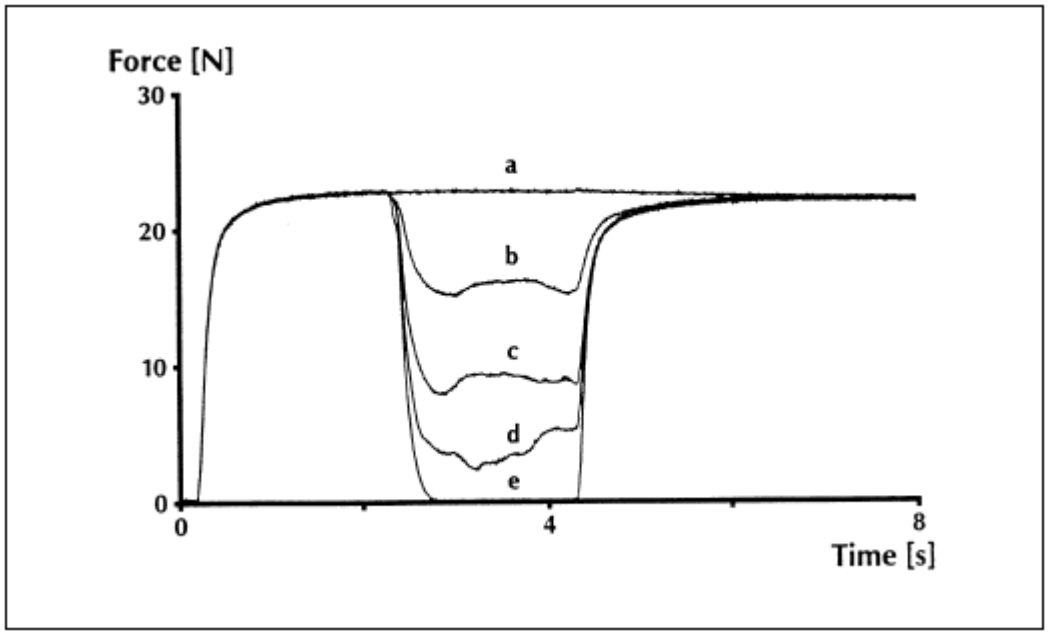

Figure A2.9: Force-time histories of isometric contractions, in which recruitment was decreased for a 2 second period (at different levels) following full force development. (From [155]).

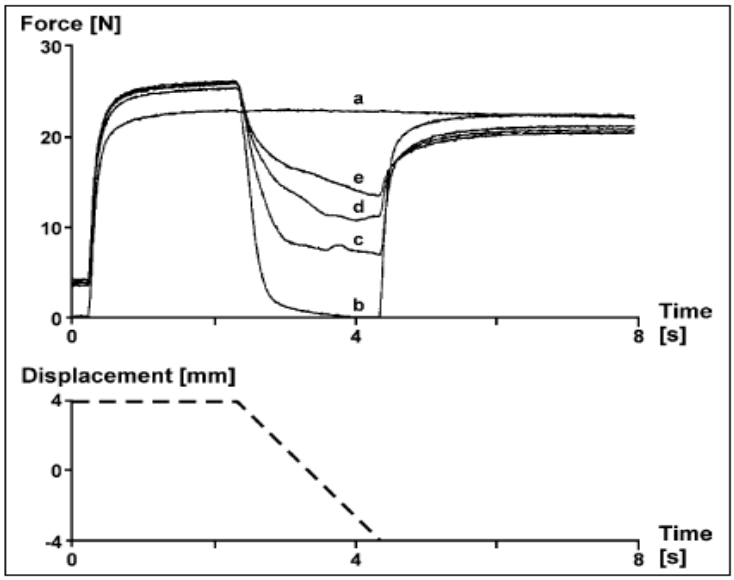

Figure A2.10: Force depression increases with increasing force during shortening. Results shown are from cat soleus at $37\,C^{o}$. The different force levels were achieved by changing the stimulation voltage. (From [13]).

In figure A2.11, the shortening was done from the ascending limb to the ascending limb; at six levels of recruitment during the shortening phase, ranging from full recruitment (3T) to zero recruitment (0). Isometric reference contraction (i) at -4 mm was performed at the final length of the dynamic contraction after shortening. Force depressions are directly related to the force during the shortening phase.

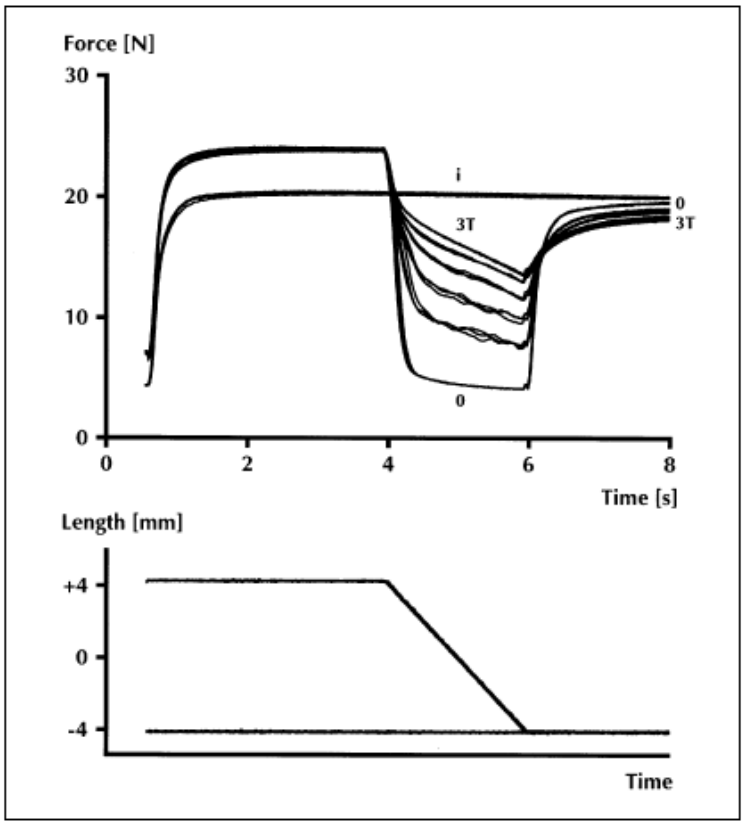

Figure A2.11: Force-time history for shortening of 8 mm from +4 to -4 mm at six levels of recruitment during the shortening phase.(From [170]).

In figure A2.12, the activation of the muscle was varied by frequency modulation between (0) and (100) Hz to produce different force levels during shortening, similar results were obtained when varying the recruitment level between 100% and 0.0%. Force depression decreased with decreasing activation/recruitment during the shortening phase.

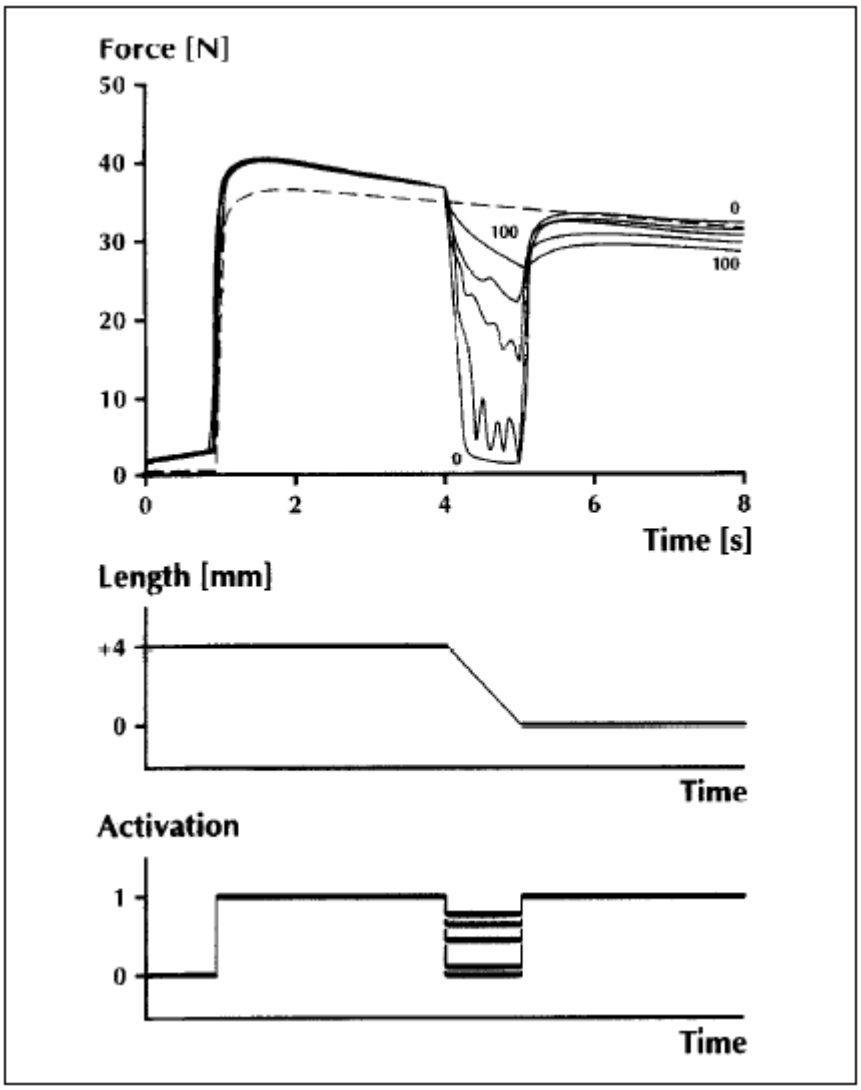

Figure A2.12: Force-time, length-time and recruitment -time histories of shortening contractions. (From [152]).

In figure A2.13, the force-time histories shown are for shortening of 8 mm amplitude at constant speed of 4 mm/s, and force-time history of an isometric reference contraction at the final muscle length of -4 mm. The recruitment during shortening was varied by de-recruiting the muscle for the first 0.5, 1, 1.5, and 2 seconds and then re-recruiting it maximally.

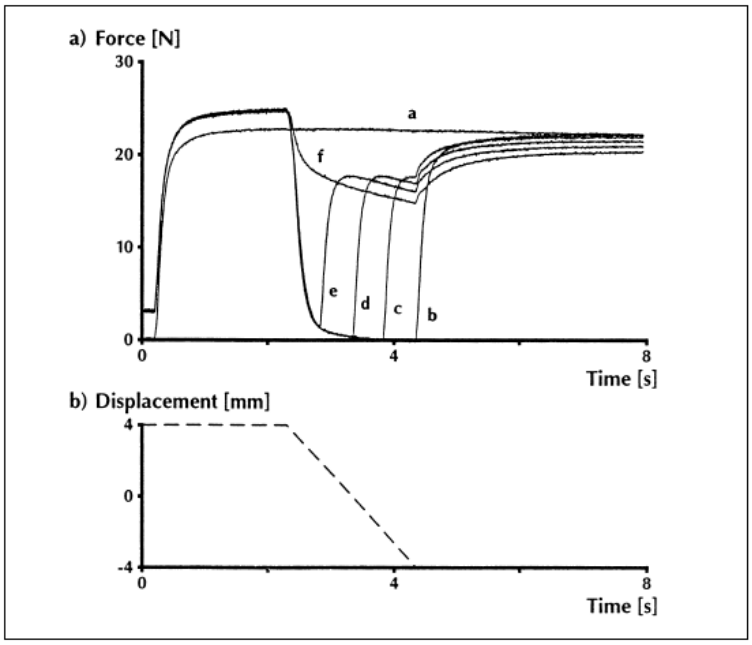

Figure A2.13: Force-time histories of shortening at constant speed , the recruitment during shortening was varied by de-recruiting the muscle for different times. (From [185]).

In figure A2.14, (A) Force depression as a function of recruitment during the shortening phase. The higher the force during shortening, the more the force depression. (B) Force depression as a function of the time period of de-recruitment during the isometric contraction following shortening. The smaller the interruption, the more the force depression.

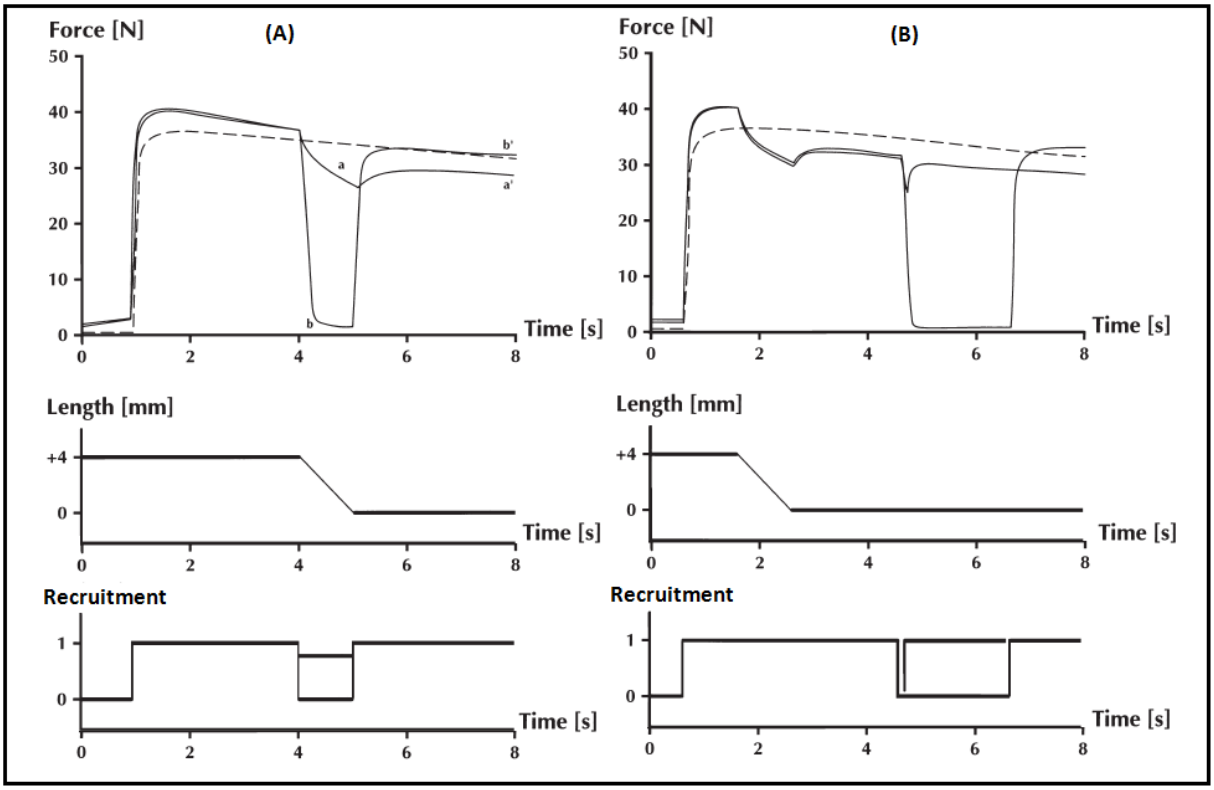

Figure A2.14: (A) Force depression as a function of recruitment during the shortening phase. (B) Force depression as a function of the time period of de-recruitment during the isometric contraction following shortening. (From [173]).

In figure A2.15, during the second isometric phase (i.e. after the shortening had occurred), the recruitment was interrupted for variable time periods to allow the muscle force to decrease to different levels. The force depressions following de-recruitment were smaller for longer periods of de-recruitment (i.e. longer interruption). When the de-recruitment periods were so long that the muscle force dropped to zero, or even stayed at zero for a period of time, the forces following re-recruitment came close to or exceeded the isometric reference force (dashed line).

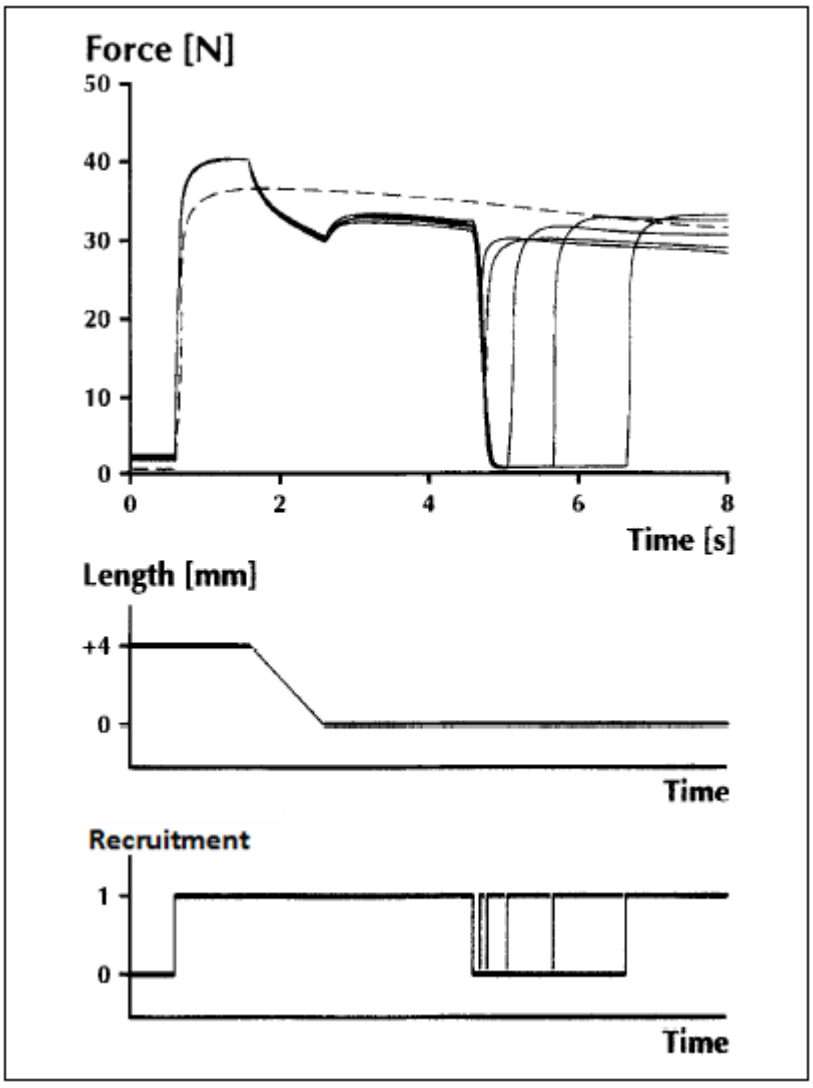

Figure A2.15: Force-time, length-time and recruitment-time histories of isometric-shortening-isometric contractions for one representative muscle. (From [152]).

A2.4 Instability on the descending limb of the force-length relationship

Almost six decades ago, A. V. Hill proposed that sarcomere behaviour was unstable on the descending limb of the force-length relationship [186], since then this has been a topic of great debate [18, 182], see Figure A2.16. A system is considered stable if, following a perturbation, the system will return to its original state.

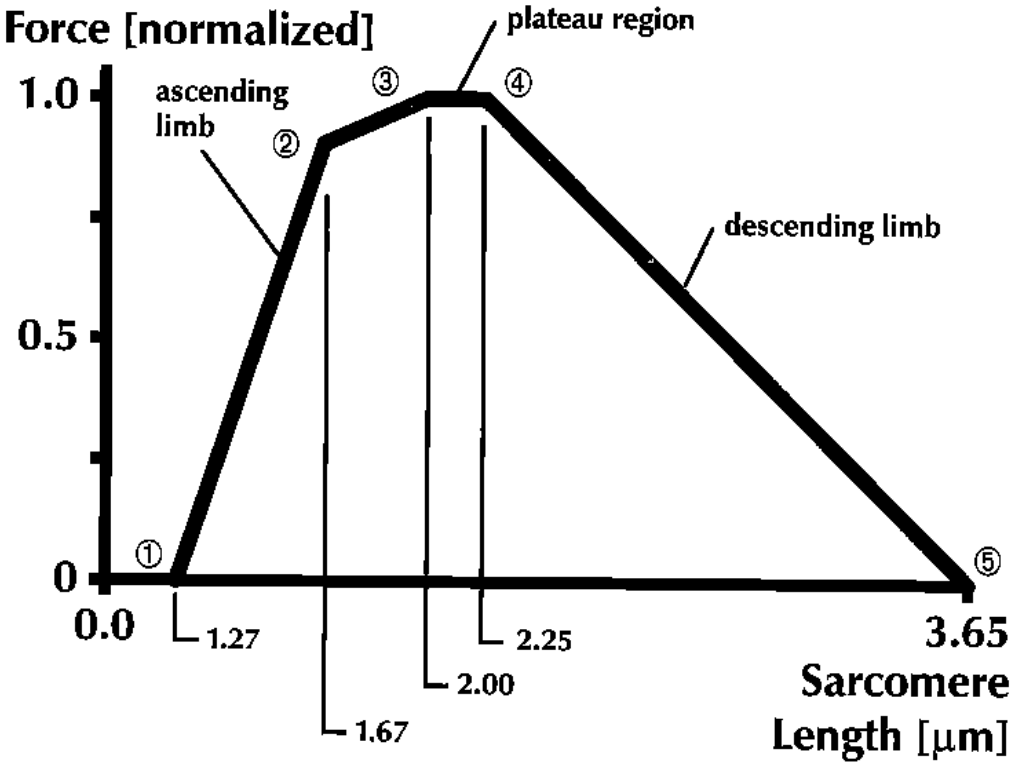

Figure A2.16: The sarcomere force-length relationship of frog skeletal muscle. (From [18])

The negative slope of the descending limb has the characteristics of a softening material (i.e. force becomes less as the material is stretched), and any material with such properties would be highly unstable if this was a dynamic property. But, the softening behaviour of skeletal muscle has not been observed experimentally.

The isometric force-length relationships represent a series of isolated and independent static experimental observations because they are obtained for isometric contractions at discrete lengths, the sarcomere force-length relationship of frog skeletal muscle is shown in Figure A2.16.

If an active sarcomere was stretched or shortened to a new length, the force would not follow the continuous isometric force-length relationship. The steady-state force after stretch would be larger, and after shortening, would be lower than the isometric force corresponding to the new length (Figure A2.17). This result indicates that sarcomere stiffness is always positive, including the descending limb, and sarcomere stability is guaranteed [18].

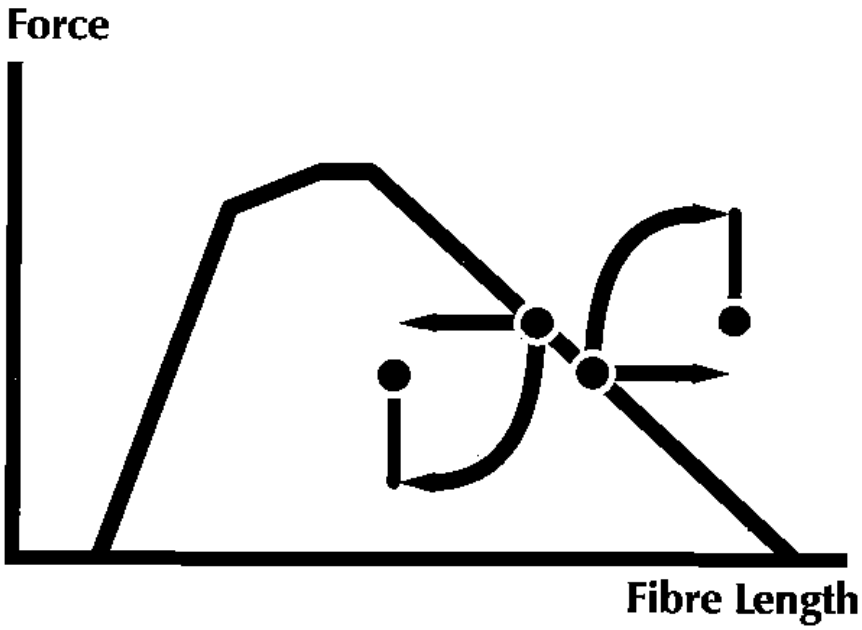

Figure A2.17: Schematic representation of the sarcomere force-length relationship. If the sarcomere was stretched or shortened to a new length, the force would not follow the isometric force-length relationship; the force would be larger after stretch and would be lower after shortening. Sarcomere stiffness observed experimentally is always positive and stable. (From [18]).

In all muscle models reported in the literature (except Herzog model [18]), the muscle force is dependent on the instantaneous length (l_{CE}) directly, using the isometric force-length relationship for non-isometric conditions. This leads to instability in the descending limb of the force-length relationship. To avoid this major problem, Herzog [18] assumed that the muscle remembers the length at initial recruitment l_o as long as it is still recruited (at any level). Once fully de-recruited, that length is forgotten and a new initial length will be used upon the next recruitment (at any level), details of Herzog model are provided in Appendix 6. Furthermore, the experimentally observed force enhancement (following active stretch) and force depression (following active shortening) on the ascending and descending limbs of the force-length relationship is not constant; it depends on the length at initial recruitment [18, 187, 188]. This feature can be incorporated into the muscle model either directly by making the stiffness of the parallel element depend on R and/or l_o, or indirectly by an elastic rack that is engaged upon recruitment (e.g. Forcinito elastic rack [156, 157] presented in previous section).

Why to use l_o instead of l_{CE} ?

The length at initial recruitment serves two purposes: first to avoid instability on the descending limb, and second it is more accurate on the descending limb (as can be seen in the experimental data provided in this appendix).

The force enhancement/depression need to be modelled separately, it depends mainly on the initial length. Other factors affecting the force enhancement/depression are discussed and modelled in section 2.5.5 and Appendix 2.

The *CE* length at initial recruitment (l_o) can be used with muscle models in different ways:

i) The simplest way is to use it directly as input to the F-L sub-model (e.g. the original Herzog model), see Chapter 3.

ii) A more complex way is the multiple motor-unit modelling approach. Two different ways are illustrated in Chapter 3; the $Eff.f_{iso}$ and the $Eff.f_{CE}$ multiple motor-unit models.

iii) To use l_o with l_{CE} and v_{CE} (during stretch/shortening) and magnitude of displacement (Δl_{CE}) to calculate force depression & enhancement using the new complex *IE & ID* sub-model illustrated in Chapter 6.

iv) Any other level of complexity between (i) and (iii). For example, Forcinito *IE & ID* sub-model [156, 157] which uses an elastic rack to calculate the force enhancement and depression.

<u>Does the sliding filament theory help to justify the initial length?</u>

Several possible mechanisms are presented in [13, 173, 189] and other references (see those provided in [13]). However, Herzog [13] questioned all these proposed mechanisms based on experimental evidence; only one mechanism was found to conceptually agree with experimental data. However, none of those proposed mechanisms nor the sliding filament (cross bridges) theory was helpful to justify the length at initial recruitment. Herzog [18] clearly concluded: "*Specifically, the dependence of force production on the history of contraction <u>is not</u> part of the cross-bridge model*"<u>.</u>

Herzog et al [190] experimentally examined the steady-state force enhancement in view of the cross-bridge (sliding filament) theory. They concluded that the steady-state force

enhancement following active stretch has a passive and an active component: "*The active component is associated with the cross-bridge kinetics, and the passive component is associated with a calcium-dependent increase in titin stiffness*" quoted from [190]. More discussion about history effects and possible mechanisms are provided in [182, 187, 188, 190, 191, 192, 193, 194].

A2.5 Discussion

The use of instantaneous length in dynamic contractions leads to instability on the descending limb of the force-length relationship. In order to avoid this problem, the length at initial recruitment can be used. This will make the system stable on the descending limb of the force-length relationship and also makes the corresponding isometric force more accurate than that of the instantaneous length.

As can be observed from the experimental data taken from literature, after dynamic contractions, the force-length curve was found to be different from the traditional isometric force-length curve. For the case of dynamic contractions on the ascending limb of the force-length relationship, both lengths are not good estimators. However, the instantaneous length (l_{CE}) was closer to the experimental results.

For the case of dynamic contractions on the descending limb of the force-length relationship, the initial length (l_o) was much better and very close to the experimental results.

For the case of dynamic contractions involving length changes through the whole force-length curve (on both ascending and descending limbs), the instantaneous length (l_{CE}) was close to the experimental results for the case of stretch starts on the ascending limb. For the other case of shortening starts on the descending limb, both lengths are not good estimators but the instantaneous length (l_{CE}) was closer to the experimental results.

Initial length is a good estimator in the case when the range of muscle length change lies on the descending limb, for example if the physiological range of the muscle excursions naturally lies on the descending limb. In this case, the initial length can be used with a relatively simple muscle model but in the same time keeping high level of accuracy.

Other protocols involving other cycles of stretch and shortening at different magnitudes and different speeds and happening on any part of the force-length curve are complex and difficult to predict. The experimental data available in the literature are not enough to describe confirmed characteristics, therefore any other possible protocols will be considered beyond the scope of this study.

When used for FES control; assumptions are made regarding the nominal length to use as an input to the force-velocity sub-model. Various authors use different approaches to account for lengths that vary with time, but the instantaneous CE length is commonly used. If the output of the model is joint torque, then the instantaneous joint angle and joint angular velocity are used as inputs (rather than CE length and velocity) and joint torque as output (rather than muscle force) [86].

In an attempt to address the issue of modelling partial recruitment, Herzog [18] used the initial length as an input to a relatively simple muscle model to determine the force response of the muscle, for as long as the recruitment remains on. Clearly, this is not accurate if the recruitment level does not remain constant as the muscle contracts, or lengthens. It is also not accurate to use the instantaneous length as input, if the isometric force-length relationship is used for "non-isometric" dynamic situations.

The experimental evidence provided in this appendix shows that the instantaneous length is not accurate for dynamic (non-isometric) contraction following active stretch, the observed muscle force is larger than the isometric force corresponding to instantaneous length after stretch (the difference is called force enhancement). Similarly, muscle force is less than the isometric force corresponding to instantaneous length after active shortening (force depression). Most experimental evidence suggests that the initial length (l_o) is a key parameter that determines total muscle force.

Force enhancement/ depression (f_e / f_d) are dependent on initial length; if motor-units are recruited at different lengths then each recruited motor-unit needs to be treated separately. The multiple motor-unit model proposed in Chapter 3 can be used to increase the accuracy of the muscle model to account for continuously changing recruitment levels. To make the model more accurate, more complexities have to be incorporated into the model. In the case when recruitment level is continuously changing during FES, where different motor-units are

recruited at different muscle lengths, multiple motor-unit modelling approach can be used to account for recruitment history where every recruited motor-unit is treated as a separate muscle.

Stretch induced force enhancement f_e and shortening induced force depression f_d are both dependent on the magnitude of stretch/shortening; this dependence was looked at in this study. However, force depression is also affected by forces during shortening and speed of shortening [13], some researchers also reported that speed of stretch affects force enhancement [152], these effects are not covered in this study.

However, the greater the complexity of a model, the more difficult it is to implement such a model in real-time and hence an understanding of the trade-off between model complexity and controller performance is required [74, 76, 77].

Each property of skeletal muscle can be modelled separately making the model more generic and more accurate this will make the model scalable in complexity and accuracy. The model complexity can be adjusted depending on application, the user of the model need to make decision on the balance between accuracy and the level of complexity. More complex models require more computational time and more parameters that need to be experimentally estimated. Figure A2.18 shows one possible relationship between the quality of FES controller and model complexity (assuming that extra complexity will improve model accuracy).

The hypothesis of is this research work is that the quality of FES controller is expected to increase with model accuracy, but model accuracy may not necessarily increase with model complexity (using the appropriate length l_o or l_{CE} is an example). Muscle models, used for FES control, use a variety of different levels of complexity. For most models, the "instantaneous" *CE* length is used as an input to the isometric force-length relationship to calculate force. In most cases, muscle contractions will not be occurring under isometric conditions and hence there are clear limitations with these approaches. Herzog [18] used the initial length as the input, which is also not accurate if the recruitment parameter varies at different *CE* lengths. Even if the model was complex but uses the wrong length, a simpler model can be more accurate if the right length was used.

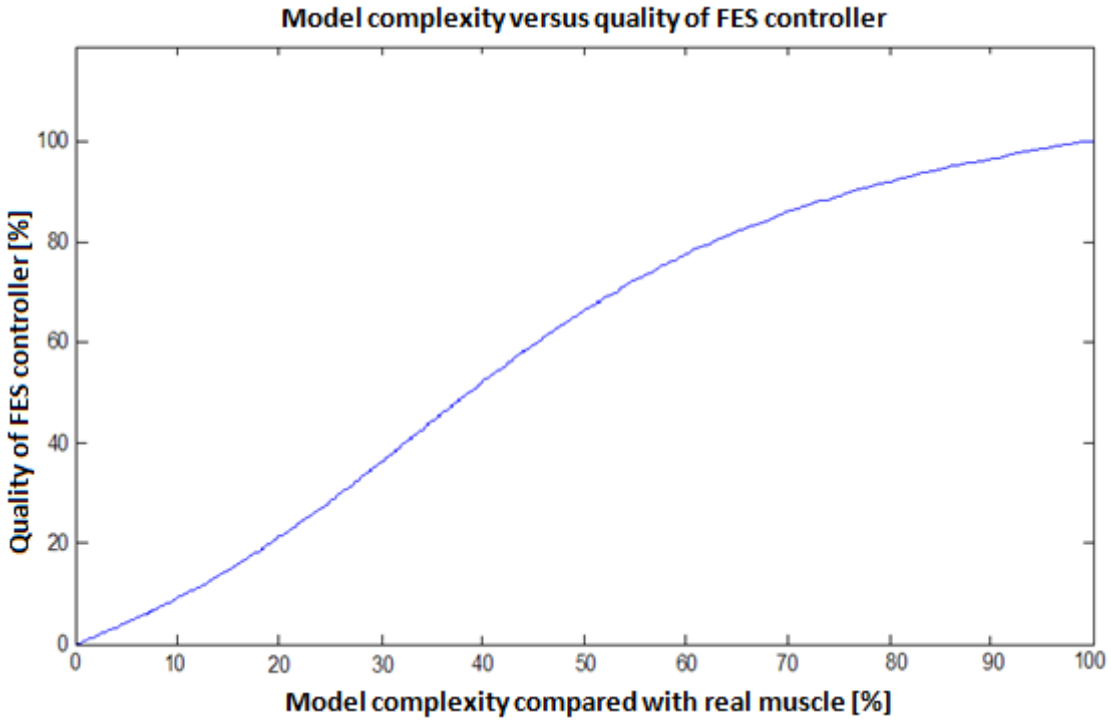

Figure A2.18: One possible relationship between the quality of FES controller and model complexity, roughly estimated relative to real skeletal muscle (assuming that extra complexity will improve model accuracy).

Figure A2.19 shows the three-dimensional relationship between *CE* length, *CE* velocity and active muscle force (f_{CE}) using the "instantaneous" *CE* length in Hill-type models. If the initial length was used instead, the isometric force-length relationship would stay constant at all lengths with the value that corresponds to the initial length.

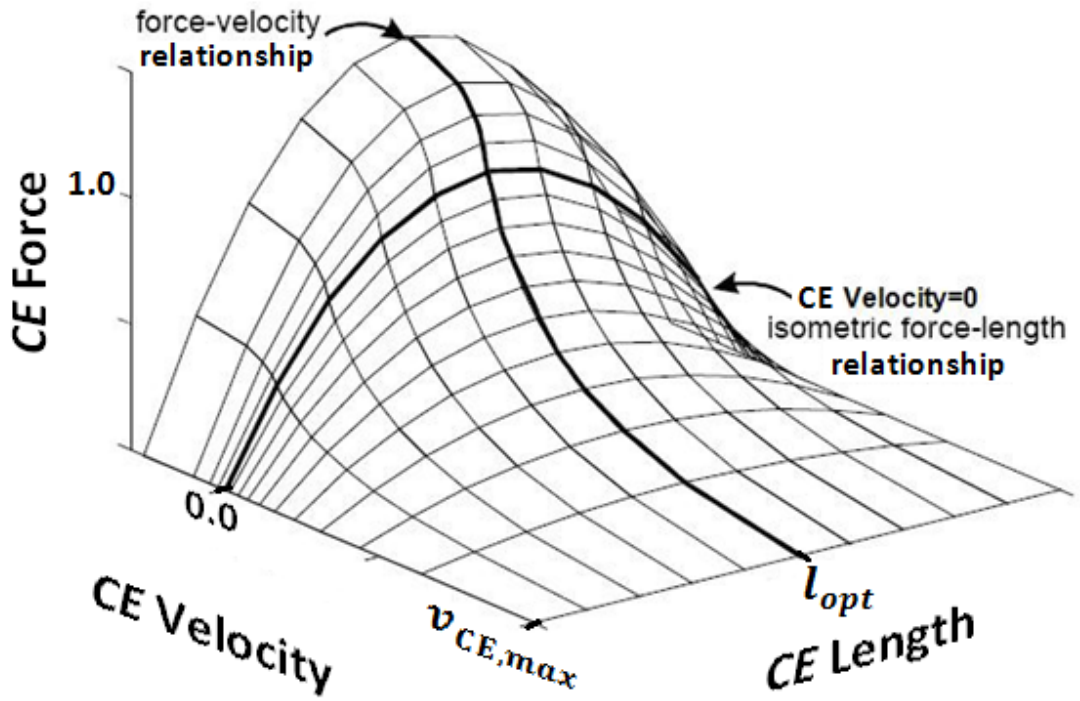

Figure A2.19: Three-dimensional relationship between "instantaneous" *CE* length (l_{CE}),*CE* velocity (v_{CE}) and *CE* force (f_{CE}). (Adapted from [18])

A2.6 Conclusions

Modelling of skeletal muscle force production can be very complicated as can be observed from the experimental data used in this study, note that this study only covers some of the effects of stretch/shortening on the steady-state force enhancement/depression. However, for applications where simplicity of the model is required, the initial length l_o can be used with good accuracy for dynamic contractions on the descending limb (l_o is more accurate than the instantaneous length l_{CE}). On the ascending limb, both lengths were not good estimators but the instantaneous length was closer to the experimental results.

The initial length (l_o) is a key parameter that determines total muscle force as can be observed from the experimental data. The isometric steady-state muscle force is highly affected by the length of the muscle fibres. Muscle fibres length is the most important factor in the force-length relationship.

In dynamic movements, when recruitment levels are changing continuously, different motor-units will be recruited at different initial lengths and at different times. This will make significant differences in the forces produced by recruited motor-units. Isometric steady-state force, f_d / f_e, fatigue, and other muscle properties depend on initial length and time since initially recruited.

The multiple motor-unit modelling approach can be used to account for the recruitment history during FES control whilst allowing the recruitment to change continuously at different lengths. This approach of modelling can also account for different types of motor-units of different properties, within one muscle.

In order to model muscle force properly, all important muscle properties have to be taken into account and incorporated into the model in order to increase the accuracy of the model, but this will make the model and parameters' estimation much more complex. A compromise between model complexity and accuracy has to be decided.

A2.7 Summary

The isometric steady-state force of skeletal muscle after stretch or shortening is history-dependent [13, 152, 154, 155, 168, 169, 170, 171, 172, 184, 185]. In this appendix, the initial length and the instantaneous length were compared for the purpose of estimating the steady-state skeletal muscle force following stretch and/or shortening from the traditional force-length curve. A review was made to the existing evidence, in the literature, on the isometric steady-state muscle force and the relationship with the history of *CE* length. The experimental isometric steady-state force following stretch/shortening is compared at the final *CE* length (after stretch/shortening) with the corresponding force of purely isometric contraction and also compared with the force at the initial *CE* length (before stretch/shortening). Results of the comparison are discussed. It was concluded that the initial length is much more accurate for dynamic contractions on the descending limb. On the ascending limb, both lengths are not good estimators, but the error was less when using instantaneous length. Improvement of model accuracy by incorporating more complexities into the basic Hill model is also discussed.

In chapter 3 of this thesis, Matlab simulations for different protocols of stretch and shortening using the initial and instantaneous lengths are tested for the single and multiple motor-unit models.

Appendix 3: Herzog Model

Herzog muscle model [18] is a basic Hill-type model (not complex); the main difference from other models in the literature is that Herzog uses the *CE* length at initial recruitment (l_o) instead of the instantaneous *CE* length (l_{CE}) which is typically used with Hill-type muscle models. Another feature of Herzog model is in the modelling of the maximum shortening and stretch velocities ($v_{CE,\max}$ and $v^{str}_{CE,\max}$), where both of $v_{CE,\max}$ and $v^{str}_{CE,\max}$ depend on $f_{iso}(l_0)$, see summary of Herzog F-V sub-model in section 2.5.3.2. Summary of the "original" Herzog model (as introduced in [18]) is given here:

A3.1 The standard Herzog model

Herzog used the three-element Hill-type model, the model consists of a parallel elastic element (k_p) in parallel with a series elastic element (k_s) and a contractile element (*CE*), see Figure A3.1.

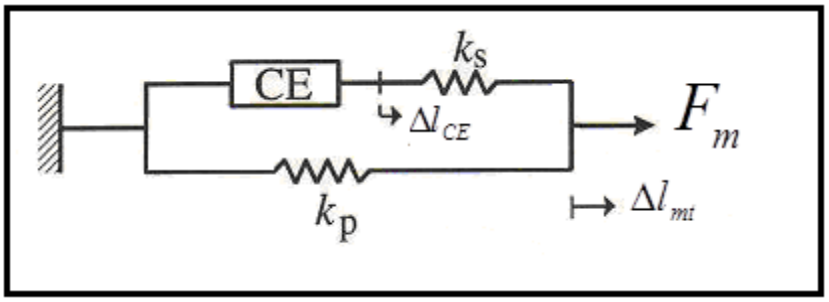

Figure A3.1: Topology of Herzog model [18].

For a skeletal muscle at full recruitment ($R = 1$), the isometric muscle force is approximated by the following equation:

$$f_{iso}(l_o) = f_{iso,\max}.[-c_1(l_o / l_{opt})^2 + c_2(l_o / l_{opt}) - c_3] \quad \text{(A3.1)}$$

Where, l_o is Length of the contractile element (*CE*) at the moment of initial recruitment, l_{opt} is the optimal *CE* length, $f_{iso}(l_o)$ is the isometric muscle force corresponding the *CE* length at initial recruitment and $f_{iso,\max}$ is the maximum isometric muscle force. c_1, c_2 and c_3 are

constants, their values depend on the force-length experimental curve of the muscle. For a typical mammalian skeletal muscle the normalized isometric muscle force can be approximated by the parabola given in equation A3.2 and illustrated in Figure A3.2.

$$f_{iso}(l_o) = f_{iso,\max} \times [-2.777(l_o / l_{opt})^2 + 5.554(l_o / l_{opt}) - 1.777] \qquad \text{(A3.2)}$$

This equation can be simplified to reduce the number of constant coefficients to one coefficient only.

$$FL(l_o) = \frac{f_{iso}(l_o)}{f_{iso,\max}} = \begin{Bmatrix} c_1(\bar{l}_o - 1)^2 + 1 & for \ \ positive \ \ values \\ 0.0 & for \ \ negative \ \ values \end{Bmatrix} \qquad \text{(A3.2A)}$$

$$\bar{l}_o = \frac{l_o}{l_{opt}},\ c_1 = -2.777\,.$$

Note that this parabola achieves positive values within the range: $0.4 < \bar{l}_o < 1.6$, else for negative values the isometric force is zero ($f_{iso}(l_o)$ = 0).

Equations A3.1, A3.2 and A3.3 give the *CE* active muscle force only; the passive muscle force of the parallel element *PE* will be considered in the equation of total muscle force (F_m).

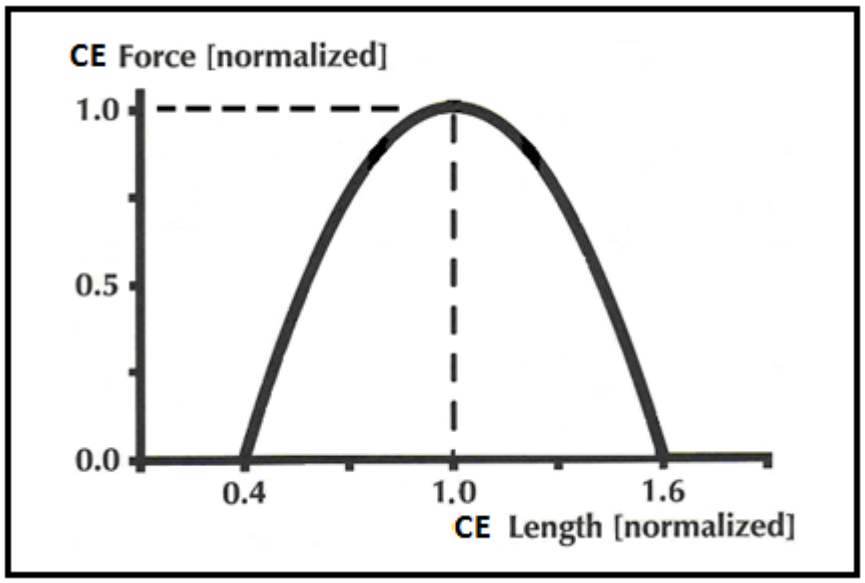

Figure A3.2: The normalised force-length relationship of a skeletal muscle obeying equation A3.2. (From [18]).

The contractile element *CE* of Hill model, originally conceived to operate at the plateau of the force-length relationship, can be generalized to include the full force-length response. Such a generalized *CE* is governed by an all-or-nothing recruitment ($R = 1$ if the muscle is recruited, otherwise $R = 0$).

In the inactive state, the *CE* cannot sustain any force, and its length can be adjusted at will. In the active state (providing the force as a function of *CE* velocity (v_{CE}), and *CE* initial length (l_0), the behaviour of the *CE* is related to empirical data as follows:

$$f_{CE} = f_{CE}(v_{CE}, l_0) = \left\{ \begin{array}{c} 0 \quad for \quad v_{CE} \le -f_{iso}(l_0)\dfrac{b}{a} \\ \dfrac{f_{iso}(l_0)b + av_{CE}}{-v_{CE} + b} \quad for \quad -f_{iso}(l_0)\dfrac{b}{a} < v_{CE} \le 0 \\ 1.5 f_{iso}(l_0) - 0.5\dfrac{f_{iso}(l_0)b' + a'v_{CE}}{v_{CE} + b'} \quad for \quad 0 < v_{CE} \le f_{iso}(l_0)\dfrac{b'}{a'} \\ 1.5 f_{iso}(l_0) \quad for \quad v_{CE} > f_{iso}(l_0)\dfrac{b}{a'}' \end{array} \right\} \quad \text{(A3.3)}$$

a, b, a' and b': are constants. f_{CE}: is the instantaneous force produced by the contractile element *CE*.

In the shortening range equation A3.3 is a direct rewriting of Hill's law [97], with *CE* velocity (v_{CE}) considered positive in elongation. The overall appearance of equation A3.3 is plotted in Figure A3.3.

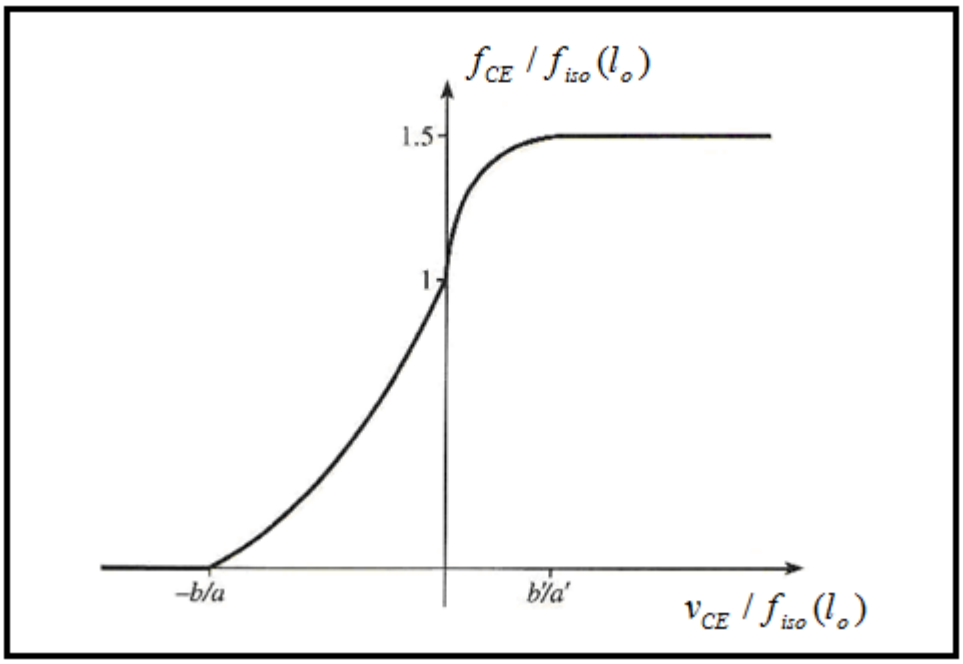

Figure A3.3: The normalised force-velocity relationship of Herzog model. (From [18]).

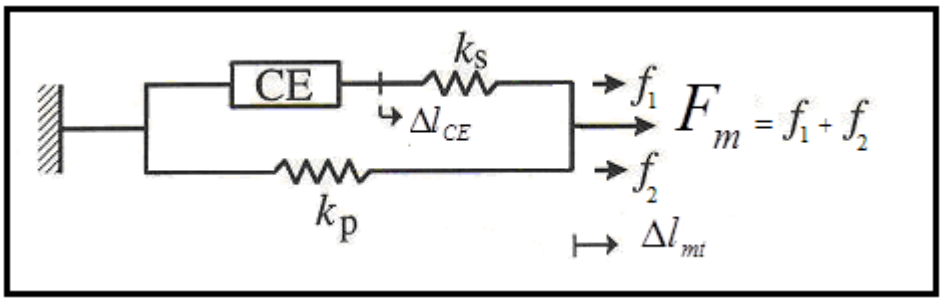

Figure A3.4: Total force in Herzog model is the sum of the two parallel forces.

The forces of elements in series are always the same in both elements while the elongations sum to the total elongation of the combined element. In parallel elements the elongations are the same and the forces are added as shown in Figure A3.4. The response of the three-element model is governed by equations A3.4 and A3.5, derived as follows:

$$f_1 = k_s(\Delta l_{mt} - \Delta l_{CE}) = f_{CE}(v_{CE}, l_0)$$
$$f_2 = k_p \times \Delta l_{mt}$$
$$F_m = f_1 + f_2$$
$$F_m = (k_p \times \Delta l_{mt}) + k_s(\Delta l_{mt} - \Delta l_{CE}) \quad \text{(A3.4)}$$
$$F_m - f_2 = f_1 = f_{CE}(v_{CE}, l_0)$$
$$F_m - (k_p \times \Delta l_{mt}) = f_{CE}(v_{CE}, l_0) \quad \text{(A3.5)}$$

With l_0 given by ($l_0 = l_{PE} + u_0 - l_S^t = l_{rest} + u_0$) and Δl_{CE} denotes the elongation of the *CE* with respect to its length at the unique resting state of the system. It is possible to eliminate the internal degree of freedom v_{CE} by rearranging equation A3.4 and introducing the result into equation A3.5 to obtain the first order nonlinear differential equation:

From equation A3.4: $\dfrac{F_m - (k_p \times \Delta l_{mt})}{k_s} = (\Delta l_{mt} - \Delta l_{CE})$

$$\Delta l_{CE} = (1 + \frac{k_p}{k_s}) \times \Delta l_{mt} - \frac{F_m}{k_s}$$

By taking the time derivative, the instantaneous *CE* velocity is:

$$v_{CE} = \left(1 + \frac{k_p}{k_s}\right) \times v_{mt} - \left(\frac{\dot{F}_m}{k_s}\right) \qquad \text{(A3.6)}$$

By introducing the last result (equation A3.6) into equation A3.5, the total muscle force for a fully recruited muscle can be expressed as:

$F_m = (k_p \times \Delta l_{mt}) + f_{CE}(v_{CE}, l_0)$

$$F_m - (k_p \times \Delta l_{mt}) = f_{CE}\left[\left(\left(1 + \frac{k_p}{k_s}\right) \times v_{mt} - \frac{\dot{F}_m}{k_s}\right), l_0\right] \qquad \text{(A3.7)}$$

The muscle is considered to be at full recruitment ($R = 1$) in equation A3.7. The variations in R have to be considered when modelling muscle force, any complete muscle model should allow for such variations, but definitive experimental data are not available yet [18]. Until the proper experimental data becomes available, provisional solutions which at least do not violate the basic laws of physics can be used. Herzog [18] assumed that the muscle remembers the *CE* length l_0 at which it was initially recruited for as long as any level of recruitment remains. If, and only if, the recruitment completely disappears, then that length is forgotten and a new initial length will be determined upon a new recruitment. For partial recruitment; equation A3.7 can be modified to:

$$F_m = (k_p \times \Delta l_{mt}) + R \times f_{CE}\left(\left(\left(1 + \frac{k_p}{k_s}\right) \times v_{mt} - \left(\frac{\dot{F}_m}{k_s}\right)\right), l_0\right) \qquad \text{(A3.8)}$$

In order to solve the differential equation in A3.8, Herzog used the forward finite-difference scheme. The time derivative of total muscle force is approximated using the known value at time (i) and the unknown value at time (i+1) as follows:

$$\dot{F}_m \cong \frac{\dot{F}_m(i+1) - \dot{F}_m(i)}{h}$$

h: small time increment.

The forward finite- difference scheme used by Herzog to solve the differential equation in A3.8 is not explained in [18], details are not provided in that reference.

A3.2 The formulated Herzog model

The original Herzog muscle model is summarised in the previous section of this appendix. The purpose of the work described in this section is to re-analyse the equations presented by Herzog [18] in order to produce an expression for the rate of change of total muscle force $\dot{F}_m$ as a function of relevant parameters.

The elongation of the whole muscle (the musculotendon complex) Δl_{mt} will be measured from the unique resting state (inactive, force-free) corresponding to the un-stretched length l_{PE}^{S} of the parallel element *PE* and the un-stretched length l_S^t of the series elastic element *SE* as shown in Figure A3.5. In the inactive state ($R = 0$), the *CE* cannot produce any force, and its length can be adjusted at will according to the following equation:

$$l_{CE} = l_{PE} - l_S^t \qquad \text{(A3.10)}$$

Where: $l_{rest} = l_{PE}^{S} - l_S^t$

l_{rest} is the resting length of the inactive contractile element CE (at the unique resting state).

l_S^t: *SE* slack length (at the unique resting state), *SE* length beyond which *SE* begins to develop force.

l_{PE}^{S}: The slack length of *PE* (at the unique resting state), the length beyond which *PE* begins to develop force.

The unique resting state is considered “unique” because for any stretch beyond this length, the musculotendon complex will develop passive force.

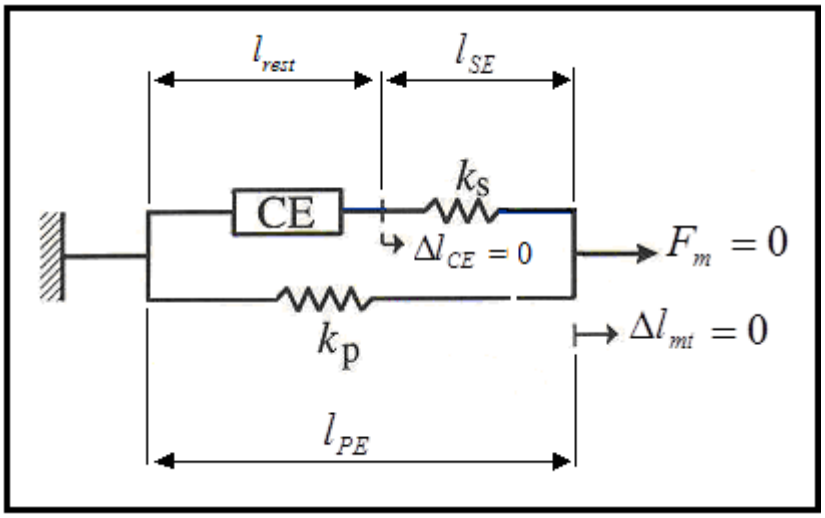

Figure A3.5: Herzog model at the unique resting state.

The elongation value for the entire muscle Δl_{mt} at the instant at which the recruitment is applied is u_0. At this moment, the elongation of the contractile element Δl_{CE} will also be u_0, since the force in the serial element *SE* (and its elongation) will vanish up to the moment just before the initial recruitment, see Figure A3.6. The length of the contractile element *CE* at the moment of recruitment (l_0) can be represented as:

$$l_0 = l_{PE} + u_0 - l_S^t = l_{rest} + u_0 \qquad \text{(A3.11)}$$

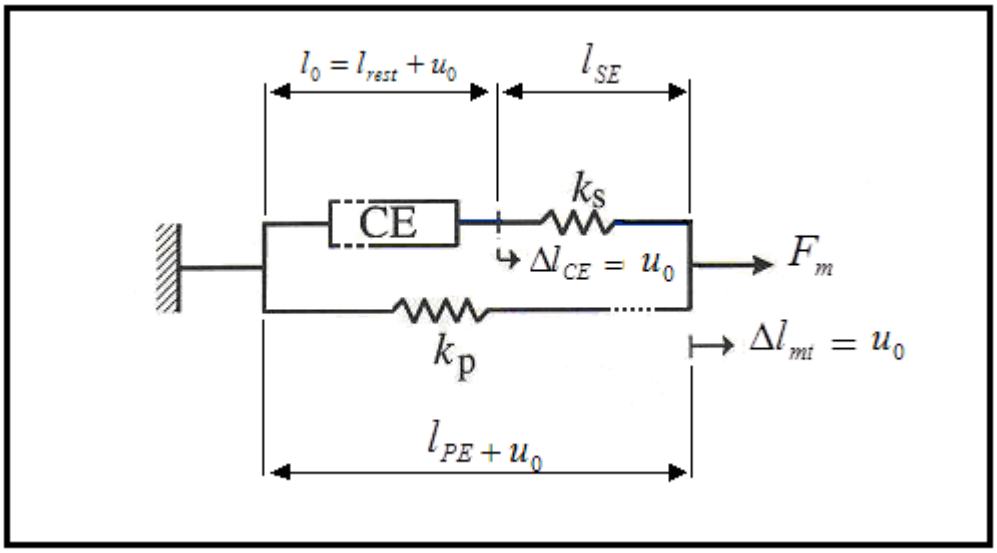

Figure A3.6: Herzog model at the moment of initial recruitment.

In the original form of Herzog model, the *CE* velocity (v_{CE}) is expressed as a first order differential equation:

$$v_{CE} = \left(1 + \frac{k_p}{k_s}\right) v_{mt} - \left(\frac{\dot{F}_m}{k_s}\right) \qquad \text{(A3.12)}$$

The total muscle force for partial recruitment is given as follows:

$$F_m = (k_p \times \Delta l_{mt}) + f_{CE}(v_{CE}, l_0) = (k_p \times \Delta l_{mt}) + R \times f_{CE}\left(\left(\left(1 + \frac{k_p}{k_s}\right) v_{mt} - \left(\frac{\dot{F}_m}{k_s}\right)\right), l_0\right) \qquad \text{(A3.13)}$$

F_m: Total muscle force, including all active and passive forces (all forces produced by the musculotendon complex). k_p: Stiffness of the linear un-damped purely elastic element in parallel (*PE*). k_s: Stiffness of the linear un-damped purely elastic element in series (*SE*). Δl_{mt} : Elongation of the musculotendon complex from the unique resting state. $v_{mt} = dl_{mt} / dt$: Instantaneous velocity of the musculotendon complex (including muscle fibres and tendon). v_{CE}: Instantaneous *CE* velocity, assumed the same for all motor-units. $v_{CE} = dl_{CE} / dt$, $v_{CE} < 0$ for muscle shortening.

The author's implementation of Herzog's F-V sub-model depends on the instantaneous *CE* velocity and is calculated as follows:

To solve the differential equation in A3.13, the time derivative of the total muscle force $\dot{F}_m$ as a function of ($R, \Delta l_{mt}, v_{mt}, f_{iso}(l_o), F_m$) is calculated from equations A3.3 A3.12 and A3.13, the derivation is provided in Chapter 3.

Finally, $\dot{F}_m$ of the formulated Herzog's single motor-unit model is represented as:

$$\dot{F}_m = \begin{cases} k_p v_{mt} & for \quad v_{mt} \le \left(\dfrac{\dot{F}_m}{(k_p + k_s)} - \dfrac{b.f_{iso}(l_o)}{a.\left(1 + \dfrac{k_p}{k_s}\right)} \right) \\ \dfrac{b(R.f_{iso}(l_o) - F_m + k_p \Delta l_{mt}) + \left(1 + \dfrac{k_p}{k_s}\right)(R.a + F_m - k_p \Delta l_{mt}) v_{mt}}{\dfrac{1}{k_s}(R.a + F_m - k_p \times \Delta l_{mt})} & for \quad \left(\dfrac{\dot{F}_m}{(k_p + k_s)} - \dfrac{b.f_{iso}(l_o)}{a.\left(1 + \dfrac{k_p}{k_s}\right)} \right) < v_{mt} \le \dfrac{\dot{F}_m}{(k_p + k_s)} \\ \dfrac{2b'\left[R.f_{iso}(l_o) - (F_m - k_p \Delta l_{mt})\right] + \left[R.(3f_{iso}(l_o) + a') - 2(F_m - k_p \Delta l_{mt})\right]\left(1 + \dfrac{k_p}{k_s}\right) v_{mt}}{\dfrac{1}{k_s}\left[R.(3f_{iso}(l_o) + a') - 2(F_m - k_p \Delta l_{mt})\right]} & for \quad \dfrac{\dot{F}_m}{(k_p + k_s)} < v_{mt} \le \left(\dfrac{\dot{F}_m}{(k_p + k_s)} - \dfrac{b'.f_{iso}(l_o)}{a'.\left(1 + \dfrac{k_p}{k_s}\right)} \right) \\ k_p v_{mt} & for \quad \left(\dfrac{\dot{F}_m}{(k_p + k_s)} - \dfrac{b'.f_{iso}(l_o)}{a'.\left(1 + \dfrac{k_p}{k_s}\right)} \right) < v_{mt} \end{cases} \quad \text{(A3.9)}$$

Then total muscle force (F_m) is obtained by integration of $\dot{F}_m$ with respect to time:

$$F_m = \int \dot{F}_m \quad dt$$

A3.3 Matlab simulation results

Matlab codes were developed for simulating the responses to open-loop stimulation protocols of different versions of Herzog muscle model. In order to solve the differential equation in A3.8, Herzog used the forward finite-difference scheme. However, the author used two other different methods; one method with the formulated Herzog model (equations A3.9) and another method with the standard (original) Herzog model (equations A3.8) using an iterative approach (details are provided in Chapter 3). Both of these two methods can be used with single or multiple motor-unit models.

Matlab simulation results were found to be exactly the same for the steady-state force response. However, for the transient-state force response, there can be very small differences. These very small differences are expected because in every method, a different approach is used to estimate the lengths of *CE* and *SE* (e.g. in equation A3.9, the previous value of $\dot{F}_m$ is used to solve the current value of $\dot{F}_m$, while the iterative approach used different method as explained in Chapter 3).

Another important point about the initial length (l_o) is worthy of notice; the *CE* length before and just after recruitment is not the same, this is due to the tendon compliance (modelled as k_s). The initial length at rest (before recruitment) is not accurate since the experimental F-L relationship is measured after recruitment not before. Therefore, it would be more accurate to use the instantaneous $l_{CE}(t)$ at onset of recruitment at rest until *CE* length settles, and then use that *CE* length for those recruited motor-units throughout the protocol as long as they are still recruited. Modelling of other motor-units which are recruited later in the protocol will have the same problem. However, the initial length used is the length before recruitment. In the same time, experimental data are taken for the length just after recruitment not the length before recruitment, the difference can be large if the tendon compliance is small, experimental

F-L data for the tibialis anterior muscle (before and after full recruitment) are shown in Appendix 6.

The multiple motor-unit model is incorporated into Herzog's single motor-unit model by replacing [$R \times f_{iso}(l_o)$] by [$Eff \,.\, f_{iso}$] in the formulated Herzog's single motor-unit model (see details in Chapter 3.

Appendix 4: Empirical Data for the Anatomical Operating Range of Different Muscles

The anatomical operating range: is defined as the muscle belly length between l_{min} and l_{max}. l_{min} and l_{max} are defined as the position of the minimum and maximum lengths of the anatomical operating range of the muscle belly length (l_m).

The anatomical operating range varies among different muscles and different species. Moreover, different values have been reported for the anatomical operating range of the same muscle in the literature (like all other muscle parameters). This appendix some examples reported in the literature. Figures A4.1, A4.2, and A4.3 show some examples of the anatomical operating range obtained experimentally for different muscles.

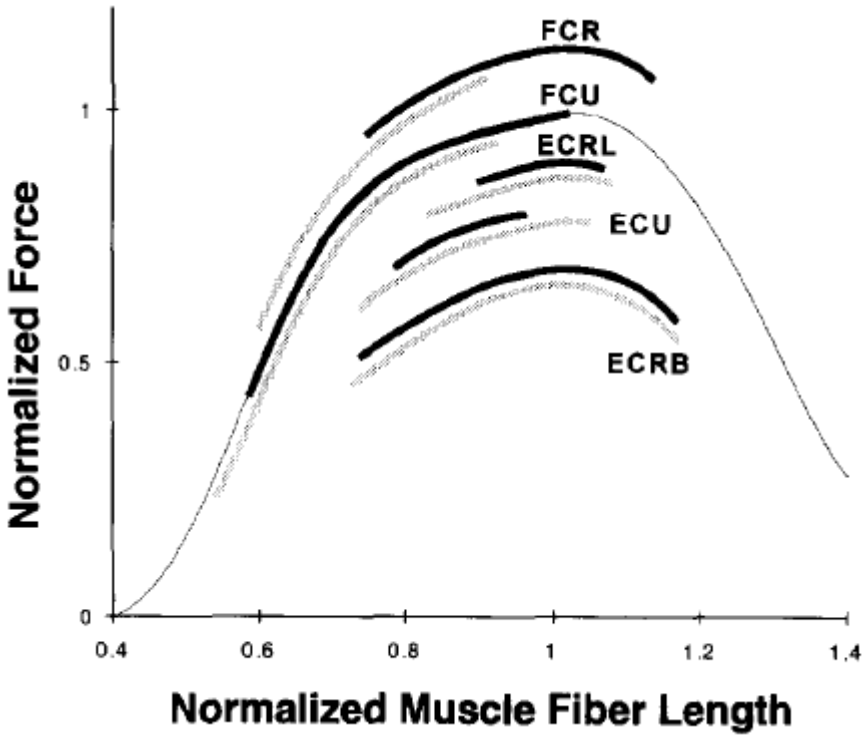

Figure A4.1: Operating lengths of five wrist muscles from 50^o flexion to 45^o extension. Model results within the operating ranges (between l_{min} and l_{max}) are the dark curves; the thin line represents the whole F-L curve. (From [159]).

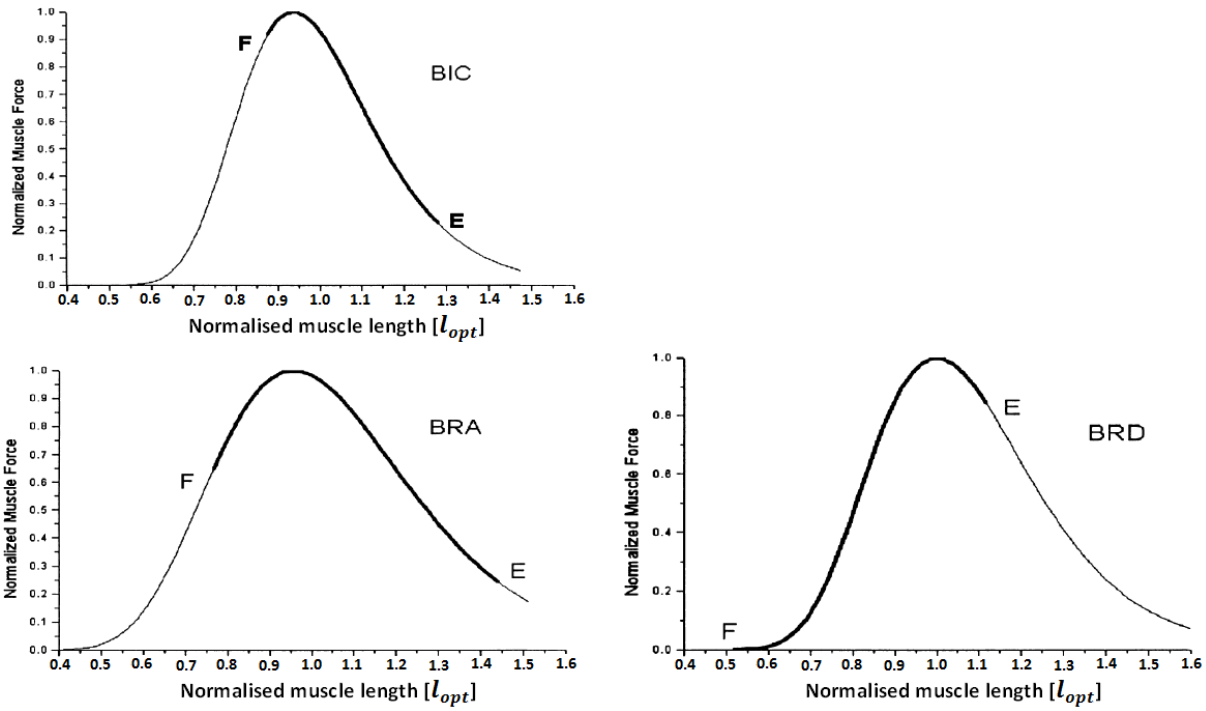

Figure A4.2: The thick lines represent the operating ranges for three major elbow flexors (BIC: Biceps Brachii; BRA: Brachialis; BRD: Brachioradialis) throughout the range of motion from 15° of elbow flexion (E at l_{max}) to 120° of elbow flexion (F at l_{min}). The thin lines represent F-L curves for the whole range. (From [195]).

In figure A4.3, the operating ranges are ordered from l_{min} to l_{max} within a study and are colour-coded according to the species from which the experimental data were obtained. Numbers shown on the right of each operating range indicate the reference which this particular data were taken from (the full list of references used to make this figure are provided in [196]).

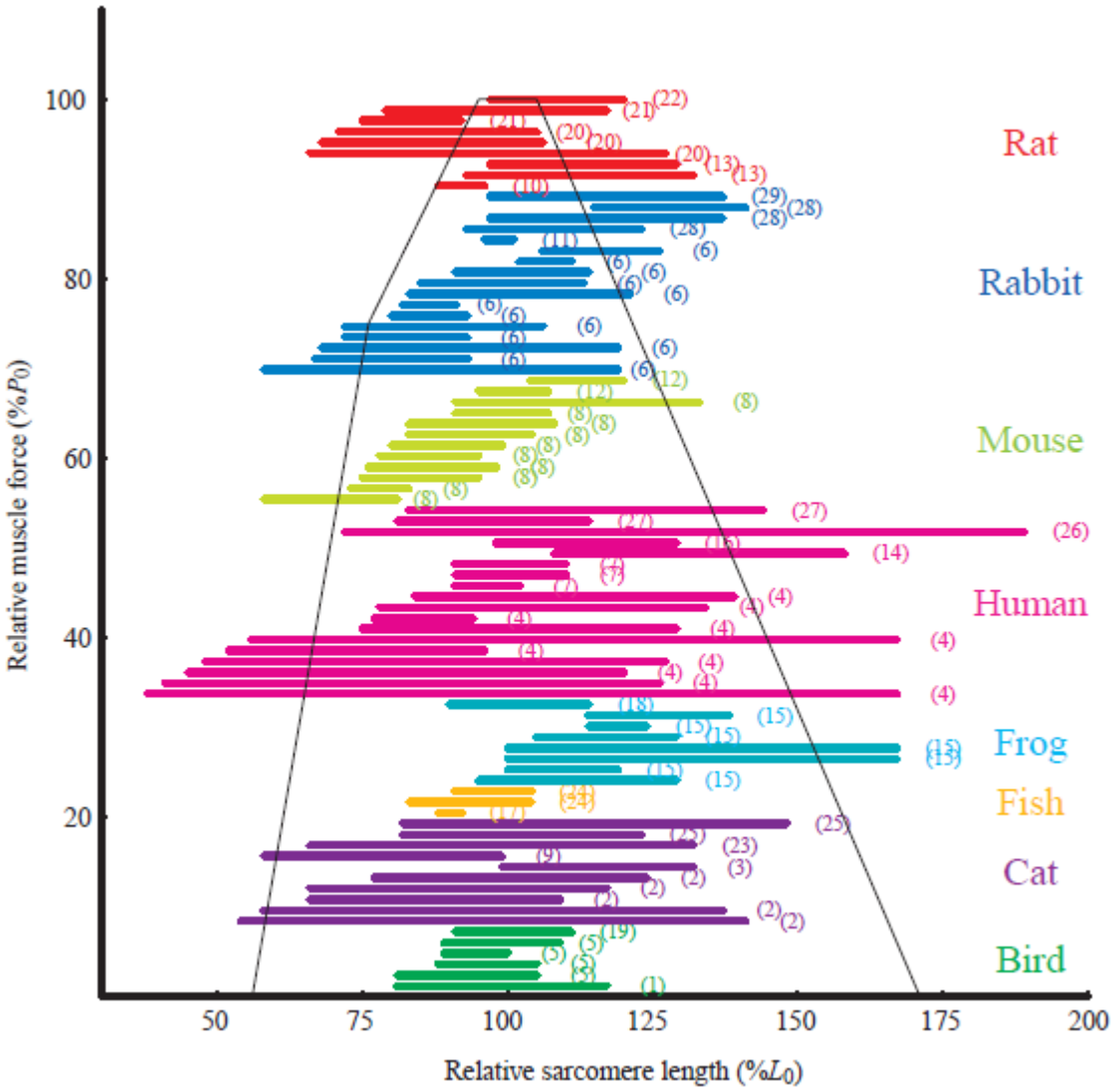

Figure A4.3: Sarcomere length operating ranges reported in the literature, graphically superimposed upon a normalized sarcomere F-L curve. (From [196]).

Appendix 5: Effects of *CE* Length on Force Response to Open-Loop Simulation Protocols

The dynamic variations in $R(t)$ during FES and the effects of different *CE* lengths are examined here. Protocol-I and protocol-II were used to investigate the effects of different *CE* lengths on force response when protocol-I and protocol-II are applied on the "$Eff.f_{iso}$" model (all other muscle parameters and constants values in the model equations are the same for all *CE* lengths with $\frac{l_{rest}}{l_{opt}}$=1.25). Note that the ratio of the magnitude of stretch or shortening to *CE* lengths is different when same protocols are applied on different *CE* lengths and hence the normalised isometric force values at the end of stretch are different.

The muscle parameters used here are the same as those provided in chapter 3 (section 3.4.1), more *CE* lengths are be tested, in addition to that *CE* length used in chapter 3, which is used as a reference for comparison. The force responses for the range of *CE* lengths is compared with that of the single motor-unit model, where $f_{iso}(l_o)$ at initial recruitment is used through the protocols regardless of the dynamic variations in $R(t)$.

Protocol-I: The *CE* lengths examined with protocol-I are shown in Table A5.1. The simulation results are shown in Figure A5.1. As can be observed from this figure, force response looks similar for all *CE* lengths until 5seconds when the 50% recruitment was increased to 100%. The force response is shown magnified in Figure A5.2.

Table A5.1: *CE* lengths used with protocol-I.

	*CE*1	*CE*2	*CE*3	*CE*4	*CE*5	*CE*6
l_{opt}	200mm	80mm	50mm	30mm	20mm	15mm
l_{rest}	250mm	100mm	62.5mm	37.5mm	25mm	18.75mm

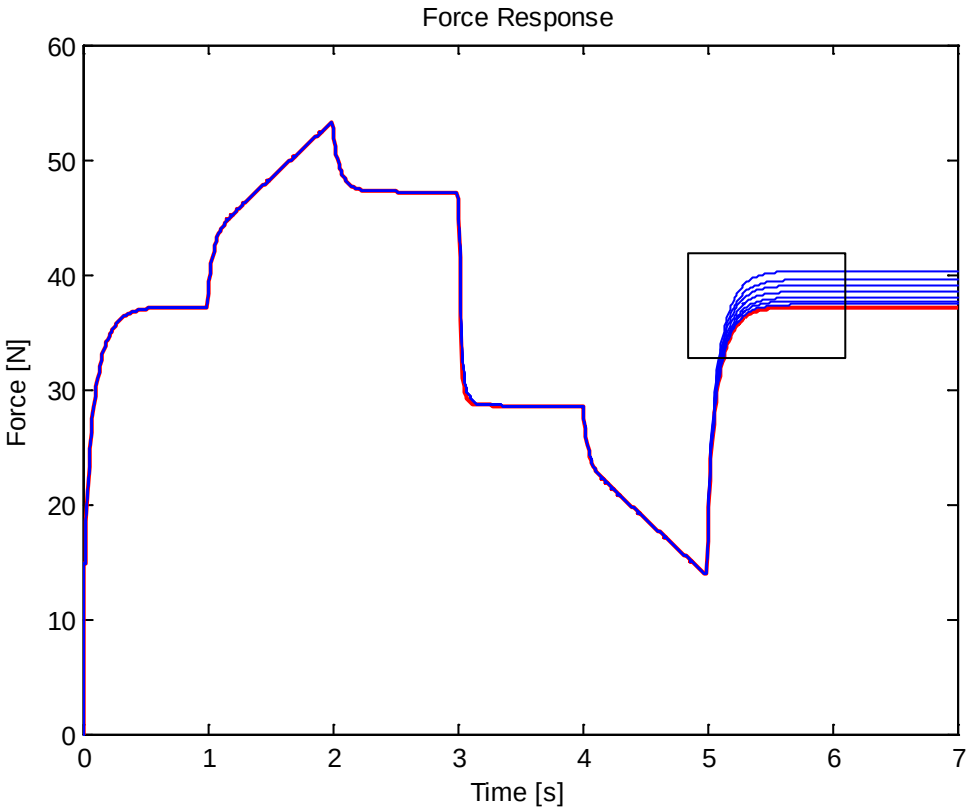

Figure A5.1: Force response of the $Eff.f_{iso}$ model, the input is protocol-I with different *CE* lengths.

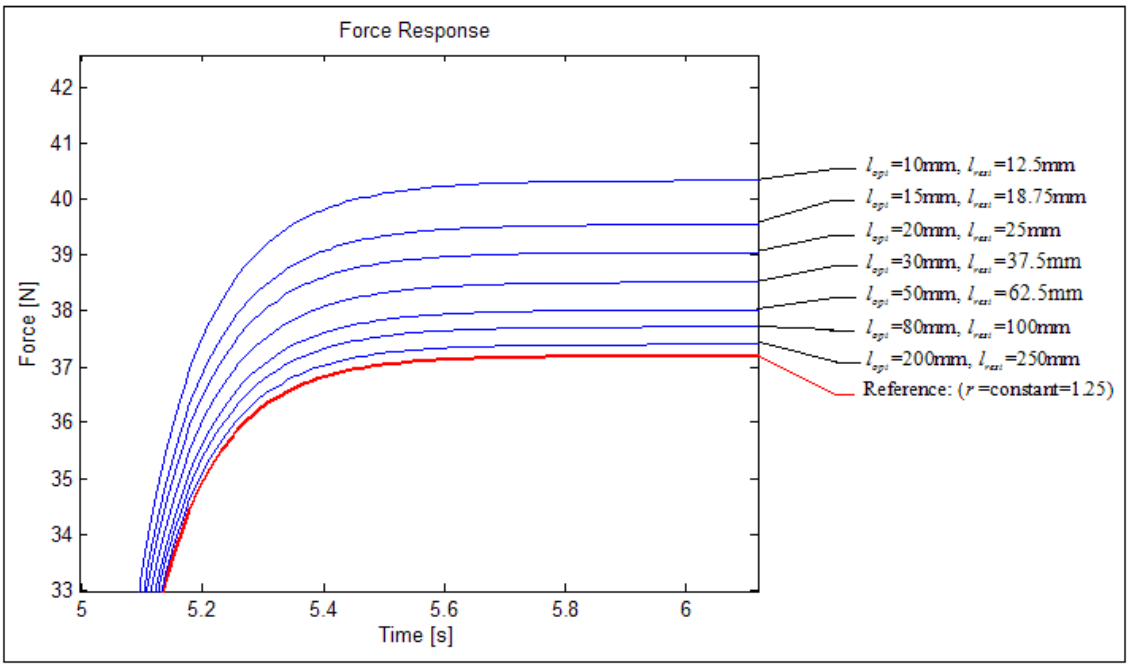

Figure A5.2: *CE* lengths used to examine the force response of protocol-II.

Protocol-I started with 100% recruitment (all motor-units are recruited) then reduced to 50% (this means 50% of the motor-units have been de-recruited) and later increased again to 100%

(all motor-units are recruited again) at the same *CE* length as that at the beginning of the protocol at unique resting state ($\Delta l_{mt} = 0$). All motor-units now are recruited and were initially recruited at the same *CE* length at unique resting state ($\Delta l_{mt} = 0$), but the *CE* length was not the same at initial recruitment for all motor-units. When the recruitment increased again to 100%, the *CE* is already contracted with 50% of the motor-units already recruited and produce force causing *SE* to stretch. *CE* length is slightly shorter than its previous length at the beginning of the protocol when it was at the unique resting state. Therefore, the *CE* length at which the first 50% of motor-units where initially recruited is slightly longer than that for the other 50% of motor-units recruited later. The force response is slightly different as shown in Figure A5.1 and Figure A5.2. Note that this difference is increasing with shorter *CE* lengths; this is because the small difference in *CE* lengths in both cases (before stretch and after stretch) is relatively larger on isometric force-length relationship for those shorter muscles. .

Protocol-II: The *CE* lengths examined with protocol-II are shown in Table A5.2. The simulation results are shown in Figure A5.3. As can be observed from this figure, force response looks similar for all *CE* lengths until 3 seconds when the 50% recruitment was increased to 100%. The force responses for the range of *CE* lengths were largely different with the shortest muscle with very little increase in force after the full recruitment.

Table A5.2: *CE* lengths used with protocol-II.

	*CE*1	*CE*2	*CE*3	*CE*4	*CE*5	*CE*6	*CE*7
l_{opt}	600mm	200mm	100mm	70mm	40mm	32mm	24mm
l_{rest}	750mm	250mm	125mm	87.5mm	50mm	40mm	30mm

Lengths shorter than (l_{opt} =24mm) are not suitable for this protocol because a stretch of 10mm is more than the maximum stretch allowed for Herzog F-L sub-model, which is $(1.4 l_{opt})$.

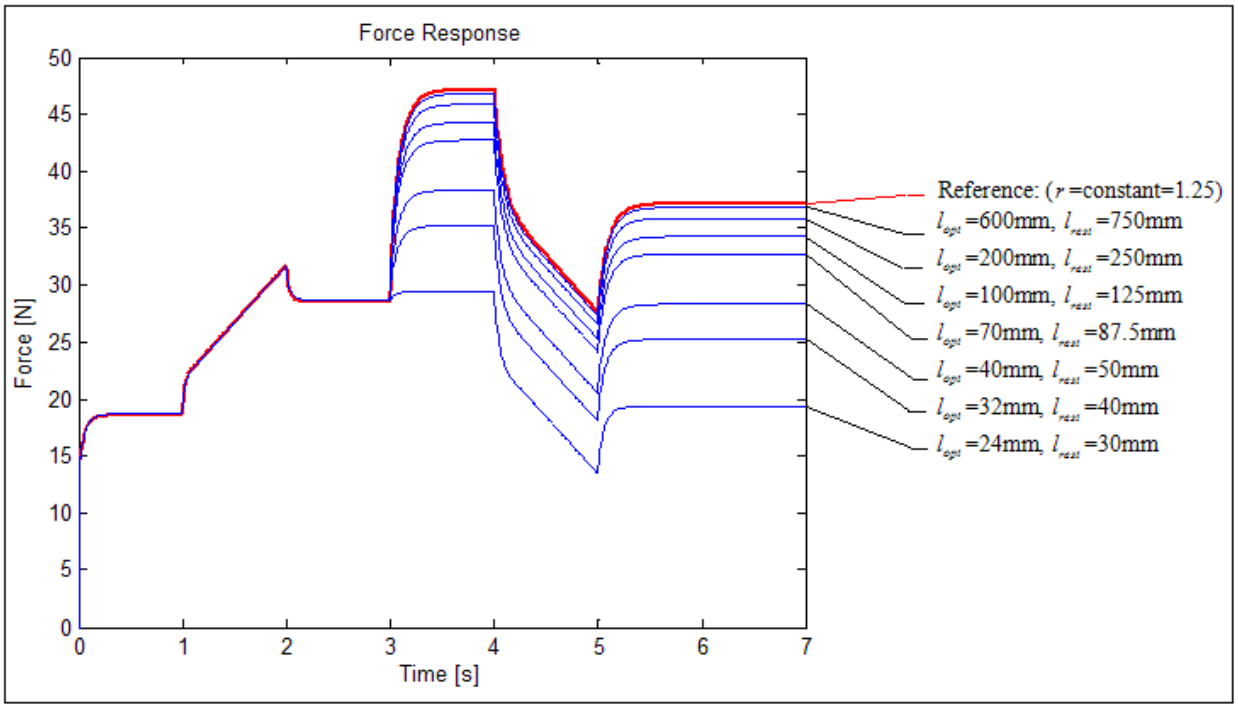

Figure A5.3: Force response for the $Eff.f_{iso}$ model, the input is protocol-II at range of *CE* lengths.

In protocol-II, the recruitment level (R) was increased (at 3 seconds) at a range of *CE* lengths. The force response was found to be dependent on the *CE* length, see Figure A5.3. This is also true for any other protocol if R was increased at different *CE* length other than the initial length providing that the corresponding isometric forces for these two lengths are not the same (when the isometric force of one length lies on the descending limb and the other one lies on the ascending limb and having the same value). This can be compared with Protocol-I force response (in Chapter 3). For both protocols, shorter *CE* lengths produce larger difference in the force response.

The initial length for protocol-II at 0 seconds was l_{rest} and the ratio: $\frac{l_0}{l_{opt}} = \frac{l_{rest}}{l_{opt}} = 1.25$ for the first 50% recruited motor-units. Then at 3 seconds; for the other 50% of motor-units the ratio is: $\frac{l_{rest} + \Delta l_{CE}}{l_{opt}}$, this is larger than the previous ratio.

Lengths longer than (l_{opt} =600mm) were also examined, the difference in force response was very small, just between the reference force response and the response of the *CE* length (l_{opt} =600). For the longest *CE* length (l_{opt} =600mm), a stretch of the value $u = 10mm$ is relatively small and the corresponding isometric force for the *CE* length ($l_{rest} + \Delta l_{CE}$) becomes very near to the isometric force for *CE* length (l_{rest}), and this is why the difference from the reference results was very small. For the shortest *CE* length (l_{opt} =24mm), $\Delta l_{mt} = 10mm$ becomes relatively large and the corresponding isometric force for the *CE* length ($l_{rest} + \Delta l_{CE}$) becomes very small (almost zero) because it lies nearly at the bottom of the descending limb of the force-length relationship. So, when recruitment increased from 50% to 100%, the force produced by the recently recruited 50% of motor-units is very small and added very little extra on the total muscle force.

Appendix 6: Ankle-Joint and Tibialis Anterior Parameters

Some parameters of the ankle-joint and Tibialis Anterior (TA) muscle (Figure A6.1) are shown here in this appendix. Figure A6.2 shows experimental data for the F-L relationship of TA muscle belly and for the TA musculotendon complex. More detailed data, for the same muscle, are shown in Table A6.1.

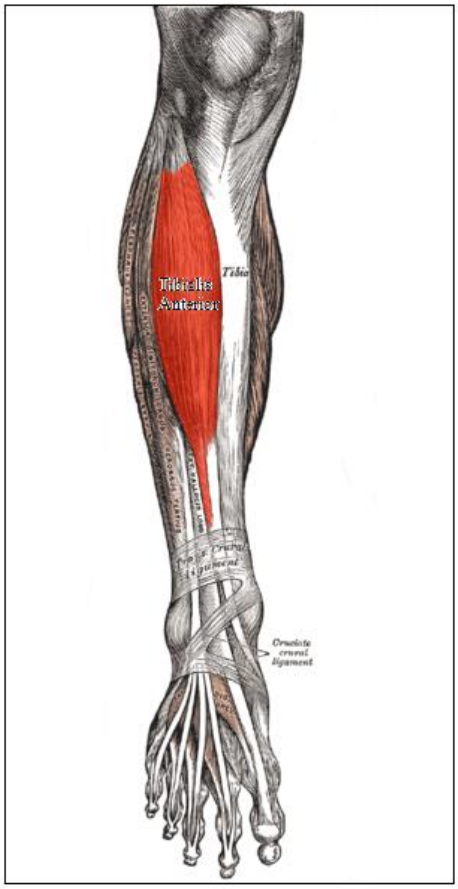

Figure A6.1: The Tibialis Anterior muscle. (from [15]).

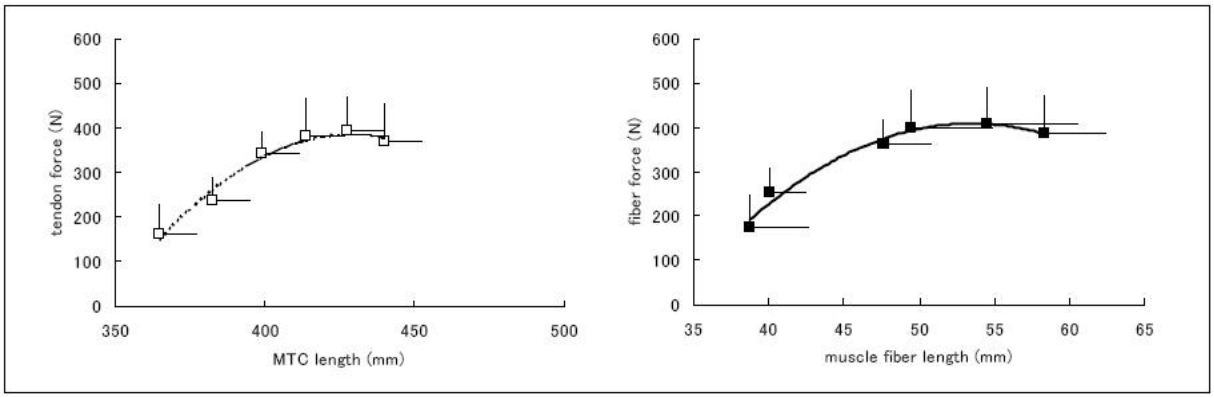

Figure A6.2: F-L relationship on muscle fibre (MF) and the musculotendon complex (MTC). (From [197]).

Table A6.1: Ankle-joint angle, pennation angle and the corresponding elongation of tendon structures, muscle fibre (MF) length and force, and musculotendon complex (MTC) length and force. (From [197]).

Joint Angle [deg]	**-20**	**-10**	**0**	**+10**	**+20**	**+30**
Pennation Angle [deg] (during contraction)	**22.8**	**20.5**	**19.2**	**15.7**	**15.6**	**16**
Elongation of tendon structures [mm]	**12.3**	**15.4**	**15**	**16.4**	**16.6**	**18.6**
MF length (at rest) [mm]	**51**	**55**	**62.5**	**66.5**	**71**	**74**
MF length [mm] (during contraction)	**38.8**	**40.2**	**47.8**	**49.5**	**54.5**	**58.3**
MF force [N]	**174.2**	**253**	**364**	**400**	**408.8**	**388**
MTC length [mm]	**365.1**	**383.3**	**399.4**	**414.1**	**427.6**	**440.1**
MTC force [N]	**160.5**	**235**	**342**	**382.5**	**393**	**369**

The length change of MTC was determined by multiplying the moment arm at the middle value in the range of joint angle change by the amplitude of joint angle change (converted to radians), e.g. if joint angle changed from 0^o to 20^o, the moment arm at 10^o was multiplied by $(\frac{20}{180}\pi)$ rad [197].

Experimental F-L data are usually taken for lengths after recruitment (at fixed musculotendon length) not the length before recruitment; the difference can be large if the tendon compliance is small. F-L experimental data of the tibialis anterior are shown in Figure A6.3. The muscle fibre operates in the plateau region and ascending limb by elongating tendon structures, although the length-force relationship predicted from the muscle fibre length in a resting state is on the descending limb and plateau region).

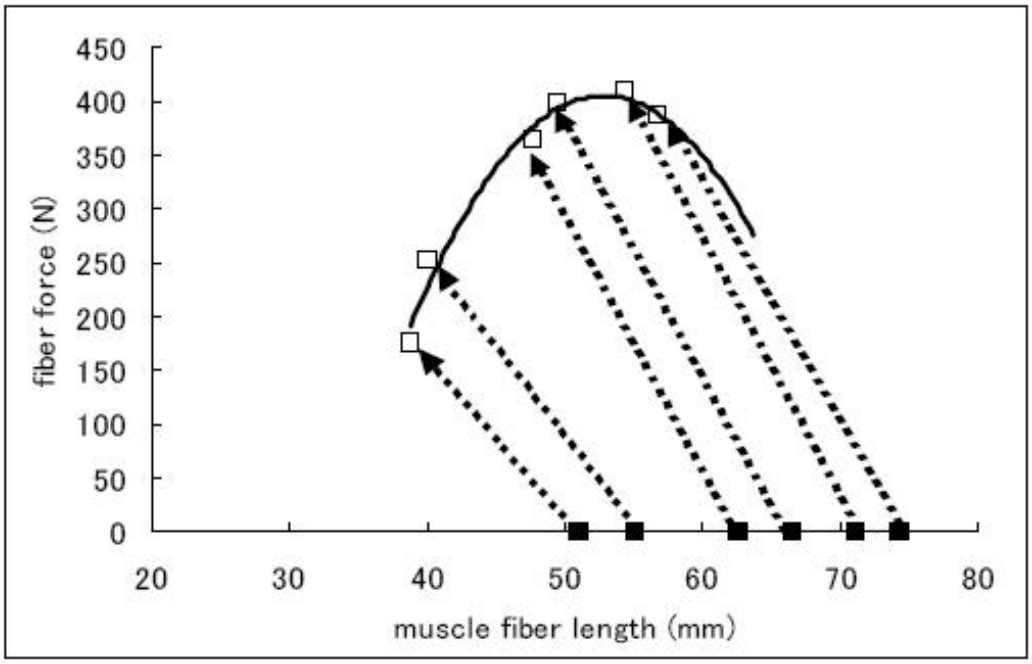

Figure A6.3: Length change of muscle fibre at rest and during contraction. The initial length at rest is the measured data in the pre-set study. (From [197]).

If a constant value of 5.0 cm length is used for the moment arm model of both the Achilles tendon and TA for the full range of ankle joint angle, this length (5.0 cm) is only accurate at about 100^{o} ankle joint angle. At 150^{o} the difference between the constant value (5.0 cm) moment arm and the real moment arm is about 20% for the Achilles tendon and 30% for the TA. Some experimental data are shown in Figure A6.4, Figure A6.5, and Table A6.2.

Muscle moment arms are estimated empirically, accuracy of moment arms values are critical in the field of musculoskeletal modelling [198, 199]. The sensitivity of muscle force calculations to changes in muscle input variables was investigated by Herzog [200], an error in moment arm values of 20% produced errors of up to 50% in the calculated muscle force.

Therefore, accurate estimates and angle-specific values for the moment arm may significantly reduce errors in muscle force estimates [198]

Figure A6.4: Ankle angle and moment arm lengths: (a) Achilles tendon moment arm. (b) Tibialis Anterior moment arm, and (c) ankle angle. (From [198]).

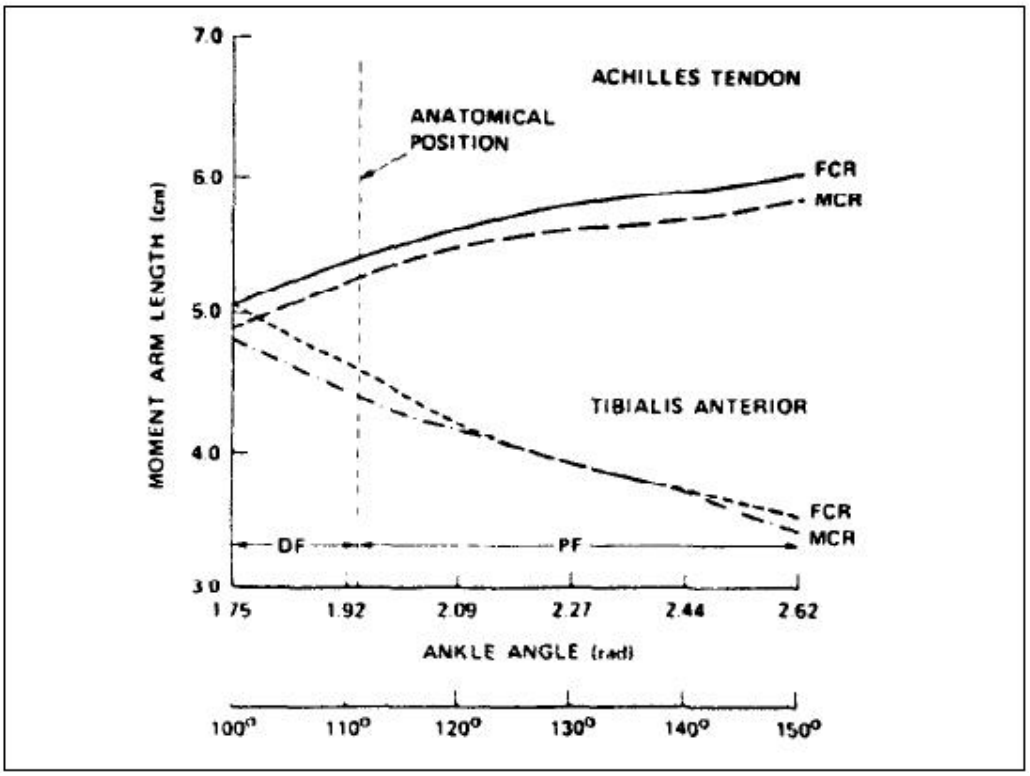

Figure A6.5: Average moment arm values for the Achilles tendon and Tibialis Anterior measured using a fixed centre of rotation (FCR) and a moving centre of rotation (MCR). DF= dorsi-flexion and PF= plantar flexion. Anatomical position was recorded at an ankle angle of approximately 1.94 radians (about 111^{o}) using both an FCR and MCR. (From [198]).

Table A6.2: Mean (2S.D.) moment arm values (N = 10) for the Achilles tendon and tibialis anterior measured using a fixed centre of rotation (FCR) and a moving centre of rotation (MCR). * Differences in moment arm values measured using fixed CR versus moving CR were statistically significant at the O.05 level. (From [198]).

Ankle angle (radians)	Achilles tendon moment arms (cm) FCR	MCR	Tibialis anterior moment arms (cm) FCR	MCR
1.75	5.1 ± 0.3	4.9 ± 0.4	5.1 ± 0.3	4.8 ± 0.3
1.92	5.4 ± 0.3	5.2 ± 0.4	4.6 ± 0.4	4.4 ± 0.3
2.09	5.6 ± 0.3*	5.5 ± 0.4	4.2 ± 0.3	4.2 ± 0.3
2.27	5.8 ± 0.4*	5.6 ± 0.4	3.9 ± 0.3	3.9 ± 0.3
2.44	5.9 ± 0.4*	5.7 ± 0.4	3.7 ± 0.2	3.7 ± 0.3
2.62	6.0 ± 0.3	5.9 ± 0.4	3.5 ± 0.2	3.4 ± 0.3

Appendix 7: Basic Laws of Geometry Related to Pennation Angle

Basic laws of geometry which can be used to calculate the effect of pennation angle on the F-V and F-L relationships are given here, this include the effect on length change (displacement due to stretch/shortening) of muscle belly (Δl_m) and muscle fibre (Δl_f), and also the rate of length change (velocity) for muscle belly (v_m) and muscle fibre (v_f). Note that for pennated muscle (pennation angle > 0): Δl_f and Δl_m are different, and consequently v_f and v_m are also different. The main basic laws of geometry related to this issue are shown in Figure A7.1 and Figure A7.2.

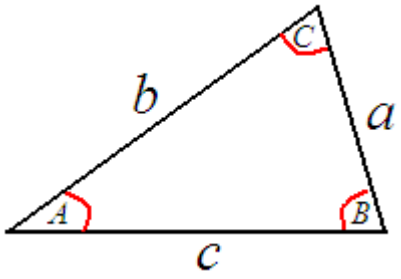

Figure A7.1: $\frac{\sin(A)}{a} = \frac{\sin(B)}{b} = \frac{\sin(C)}{c}$

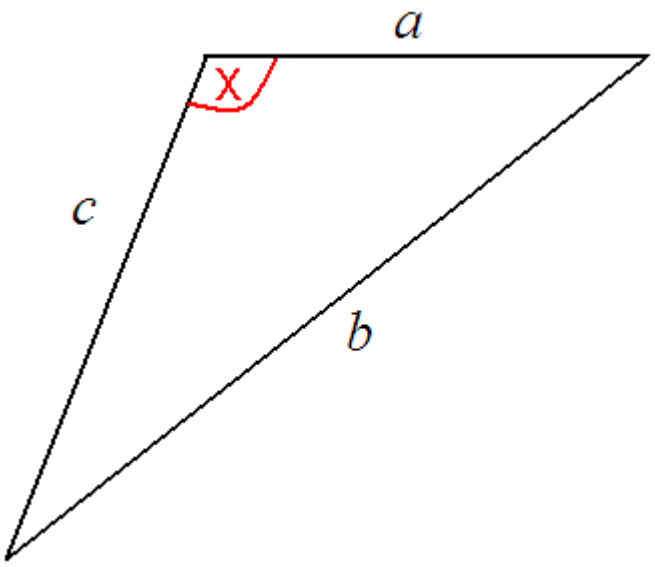

Figure A7.2: $b^2 = a^2 + c^2 - 2 \times a \times c \times \cos(x)$, $b = \sqrt{a^2 + c^2 - 2 \times a \times c \times \cos(x)}$.

Appendix 8: Forcinito Force Enhancement & Depression Sub-Model

Forcinito force enhancement & depression sub-models [156, 157] were modified in order to be used in the General Model, details are provided in this appendix.

In this sub-model, the initial length is used to calculate the isometric force $\left[f_{CE} = f_{iso}(l_o)\right]$, where in the majority of Hill-type models the instantaneous length is used $\left[f_{CE} = f_{iso}(l_{CE})\right]$. For fully recruited muscle ($R = 1$), the steady-state force depression/enhancement is modelled by an extra parallel elastic rack (parallel to *CE*), where a relay will engage the elastic rack at the moment when the muscle is initially recruited, this relay will continue to be active as long as the muscle is still recruited ($R > 0$). The stiffness of the rack is given by: $(E.A/l_{ER,0})$, where A is the cross-sectional area of the elastic rack, and E is the modulus of elasticity. The stiffness of the rack decreases linearly with increasing initial length ($l_{ER,0}$). The instantaneous active muscle force (f_m) including force enhancement and force depression is given by:

$$\begin{aligned} F_m = \quad & f_{iso}(l_o) + \left(\frac{E.A}{l_{ER,o}} \times (l_{ER} - l_{ER,o})\right) \\ & + \left(1 + \frac{E.A}{k \times l_{ER,o}} - \frac{E.A}{l_{ER,o}}\right) \times (l_{ER} - l_{ER,o}) \times \exp(-(k/c) \times t) \end{aligned} \qquad \text{(A8.1)}$$

In order to use Forcinito *IE & ID* sub-models in the "General Model" (it can only be used with Herzog since Herzog also used the initial length); it has to be in the standard form as presented in section 6.2. Therefore it needs to be re-formulated by normalising it to $\left[f_{iso}(l_o)\right]$ and optimal length (l_{opt}), also making the time t starts after end of stretch/shortening (in the original Forcinito model, time starts at onset of stretch/shortening).

The normalised *IE & ID* sub-models are represented by:

$$IE \quad or \quad ID = \left\{1 + (\frac{E.A}{\bar{l}_{ER,o}} \times (\bar{l}_{ER} - \bar{l}_{ER,o}))\right\} + \left[\left\{\left((1 + \frac{E.A}{k \times \bar{l}_{ER,o}}) \times (\bar{l}_{ER} - \bar{l}_{ER,o})\right) - \left((\frac{E.A}{\bar{l}_{ER,o}}) \times (\bar{l}_{ER} - \bar{l}_{ER,o})\right)\right\} \times \exp\left[-(\frac{k}{c} \times t)\right]\right] \quad \text{(A8.2)}$$

Note that the first term represents (IE_{∞}) and the second term represents the exponentially decaying transient-state. The re-formulation of Forcinito *IE & ID* sub-models is complicated because of the following: it was developed using a simple linear F-V relationship and also assumed that the time t starts at onset of stretch/shortening. Another problem is that the equations provided in [157] do not agree with the arrangement of rheological elements presented in the given figure, (see [157] for details).

Therefore the exponentially decaying term:

$$\left\{\left((1 + \frac{E.A}{k \times \bar{l}_{ER,o}}) \times (\bar{l}_{ER} - \bar{l}_{ER,o})\right) - \left((\frac{E.A}{\bar{l}_{ER,o}}) \times (\bar{l}_{ER} - \bar{l}_{ER,o})\right)\right\}$$

Which represents the maximum force reached during stretch or the minimum force reached during shortening, will be formulated in a form similar to Hawkins *IE* sub-model. Hence, IE_{∞} is the plateau level of *IE & ID* after very large value of time ($t \to \infty$), in its original form as provided in [156, 157] is given by:

$$IE_{\infty} = 1 + \left(\frac{E.A}{\bar{l}_{ER,j,o}} \times \Delta\bar{l}_{ER}\right) \quad , \quad \Delta\bar{l}_{ER,j} > 0 \qquad \text{(A8.3)}$$

$$ID_{\infty} = 1 + \left(\frac{E.A}{\bar{l}_{ER,j,o}} \times \Delta\bar{l}_{ER}\right) \quad , \quad \Delta\bar{l}_{ER,j} < 0 \qquad \text{(A8.4)}$$

Both of IE_{∞} and ID_{∞} have the same equation but $\Delta\bar{l}_{ER}$ will be positive in case of stretch and negative in case of shortening.

The maximum/minimum *IE* or *ID* at end of stretch/shortening will be taken as the normalised maximum/minimum force at end of stretch/shortening of Hill-type models (as defined in the notation list):

$$IE_{\max} = \frac{\text{maximum muscle force during stretch}}{\text{isometric force corresponding to the length at end of stretch}}$$

$$ID_{\min} = \frac{\text{minimum muscle force during shortening}}{\text{isometric force corresponding to the length at end of shortening}}$$

The steady-state IE_{SS} or ID_{SS} at $t = 4$:

$$IE_{SS} = IE_{\infty} + \left[(IE_{\max} - IE_{\infty}) \times \exp(c_{TS} \times 4)\right], \text{ for stretch.} \quad \text{(A8.5)}$$

$$ID_{SS} = ID_{\infty} + \left[(ID_{\min} - ID_{\infty}) \times \exp(c_{TS} \times 4)\right], \text{ for shortening.} \quad \text{(A8.6)}$$

$$\text{Finally: } c_{TS} = -(\frac{k}{c}) \quad \text{(A8.7)}$$

Appendix 9: Published Papers

Two paper abstracts were published during this study:

[1] A. Hamouda, D. Howard, L. Kenney, and G. Cooper, "A new multiple motor-unit muscle model for FES applications," In Proceedings 1st Annual Conference IFESS (UK and Ireland Chapter), Salford, UK, 47, April 2010.

[2] A. Hamouda, D. Howard, L. Kenney, and G. Cooper, "Modelling the Length-History Dependence of Muscle for FES Applications Using a Multiple Motor-Unit Approach," In Proceedings 2nd Annual Conference IFESS (UK and Ireland Chapter), University College Dublin, March 2011.

Copies of the two paper abstracts are shown in the next two pages.

A New Multiple Motor-Unit Muscle Model for FES Applications

Hamouda A[1], Howard D[1*], Kenney L[2], Cooper G[2].

[1*] School of Computing, Science & Engineering
[2] School of Health, Sports and Rehabilitation Sciences
University of Salford, UK.
Email d.howard@salford.ac.uk

1. Introduction

Many FES controllers have been developed using a simulation approach and the performance of these controllers depends on the muscle model accuracy. During FES, the activation level can change in a continuous fashion such that different motor units are recruited at different muscle lengths. Furthermore, it is the length at initial activation that should be the input to the muscle force-length relationship [1]. Therefore, it seems reasonable to account for these facts in muscle models that are to be used in the development of FES controllers. However, in most previous work on FES control [2,3], the instantaneous muscle length is used rather than the length at initial activation.

Whilst not commonly used in FES control studies, the Hill-type model described by Epstein & Herzog [1] does use the length at initial activation of the muscle (i.e. when the first motor unit is recruited). However, this does not properly model the situation where the activation varies with time and muscle length (i.e. different motor units are recruited at different lengths).

We present a Hill-type muscle model which accounts for different motor units being recruited at different lengths. Hence the model can account for a continuously changing activation level whilst using the individual motor unit lengths at initial activation as input to the force-length relationship (i.e. modelling the history effect).

2. The Model

Referring to Figure 1, a Hill-type model is used in which each recruited motor unit is treated as a separate fully activated muscle for the purposes of calculating the isometric force. The number of recruited motor units depends on the activation level, *β(t)*. The isometric force ($f_{iso,i}$) produced by each motor unit depends on the length at which it was initially recruited. The effective isometric force for the entire muscle ($Eff \cdot f_{iso}$) is the sum of the individual motor units' isometric forces.

$$Eff \cdot f_{iso} = \sum_{i=1}^{n} f_{iso,i} \qquad (1)$$

This effective isometric force is used as input to the force-velocity relationship of a Hill-type muscle model. Thus the total muscle force is determined by the number of recruited motor units, the length of each motor unit when initially recruited, and the instantaneous muscle velocity.

It should be noted that the virtual motor units in the model don't correspond to real motor units. Rather, the number of virtual motor units used in the model is chosen to give the required force resolution. For example if we want a resolution of 1%, then we would use a model based on 100 motor units.

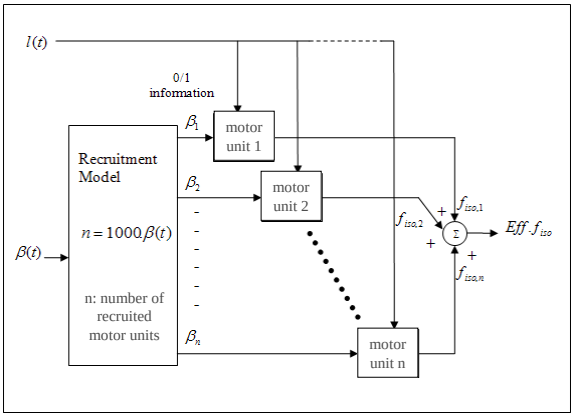

Figure 1 Calculating effective isometric force

3. Discussion

The new muscle model accounts for the activation history during FES control whilst allowing the activation to change continuously. As such, the model is suitable for the design, development and simulation of feedback control systems prior to clinical trials; with the proviso that other important features, such as a fatigue model, are included.

References

1. Epstein M & Herzog W. *Theoretical Models of Skeletal Muscle: Biological and Mathematical Considerations.* Wiley, 1998.
2. Lynch L & Popovic M. *Functional Electrical Stimulation: Closed-loop control of induced muscle contractions.* IEEE Control Systems Mag. 2008. 28(2): 40-50.
3. Riener R & Fuhr T. *Patient-driven control of FES-supported standing up: a simulation study.* IEEE Trans. Rehab. Eng. 1998. 6(2):113-124.

Modelling the Length-History Dependence of Muscle for FES Applications Using a Multiple Motor-Unit Approach

Hamouda A[1], Howard D[1*], Kenney L[2], Cooper G[2].

[1] School of Computing, Science & Engineering.
[2] School of Health, Sports and Rehabilitation Sciences.
University of Salford, Salford, Greater Manchester, UK.
Email: d.howard@salford.ac.uk

1. Introduction

Skeletal muscle force production is history dependent, yet this aspect of muscle modelling has received little attention in FES control studies. Force depression following shortening and force enhancement following stretch can reach values of up to almost 50% of the corresponding isometric muscle force. Therefore, if not properly accounted for during the design, it is reasonable to assume that this effect may adversely influence the performance of FES controllers [2]. To the best of the authors' knowledge, this length-history dependence has yet to be incorporated in muscle models in the context of FES control. We have developed a multiple motor-unit model for force depression and enhancement which accounts for time-varying activation levels (i.e. different motor-units being recruited at different lengths).

2. The Model

In our previous study [1], we developed a Hill-type multiple motor-unit muscle model that accounts for the activation history during FES control. We have extended this by incorporating the model of force depression and enhancement proposed by Forcinito, M., et al. [3] for a fully activated muscle treated as a single motor-unit. Based on their model, we have included an elastic rack in parallel with each motor-unit (Figure 1). When a motor-unit is recruited, its elastic rack is engaged and thus the passive force produced by that motor-unit will be a function of its change in length, x_i, since initial activation.

$$(f_{d/e})_i = \left(\frac{E.A}{l_{0,i}}(x_i) \right) \qquad (1)$$

Where A is the cross-sectional area of the elastic rack, E is the modulus of elasticity, and $l_{0,i}$ is the length at initial activation.

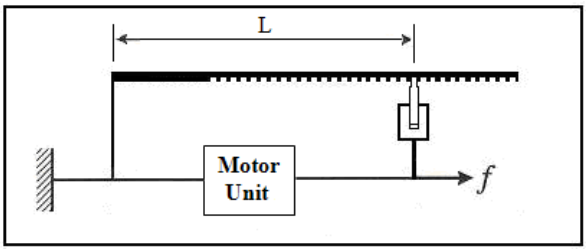

Figure (1) Motor unit with parallel elastic rack.

The effective isometric force of the entire muscle, including force depression or enhancement for each motor unit recruited, is the sum of the individual motor unit forces as follows:

$$Eff \cdot f_{iso+d/e} = \sum_{i=1}^{n} (f_{iso})_i + (f_{d/e})_i \qquad (2)$$

3. Discussion

We have incorporated force depression and enhancement in our multiple motor-unit muscle model, further improving the way in which the activation-history and length-history are accounted for. By correctly modelling the effects of continuously changing recruitment and length, as seen during FES control, we hope that better FES controllers can be designed.

References

1. Hamouda, A., Howard, D., Kenney, L. and Cooper G., *A new multiple motor-unit muscle model for FES applications.* In Proc. 1st Ann Conf IFESS (UK and Ireland Chapter), Salford, UK, April 2010. p. 47.
2. Herzog, W., *History dependence of skeletal muscle force production: implications for movement control*. Human Movement Science, 2004. 23: p. 591–604.
3. Forcinito, M., Epstein, M. and Herzog, W., *Can a rheological muscle model predict force depression/enhancement?* J Biomechanics, 1998. 31: p. 1093-9.

REFERENCES

[1] C. L. Lynch, and M. R. Popovic, "Functional Electrical Stimulation: Closed-Loop Control of Induced Muscle Contractions," IEEE Control Systems Magazine, 28 (2), 40-50, 2008.

[2] L. R. Sheffler, and J. Chae, "Neuromuscular Electrical Stimulation in Neurorehabilitation," Muscle & Nerve, 35, 562-590, 2007.

[3] L. Baker, C. Wederich, D. McNeal, C. Newsam, and R. L. Waters, "Neuromuscular Electrical Stimulation: A Practical Guide," 4th edition, Downey, CA: Rancho Los Amigos National Rehabilitation Centre, 2000.

[4] D. B. Popovic, and T. Sinkjaer, "Control of Movement for the Physically Disabled," Centre for Sensory-Motor Interaction, Aalborg University, 2003.

[5] D. Prodanov, E. Marani, and J. Holsheimer "Functional Electrical Stimulation for Sensory and Motor Functions: Progress and Problems," Biomedical Reviews, 14, 23-50, 2003.

[6] S. J. Dorgan, and T. Fuhr, "Mathematical Modelling and Control of Human Skeletal Dynamics," Engineering Science and Education Journal, 8 (4), 185-192, 1999.

[7] G. I. Barsi, D. B. Popovic, I. M. Tarkka, T. Sinkjær, and M. J. Grey, "Cortical Excitability Changes Following Grasping Exercise Augmented with Electrical Stimulation," Exp. Brain Res., 191, 57-66, 2008.

[8] S. Salmons, Z. Ashley, H. Sutherland, M. F. Russold, F. Li, and J. C. Jarvis "Functional Electrical Stimulation of Denervated Muscles: Basic Issues," Artificial Organs, 29 (3), 199-202, 2005.

[9] M. R. Popovic, A. Curt, T. Keller, and V. Dietz, "Functional electrical stimulation for grasping and walking: indications and limitations," Spinal Cord, 39, 403-412, 2001.

[10] M. R. Popovic, T. Keller, I. P. Pappas, V. Dietz, and M. Morari, "Surface-Stimulation Technology for Grasping and Walking Neuroprosthesis," IEEE Engineering in Medicine and Biology Magazine, 20 (1), 82–93, 2001.

[11] R. Stein, P. Peckham, and D. Popovic, "Neural Prostheses – Replacing Motor Function after Disease or Disability," New York and Oxford, Oxford University Press, 58-87, 1992.

[12] D. Zhang, T. H. Guan, F. Widjaja, and W. T. Ang, "Functional Electrical Stimulation in Rehabilitation Engineering: A Survey," Proceedings of the 1st International Convention on Rehabilitation Engineering & Assistive Technology, Singapore, 2007.

[13] W. Herzog, "History Dependence of Skeletal Muscle Force Production: Implications for Movement Control," Human Movement Science 23, 591-604, 2004.

[14] E. N. Marieb, "Human Anatomy and Physiology," 8th edition, Pearson Education Inc. USA, 2010.

[15] R. L. Lieber, "Skeletal Muscle Structure, Function & Plasticity," 2nd edition, Baltimore, MD: Williams &Wilkins, 2002.

[16] A. F. Huxley, "Muscle Structure and Theories of Contraction," Progress in Biophysics and Biophysical Chemistry, **7**, 255-318, 1957.

[17] D. Jones, J. Round, and A. de Haan, **"**Skeletal Muscle: from Molecules to Movement," Churchill Livingstone, 2008.

[18] W. Herzog, and M. Epstein, "Theoretical Models of Skeletal Muscle: Biological and Mathematical Considerations," John Wiley & Sons Ltd., 1998.

[19] W. Scott, J. Stevens, and S. A. Binder-Macleod, "Human Skeletal Muscle Fiber Type Classifications," Physical Therapy, 81 (11), 1810-1816, 2001.

[20] A. V. Hill, "First and Last Experiments in Muscle Mechanics," Cambridge University Press, Cambridge, 1970.

[21] M. Ariano, R. Armstrong, and V. Edgerton, "Hindlimb Muscle Fibre Populations of Five Mammals," Journal of Histochemistry and Cytochemistry, 21 (1), 51-55, 1973.

[22] B. Walmsley, J. Hodgson, and R. Burke, "Force Produced by Medial Gastrocnemius and Soleus Muscles during Locomotion in Freely Moving Cats," Journal of Neurophysiology, 41 (5), 1203-1216, 1978.

[23] W. Herzog, R. Leonard, and A. Guimaraes, "Forces in Gastrocnemius, Soleus, and Plantaris Muscles of the Freely Moving Cat," Journal of Biomechanics, 26, 945-953, 1993.

[24] J. T. Mortimer, "Motor Prostheses," in Handbook of Physiology-The Nervous System II, (Ed. V. B. Brooks.), American Physiological Society Bethesda, Maryland, 1981.

[25] J. Kiernan, J. Alan, and M. L. Barr, "Barr's The Human Nervous System: An Anatomical Viewpoint," 9th edition, Lippincott Williams & Wilkins, 2009.

[26] K. W. Horch, and G. S. Dhillon, "Neuroprosthetics: Theory and Practice," Series on Bioengineering & Biomedical Engineering, 2, Singapore, World Scientific Publishing, 2004.

[27] P. Cull, and L. Hague, "The Sourcebook of Medical Illustration," Park Ridge, USA: The Parthenon Publishing Group, 1989.

[28] J. P. Reilly, "Applied Bioelectricity from Electrical Stimulation to Electropathology," New York, Springer-Verlag, 1998.

[29] G. J. Tortora, “Introduction to the Human Body: the Essentials of Anatomy and Physiology,” 7th edition, New York, John Wiley, 2007.

[30] J. Z. L., R. W. Brown, and G. H. Yue, “A Dynamical Model of Muscle Activation, Fatigue and Recovery,” Biophysical Journal, 82 (5), 2344-2359, 2002.

[31] A. C. Guyton, and J. E. Hall, “Textbook of Medical Physiology,” 10th edition, Philadelphia, PA: Saunders, 2000.

[32] L. Sherwood, "Human Physiology: from Cells to Systems,” 7th edition, 2008.

[33] A. McPhedran, R. Wuerker, and E. Henneman, “Properties of Motor Units in a Homogeneous Red Muscle (Soleus) of the Cat,” Journal of Neurophysiology, 28, 71-84, 1965.

[34] R. Wuerker, A. McPhedran, and E. Henneman, “Properties of Motor Units in a Heterogeneous Pale Muscle (M. Gastrocnemius) of the Cat,” Journal of Neurophysiology, 28, 85-99, 1965.

[35] B. M. Nigg, and W. Herzog, “Biomechanics of the Musculo-skeletal System,” 2nd edition, John Wiley and Sons, Inc., 2002.

[36] D. Winter, “Biomechanics and Motor Control of Human Movement,” 4th edition, John Wiley and Sons, inc., 2009.

[37] H. S. Milner-Brown, R. B. Stein, and R. Yemm, “Changes in Firing Rate of Human Motor Units during Linearly Changing Voluntary Contractions,” Journal of Physiology, 230, 371-390, 1973.

[38] C. J. De Luca, R. S. LeFever, M. P. McCue, and A. P. Xenakis, “Behaviour of Human Motor Units in Different Muscles during Linearly Varying Contractions,” The Journal of Physiology, 329, 113-128, 1982.

[39] J. A. Hoffer, G. E. Loeb, W. B. Marks, M. J. O’donovan, C. A. Pratt, and N. Sugano, “Cat Hindlimb Motoneurons during Locomotion. I: Destination, Axonal Conduction Velocity, and Recruitment Threshold,” Journal of Neurophysiolgy, 57 (2), 510-529, 1987.

[40] J. A. Hoffer, N. Sugano, G. E. Loeb, W. B. Marks, M. J. O’donovan, C. A. Pratt, and, “Cat Hindlimb Motoneurons during Locomotion. II: Normal Activity Patterns,” Journal of Neurophysiolgy, 57 (2), 530-553, 1987.

[41] I. E. Brown, “Measured and Modeled Properties of Mammalian Skeletal Muscle,” PhD thesis, Queen’s University, Canada, 1998.

[42] Z. Erim, C. J. De Luca, K. Mineo, and T. Aoki, “Rank-Ordered Regulation of Motor Units,” 19 (5), 563-573, 1996.

[43] C. J. De Luca, P. J. Foley, and Z. Erim, “Motor Unit Control Properties in Constant-Force Isometric Contractions,” Journal of Neurophysiology, 76, 1503-1516, 1996.

[44] H. S. Milner-Brown, R. B. Stein, R. Yemm, “The Orderly Recruitment of Human Motor Units during Voluntary Isometric Contractions,” Journal of Physiology, 230, 359-370, 1973.

[45] B. R. MacIntosh, P. F. Gardiner, and A. J. McComas, “Skeletal Muscle: Form and Function,” Human Kinetics, 2006.

[46] P. H. Gorman, and J. T. Mortimer, “The Effect of Stimulus Parameters on the Recruitment Characteristics of Direct Nerve Stimulation,” IEEE Transactions on Biomedical Engineering, 30 (7), 407-414, 1983.

[47] P. H. Peckham, and J. S. Knutson “Functional electrical stimulation for Neuromuscular Applications,” Annual Review of Biomedical Engineering, 7, 327-360, 2005.

[48] M. Levy, J. Mizrahi, and Z. Susak, “Recruitment, Force and Fatigue Characteristics of Quadriceps Muscles of Paraplegics Isometrically Activated by Surface Functional Electrical Stimulation,” Journal of Biomedical Engineering, 12 (2), 150-156, 1990.

[49] C. M. Gregory, and C. S. Bickel, “Recruitment Patterns in Human Skeletal Muscle during Electrical Stimulation,” Physical Therapy, 85 (4), 358-364, 2005.

[50] K. Singh, F. J. R. Richmond, and G. E. Loeb, “Recruitment Properties of Intramuscular and Nerve-Trunk Stimulating Electrodes,” IEEE Transactions on Rehabilitation Engineering, 8 (3), 2000.

[51] Z. Lertmanorat, K. J. Gustafson, and D. M. Durand, “Electrode Array for Reversing the Recruitment Order of Peripheral Nerve Stimulation: Experimental Studies,” Annals of Biomedical Engineering, 34 (1), 152-160, 2006.

[52] H. Lanmüller, S. Sauermann, E. Unger, G. Schnetz, W. Mayr, M. Bijak, and W. Girsch, “Multi-Functional Implantable Nerve Stimulator for Cardiac Assistance by Skeletal Muscle,” Artificial Organs, 23 (4), 352-359, 1999.

[53] Z. -P. Fang, and J. T. Mortimer, “A Method to Effect Physiological Recruitment Order in Electrically Activated Muscle,” IEEE Transactions on Biomedical Engineering, 38 (2), 175-179, 1991.

[54] P. E. Crago, P. H. Peckham, and G. B. Thrope, “Modulation of Muscle Force by Recruitment during Intramuscular Stimulation,” IEEE Transaction on Biomedical Engineering, 27, 12, 679-684, 1980.

[55] R. Riener, J. Quintern, and G. Schmidt, “Biomechanical Model of the Human Knee Evaluated by Neuromuscular Stimulation,” Journal of Biomechanics, 29, 1157-1167, 1996.

[56] M. R. Popovic, T. A. Thrasher, V. Zivanovic, J. Takaki, and V. Hajek, “Neuroprosthesis for Restoring Reaching and Grasping Functions in Severe Hemiplegic Patients,” Neuromodulation, 8 (1), 60-74, 2005.

[57] M. M. Adamczyk, and P. E. Crago, “Simulated Feed forward Neural Network Coordination of Hand Grasp and Wrist Angle in A Neuroprosthesis,” IEEE Transactions on Biomedical Engineering, 8 (3), 297-304, 2000.

[58] A. Kralj, and T. Bajd, “Functional Electrical Stimulation: Standing and Walking after Spinal Cord Injury,” CRC Press, Baca Raton, FL, USA, 1989.

[59] Z. Matjacic, and T. Bajd, “Arm-Free Paraplegic Standing-Part II: Experimental Results,” IEEE Transactions on Rehabilitation Engineering, 6 (2), 139-150, 1998.

[60] W. Holderbaum, K. J. Hunt, and H. Gollee, “H∞ Robust Control Design for Unsupported Paraplegic Standing: Experimental Evaluation,” Control Engineering Practice, 10, 1211-1222, 2002.

[61] R. Davoodi, and B. J. Andrews, “Fuzzy Logic Control of FES Rowing Exercise in Paraplegia,” IEEE Transaction on Biomedical Engineering, 51 (3), 541-543, 2004.

[62] N. Donaldson, T. A. Perkins, R. Fitzwater, D. E. Wood, and F. Middleton, “FES Cycling May Promote Recovery of Leg Function after Incomplete Spinal Cord Injury,” Spinal Cord, 38, 11, 680-682, 2000.

[63] T. J. Demchak, J. K. Linderman, W. J. Mysiw, R. Jackson, J. Suun, and S. T. Devor, “Effects of Functional Electrical Stimulation Cycle Ergometry Training on Lower Limb Musculature in Acute SCI Individuals,” Journal of Sports Science and Medicine., 4 (3), 263-271, 2005.

[64] T. A. Thrasher, H. E. Flett, and M. R. Popovic, “Gait Training Regimen for Incomplete Spinal Cord Injury Using Functional Electrical Stimulation,” Spinal Cord, 44, 357-361, 2006.

[65] A. Kralj, T. Bajd, and R. Turk, “Enhancement of Gait Restoration in Spinal Injured Patients by Functional Electrical Stimulation,” Clinical Orthopaedics & Related Research, 223, 34-43, 1988.

[66] D. Graupe, R. Davis, H. Kordylewski, and K. H. Kohn, “Ambulation by Traumatic T4-12 Paraplegics Using Functional Neuromuscular Stimulation,” Critical Review in Neurosurgery, 8, 221-231, 1998.

[67] R. Riener, “Model-Based Development of Neuroprostheses for Paraplegic Patients,” Royal Philosophical Transactions: Biological Sciences, 354, 877-894, 1999.

[68] C. L. Lynch, and M. R. Popovic, “Closed-Loop Control of FES: Past Work and Future Directions,” Proceedings of the 10th Annual Conference of the International FES Society (IFESS ‘05), Montreal, Canada, 47-49, 2005.

[69] B. Jacques, “Can Muscle Models Improve FES-Assisted Walking after Spinal Cord Injury?” Journal of Electromyography and Kinesiology, 8, 125-132, 1998.

[70] J. J. Abbas, and R. Riener, “Using Mathematical Models and Advanced Control Systems Techniques to Enhance Neuroprosthesis Function,” Neuromodulation, 4, 187-195, 2001.

[71] R. Davoodi, C. Urata, M. Hauschild, M. Khachani, and G. E. Loeb, “Model-Based Development of Neural Prostheses for Movement,” IEEE Transactions on Biomedical Engineering, 54 (11), 1909-1918, 2007.

[72] R. Riener, and T. Fuhr, “Patient-Driven Control of FES-Supported Standing-Up: A Simulation Study,” IEEE Transactions on Rehabilitation Engineering, 6 (2), 113-124, 1998.

[73] R. Riener, and J. Quintern, “A Physiologically Based Model of Muscle Activation Verified by Electrical Stimulation,” Journal of Bioelectrochemistry and Bioenergetics, 43, 257-264, 1997.

[74] M. Ferrarin, F. Palazzo, R. Riener, and J. Quintern, “Model-Based Control of FES-Induced Single Joint Movements,” IEEE Transactions on Neural Systems and Rehabilitation Engineering, 9 (3), 2001.

[75] G. I. Zahalak, "An Overview of Muscle Modelling, ”Neural Prostheses – Replacing Motor Function after Disease or Disability (eds. R. Stein, P. Peckham, and D. Popovic), New York and Oxford, Oxford University Press, 17-57, 1992.

[76] G. Khang, and F. E. Zajac, “Paraplegic Standing Controlled by Functional Neuromuscular Stimulation: Part I-Computer Model and Control-System Design,” IEEE Transactions on Biomedical Engineering, 36, 873-884, 1989.

[77] G. T. Yamaguchi, and F. E. Zajac, “Restoring Unassisted Natural Gait to Paraplegics via Functional Neuromuscular Stimulation: a Computer Simulation,” IEEE Transactions on Biomedical Engineering, 37, 886-902, 1990.

[78] F. Previdi, “Identification of Black-Box Nonlinear Models for Lower Limb Movement Control Using Functional Electrical Stimulation,” Control Engineering Practice, 10, 91-99, 2002.

[79] Z. Cai, E. Bai, and R. K. Shields, “Fatigue and Non-Fatigue Mathematical Muscle Models during Functional Electrical Stimulation of Paralyzed Muscle,” Biomedical Signal Processing and Control, 5 (2), 87-93, 2010.

[80] W. K. Durfee, “Model Identification in Neural Prosthesis Systems, ”Neural Prostheses – Replacing Motor Function after Disease or Disability (eds. R. Stein, P. Peckham and D. Popovic), New York and Oxford, Oxford University Press, 58-87, 1992.

[81] I. E. Brown, and G. E. Loeb, “Measured and Modeled Properties of Mammalian Skeletal Muscle: I. The Effects of Post-Activation Potentiation on the Time-Course and Velocity Dependencies of Force Production,” Journal of Muscle Research and Cell Motility, 20, 443-456, 1999.

[82] I. E. Brown, E. J. Cheng, and G. E. Loeb, “Measured and Modeled Properties of Mammalian Skeletal Muscle: II. The Effects of Stimulus Frequency on Force-Length and Force-Velocity Relationships,” Journal of Muscle Research and Cell Motility, 20, 627-643, 1999.

[83] I. E. Brown, and G. E. Loeb, “Measured and Modeled Properties of Mammalian Skeletal Muscle: III. The Effects of Stimulus Frequency on Stretch-Induced Force Enhancement and Shortening-Induced Force Depression,” Journal of Muscle Research and Cell Motility, 21, 21-31, 2000.

[84] I. E. Brown, and G. E. Loeb, “Measured and Modeled Properties of Mammalian Skeletal Muscle: IV. Dynamics of Activation and Deactivation,” Journal of Muscle Research and Cell Motility, 21, 33-47, 2000.

[85] A. Hammerstein, “Nichlineare Integralgleichungen nebst Anwendungen,” Acta Mathematica, 54, 117-176, 1930.

[86] K. Hunt, M. Munih, N. Donaldson, and F. Barr, “Investigation of the Hammerstein Hypothesis in the Modeling of Electrically Stimulated Muscle,” IEEE Transactions on Biomedical Engineering, l45 (8), 998-1009, 1998.

[87] E. -W Bai, Z. Cai, S. Dudley-Javorosk, and R. K. Shields, “Identification of a Modified Wiener-Hammerstein System and its Application in Electrically Stimulated Paralyzed Skeletal Muscle Modelling,” Automatica, 45, 736-743, 2009.

[88] M. Bijanzadeh, D. Kahani, E. D. Kohan, M. Joghatai, S. C. Gharooni, and M. O. Tokhi, “NARMAX_OLS Representation of a Semi-Active Dynamic Leg Joint Model for a Paraplegic Subject Using Functional Electrical Stimulation,” Proceedings of the World Congress on Engineering II, WCE 2013, London, U.K., 1303–1308, 3 – 5 July, 2013.

[89] B. S. K. Ibrahim, M. O. Tokhi, S. C. Gharooni, and M. S. Huq, "Development of Fuzzy Muscle Contraction and Activation Model Using Multi-Objective Optimisation," 4th Annual IEEE International Systems Conference, 444–449. ISBN: 978-1-4244-5883-7, San Diego, CA, USA, 5-8 April, 2010.

[90] B. S. K. K. Ibrahim, M. O. Tokhi, M. S. Huq, R. Jailani, and S. C. Gharooni, "Fuzzy Modelling of Knee Joint with Genetic Optimisation," Applied Bionics and Biomechanics, 8 (1), 85 - 99, 2011.

[91] B. S. K. K. Ibrahim, M. S. Huq, M. O. Tokhi, S. C. Gharooni, R. Jailani, and Z. Hussain, "Identification of Active Properties of Knee Joint Using GA Optimization," Proceedings of ICBST 2009: International Conference on Biomedical Sciences and Technologies, Oslo, Norway, World Academy of Science, Engineering and Technology, ISSN: 2070-3724, 55, 441 - 446, 29 - 31 July, 2009.

[92] B. S. K. K. Ibrahim, M. O. Tokhi, M. S. Huq, and S. C. Gharooni, "Muscle Modelling: Comparative Study of Fuzzy and Mathematical Modelling Approaches," Proceedings of CLAWAR2010: 13th International Conference on Climbing and Walking Robots and the Support Technologies for Mobile Machines, Nagoya, Japan, World Scientific Publishing Company, Singapore, ISBN: 13 978-981-4327-97-8, 10 981-4327-97-2, 1247 - 1254, 31 August - 3 September, 2010,.

[93] B. S. K. K. Ibrahim, M. S. Huq, M. O. Tokhi, S. C. Gharooni, R. Jailani, and Z. Hussain, "Knee Joint Model Identification Using Genetic Algorithms," Proceedings of CLAWAR 2009: The 12th International Conference on Climbing and Walking Robots and the Support Technologies for Mobile Machines, Istanbul, Turkey, World Scientific Publishing Company, Singapore, ISBN: 13 978-981-4291-26-2, 10 981-4291-26-9, 1145 - 1152, 09 - 11 September, 2009,.

[94] R. Jailani, M. O. Tokhi, S. Gharooni, and Z. Hussain, "A Novel Approach in Development of Dynamic Muscle Model for Paraplegic with Functional Electrical Stimulation," Journal of Engineering and Applied Sciences, 4 (4), 272 - 276, 2009.

[95] R. Jailani, and M. O. Tokhi, "Development of Hamstrings Muscle Model for Paraplegic with Functional Electrical Stimulation," Proceedings of ISMS 2012: 3rd International Conference on Intelligent Systems Modelling and Simulation, Kota Kinabalu, Malaysia, 177-180, ISBN 978-0-7695-4668-1/12. DOI: 10.1109/ISMS. 2012.59, 8 - 10 February 2012.

[96] R. Jailani, M. O. Tokhi, S. Gharooni, and Z. Hussain, "Development of Dynamic Muscle Model with Functional Electrical Stimulation," Proceedings of COMPENG

2010: IEEE Conference on Complexity in Engineering, Rome, Italy, ISBN: 978-0-7695-3974-4, 132-134, 22-24 February 2010.

[97] A. V. HILL, "The Heat of Shortening and the Dynamic Constants of Muscle," Proceedings of the Royal Society of London, Series B, Biological Sciences, 126 (843), 136-195, 1938.

[98] G. I. Zahalak, "Modeling Muscle Mechanics (and Energetics) ," in Multiple Muscle Systems: Biomechanics and Movement Organization, (eds. J. M. Winters and S. L. -Y. Woo), New York, Springer-Verlag, 1-23, 1990.

[99] F. E. Zajac, "Muscle and Tendon: Properties, Models, Scaling and Application to Biomechanics and motor Control," Critical Reviews in Biomedical Engineering, 17 (4), 359-411, 1989.

[100] E. J. Cheng, I. E. Brown, and G. E. Loeb, "Erratum to 'Virtual Muscle: A Computational Approach to Understanding the Effects of Muscle Properties on Motor Control' " [Journal of Neuroscience Methods 101 (2000) 117-130]," Journal of Neuroscience Methods, 106, 111-112, 2001.

[101] D. A. Hawkins, "A Cellular Based Muscle Model: Formulation and Application for Studying Muscle Mechanics," PhD thesis, University of California, Davis, 1990.

[102] W. K. Durfee, and K. I. Palmer, "Estimation of Force-Activation, Force-Length and Force-Velocity Properties in Isolated Electrically Stimulated Muscle," IEEE Transactions on Biomedical Engineering, 41, 205-216, 1994.

[103] T. Siebert, C. Rode, W. Herzog, O. Till, and R. Blickhan, "Nonlinearities Make a Difference: Comparison of Two Common Hill-Type Models with Real Muscle," Biological Cybernetics, 98, 133-143, 2008.

[104] B. R. Jewell, and D. R. Wilkie, "An Analysis of the Mechanical Components in Frog's Striated Muscle," Journal of Physiology, 143, 515-540, 1958.

[105] B. W. Hoffman, G. A. Lichtwark, T. J. Carroll, and A. G. Cresswell, "A Comparison of Two Hill-Type Skeletal Muscle Models on the Construction of Medial Gastrocnemius Length-Tension Curves in Humans in Vivo," Journal of Applied Physiology, 113, 90-96, 2012.

[106] C. Rode, T. Siebert, W. Herzog, and R. Blickhan, "The Effects of Parallel and Series Elastic Components on the Active Cat Soleus Force-Length Relationship," Journal of Mechanics in Medicine and Biology, 9 (1), 105-122, 2009.

[107] Y. C. Fung, "Comparison of Different Models of the Heart Muscle," Journal of Biomechanics, 4, 289-295, 1971.

[108] M. Ferrarin, and A. Pedotti, "The Relationship between Electrical Stimulus and Joint Torque: A Dynamic Model," IEEE Transactions on Rehabilitation Engineering, 8, 342-352, 2000.

[109] P. H. Veltink, H. J. Chizeck, P. E. Crago, and A. El-Bialy, "Nonlinear Joint Angle Control for Artificially Stimulated Muscle," IEEE Transactions on Biomedical Engineering, 1992.

[110] J. Ding, A. S. Wexler, and S. A. Binder-Macleod, "A Mathematical Model that Predicts the Force-Frequency Relationship of Human Skeletal Muscle," Muscle & Nerve, 26 (4), 477-485, 2002.

[111] G. H. Shue, and P. E. Crago, "Muscle-Tendon Model with Length History Dependent Activation-Velocity Coupling," Annual Biomedical Engineering, 26 (3), 369-380, 1998.

[112] D. Zhang, and K. Zhu, "Modeling Biological Motor Control for Human Locomotion with Functional Electrical Stimulation," Biological Cybernetics, 96, 79-97, 2007.

[113] T. Schauer, N. -O. Negard, F. Previdi, K. J. Hunt, M. H. Fraser, E. Ferchland, and J. Raisch, "Online Identification and Nonlinear Control of the Electrically Stimulated Quadriceps Muscle," Control Engineering Practice: 13, 1207-1219, 2005.

[114] G. I. Zahalak, and S. P. Ma, "Muscle Activation and Contraction: Constitutive Relations Based Directly on Cross-Bridge Kinetics," Journal of Biomechanical Engineering, 112, 52-62, 1990.

[115] H. El Makssoud, D. Guiraud, P. Poignet, M. Hayashibe, P. B. Wieber, K. Yoshida, and C. Azevedo-Coste, "Multiscale Modeling of Skeletal Muscle Properties and Experimental Validations in Isometric Conditions," Biological Cybernetics, 105, 121-138, 2011.

[116] S. Dorgan, and M. O'Malley, "A Mathematical Model for Skeletal Muscle Activated by N-Let Pulse Trains," IEEE Transactions on Rehabilitation Engineering, 6 (3), 1998.

[117] S. J. Dorgans, and R. Riener, "A Physiologically Based Neuromusculoskeletal Model for the Design of FNS Control Strategies," Proceedings of the 20th Annual International Conference of the IEEE Engineering in Medicine and Biology Society, 5, 28 Oct - 1 Nov, 1998.

[118] S. J. Dorgan, and M. J. O'Malley, "A Nonlinear Mathematical Model of Electrically Stimulated Skeletal Muscle," IEEE Transactions on Rehabilitation Engineering, 5, 179-194, 1997.

[119] R. Riener, ”Neurophysiologische und biomechanische Modellierung zur Entwicklung geregelter Neuroprothesen,” PhD dissertation, Technical University of Munich, Germany, 1997.

[120] R. Massoud, “Intelligent Control Techniques for Spring Assisted FES-Cycling,” PhD thesis, Department of Automatic Control and System Engineering, University of Sheffield, Sheffield, UK, 2007.

[121] Z. Hussain, and M. O. Tokhi, "Modelling of Muscle Extension and Flexion for FES-Assisted Indoor Rowing Exercise," Proceeding of 2nd Asia International Conference on Modelling and Simulation (AMS 2008), 963-967, 2008.

[122] Z. Hussain, M. A. Zaidan, M. O. Tokhi, and R. Jailani, “The Adaptive Control of FES-assisted Indoor Rowing Exercise,” Proceedings of 2009 CACS International Automatic Control Conference National Taipei University of Technology, Taipei, Taiwan, 27-29 November, 2009.

[123] Z. Hussain, M. O. Tokhi, R. Jailani, S. Ahmad, B. S. K. S. M. K. Ibrahim, "Effect of Inclined Rowing Machine on FES-Assisted Indoor Rowing Exercise Performance," 3rd Asia International Conference on Modelling & Simulation, 242-245, 2009.

[124] Z. Hussain, S. Z. Yahaya, R. Boudville, K. A. Ahmad, and M. H. M. Noor, “Self Adaptive Neuro-Fuzzy Control of FES-Assisted Paraplegics Indoor Rowing Exercise,” IEEE International Conference on Control System, Computing and Engineering, 7-11, 2011.

[125] D. Zhang, and W. T. Ang, “Tremor Suppression of Elbow Joint via Functional Electrical Stimulation: A Simulation Study,” Proceeding of the 2006 IEEE International Conference on Automation Science and Engineering, Shanghai, China, 7-10 October, 2006.

[126] F. Previdi, M. Ferrarin, S. M. Savaresi, and S. Bittanti, “Closed-Loop Control of FES Supported Standing up and Sitting Down Using Virtual Reference Feedback Tuning,” Control Engineering Practice, 13, 1173-1182, 2005.

[127] E. J. Cheng, I. E. Brown, and G. E. Loeb, “Virtual Muscle: A Computational Approach to Understanding the Effects of Muscle Properties on Motor Control,” Journal of Neuroscience Methods, 101, 117-130, 2000.

[128] D. Song, G. Raphael, N. Lan, and G. E. Loeb, “Computationally Efficient Models of Neuromuscular Recruitment and Mechanics,” Journal of Neural Engineering, 5, 175-184, 2008.

[129] D. A. Hawkins, and M. L. Hull, “An Activation-Recruitment Scheme for Use in Muscle Modeling,” Journal of Biomechanics, 25 (12), 1467-1476, 1992.

[130] D. A. Hawkins, and M. L. Hull, "Muscle Force as Affected by Fatigue: Mathematical Model and Experimental Verification," Journal of Biomechanics, 26 (9), 1117-1128, 1993.

[131] W. K Durfee, and K. E. MacLean, "Methods for Estimating Isometric Recruitment Curves of Electrically Stimulated Muscles," IEEE Transactions on Biomedical Engineering, 36 (7), 654-666, 1989.

[132] H. Gareis, M. Solomonow, R. Baratta, R. Best, and R. D'ambrosia, "The Isometric Length-Force Models of Nine Different Skeletal Muscles," Journal of Biomechanics, 25 (8), 903-916, 1992.

[133] C. J. Zuurbier, and P. A. Huijing, "Influence of Muscle Geometry on Shortening Speed of Fibre, Aponeurosis and Muscle," Journal of Biomechanics, 25 (9), 1017-1026, 1992.

[134] E. Otten, "A Myocybernetic Model of the Jaw System of the Rat," Journal of Neuroscience Methods, 21, 287-302, 1987.

[135] C. A. Phillips, and J. S. Petrofsky, "Velocity of Contraction of Skeletal Muscle as a Function of Activation and Fiber Composition: a Mathematical Model," Journal of Biomechanics, 13, 549-558, 1979.

[136] AnyBody Modelling System. Anybody Tutorials, Lesson 5: Muscle Models. Retrieved 16 December, 2012, from: http://www.anybodytech.com/fileadmin/AnyBody/Docs/Tutorials/chap5_Muscle_modeling/lesson5.html.

[137] LifeMOD Biomechanics Modeller. LifeMOD Manual, Muscle Formulation. Retrieved 16 December, 2012, from: http://www.lifemodeler.com/LM_Manual/A_musclesform.shtml.

[138] LifeMOD Biomechanics Modeller. LifeMOD Manual, Choosing Model Parameters. Retrieved 16 December, 2012, from: http://www.lifemodeler.com/LM_Manual/A_parameters.shtml.

[139] J. Z. Liu, "FMRI Studies on Human Brain Function & Model of Muscle Activation And Fatigue," PhD Dissertation, Case Western Reserve University, Cleveland, OH, 2000.

[140] R. H. Fitts, "Cellular Mechanisms of Muscle Fatigue," Physiological reviews, 74, 49-94, 1994.

[141] R. M., Enoka, and D. G. Stuart, "Neurobiology of Muscle Fatigue," Journal of Applied Physiology 72, 1631-1648, 1992.

[142] A. Thrasher, G. M. Graham, and M. R. Popovic, “Reducing Muscle Fatigue Due to Functional Electrical Stimulation Using Random Modulation of Stimulation Parameters,” Artificial Organs, 29 (6), 453-458, 2005.

[143] Y. Giat, J. Mizrahi, and M. Levy, “A Musculotendon Model of the Fatigue Profiles of Paralyzed Quadriceps Muscle under FES,” IEEE Transactions on Biomedical Engineering, 40 (7), 1993.

[144] Y. Giat, J. Mizrahi, and M. Levy, “A model of Fatigue and Recovery in Paraplegic's Quadriceps Muscle Subjected to Intermittent FES,” Journal of Biomechanical Engineering, 118, 357-366, 1996.

[145] J. Mizrahi, D. Seelenfreund, E. Isakov, and Z. Susak, “Predicted and Measured Muscle Forces after Recoveries of Differing Durations Following Fatigue in Functional Electrical Stimulation,” Artificial Organs, 21 (3), 236-239, 1997.

[146] M. Levy, T. Kushnir, J. Mizrahi, and Y. Itzchak, “In Vivo ^{31}P NMR Studies of Paraplegics’s Muscles Activated by Functional Electrical Stimulation,” Magnetic Resonance in Medicine, 29, 53-58, 1993.

[147] J. Freund, and E. -P. Takala, “A Dynamic Model of the Forearm Including Fatigue,” Journal of Biomechanics, 34, 597-605, 2001.

[148] L. Ma, D. Chablat, F. Bennis, and W. Zhang, “A New Simple Dynamic Muscle Fatigue Model and its Validation,” International Journal of Industrial Ergonomics, 39, 211-220, 2009.

[149] L. Ma, D. Chablat, F. Bennis, W. Zhang, and F. Guillaume, “A New Muscle Fatigue and Recovery Model and Its Ergonomics Application in Human Simulation,” Virtual and Physical Prototyping, 5 (3), 123-137, 2010.

[150] K. A. P. Edman, G. Elzinga, and M. I. M. Noble, “Residual Force Enhancement after Stretch of Contracting Frog Single Muscle Fibers,” Journal of General Physiology, 80, 769–784, 1982.

[151] D. L. Morgan, N. P. Whitehead, A. K. Wise, J. E. Gregory, and U. Proske, “Tension Changes in the Cat Soleus Muscle Following Slow Stretch or Shortening of the Contracting Muscle,” Journal of Physiology, 522 (3), 503–513, 2000.

[152] W. Herzog, and T. R. Leonard, “Depression of Cat Soleus Forces Following Isokinetic Shortening,” Journal of Biomechanics, 30, 865-872, 1997.

[153] D. E. Rassier, W. Herzog, J. Wakeling, and D. Syme, “Stretch-Induced, Steady-State Force Enhancement in Single Skeletal Muscle Fibers Exceeds the Isometric Force at Optimal Fibre Length,” Journal of Biomechanics, 36, 1309–1316, 2003.

[154] B. Hisey, T. Leonard, and W. Herzog, “Does Residual Force Enhancement Increase with Increasing Stretch Magnitudes?” Journal of Biomechanics, 42, 1488-1492, 2009.

[155] W. Herzog, T. R. Leonard, and J. Z. Wu, “The Relationship between Force Depression Following Shortening and Mechanical Work in Skeletal Muscle,” Journal of Biomechanics, 33, 659-668, 2000.

[156] M. Forcinito, M. Epstein, and W. Herzog, “A Rheological Muscle Model Capable to Predict Force Depression/Enhancement,” North American Congress on Biomechanics NACOB98, University of Waterloo, Waterloo, Ontario, Canada, 14-18, 1998.

[157] M. Forcinito, M. Epstein, and W. Herzog, "Can a Rheological Muscle Model Predict Force Depression/Enhancement?” Journal of Biomechanics, 31, 1093-1099, 1998.

[158] I. E. Brown, T. L. Liinamaa, and G. E. Loeb, “Relationships between range of Motion, L_o, and Passive Force in Five Strap-Like Muscles of the Feline Hind,” Journal of Morphology, 230, 69-77, 1996.

[159] R. V. Gonzalez, T. S. Buchanan, and S. L. Delp, “How Muscle Architecture and Moment Arms Affect Wrist Flexion-Extension Moments,” Journal of Biomechanics, 30, 705-712, 1997.

[160] I. E. Brown, S. H. Scott, and G. E. Loeb, “Mechanics of Feline Soleus: II Design and Validation of A Mathematical Model,” Journal of Muscle Research and Cell Motility, 17, 221-233, 1996.

[161] H. Hatze, “A Myocybernetic Control Model of Skeletal Muscle,” Biological Cybernetics, 25, 103-19, 1977.

[162] T. Xia, and L. A. Frey Law, “A Theoretical Approach for Modeling Peripheral Muscle Fatigue and Recovery,” Journal of Biomechanics, 41, 3046-3052, 2008.

[163] B. Stojanovic, “Generalization of Hill's Phenomenological Model in Order to Investigate Muscle Fatigue,” PhD Thesis, CIMSI, University of Kragujevac Serbia, 2007.

[164] B. Stojanovic, and M. Kojic, “Modeling of Musculoskeletal Systems Using Finite Element Method,” Journal of the Serbian Society for Computational Mechanics, 1 (1), 110-119, 2007.

[165] B. Stojanovic, M. Kojic, M. Rosic, C. P. Tsui, and C. Y. Tang, “An Extension of Hill's Three-Component Model to Include Different Fibre Types in Finite Element Modelling of Muscle,” International Journal for Numerical Methods in Engineering, 71 (7), 801-817, 2007.

[166] R. B. Jailani, M. O. Tokhi, S. Gharooni, M. Joghtaei, and Z. Hussain, “Investigation into the Effect of Stimulation Frequency on Paraplegic Muscle Fatigue, “Proceedings

of 14th Annual International Functional Electrical Stimulation Society Conference 2009, Seoul, Korea, 103 - 105, 19 - 17 September, 2009.

[167] R. Jailani, and M. O. Tokhi, "The Effect of Functional Electrical Stimulation (FES) on Paraplegic Muscle Fatigue," Proceedings of CSPA 2012: IEEE 8th International Colloquium on Signal Processing and its Applications, Melaka, Malaysia, ISBN 978-1-4673-0961-5, 500 - 504, 23 - 25 March, 2012.

[168] R. Schachar, W. Herzog, and T. R. Leonard, "The Effects of Muscle Stretching and Shortening on Isometric Forces on the Descending Limb of the Force–Length Relationship," Journal of Biomechanics, 37, 917-926, 2004.

[169] W. Herzog, and D. E. Rassier, "History Dependence of Skeletal Muscle Force Production: a Forgotten Property," Journal of Mechanics in Medicine and Biology, 2, 347-358, 2002.

[170] W. Herzog, T. Leonard, and J. Wu, "Force Depression Following Skeletal Muscle Shortening is long lasting," Journal of Biomechanics, 31, 1163-1168, 1998.

[171] S. R. Bullimore, B. R. MacIntosh, and W. Herzog, "Is a Parallel Elastic Element Responsible for the Enhancement of Steady-State Muscle Force Following Active Stretch?" The Journal of Experimental Biology, 211, 3001-3008, 2008.

[172] W. Herzog, and T. R. Leonard, "The History Dependence of Force Production in Mammalian Skeletal Muscle Following Stretch-Shortening and Shortening-Stretch Cycles," Journal of Biomechanics, 33, 531-542, 2000.

[173] W. Herzog, "History Dependence of Force Production in Skeletal Muscle: a Proposal for Mechanisms," Journal of Electromyography and Kinesiology, 8, 111-117, 1998.

[174] R. Riener, T. Fuhr, and J. Schneider, "on The Complexity of Biomechanical Models Used for Neuroprostheses Development," Journal of Mechanics in Medicine and Biology, 2 (3&4), 389-404, 2002.

[175] G. C. Joyce, P. M. G. Rack, and D. R. Westbury, "Mechanical Properties of Cat Soleus Muscle during Controlled Lengthening and Shortening Movements," Journal of Physiology, 204, 461-474, 1969.

[176] J. G. Malamud, R. E. Godt, and T. R. Nichols, "Relationship between Short-Range Stiffness and Yielding in Type-Identified, Chemically Skinned Muscle Fibers from the Cat Triceps Surae Muscles," Journal of Neurophysiology, 76, 2280-2289, 1996.

[177] K. Meijer, H. J. Grootenboer, H. F. J. M. Koopman, and P. A. Huijing, "Fully Isometric Length–Force Curves of Rat Muscle Differ From Those during and After Concentric Contractions," Journal of Applied Biomechanics, 13, 164-181, 1997.

[178] K. Meijer, “Muscle Mechanics: The Effect of Stretch and Shortening on Skeletal Muscle Force,” PhD thesis, University of Twente, 1998.

[179] J. S. Petrofsky, and C. A. Phillips, “The Influence of Temperature, Initial Length and Electrical Activity on the Force-Velocity Relationship of the Medial Gastrocnemius Muscle of the Cat,” Journal of Biomechanics, 14 (5), 297-306, 1981.

[180] B. C. Abbott, and D. R. Wilkie, “The Relation between Velocity of Shortening and the Tension-Length Curve of Skeletal Muscle,” Journal of Physiology, 120, 214-223, 1953.

[181] A. S. Bahler, J. T. Fales, and K. L. Zierler, “The Dynamic Properties of Mammalian Skeletal Muscle,” The Journal of general physiology, 51, 369-382, 1968.

[182] T. L. Allinger, M. Epstein and W. Herzog, “Stability of muscle fibers on the descending limb of the force-length relation. A theoretical consideration,” Journal of Biomechanics, 29 (5), 627-633, 1996.

[183] F. D. Carlson, “The Kinematics of Retraction in Contracting Skeletal Muscle,” Journal of Cellular and Comparative Physiology, 49 (l), 291-352, 1957.

[184] W. Herzog, and T. R. Leonard, “Residual Force Depression is not Abolished Following a Quick Shortening Step,” Journal of Biomechanics, 40, 2806-2810, 2007.

[185] H. D. Lee, W. Herzog, and T. Leonard “Effects of Cyclic Changes in Muscle Length on Force Production in In-Situ Cat Soleus,” Journal of Biomechanics, 34, 979-987, 2001.

[186] A. V. Hill, “The Mechanics of Active Muscle,” Proceedings of the Royal Society of London, Series B, London, 141, 104 - 117, 1953.

[187] M. I. M. Noble, “Enhancement of Mechanical Performance of Striated Muscle by Stretch during Contraction,” The Journal of Experimental Physiology, 77, 539–552, 1992.

[188] K. A. P. Edman, and T. Tsuchiya, “Strain of Passive Elements during Force Enhancement by Stretch in Frog Muscle Fibres,” Journal of Physiology, 490, 191 - 205, 1996.

[189] D. E. Rassier, B. R. Macintosh, and W. Herzog, “Length Dependence of Active Force Production in Skeletal Muscle,” the American Physiological Society, 1445-1457, 1999.

[190] W. Herzog, T. R. Leonard, V. Joumaa, and A. Mehta, “Mysteries of Muscle Contraction,” Journal of Applied Biomechanics, 24, 1-13, 2008.

[191] W. Herzog, “The Biomechanics of Dynamically Contracting Skeletal Muscle,” University of San Francisco, Biomechanics Symposia 2001.

[192] R. Schachar, W. Herzog, T. R. Leonard, “Force Enhancement above the Initial Isometric Force on the Descending Limb of the Force–Length Relationship,” Journal of Biomechanics, 35, 1299–1306, 2002.

[193] W. Herzog and T. R. Leonard, “Force Enhancement Following Stretching of Skeletal Muscle: A New Mechanism,” The Journal of Experimental Biology, 205, 1275–1283, 2002.

[194] D. R. Peterson, D. E. Rassier and W. Herzog, “Force Enhancement in Single Skeletal Muscle Fibres on the Ascending Limb of the Force–Length Relationship,” The Journal of Experimental Biology 207, 2787-2791, 2004.

[195] Y. -W. Chang, F. -C. Su, H. -W. Wu, and K. -N. An, “Optimum length of Muscle Contraction,” Clinical Biomechanics, 14, 537-542, 1999.

[196] T. J. Burkholder, and R. L. Lieber, “Sarcomere Length Operating Range of Vertebrate Muscles during Movement,” The Journal of Experimental Biology, 204, 1529-1536, 2001.

[197] T. Oda, H Kanehisa, K Chino, T. Kurihara, T. Nagayoshi, E. Kato, T. Fukunage, and Y. Kawakami, “In Vivo Length-Force Relationship on Muscle Fiber and Muscle Tendon Complex in the Tibialis Anterior Muscle,” International Journal of Sport and Health Science, 3, 245-252, 2005.

[198] S. G. Rugg, R. J. Gregor, B. R Mandelbaum, and L. Chiu, “In Vivo Moment Arm Calculations at the Ankle Using Magnetic Resonance Imaging (MRI),” Journal of Biomechanics, 23, 495-501, 1990.

[199] C. N. Maganaris, “Imaging-Based Estimates of Moment Arm Length in Intact Human Muscle-Tendons,” European Journal of Applied Physiology, 91, 130-139, 2004.

[200] W. Herzog, “Sensitivity of Muscle Force Calculations Using Nonlinear Optimal Designs to Changes in Muscle Input Variables,” Journal of Biomechanics, 20, 895, 1987.